AN EXPERIMENTAL AND ANALYTICAL STUDY OF ELECTROKINETIC CONSOLIDATION

by

MyungHo Lee

A thesis submitted for the degree of Master of Science

at the University of Oxford

St. Catherine's College

Hilary term, 2000

To my beloved parents
Prof. KeunSik Lee and Dr. YoungHee Yim

Abstract

AN EXPERIMENTAL AND ANALYTICAL STUDY OF ELECTROKINETIC CONSOLIDATION

A thesis submitted for the degree of Master of Science

MyungHo Lee

St. Catherine's College, Oxford

Hilary term, 2000

This thesis describes settling process of clay particles in suspension and subsequent consolidation behaviour of Speswhite kaolin clay under the influence of electrokinetics. Comprehensive experimental investigations on soil behaviour under different stress conditions (e.g. electrokinetics, self-weight, and hydraulic gradient) were performed and reported. For comparing soil behaviour under electrokinetics with self-weight consolidation, the electrode configuration of closed anode and open cathode (the anode at the base and the cathode at the top of the soil) was used. One of the problems with this electrode arrangement was the gas produced at the anode electrode entering the soil and destroying the developing structure of soils. This problem was overcome by developing a specially designed electrokinetic cell. The density measurements of soil were achieved by an accurate and non-destructive X-ray technique, and pore pressures were also measured during the process.

The experimental results revealed that the electrically induced surface settlement was greater in magnitude and faster in rate than that under self-weight stresses; the dissipation rate of excess pore pressure was directly related to the applied electric field strength; the density in the anode region was increased significantly by the development of effective stress due to the effect of electroosmosis; the movement of acid and base fronts due to electrolysis was identified by the variation of pH; and the development of the denser layer at the soil surface was caused by the additional effects of electrokinetics, such as the variation of zeta potential and voltage gradient.

Numerical simulations using the simple diffusion equation with constant coefficients were investigated in order to predict the soil behaviour under the influence of electrokinetics. The normal small strain assumption (equivalent to the boundary remaining fixed) made in previous solutions of the equation has been replaced by boundary movement coupled with the requirement of conservation of mass. Remarkably good agreement between the measured and simulated surface settlement, density, and excess pore pressure profiles has been achieved using the method above, with appropriate soil parameters, such as C_c, C_v, k_h, and k_e.

Acknowledgements

I would like to express my gratitude and appreciation to my supervisor, Dr Gilliane Sills, for her constant support, guidance and friendship throughout the last few years. Dr Sills kindly provided EPSRC funds to allow construction of the experimental apparatus.

There are so many people I would like to thank for their technical support, discussion, encouragement, and assistance throughout the course of this thesis. Those people know who they are, and how grateful I am for their help.

MyungHo Lee

Contents

List of Symbols

English

A	total cross-sectional area (m^2)
$A_1 \sim A_5$, A_n	constant
B	constant
C_c	compression index
C_v	coefficient of consolidation (m^2/sec)
D	relative permittivity
e	void ratio
e_i	initial void ratio
e_f	final void ratio
E	electrical potential (V)
E_m	maximum electrical potential (V)
G_s	specific gravity of soil
g	gravitational constant
H	distance between electrodes (m)
h	thickness of soil element or hydraulic head (m)
h_s	height of slurry surface
Δh_i	difference in elevation
I	transmitted radiation intensity
I_o	intensity corresponding to transmission in a vacuum
i_e	electrical potential gradient (V/m)
i_h	hydraulic gradient
k	average attenuation constant ($=\mu_m x$)
k_e	electroosmotic permeability ($m^2/V \cdot sec$)
k_h	hydraulic permeability (m/sec)
L	length (m)
m_v	coefficient of compressibility (m^2/kN)
N	scintillation count rate with sample present
N_o	scintillation count rate with no sample present
N_s	transmitted count rates for the slurry
N_w	transmitted count rates for water
N_i, N_{i+1}	count rates at consecutive elevations
n	porosity
Q	volume flow rate (m^3/sec)
t	time (sec)
T_v	dimensionless time factor
u_e	excess pore pressure (kN/m^2)
u_{ei}	initial excess pore pressure (kN/m^2)
u_{em}	maximum excess pore water pressure (kN/m^2)
U_{av}	average degree of consolidation
v	pore fluid velocity, ion velocity (m/sec)
v_e	electrically induced flow velocity (m/sec)

v_f	velocity of pore fluid with respect to a fixed plane in the column (m/sec)
v_h	hydraulically induced flow velocity (m/sec)
v_r	relative velocity of pore fluid to soil particles (m/sec)
v_s	velocity of soil particles (m/sec)
x	absorber thickness
z	distance from soil surface or the cathode(m)

Greek

γ_s	unit weight of slurry (kN/m^3)
γ	density of absorbing material
γ_w	unit weight of water (kN/m^3)
δ	distance from clay surface to electrokinetic slip plane (m)
ε	static electrical permittivity of the liquid (F/m or C^2/Jm)
ε_o	vacuum permittivity (F/m or C^2/Jm)
ζ	zeta potential (V)
η	dynamic viscosity of the liquid phase (Ns/m^2)
ξ	dummy variable
ρ_f	final consolidation settlement (m)
σ	surface charge density, double layer charge (C/m^2)
σ_{ex}	total vertical stress above hydrostatic at the base of a column (kN/m^2)
σ_f'	vertical effective stress at the end of consolidation (kN/m^2)
σ_i'	vertical effective stress at the beginning of consolidation (kN/m^2)
σ_{vi}'	initial vertical effective stress (kN/m^2)
σ_{vf}'	final vertical effective stresse (kN/m^2)
σ_v'	vertical effective stress (kN/m^2)
μ_m	total mass absorption coefficient
Δt	time interval (s)
ΔE	electrical potential difference (V)
ΔL	distance between electrical charge (m)
ψ	electrical potential at a point within the double layer (V)
ψ_o	electrical surface potential (V)

List of Constant

D	relative permittivity for water at 25 °C (78.303)
g	acceleration due to gravity (9.81 m/sec^2)
ε_o	vacuum permittivity (8.8542 $\times$ 10^{-12} C^2/Jm)

Subscripts

av	average
c	compression
e	electroosmotic or excess
f	final
h	hydraulic
i	initial or time increment
m	maximum
s	soil
v	vertical
w	water

List of Figures

List of Plates

List of Tables

CHAPTER 1 INTRODUCTION

1. INTRODUCTION

1.1 General

In many areas of the world, soft soils of very high water content make construction extremely difficult. For example, it usually takes a long time for materials such as polluted dredged materials, mine tailings, coal washeries, slimes, or wastewater sludges to settle by gravity in storage ponds or to consolidate enough to support even light structures. Furthermore, several studies have shown that the dumping of polluted waste in the ground has contaminated both soil and groundwater. Thus, reliable *in situ* techniques are currently needed to dewater and stabilise these materials for reuse in these disposal sites.

1.2 An Overview of Literature

In order to provide an overall view of soft soil research and the application of electrokinesis, a brief literature review is given here. A more detailed survey of literature relevant to the research programme reported in this thesis is contained in Chapter 2.

1.2.1 Soft Soil Research

Sedimentation is the process of particles settling in a suspension. In a very dilute suspension of natural slurries, the distances between dispersed individual particles or flocs (discrete clusters of particles) are sufficiently large that they effectively settle independently of one another. The forces governing the settling behaviour are gravity and fluid drag.

In suspensions of intermediate concentration, there are electrochemical interactions (i.e. attractions and repulsions) occurring between settling particles and flocs due to the charged surface of particles. The settling behaviour under electrochemical interactions is referred to as hindered settling. During the process of hindered settling, pore pressures are equal to total stresses (e.g. total mass of sediment and fluid at any point) and interparticle distances decrease until a continuous matrix of interacting particles forms a sedimenting bed. These processes in which the soil is effectively behaving as a dense fluid have been described theoretically by Kynch (1952).

Structural continuity allows an external force to be transmitted throughout the sediment via networks of interparticle forces. With the development of soil structure from the bottom of the sedimenting bed, particles become partially self-supporting and pore pressures reduce to less than total stresses with time. The difference between pore pressure and total stress is called effective stress. Consolidation is, therefore, the time dependent process of pore fluid escaping from the sedimenting bed, resulting in compaction of the soil skeleton.

Been and Sills (1981) carried out a number of experiments in settling columns in which a dilute soil slurry was allowed to settle under its own weight. They examined the transition process from sedimentation to consolidation. Further experiments examined the significance of soil conditions, such as salinity and initial density, and identified the existence of creep in parallel with consolidation (Elder & Sills, 1984; Pane & Schiffman, 1985; Tan *et al.*, 1990; Sills, 1995).

One-dimensional consolidation theory was first presented by Terzaghi (1923), based on an infinitesimal strain theory. However, Terzaghi's theory cannot be applied to a soft clay consolidating under its own weight; large strains due to self-weight stresses and variations in soil compressibility and permeability must be taken into account. Gibson *et al.* (1967) published a non-linear finite strain theory for one-dimensional consolidation of a sedimenting clay layer with self-weight stresses.

1.2.2 Electrokinetic Research for Geotechnical Applications

In 1809, Reuss discovered the phenomenon of water flow across porous medium under an electrical gradient. Ions in the pore fluid are attracted to the oppositely charged electrodes and tend to drag with them their surrounding water. Clay particles carry a net negative charge, balanced by net positive ions in the pore water. In a clay soil, therefore, the application of an electric field leads to a flow of water dragged with these net positive ions. This process is termed electroosmosis, which is described more fully in Chapter 2.

As a method of dewatering, it is particularly suitable for low permeability soils where hydrodynamic techniques require much longer time scales. It was first employed by L. Casagrande in 1939 for stabilising a long railroad cutting. Following this first successful field application in Germany, electroosmosis became an established technique for stabilising slopes, dams, embankments, and excavation sites for construction (Lomize *et al.*, 1957; Casagrande *et al.*, 1961; Perry, 1963; Fetzer, 1967; Chappell & Burton, 1975; Wade, 1976). The process has been applied to different types of soils, ranging from sensitive silt (Wade, 1976) to soft clay (Fetzer, 1967) to very sensitive clay (Bjerrum, 1967).

1.2.3 Electrokinetic Research for Environmental Applications

Numerous techniques have been proposed for *in situ* remedial treatment of polluted ground. These currently involve thermal, physical, chemical, and biological processes. Thermal processes can be used to treat organic contaminants from soils. Physical processes such as soil washing and vacuum extraction can treat both organic and inorganic pollutants. Chemical processes involve the addition of chemicals and surfactants to soils to

desorb pollutants from soil particles, which then can be extracted by advection. Biological processes can destroy or transform pollutants by the action of microbes in soils. However, a major limitation of these remediation technologies is that they are not appropriate for soils with low hydraulic permeability, and some of them are not effective in extraction of pollutants adsorbed on soil particles. After relatively little attention for several years, the detection of high concentrations of organic materials and heavy metals in electrically drained effluent from a dredged soil was reported by Segall *et al.* (1980). Since then, the use of electrokinesis in environmental geotechnology has increased.

Numerous laboratory and field investigations have been performed in order to study the feasibility of using electrokinesis to mobilise and remove heavy metals such as arsenic, cadmium, chromium, copper, iron, lead, mercury, nickel, and zinc from soils (Lageman *et al.*, 1989; Banerjee *et al.*, 1990; Hamed *et al.*, 1991; Pamukcu & Wittle, 1992; Acar *et al.*, 1994; Rødsand *et al.*, 1995; Acar & Alshawabkeh, 1996). In addition, the electrokinetic removal of organic and inorganic contaminants such as benzene, toluene, ethylene, m-xylene, phenol, and acetic acid has been also demonstrated by laboratory studies (Shapiro *et al.*, 1989; Acar & Gale, 1992; Bruell *et al.*, 1992; Shapiro & Probstein, 1993).

The earlier research identified the importance of changes in soil conditions such as pH, concentration distributions of contaminants, soil and pore fluid conductivities, Atterberg limits and water content distributions, that take place during the electrokinetic process due to changes in the ion concentrations in the pore fluid (Lockhart, 1983abc; Mitchell & Yeung, 1990; Hamed *et al.*, 1991). This has led to efforts to improve the flow efficiency by the use of buffer solutions at the electrodes which control the ion concentration and stabilise the pH values (Acar & Alshawabkeh, 1993; Eykholt & Daniel, 1994; Rødsand *et al.*, 1995).

1.3 Research Objectives

The most common applications of electroosmosis have been to induce a lateral flow of water, since it is easier to install electrodes in this configuration and contaminants that arrive at an electrode can be removed by pumping. Much less emphasis has been placed on vertical electroosmotic flow with electrodes placed one above the other. Such an arrangement has applications in dewatering of hydraulic fill and related topics, and also provides a one-dimensional flow and consolidation process, that is a simpler basis for a fundamental study and for modelling. The purpose of the present research is to understand the processes occurring in electroosmosis, and to develop a simple one-dimensional model to describe the behaviour.

These research aims may most effectively be achieved by experiments observing the consolidation process of a soft soil slurry with and without the application of a vertical potential difference. Measurements are made of settlement, density, pore pressure, voltage, and pH. The results are analysed in terms of material parameters such as compressibility and permeability (i.e. hydraulic and electroosmotic).

1.4 Outline of the Thesis

Chapter 2 reviews the basic concepts of soil behaviour under various stress conditions and electrokinetic phenomena, the theory for electroosmotic flow, the theory of one-dimensional electrokinetic consolidation, and the current literature relevant to the soil behaviour under the influence of electrokinesis.

Chapter 3 is a detailed description of the testing apparatus and the development of the electrokinetic cells employed in the experimental programme. The experimental set up, laboratory testing procedures, and experimental techniques including density and pore pressure measurements are also presented.

Chapter 4 presents experimental results and discusses the significance of the influence of electrokinesis on soft soil by comparison with the results from self-weight and hydraulic gradient consolidation tests.

Chapter 5 reviews the material properties of Speswhite kaolin clay and summarises some mechanical properties including compressibility and hydraulic permeability obtained from the laboratory experimental programme given in Chapter 4. The electroosmotic permeability has also been investigated experimentally and evaluated theoretically.

Chapter 6 presents analytical models for self-weight and electrokinetic consolidation and examines the validity of the models to predict consolidation behaviour using the data obtained from the laboratory experiments.

Chapter 7 summarises the main conclusions of this research, and suggests some areas requiring further work.

REFERENCES

Acar, Y. B. and Gale, R. J. (1992). Phenol removal from kaolinite by electrokinetics. *J. Geotech. Engng. ASCE*, 118(11), 1837-1851.

Acar, Y. B. and Alshawabkeh, A. N. (1993). Principles of electrokinetic remediation. *Envir. Sci. Technol.* 27(13), 2638-2647.

Acar, Y. B., Hamed, J. T., Alshawabkeh, A. N., and Gale, R. J. (1994). Removal of cadminm(II) from saturated kaolinite by the application of electrical current. *Geotechnique* 44(2), 239-254.

Acar, Y. B. and Alshawabkeh, A. N. (1996). Electrokinetic remediation. I: pilot-scale tests with lead-spiked kaolinite. *J. Geotech. Engng. ASCE*, 122(3), 173-185.

Banerjee, S., Horng, J., Ferguson, J., and Nelson, P. (1990). Field scale feasibility of electrokinetic remediation. *Rep. presented to USEPA, Land Pollution Control Div., University of Washington, Seattle.*

Been, K. and Sills, G. C. (1981). Self-weight consolidation of soft soils: an experimental and theoretical study. *Geotechnique* 31(4), 519-535.

Bjerrum, L., Moum, J. and Eide, O. (1967). Application of electroosmosis to a foundation problem in a Norwegian quick clay. *Geotechnique* 17(3), 214-235.

Bruell, C. J., Segall, B. A., and Walsh, M. T. (1992). Electroosmotic removal of gasoline hydrocarbons and TCE from clay. *J. Envir. Engng. ASCE*, 118(1), 68-73.

Casagrande, L., Loughney, R. W., and Matich, M. A. J. (1961). Electro-osmotic stabilization of a high slope in loose saturated silt. *Proc. 5th ICSMFE, Paris*, 2, 555-561.

Chappell, B. A. and Burton, P. L. (1975). Electro-osmosis applied to unstable embankment. *J. Geotech. Engng. ASCE*, 101(8), 733-739.

Elder, D. McG. and Sills, G. C. (1984). Time and stress dependent compression in soft sediments. *Proc. ASCE Symp. On Prediction and Validation of Consolidation, San Francisco*, 425-444.

Eykholt, G. R. and Daniel, D. E. (1994). Impact of system chemistry on electroosmosis in contaminated soil. *J. Geotech. Engng. ASCE*, 120(5), 797-815.

Fetzer, C. A. (1967). Electroosmotic stabilization of west branch dam. *J. Soil Mech. Fdns. Div. ASCE*, 93(4), 85-106.

Gibson, R. E., England, G. L., and Hussey, M. J. L. (1967). The theory of one-dimensional consolidation of saturated clays-I. *Geotechnique* 17, 261-273.

Hamed, J., Acar, Y. B., and Gale, R. J. (1991). PB(II) removal from kaolinite by electrokinetics. *J. Geotech. Engng. ASCE*, 117(2), 241-271.

Kynch, G. J. (1952). A theory of sedimentation. *Transactions of the Faraday Society* 48, 166-176.

Lageman, R., Pool, W., and Seffinga, G. (1989). Electro-reclamation: theory and practice. *Chemistry and Industry* 18(9), 585-590.

Lockhart, N. C. (1983a). Electroosmotic dewatering of clays: I. influence of voltage. *Colloids Surf.* 6(3), 229-238.

Lockhart, N. C. (1983b). Electroosmotic dewatering of clays: II. influence of salt, acid, and flocculants. *Colloids Surf.* 6(3), 239-251.

Lockhart, N. C. (1983c). Electroosmotic dewatering of clays: III. influence of clay type, exchangeable cations, and electrode materials. *Colloids Surf.* 6(3), 253-269.

Lomize, G. M., Netushil, A. V., and Rzhanitzin, B. A. (1957). Electro-osmotic processes in clayey soils and dewatering during excavations. *Proc. 4th ICSMFE, London*, 1, 62-67.

Mitchell, J. K. and Yeung, A. T. (1990). Electro-kinetic flow barriers in compacted clay. *Transportation Res. Rec.* 1288, 1-9.

Pamukcu, S., and Wittle, J. K. (1992). Electrokinetic removal of selected heavy metals from soil. *Envir. Progress* 11(3), 241-250.

Pane, V. and Schiffman, R. L. (1985). A note on sedimentation and consolidation. *Geotechnique* 35(1), 69-72.

Perry, W. (1963). Electro-osmosis dewaters foundation excavation. *Constr. Methods Equip.* 49(9), 116-119.

Rødsand, T., Acar, Y. B., and Breedveld, G. (1995). Electrokinetic extraction of lead from spiked Norwegian marine clay. *Geoenvironment 2000, Geotechnical Special Publication 46*, 1518-1534.

Segall, B. A., O'Bannon, C. E., and Mathias, J. A. (1980). Electroosmosis chemistry and water quality. *J. Geotech. Engng. ASCE*, 106(10), 1148-1152.

Shapiro, A. P., Renaud, P. C., and Probstein, R. F. (1989). Preliminary studies on the removal of chemical species from saturated porous media by electroosmosis. *PhysicoChemical Hydrodynamics* 11(5/6), 785-802.

Shapiro, A.P. and Probstein, R. F. (1993). Removal of contaminants from saturated clay by electroosmosis. *Envir. Sci. Technol.* 27, 283-291.

Sills, G. C. (1995). Time dependent processes in soil consolidation. *Proc. Int. Symp. Compression and Consolidation of Clayey Soils. Hiroshima*, Japan 875-890.

Tan, T. S., Yong, K. Y., Leong, E. C., and Lee, S. L. (1990). Sedimentation of clayey slurry. *J. Geotech. Engng. ASCE*, 116(6), 885-898.

Terzaghi, K. (1936). The shearing resistance of saturated soils and the angles between the planes of shear. *Proc. 1st Int. Conf. Soil Mechanics*, 1, 54-56.

Wade, M. H. (1976). Slop stability by electroosmosis. *Proc. 29th Canadian Geotechnical Conference, Vancouver*, 10, 44-66.

CHAPTER 2 LITERATURE REVIEW

2. LITERATURE REVIEW

2.1 Introduction

This chapter introduces the literature relevant to the principles of electrokinetic processes. Basic concepts and definitions of electrokinetic processes are presented and discussed. The theoretical model for pore fluid flow induced by electroosmosis and the development of pressure gradients under various drainage conditions during the electrokinetic process are described. Some settling column experiments are introduced and discussed. Finally, the theory of one-dimensional electrokinetic consolidation is reviewed.

2.2 Clay Structure

In general, clay minerals have layered sheet structures consisting of silica tetrahedral and octahedral units. The silica tetrahedral unit is formed by one silicon atom surrounded by four oxygens, whereas the octahedral unit consists of magnesium or aluminum coordinated octahedrally with oxygens or hydroxyls as shown in Figure 2.1.

Clay particles have a net negative surface charge due to isomorphous substitutions, which occur during the formation of clay minerals by the replacement of cations in the structure with another type of similar size but lower valence. The lower valence results in a net negative surface charge (Goldman *et al.*, 1986). Clay minerals can be categorised into four groups; kaolinite, smectite, illite, and chlorite. Speswhite kaolin clay was used in this study, and therefore some details of kaolinite minerals are reviewed below.

Kaolinite minerals are composed of alternating silica and octahedral sheets, which are held by both van der Waals forces and hydrogen bonds as shown in Figure 2.2. As kaolinite minerals have little isomorphous substitution, their net negative surface charge is low, resulting in a low cation exchange capacity. The negative surface charge is due to broken bonds at the edges of the particles, which have unsatisfied valence charges that are balanced by adsorbed cations from the pore fluid. Therefore, the charges are affected by the pH level. Kaolinite particles are charged negatively in a high pH environment, whereas in a low pH environment, the broken bonds attract hydrogen ions producing positively charged sites on their edges (Mitchell, 1993).

2.3 Electric Double Layer

Clay particles generally carry a net negative charge distributed as negative charges on their faces and positive charges at their edges. Thus, ions of opposite charge are electrostatically held by the negatively charged clay surfaces to maintain electrical neutrality

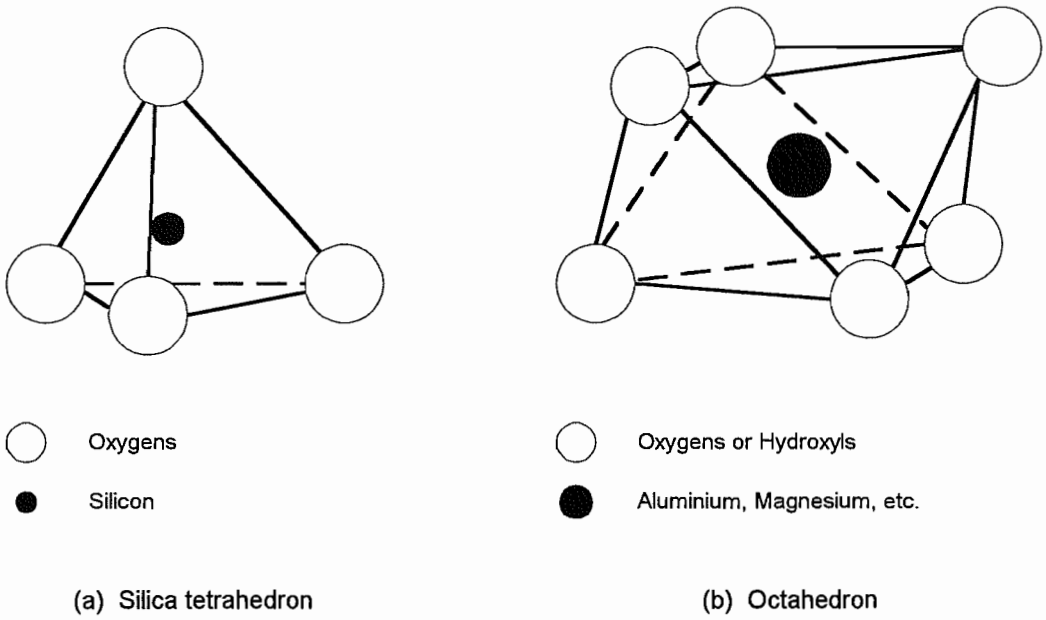

Figure 2.1 Basic units of clay minerals: (a) silica tetrahedron; (b) octahedron (After Mitchell, 1993)

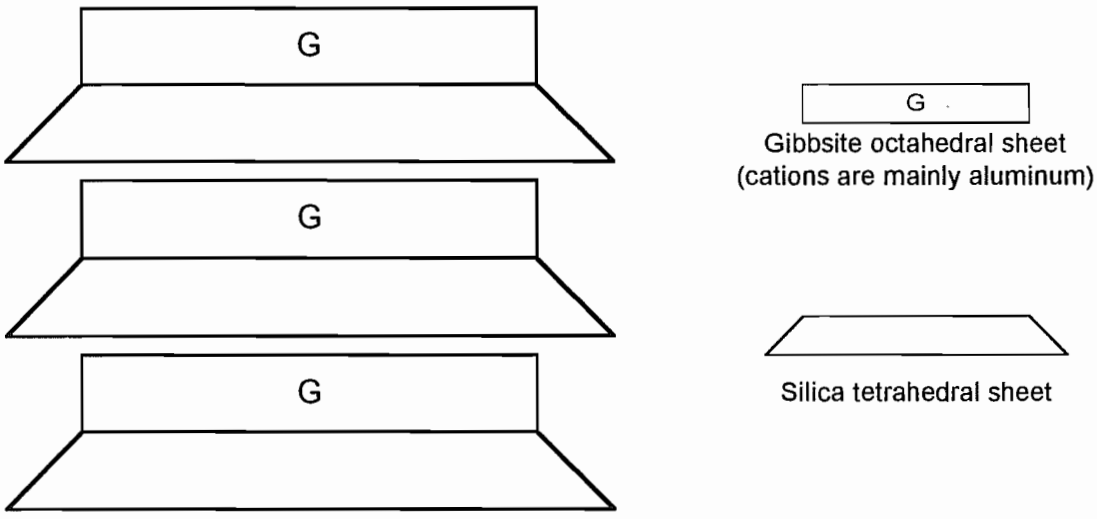

Figure 2.2 Schematic of kaolinite structure (After Mitchell, 1993)

as illustrated in Figure 2.3. The distribution of ions adjacent to the surfaces of clay particles and the electrical potential distribution caused by the interaction between the negative charges on the surface and the counter ions are briefly reviewed in this section.

2.3.1 Helmholtz Model

Several theories have been proposed to describe quantitatively the ion distributions within charged surfaces. One of the earliest models is the *Helmholtz Double Layer*, proposed by Helmholtz in 1879. It is assumed that the electrically balanced positive charges (cations) are concentrated in a plane parallel to the uniformly charged particle surface with a small distance. Therefore, the electrical potential is maximum at the surface and decreases linearly with increasing distance from the surface as shown in Figure 2.4(a).

2.3.2 Gouy-Chapman Model

The influence of the layer of mobile counter ions on other ions in the bulk pore fluid was recognised by Gouy in 1910 and Chapman in 1913. When water is added to clay, the counter ions (cations) adsorbed on the negatively charged clay particles produce a higher concentration near the soil surfaces, so that they try to diffuse away from the soil to make equal concentrations throughout. The charged surface and the mobile counter ions in the bulk solution are together termed the *Gouy-Chapman Diffuse Double Layer*. The model assumes that the total electrical charges on the particle surface are considered to be balanced by excess cations, so that the electrical potential is maximum at the surface and decreases exponentially with the distance from the surface as illustrated in Figure 2.4(b).

2.3.3 Stern Model

The Gouy-Chapman model did not consider the effect of ion size. In 1924, Stern made corrections in the Gouy-Chapman model by taking ion size into account. The model assumes that the electric double layer consists of two regions where adsorbed ions are in the inner region (i.e. Stern layer) and the counter ions are distributed under the influence of the interparticle forces in the outer region (i.e. diffuse layer). The electric double layer is separated by the Stern plane, located at about a hydrated ion radius from the surface. The Stern layer is tightly packed with cations, and the electrical potential decreases linearly with distance from the surface, according to the Helmholtz model. In the diffuse layer, the electrical potential decreases exponentially with distance from the surface, according to the Gouy-Chapman model as shown in Figure 2.4(c).

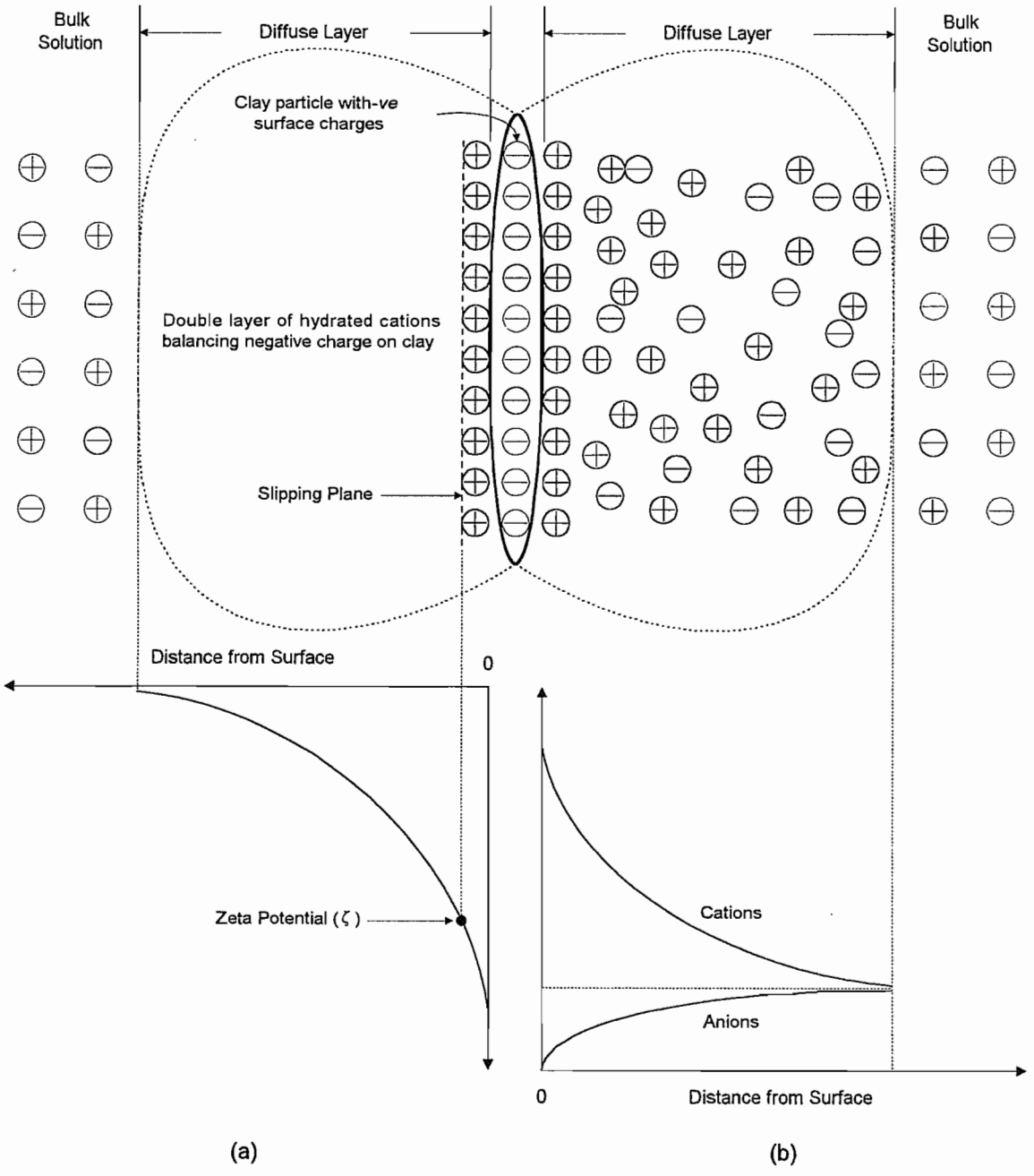

Figure 2.3 Electric double layer: (a) variation of electrical potential with distance from a charged surface; (b) distributions of ions adjacent to a clay surface (After Tan, 1993; Mitchell, 1993; Rowe *et al.*, 1995)

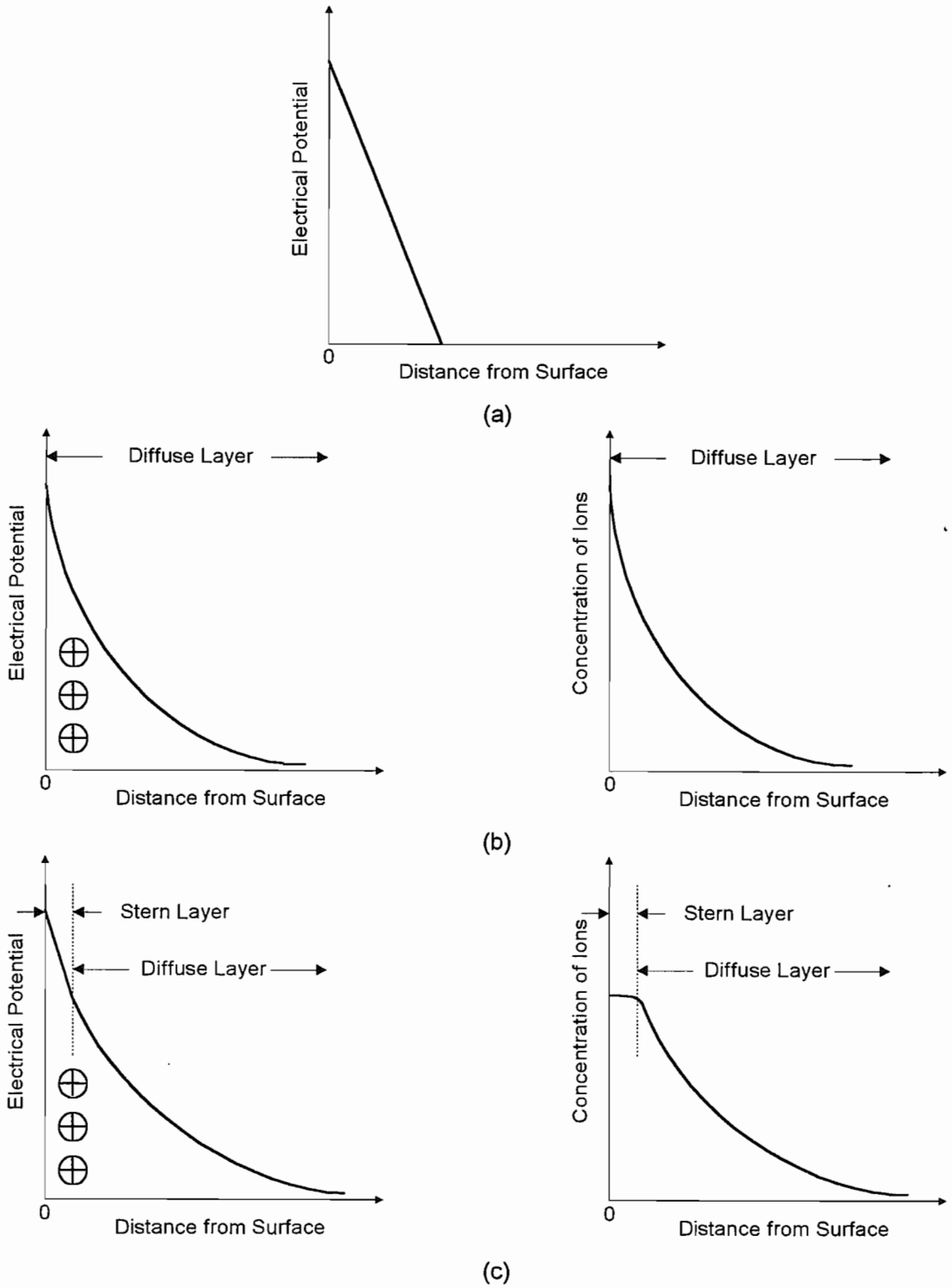

Figure 2.4 Double layer models: (a) Helmholtz double layer; (b) Gouy-Chapman diffuse double layer; (c) Stern double layer (After Tan, 1993; Mitchell, 1993)

2.3.4 Zeta Potential

If a colloidal suspension is placed in an electric field, the colloidal particles move in one direction towards the positive pole (Section 2.4.2). The counter ions move in another direction towards the negative pole. The electrical potential developed at the junction between the fixed and mobile parts of the electric double layer is called the zeta potential (see Figure 2.3(a)).

The zeta potential is not a unique property of the colloid, but depends on the electrical surface potential of the suspension using the following equation:

$$\zeta = \frac{4\pi\eta}{DE} v_e \qquad (2.1)$$

where ζ is the zeta potential, η is the viscosity of the liquid, D is the relative permittivity, E is the electrical surface potential, and v_e is the electrically induced flow velocity.

The zeta potential is related to the thickness of the electric double layer and electrical surface potential, which are affected by pH, relative permittivity, and concentration of ions and their valence (van Olphen, 1977; Tan, 1993; West & Stewart, 1995). It was assumed that the electrical surface charge remains constant and that zeta potential is dependent on electrical surface potential (Mitchell, 1993). However, increasing the ion concentration in the solution usually results in decreasing the thickness of the electric double layer; the thickness of the double layer affects the magnitude of the zeta potential. As a result, the zeta potential ranges from 0 to -50 mV for most clays.

Figure 2.5 presents an example of the change in the magnitude of zeta potential according to the change in ion concentrations. The zeta potential in a dilute solution has a value represented by ζ_1. By adding salt to the solution, the diffuse layer is suppressed and more counter ions are forced to the colloid surface within the slipping plane. Hence, the zeta potential becomes small (i.e. from ζ_1 to ζ_2) due to the change in the total potential distribution as related to distance from the colloid at high salt concentration; the potential distribution at high salt concentration is represented by the dotted line. Thus, the zeta potential is expected to decrease in magnitude with increasing ion concentration.

West and Stewart (1995) investigated the influence of pH and ionic strength on the zeta potential of Speswhite kaolin clay. The pH was controlled by the addition of nitric acid and sodium hydroxide. As shown in Figure 2.6, increasing the pH in the solution resulted in increasing the magnitude of the zeta potential to -30 mV at pH 12 from 0 mV at pH 2.

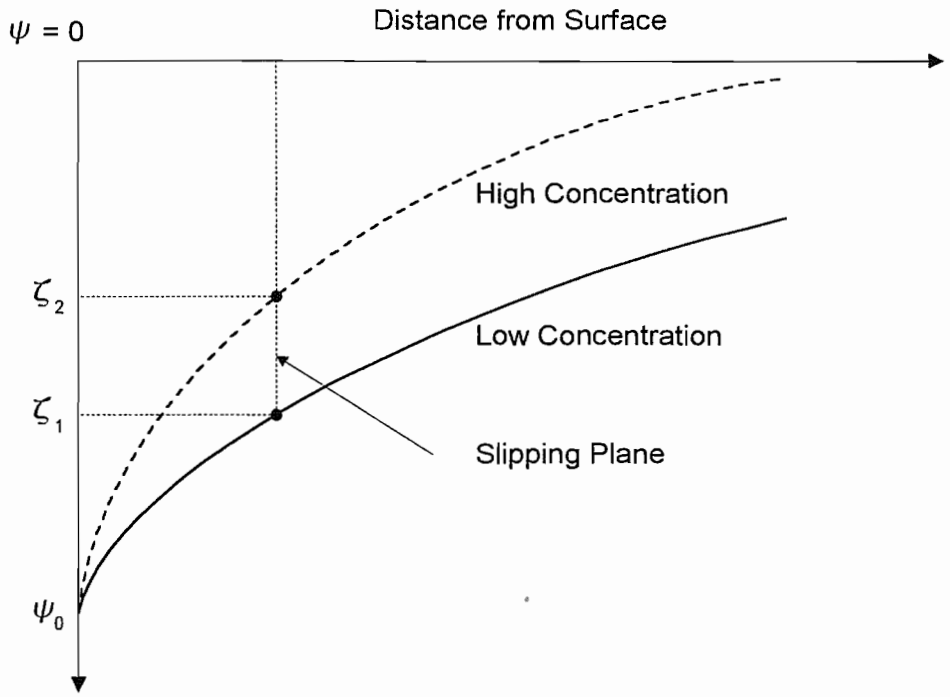

Figure 2.5 Variations of zeta potential (After Tan, 1993)

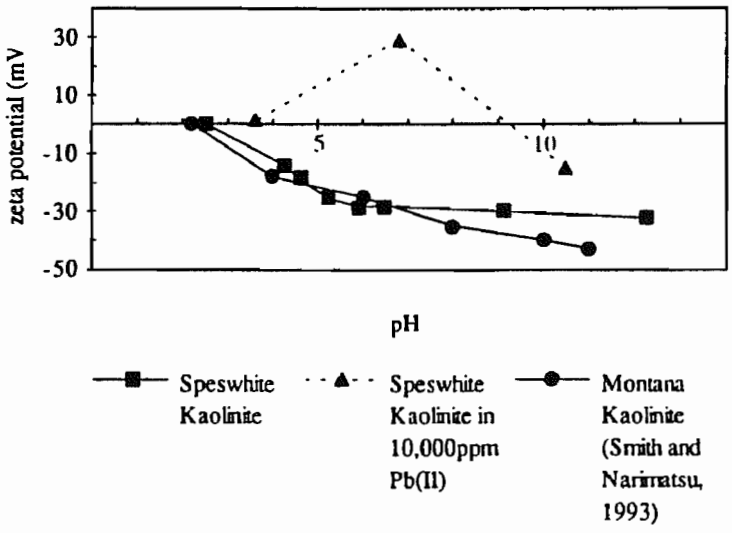

Figure 2.6 Influence of pH on ζ potential (After West & Stewart, 1995)

Increasing the ionic strength of the solution to 10,000 ppm of Pb(II) resulted in the positive zeta potential between pH 4 and 9. They also reported that high concentrations of ions in the soil (i.e. low pH condition) can reduce the electroosmotic flow significantly, or even reverse the direction of flow due to the change in zeta potential. A similar effect of ion concentration on electroosmosis was also found by several researchers (Eykholt & Daniel, 1994; Vane & Zang, 1995; Eykholt, 1997).

Vane and Zang (1997) conducted similar laboratory experiments with Georgia kaolinite and Wyoming bentonite samples treated by electrokinesis in order to investigate the influence of pH on the zeta potential. They found that the zeta potential of kaolinite was a strong function of pH, ranging from 0.7 mV at pH 2 to -52 mV at pH 10, whereas that of the bentonite did not change by more than 20 % over a pH range of 2 to 10 (-31 mV to -36 mV) as shown in Figure 2.7.

2.4 Electrokinetic Phenomena

In general, several electrokinetic phenomena can arise when the counter ions in the mobile part of the double layer adjacent to the surface of charged particles are subject to shear by external forces. These phenomena can be classified into two main groups. The first group consists of *electroosmosis* and *electrophoresis*, in which the liquid or solid phase moves relative to the other under the influence of an externally applied electric field. The second group consists of *streaming potential* and *migration or sedimentation potential*, in which the liquid or solid phase moves relative to the other under the influence of hydraulic or gravity force, thus inducing an electrical potential. These four electrokinetic phenomena are illustrated in Figure 2.8.

In addition to the migration of water and the movement of soil particles due to the externally applied electric field, some other effects may develop: electrolysis, hydrolysis, ion diffusion and exchange, oxidation, reduction, gas generation, pH change, physical and chemical adsorption, mineral decomposition, fabric changes, precipitation, and desiccation (Mitchell, 1993). A simplified schematic diagram of overall electrokinetic processes within a soil mass is illustrated in Figure 2.9.

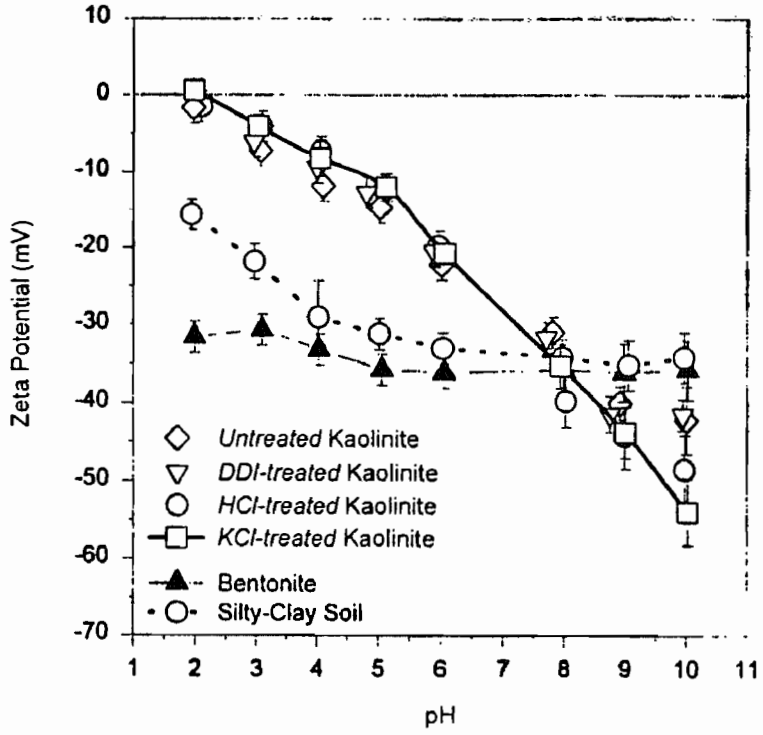

Figure 2.7 Effect of pH on zeta potential of kaolinite, bentonite and silty-clay soil samples. All samples: 0.1 g-clay/1 suspensions in 0.01 M KCL at 25°C (After Vane & Zang, 1997)

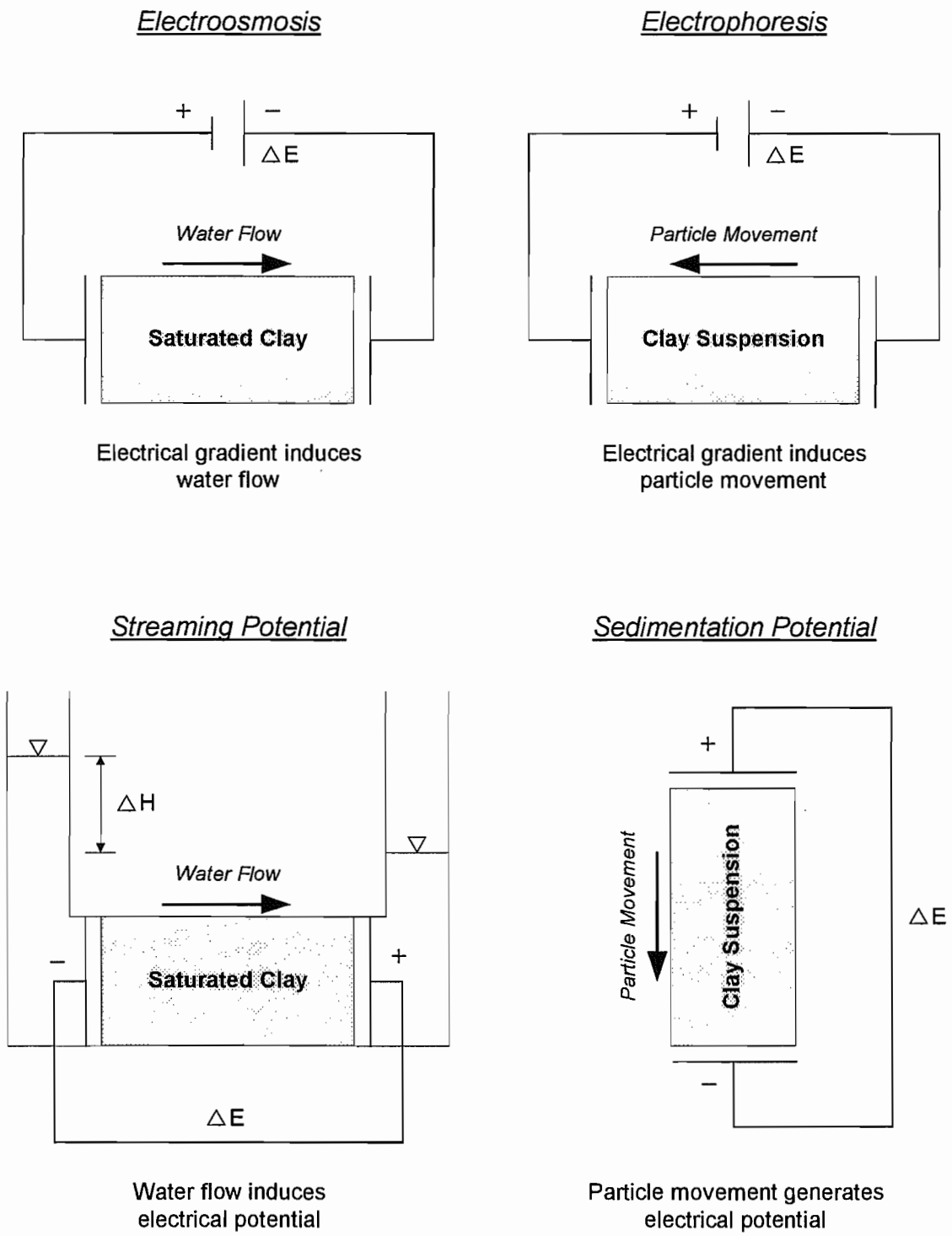

Figure 2.8 Electrokinetic phenomena in soils (After Mitchell, 1993)

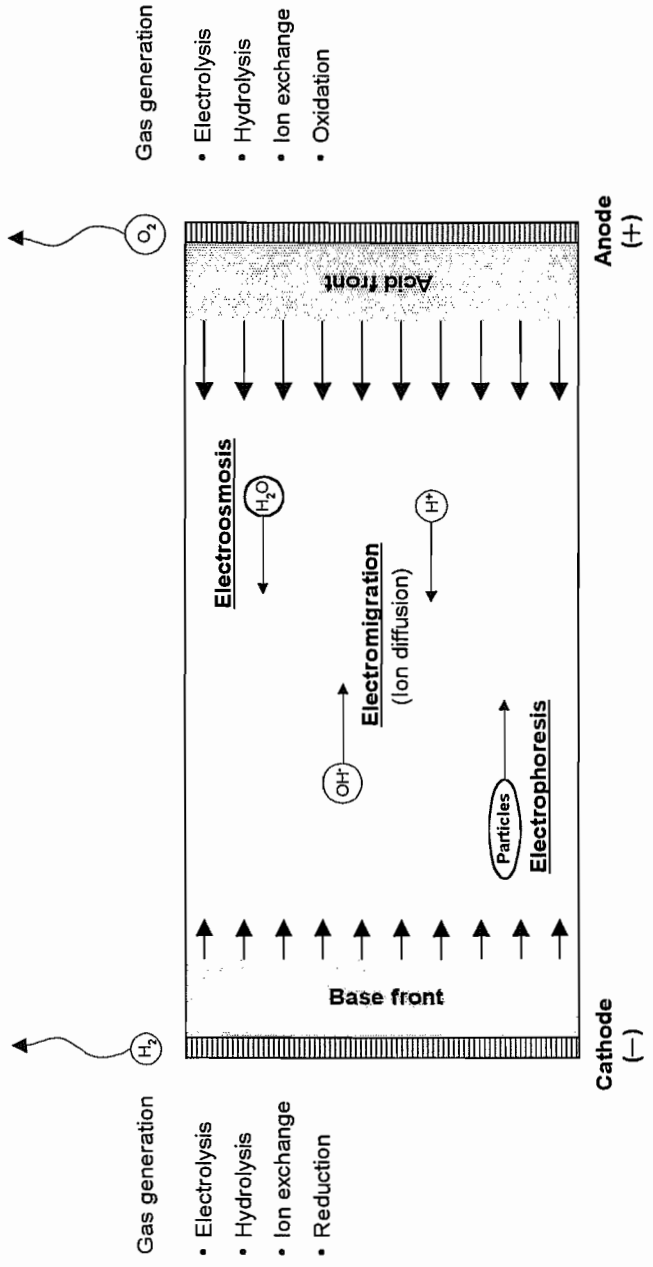

Figure 2.9 Schematic of electrokinetic processes in a soil mass

2.4.1 Electroosmosis

In general, the hydrated water held by molecular forces to the soil particle in the electric double layer does not participate in the water flow by a hydraulic gradient. However, if an electric field is applied to a soil mass, the free ions within the pore water migrate carrying their hydrated water molecules surrounding them. Since the soil mass contains more cations than anions as a result of the negatively charged particles (Sections 2.2 and 2.3), a net water flow is generated towards the cathode by a plug flow mechanism as shown in Figures 2.10 and 2.11. This water flow through a saturated soil mass under an electric field is termed *electroosmosis*, which was first discovered by Reuss in 1809. Several analytical models have been proposed to quantify the water flow by electroosmosis. The most prominent model, *Helmholtz-Smoluchowski theory*, is reviewed in Section 2.5.1.

2.4.2 Electrophoresis

When an electric field is placed across a colloidal suspension, charged particles are electrostatically attracted to one of the electrodes and repelled from the other. As most soil particles are negatively charged, they migrate towards the anode in suspensions under an externally applied electric field. This phenomenon is known as *electrophoresis*, and first observed by Reuss in 1809.

The electrophoretic force on a single clay particle can be quantitatively calculated by knowing the zeta potential of the particle (Section 2.3.4). The electrophoretic mobilities are usually in the range of 1×10^{-4} to 3×10^{-4} $cm^2/V \cdot sec$. (van Olphen, 1977). Because of its ability and efficiency to move charged fine particles in suspensions, electrophoresis has been used successfully to densify mine tailings, coal washery slimes, and fine particle suspensions in which mechanical dewatering operation such as gravitational method, centrifugal method, compression, and vibrational method are ineffective (Lockhart, 1981; Sprute & Kelsh, 1982; Lockhart & Stickland 1984).

2.4.3 Electrolysis

Electrolysis is the production of chemical changes by passing an electrical current through an aqueous solution, resulting in a change of pH; H^+ ions decrease the pH at the anode and OH^- ions increase the pH at the cathode. During the electrolytic reactions, the ions react at the electrode, either receiving or giving up electrons. The resultant atoms may be liberated as a gas, or deposited as a solid on the electrode; oxygen gas is evolved at the anode by hydrolysis and hydrogen gas at the cathode.

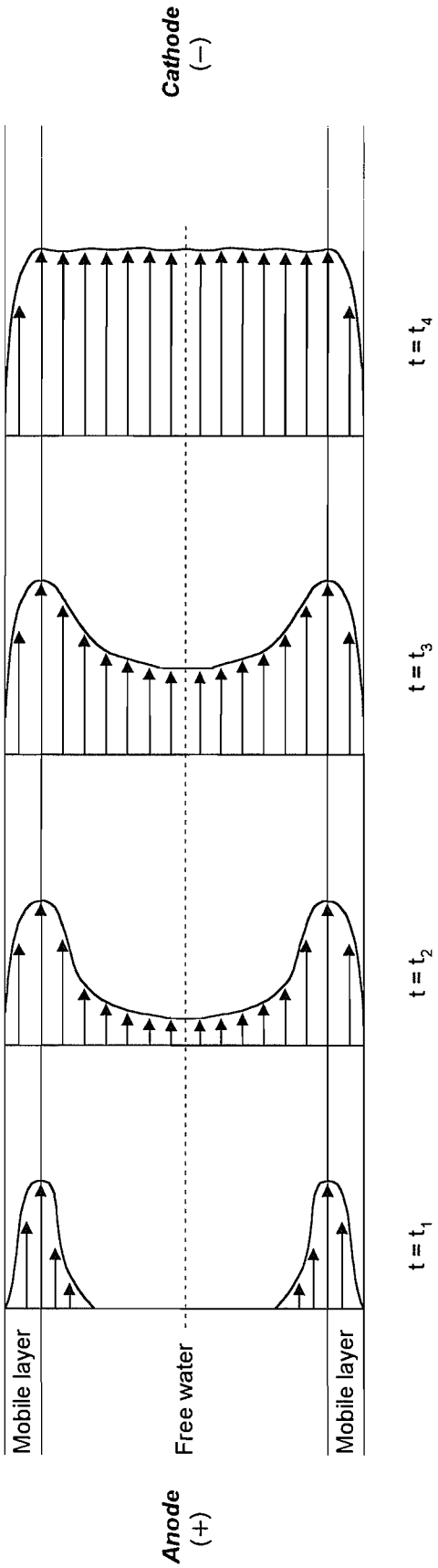

Figure 2.10 Development of water flow by electroosmosis (Redrawn from Pamukcu, 1998)

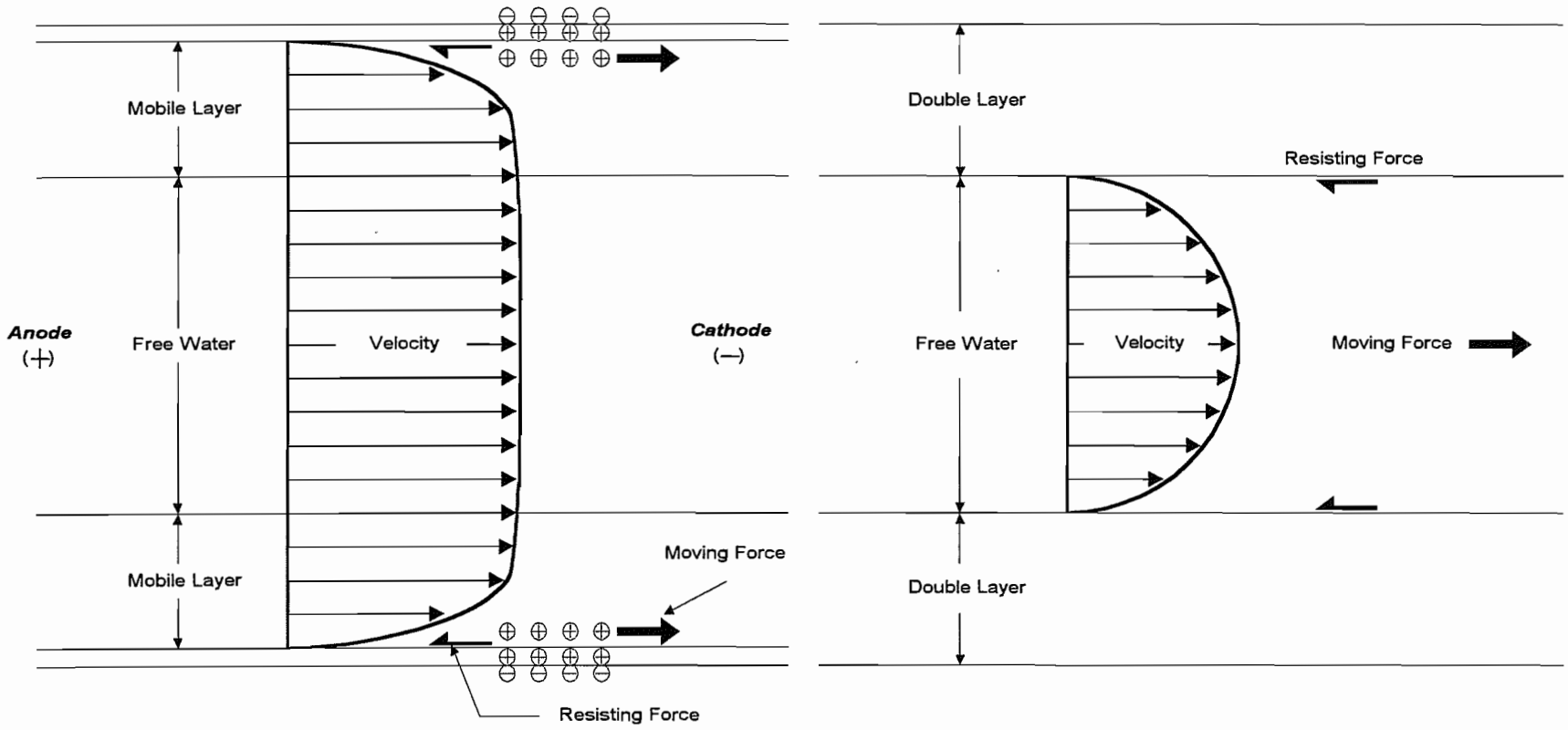

Figure 2.11 Comparison of water flow by electroosmosis with hydraulic flow in a single capillary (After Casagrande, 1952)

A simplified mechanism of the processes of electrolysis at electrodes is as follows:

$$\textit{Positive Electrode (Anode)} : 2H_2O - 4e^- \rightarrow O_2\uparrow + 4H^+ \quad (\textit{Oxidation})$$
$$\textit{Negative Electrode (Cathode)} : 4H_2O + 4e^- \rightarrow 2H_2\uparrow + 4OH^- \quad (\textit{Reduction})$$

The hydrogen ions decrease the pH at the anode and the hydroxyl ions increase the pH at the cathode, depending on the total current applied.

2.4.4 Electromigration

Electromigration is the transportation of chemical species, either present in solution or products of electrolysis, under an electric field towards the opposite electrodes. The values for ionic mobility are typically of the order of 5×10^{-8} $m^2/V \cdot sec$ (Lageman *et al.*, 1989).

In general ionic mobility is greater than the electroosmotic permeability, so that anions can migrate towards the anode, despite being transported in the opposite direction in the electroosmotic flow. The velocity of electromigration depends on the intensity of electric field and the charge on the ions (West & Stewart, 1995).

2.4.5 pH Change

Stewart and West (1996) observed in their electrokinetic decontamination tests that the pH of soil samples increased near the cathode and decreased over the remainder of the specimens as a result of transport of electrolysis products. The hydrogen and hydroxyl ions produced during electrolysis migrate through the soil towards the electrodes of opposite charge, creating acid and base fronts respectively. The migration of pH fronts through the soil has been observed by several researchers (Gray, 1970; Shapiro *et al.*, 1989; Acar *et al.*, 1990).

The advancing process of acid and base fronts is governed by different transport mechanisms including ionic migration due to electrical gradient (i.e. electromigration), pore fluid advection by electroosmosis or any externally applied hydraulic gradient, and diffusion by chemical concentration gradient (Acar *et al.*, 1992). As the ionic mobility of the hydrogen ion is about 1.8 times the hydroxyl ion, the pH was found to have decreased throughout the soil after the electrokinetic process (Acar & Alshawabkeh, 1993). Furthermore, the pore fluid advection towards the cathode by electroosmosis aids the acid front whereas the base front towards the anode is hindered by the electroosmotic counter flow. Therefore, the acid and base fronts generally meet at a zone close to the cathode (Rødsand *et al.*, 1995).

Acar and Alshawabkeh (1993) suggested that electroosmotic flow may even reverse at very low pH values. The changes in pH and the resulting change in electroosmotic flow also may lead to suction development across the soil; the electroosmotic flow is greatest in cases in which the pH in the soil is highest (Eykholt & Daniel, 1994). They presented evidence of electroosmotic flow reversing its direction as a result of the changes in pH. This was caused by the change in zeta potential, and witnessed by West and Stewart (1995) in their column experiments (Section 2.3.4).

2.5 Electroosmotic Flow

Several theories have been proposed to describe the process of fluid flow by electroosmosis. The most commonly used theory is the *Electric Double Layer Theory*, introduced by Helmholtz in 1879 and refined by Smoluchowski in 1914. Theoretical consideration of this electric double layer is necessary in order to define the electroosmotic permeability (Section 2.5.2) and to consider the influence of zeta potential (Section 2.3.4).

2.5.1 Helmholtz-Smoluchowski Theory

The Helmholtz-Smoluchowski theory assumes that counter ions are concentrated at the solid/liquid interface in the double layer, and the thickness of the electric double layer is negligible relative to the pore radius. Figure 2.12 shows the Helmholtz-Smoluchowski double layer.

A slipping plane develops a small distance δ from the capillary wall (i.e. the thickness of mobile layer) and the flow velocity of liquid is v, giving a velocity gradient of v/δ. Assuming laminar flow is dominant, the frictional force per unit area is $\eta v/\delta$, where η is the dynamic viscosity of the liquid. The electrical force per unit area is $-\sigma(\Delta E/\Delta L)$, where σ is the surface charge density and $\Delta E/\Delta L$ is the electrical potential gradient. The flow rate of water is controlled by the balance between the electrical force and the frictional force between the liquid and capillary walls.

Therefore, at equilibrium:

$$\eta \frac{v}{\delta} = -\sigma \frac{\Delta E}{\Delta L} \qquad (2.2)$$

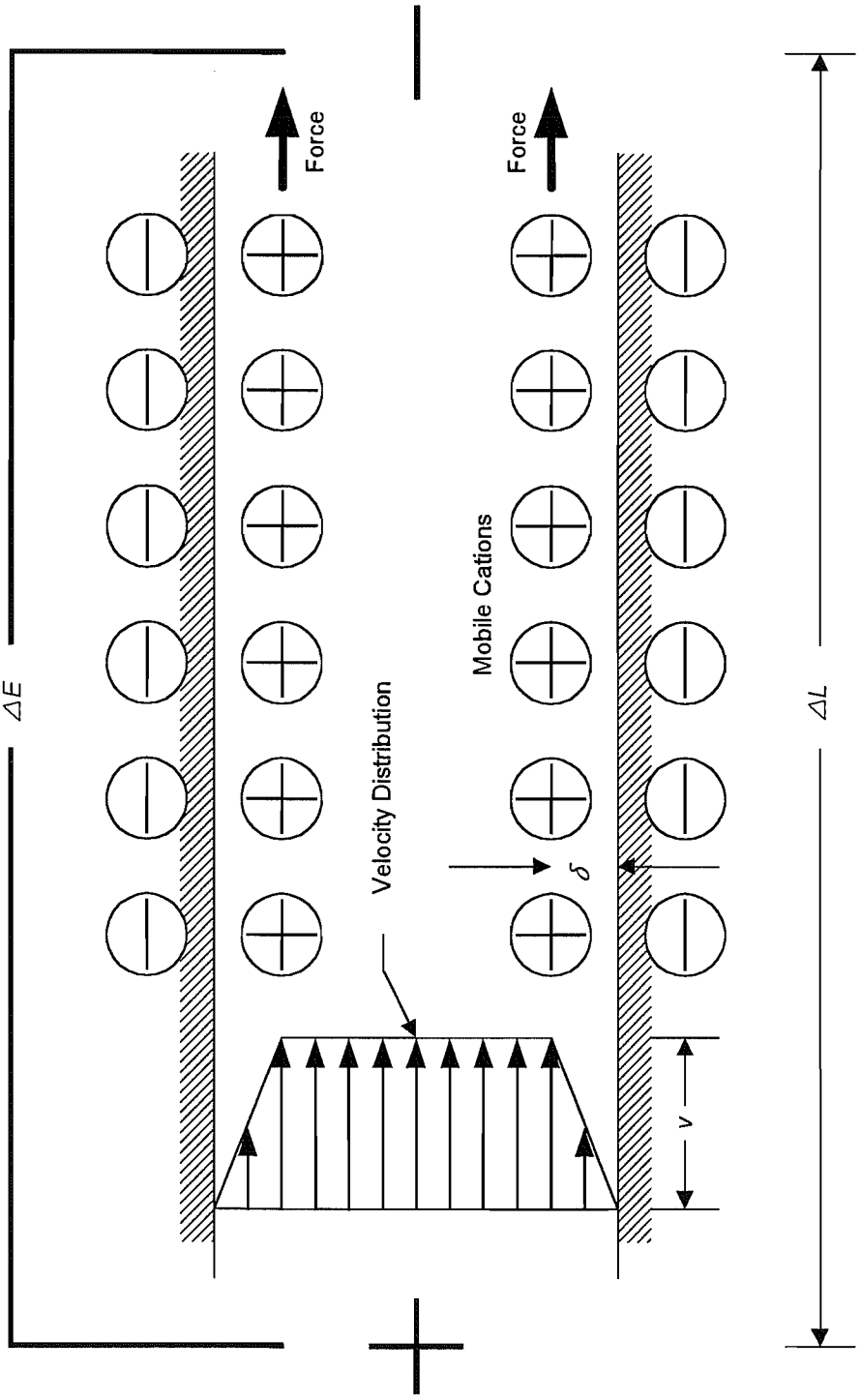

Figure 2.12 Helmholtz-Smoluchowski model for electrokinetic phenomena (After Mitchell, 1993)

From electrostatics, the potential across a parallel plate condenser can be given by:

$$-\zeta = \frac{\sigma\delta}{\varepsilon} \tag{2.3}$$

where ζ is the zeta potential and ε is the static electrical permittivity of the liquid.

Combining Equations (2.2) and (2.3), and allowing for porosity of the medium, n, and the total cross-sectional area, A, produces the volume flow rate, Q, under electroosmosis:

$$Q = vnA = \frac{n\varepsilon\zeta}{\eta}\frac{\Delta E}{\Delta L}A \tag{2.4}$$

2.5.2 Electroosmotic Permeability

By analogy with Darcy's law, the Equation (2.4) can be given as:

$$Q = k_e i_e A \tag{2.5}$$

where i_e is the electrical potential gradient ($\Delta E/\Delta L$).

Thus, the definition of electroosmotic permeability, k_e, is:

$$k_e = \frac{n\varepsilon\zeta}{\eta} \tag{2.6}$$

which relates the electroosmotic flow rate to the voltage gradient.

The coefficient of electroosmotic permeability is considered to be independent of soil type; the ranges of k_e vary between 1×10^{-9} $m^2/V \cdot sec$ and 1×10^{-8} $m^2/V \cdot sec$ for all soils (Yeung, 1990; Mitchell, 1993). For practical purposes, the coefficient of electroosmotic permeability could be considered as a constant for most soils, with a value of 5×10^{-9} $m^2/V \cdot sec$ (Casagrande, 1949). However, Acar *et al.* (1994) found in their experiments that the values of k_e ranged from 1×10^{-11} $m^2/V \cdot sec$ to 1×10^{-9} $m^2/V \cdot sec$ for Georgia kaolinite. They also reported that k_e is time dependent due to the changing pH and electrical potential gradient.

Although hydraulic flow is significantly affected by the fabric and structure of soil, according to the Helmholtz-Smoluchowski theory, electroosmotic flow mainly depends on the porosity and the zeta potential and is relatively independent of the pore size (Acar & Alshawabkeh, 1993). Therefore, electroosmotic flow through fine-grained soils with low hydraulic permeability can be effectively compared to the flow under a hydraulic gradient (Mitchell, 1993).

Stewart and West (1996) reported that localisation of the voltage gradient can occur during electrokinetic process. They noted that there was localisation in the voltage profile after two days, with most of the applied voltage drop near the cathode due to the high resistance of the precipitates.

Acar and Alshawabkeh (1996) also observed in their pilot-scale electrokinetic remediation tests that most of the increase in the potential difference occurred within the region close to the cathode compartment. They reported that the acid front from the anode compartment met the base front in the cathode region and the lead ions transported to this zone precipitated at their hydroxide solubility values. As a result of water formation and lead precipitation, the electrical conductivity within this zone decreases, also dropping the electrical potential.

2.5.3 Electroosmotic Pressure Gradients

The electrically induced water flow from the anode towards the cathode results in substantial variations in pore pressures across the soil mass. Thus, the configuration of electrodes and drainage conditions are very important in the applications of electrokinesis; the configuration depends on the local geohydrological situation and the drainage condition is associated with the purposes of electrokinetic treatment. Figure 2.13 illustrates pore pressure distributions under different drainage conditions.

In Figure 2.13(a), the electroosmotic water flow away from the closed anode causes a corresponding reduction in pore pressure from the anode producing a negative excess pore pressure. The greater the electroosmotic flow, the larger is the excess pore tension. This, in turn, sets up a hydraulic gradient, acting in the opposite direction to the electroosmotic flow. Eventually the hydraulic gradient becomes sufficiently large that pore water flow stops, and an equilibrium is achieved. In Figure 2.13(b), water moving by electroosmosis to the cathode is replaced at the anode, so that there is no change in pore pressure. In Figure 2.13(c), water is supplied at the anode with a closed cathode. Overall, the soil swells with a positive excess pore pressure developing from the cathode which produces a hydraulic gradient that eventually prevents further water flow. In Figure 2.13(d), both anode and cathode are closed, so that electroosmosis produces a redistribution of pore water with

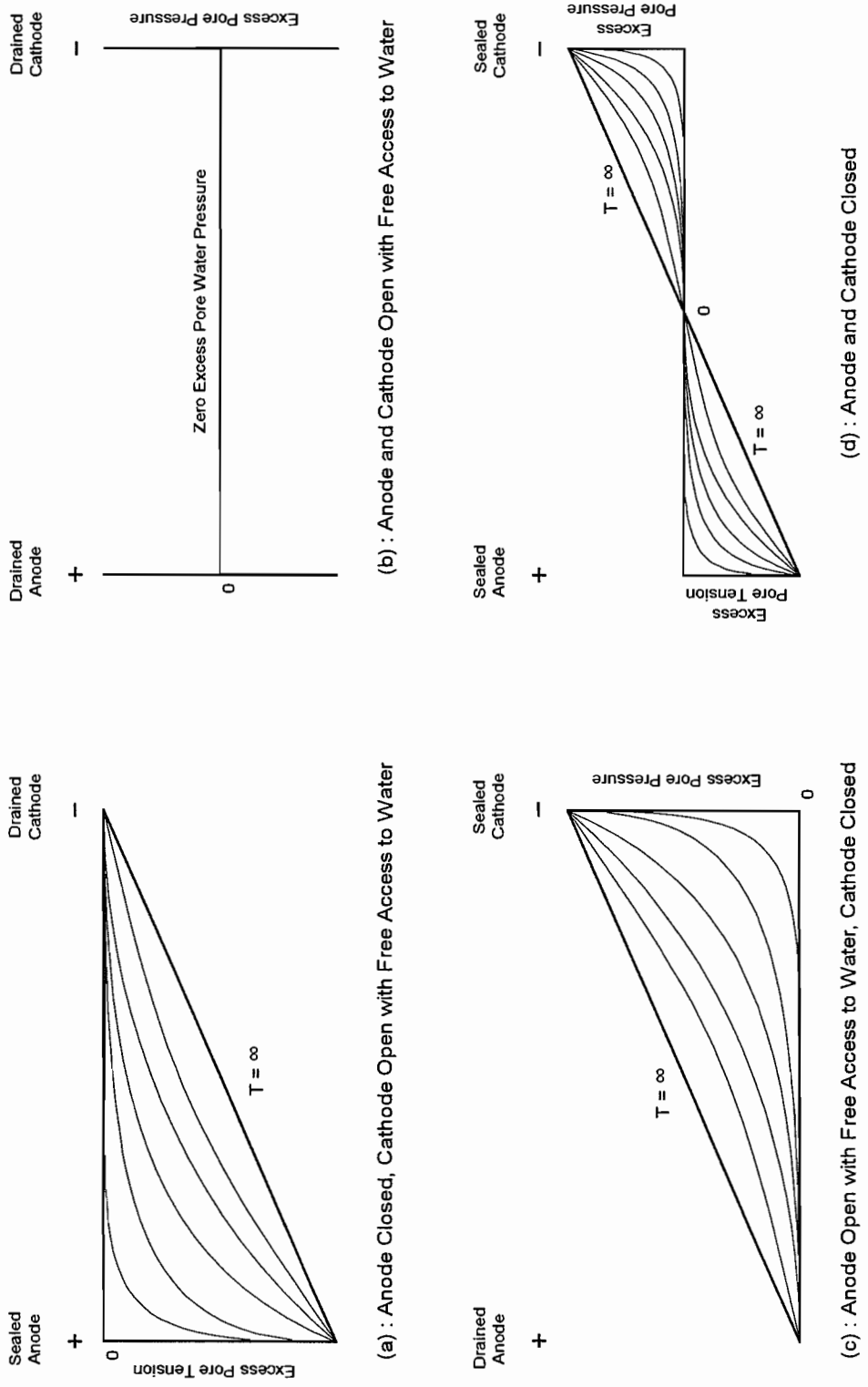

Figure 2.13 Idealised variation of pore water pressures for one-dimensional electroosmosis (Redrawn from Esrig, 1968; Butterfield & Johnston, 1980)

consolidation in the anode region and swelling in the cathode region.

It may be noted that in Figures 2.13(a) and (c), the final distribution shown for the excess pore pressure distribution is based on the idealisation that both hydraulic and electroosmotic permeabilities are independent of porosity. In practice, however, the hydraulic permeability will decrease at the anode and remain constant or increase at the cathode although the electroosmotic permeability will be close to constant. The form of the final ($T = \infty$) excess pore pressure distribution will be that which counters the electroosmotic flow and will not be linear. In the example of Figure 2.13(d), due to typically different consolidation and swelling coefficients, the magnitudes of excess pore pressure and tension will not be equal.

Experimental research has confirmed the general pattern of electroosmotic behaviour predicted from the idealisations described above, and has also identified the effects due to departures from the idealisations. Several laboratory studies have confirmed that electrically induced negative pore pressures are directly responsible for soil consolidation by the effect of electroosmosis (Esrig, 1968; Wan & Mitchell, 1976; Johnston & Butterfield, 1977). Lo *et al.* (1991) reported that the final negative pore pressures induced by electroosmosis are linearly distributed, with maximum negative pore pressure induced at the anode decreasing linearly to zero at the cathode and the maximum induced negative pore pressure is linearly related to the applied voltage.

The majority of experiments have been carried out in an open anode and cathode configuration, since this is the most appropriate for decontamination. In this case, many differences from the idealised case are observed, which can be attributed to a variety of causes, including flow and ion concentration effects.

Acar and Alshawabkeh (1996) reported that maximum pore pressures are developed close to the cathode end first, gradually moving towards the anode side. The pore pressures follow the region where the electrical potential gradient is maximum. Eykholt and Daniel (1994) also noted that negative pore pressures develop if the voltage is greater than the uniform field value. In addition, consolidation and development of negative pore pressures in laboratory experiments with an open electrode configuration have been reported by many researchers (Hamed *et al.*, 1991; Acar *et al.*, 1994).

2.6 Settling Column Experiments

Settling column experiments have been conducted by many researchers in order to investigate the process of settling and consolidation, providing insight into fundamental behaviour of soft soils as well as a means of determination of soil parameters (Been & Sills,

1981; Pane & Schiffman, 1985; Tan *et al.*, 1990; Li & Williams, 1995; Sills, 1998).

Particles and flocs are considered to settle, either independently under gravity or conditionally under electrochemical interactions, depending on the concentrations in a suspension; settling processes in a denser suspension are relatively slow and sometimes a delay occurs in the initial settling stage. During settling processes, pore pressures are equal to total stresses. Settled particles and flocs get closer together from the base of the column, forming a soil matrix, and some structure for the soil bed behaves as a frictional material where effective stress must develop. Thus, the essential difference between settling in suspension and soil consolidation is the existence of effective stresses in soils (Sills, 1998).

The transition from a fluid-supported suspension to a soil can be seen in laboratory experiments as shown in Figure 2.14. Alves (1992) carried out a series of column tests on Brazilian red mud with an initial density of 1.06 Mg/m^3 and height of 0.99 m. She observed a similar pattern of surface settling behaviour described by Kynch in her experiments that relatively faster initial surface settling associated with the fluid-supported suspension, the interface between water and sediment, was followed by a slower settlement with time. The numbers on the other curves demonstrate the developing density steps inside the bed, increasing upwards from the bottom of the settling column.

Figure 2.15 shows an example of density profile and the corresponding stress distribution after 24 hours of self-weight consolidation taken from Alves (1992). It can be seen that the excess pore pressures and excess total stress are very close in magnitude where the density is close to its initial value, 1.06 Mg/m^3, whilst in the denser part of the bed the excess pore pressures have reduced significantly below the excess total stress. The effective stresses exist in the lower part of the sample where the slurry density is higher than 1.2 Mg/m^3. This density is therefore termed the *structural density* (Sills, 1995). The density line marked 1.206 Mg/m^3 shown in Figure 2.14 started from the base of the column at the beginning of the experiment and met the water/sediment interface at the time when the surface settling rate slows down dramatically. This is further evidence in her experiment that this density marks the transition from a suspension to a soil. Such a pattern of settling behaviour was noted by Been and Sills (1981) in similar experiments carried out on a natural estuarine silty clay.

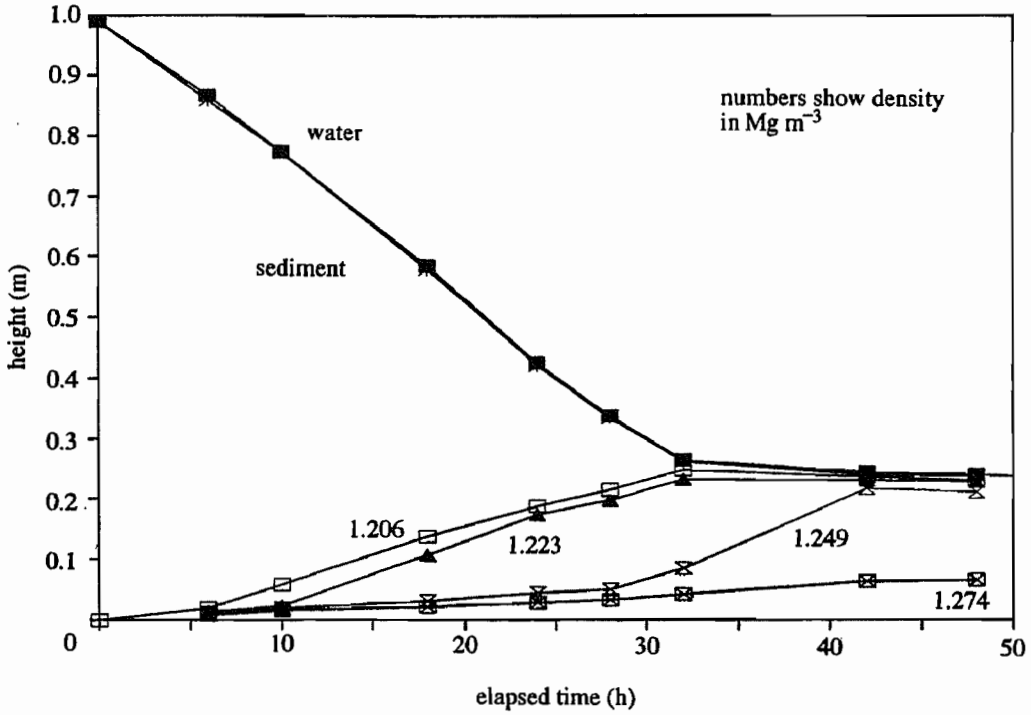

Figure 2.14 Surface settlement and upward development of density in experiment REDM05 (After Sills, 1998)

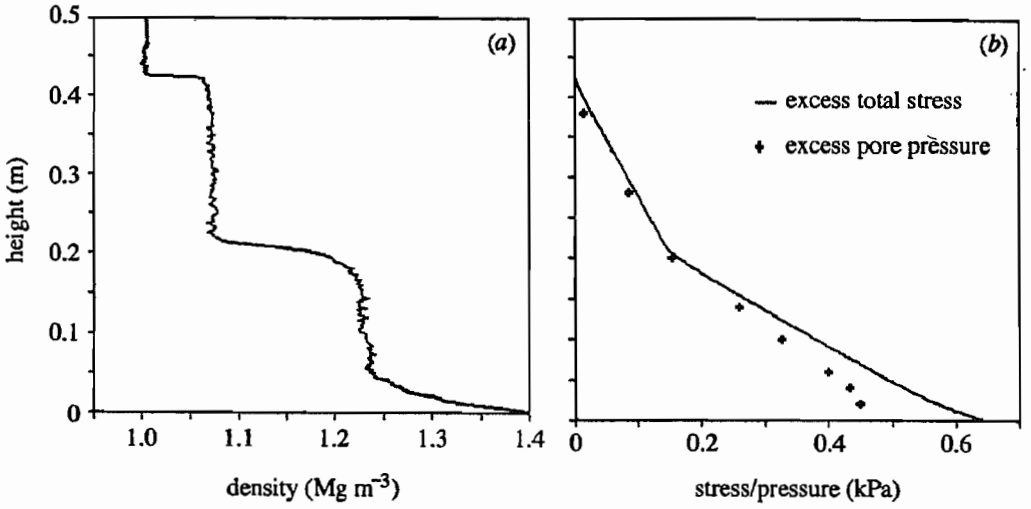

Figure 2.15 Calculation of effective stress as difference between excess total stress and excess pore pressure for experiment REDM05 (After Sills, 1998)

2.7 Electrokinetic Consolidation Theory

The theory of electrokinetic consolidation of soils has been looked at by many individuals and in many different ways. Here the theory developed by Esrig (1968) is reviewed.

2.7.1 Assumptions

Karl Terzaghi (1923, 1936) developed a one-dimensional consolidation theory that described the dissipation of excess pore pressures and the associated deformation of the soil in order to estimate the settlement rate. The assumptions made in his theory are:

- The soil is homogeneous, isotropic, and fully saturated.
- The soil particles and pore fluid are incompressible.
- Compression and flow are one-dimensional.
- Strains are small.
- Darcy's law is valid at all hydraulic gradients.
- The permeability and compressibility of the soil remain constant throughout the process.
- There is a unique relationship, independent of time, between void ratio and effective stress.

Esrig (1968) added the following idealising conditions of electroosmotic flow in addition to those required for the Terzaghi's consolidation theory in order to predict the process of electroosmotic flow:

- The physicochemical properties of the soil mass are homogeneous and constant with time.
- Electrophoresis of fine particles does not occur.
- The electrically induced flow velocity of water through the soil is proportional to the applied voltage gradient.
- All applied voltage is useful in producing water transport.
- The electric field throughout the soil mass is constant with time.
- No chemical reactions occur at the electrodes.
- Fluid flow velocity induced by an electric field and that induced by a hydraulic gradient may be superimposed.

2.7.2 Governing Equation

Figure 2.16 shows a soil element in a consolidating ground. The net flux of water through the soil element is equal to the change in volume of soil element:

$$A(v_n(z+dz) - v_n(z)) = \frac{\partial V}{\partial t} \tag{2.7}$$

therefore

$$\frac{\partial V}{\partial t} = \frac{\partial v_n}{\partial z} V \tag{2.8}$$

where v_n is the velocity of water flow and V is the volume of soil element (i.e. Adz).

The rate of volume change can be expressed in terms of the volume compressibility:

$$\frac{1}{V}\frac{\partial V}{\partial t} = -m_v \frac{\partial \sigma_v'}{\partial t} \tag{2.9}$$

where m_v is the volume compressibility and σ_v' is the vertical effective stress.

Combining Equations (2.8) and (2.9) gives:

$$\frac{\partial v_n}{\partial z} = -m_v \frac{\partial \sigma_v'}{\partial t} \tag{2.10}$$

If the total vertical stress, σ_v, remains constant during the consolidation:

$$\frac{\partial \sigma_v}{\partial t} = \frac{\partial \sigma_v'}{\partial t} + \left(\frac{\partial u_h}{\partial t} + \frac{\partial u_e}{\partial t} \right) = 0 \tag{2.11}$$

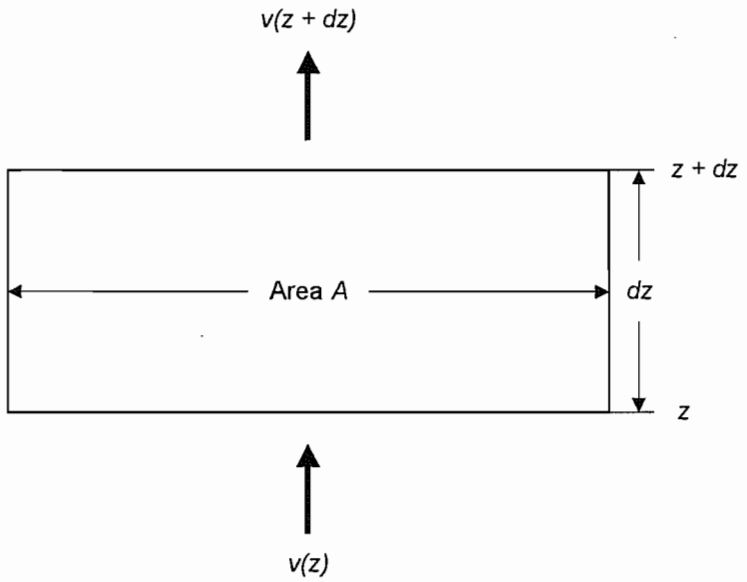

Figure 2.16 A soil element in a consolidating ground

therefore

$$\frac{\partial \sigma_v'}{\partial t} = -\frac{\partial u_e}{\partial t} \tag{2.12}$$

where u_h is the hydrostatic pressure and u_e is the excess pore pressure.

Combining Equations (2.10) and (2.12) gives:

$$\frac{\partial v_n}{\partial z} = m_v \frac{\partial u_e}{\partial t} \tag{2.13}$$

Assuming proportionality between the electrically induced velocity of water flow through the soil and the voltage gradient, the electrically induced one-dimensional flow in a coordinate direction z can be given:

$$v_e = k_e \frac{\partial E}{\partial z} \tag{2.14}$$

where v_e is the electrically induced velocity of water flow through the soil element, k_e is the

coefficient of electroosmotic permeability, and E is the electric field.

The flow velocity induced by any excess pore pressure gradient is given by Darcy's law:

$$v_h = \frac{k_h}{\gamma_w}\frac{\partial u_e}{\partial z} \tag{2.15}$$

where v_h is the hydraulically induced velocity of water flow through the soil element, k_h is the coefficient of hydraulic permeability, and γ_w is the unit weight of water.

Assuming the validity of superposing electrically and hydraulically induced flows through the soil element:

$$v_n = v_e + v_h \tag{2.16}$$

Substituting Equations (2.14) and (2.15) into Equation (2.16) yields:

$$k_e\frac{\partial^2 E}{\partial z^2} + \frac{k_h}{\gamma_w}\frac{\partial^2 u_e}{\partial z^2} = m_v\frac{\partial u_e}{\partial t} \tag{2.17}$$

Equation (2.17) can be written as:

$$\frac{\partial^2 u_e}{\partial z^2} + \frac{k_e\gamma_w}{k_h}\frac{\partial^2 E}{\partial z^2} = \frac{1}{C_v}\frac{\partial u_e}{\partial t} \tag{2.18}$$

where

$$C_v = \frac{k_h}{m_v\gamma_w} \tag{2.19}$$

and C_v is the same as the Terzaghi's coefficient of consolidation. Since k_h and m_v are assumed constant in the theory, C_v is also taken to be constant during consolidation.

Introducing a dummy variable, ξ, Equation (2.18) can be written as:

$$C_v \frac{\partial^2 \xi}{\partial z^2} = \frac{\partial \xi}{\partial t} \tag{2.20}$$

where

$$\xi = \frac{k_e \gamma_w}{k_h} E + u_e \tag{2.21}$$

Equation (2.20) is the one-dimensional diffusion equation similar to the following basic differential governing equation of Terzaghi's consolidation theory:

$$\frac{\partial u_e}{\partial t} = C_v \frac{\partial^2 u_e}{\partial z^2} \tag{2.22}$$

Therefore, Terzaghi's consolidation equation is found as a special case of Esrig's equation when the electric field is set equal to zero. The solutions of Equation (2.20) for the one-dimensional electrokinetic consolidation will be presented in Chapter 6, along with a development for large strain conditions.

REFERENCES

Acar, Y. B., Gale, R. J., Putnam, G., Hamed, J., and Wong, R. L. (1990). Electro-chemical processing of soils: theory of pH gradient development by diffusion, migration, and linear convection. *J. Envir. Sci. Engrg. ASCE*, 25(6), 687-714.

Acar, Y. B., Alshawabkeh, A. N., and Gale, R. J. (1992). A review of fundamentals of removing contaminants from soils by electrokinetic soil processing. *Envir. Geotech.*, 321-330.

Acar, Y. B. and Alshawabkeh, A. N. (1993). Principles of electrokinetic remediation. *Envir. Sci. Technol.* 27(13), 2638-2647.

Acar, Y. B., Hamed, J. T., Alshawabkeh, A. N., and Gale, R. J. (1994). Removal of cadminm(II) from saturated kaolinite by the application of electrical current. *Geotechnique* 44(2), 239-254.

Acar, Y. B. and Alshawabkeh, A. N. (1996). Electrokinetic remediation. I: pilot-scale tests with lead-spiked kaolinite. *J. Geotech. Engng. ASCE*, 122(3), 173-185.

Alves, M. C. M. (1992). *Comportamento de sedimentacao e adensamento de uma lama vermelha*. Ph.D. thesis, PUC-Rio. (In Portuguese.)

Been, K. and Sills, G. C. (1981). Self-weight consolidation of soft soils: an experimental and theoretical study. *Geotechnique* 31(4), 519-535.

Butterfield, R. and Johnston, I. W. (1980). The influence of electroosmosis on metallic piles in clay. *Geotechnique* 30(1), 17-38.

Casagrande, L. (1949). Electroosmosis in soils. *Geotechnique* 1(3), 159-177.

Casagrande, L. (1952). Electro-osmotic stabilization of soils. *J. Boston Soc. Civ. Engrs.* 39(1), 51-83.

Esrig, M. I. (1968). Pore pressures, consolidation, and electrokinetics. *J. Soil Mech. Fdns. Div. ASCE*, 94(4), 899-921.

Eykholt, G. R. and Daniel, D. E. (1994). Impact of system chemistry on electroosmosis in contaminated soil. *J. Geotech. Engng. ASCE*, 120(5), 797-815.

Eykholt, G. R. (1997). Development of pore pressures by nonuniform electroosmosis in clays. *J. Hazardous Materials* 55, 171-186.

Goldman, L. J., Greenfield, L. I., Damle, A.S., Kingsbury, G. L., Northeim, C. M., Truesdale, R. S., and Roulier, M. H. (1986). Design, construction and evaluation of clay liners for waste management facilities. *EPA/530-SW-86-007-F.*

Gray, D. H. (1970). Electrochemical hardening of clay soils. *Geotechnique* 20(1), 81-93.

Hamed, J., Acar, Y. B., and Gale, R. J. (1991). PB(II) removal from kaolinite by electrokinetics. *J. Geotech. Engng. ASCE*, 117(2), 241-271.

Johnston, I. W. and Butterfield, R. (1977). A laboratory investigation of soil consolidation by electroosmosis. *Austral. Geomech. J.* 7, 21-32.

Lageman, R., Pool, W., and Seffinga, G. (1989). Electro-reclamation: theory and practice. *Chemistry and Industry* 18(9), 585-590.

Li, H. and Williams, D. J. (1995). Sedimentation and self-weight consolidation behaviour of coal mine tailings. *Proc. Int. Symp.Compression and Consolidation of Clayey Soils, Hiroshima*, Japan 875-890.

Lo, K. Y., Inculet, I. I., and Ho, K. S. (1991). Electroosmotic strengthening of soft sensitive clays. *Can. Geotech. J.* 28, 62-73.

Lockhart, N. C. (1981). Sedimentation and electro-osmotic dewatering of coal-washery slimes. *Fuel* 60(10), 919-923.

Lockhart, N. C. and Stickland, R. E. (1984). Dewatering coal washery tailings ponds by electro-osmosis. *Powder Technol.* 40, 215-221.

Mitchell, J. K. (1993). *Fundamentals of soil behaviour.* 2nd Ed. New York: Wiley.

Pamukcu, S. (1997). Electro-chemical technologies for in-situ restoration of contaminated subsurface soils. *The Electronic Journal of Geotechnical Engineering (EJGE).*

Pane, V. and Schiffman, R. L. (1985). A note on sedimentation and consolidation. *Geotechnique* 35(1), 69-72.

Rowe, R. K., Quigley, R. M., and Booker, J. R. (1995). *Clayey barrier systems for waste disposal facilities.* Chapman & Hall.

Rødsand, T., Acar, Y. B., and Breedveld, G. (1995). Electrokinetic extraction of lead from spiked Norwegian marine clay. *Geoenvironment 2000, Geotechnical Special Publication 46*, 1518-1534.

Shapiro, A. P., Renaud, P. C., and Probstein, R. F. (1989). Preliminary studies on the removal of chemical species from saturated porous media by electroosmosis. *PhysicoChemical Hydrodynamics* 11(5/6), 785-802.

Sills, G. C. (1995). Time dependent processes in soil consolidation. *Proc. Int. Symp. Compression and Consolidation of Clayey Soils. Hiroshima*, Japan 875-890.

Sills, G. C. (1998). Development of structure in sedimenting soils. *Phil. Trans. R. Soc. Lond.* 356, 2515-2534.

Sprute, R. H. and Kelsh, R. H. (1982). Electrokinetic densification of solids in a coal mine sediment pond - a feasibility study. *U.S. Dep. Interior, Bur. Mines Rep. Invest.* 8666, 1-31.

Stewart, D. I. and West, L. J. (1996). Electrokinetic soil decontamination - effect of local resistivity variations. *Proc. 2th Int. Congress on Environmental Geotechnics, Osaka*, 10, 1101-1106.

Tan, K. H. (1993). *Principles of soil chemistry*. 2nd Ed. Marcel Dkker, Inc.

Tan, T. S., Yong, K. Y., Leong, E. C., and Lee, S. L. (1990). Sedimentation of clayey slurry. *J. Geotech. Engng. ASCE*, 116(6), 885-898.

Terzaghi, K. (1936). The shearing resistance of saturated soils and the angles between the planes of shear. *Proc. 1st Int. Conf. Soil Mechanics*, 1, 54-56.

van Olphen, H. (1977). *An introduction to clay colloid chemistry*. 2nd Ed. New York: Wiley.

Vane, L. M. and Zang, G. M. (1995). Electrokinetic soil remediation: impact of aqueous phase properties on soil surface charge and electroosmosis efficiency. *Proc. EPA 21st Annual RREL Research Symposium* 202-206.

Vane, L. M. and Zang, G. M. (1997). Effect of aqueous phase properties on clay particle zeta potential and electro-osmotic permeability: implications for electro-kinetic soil remediation processes. *J. Hazardous Materials* 55, 1-22.

Wan, T. Y. and Mitchell, J. K. (1976). Electroosmtic consolidation of soils. *J. Geotech. Engng. ASCE*, 102(5), 473-491.

West, L. J. and Stewart, D. I. (1995). Effect of zetal potential on soil electrokinesis. *Geoenvironment 2000, Geotechnical Special Publication 46*, 1535-1549.

Yeung, A. T. (1990). *Electro-kinetic barrier to contaminant transport through compacted clay*. Ph.D. dissertation, University of California, Berkeley.

CHAPTER 3 TESTING APPARATUS AND TECHNIQUES

3. TESTING APPARATUS AND TECHNIQUES

3.1 Introduction

The test equipment and instrumentation are described together with the analysis techniques used to quantify the behaviour of soft soil subjected to an electric field. A major experimental difficulty was the development of gas in the soil sample during the electrokinetic process. Various modifications to the electrokinetic cell were made in order to overcome this problem. Measurement techniques include soil density measurement by X-ray and pore pressure measurement by a pressure measuring unit.

3.2 Electrokinetic Consolidation Cell

The specialised requirements of this study of soft soil settling and consolidating under the influence of an electric field led to the design of a purpose built cell. The necessary features included:

- A uniform acrylic cell in order to enable X-ray profiles to be obtained for density measurement.
- The provision of ports in the cell walls for measurement of pore pressure and of voltage.
- The installation of electrodes to provide a uniform field from top to bottom of the cell.
- A means of preventing gas generated at the electrode in the base chamber entering the soil. This was achieved using a constant head system to flush the gas from the base chamber at appropriate intervals.

The electrokinetic consolidation cell consists of three major components: a column containing the soil sample, a base chamber housing the anode, and a top cap holding the cathode. A schematic diagram of the electrokinetic consolidation cell is illustrated in Figure 3.1.

3.2.1 The Column

The column, containing the soil sample, was constructed from clear acrylic tube (102 mm i.d., 114 mm o.d., and 250 mm long) equipped with pore pressure ports and voltage probes along the side of the wall. Acrylic was chosen as the material for the testing cell as the soil appearance can be observed during the test. All accessory valves and fittings were made of brass and the connecting tubing was made of polyurethane. A schematic diagram

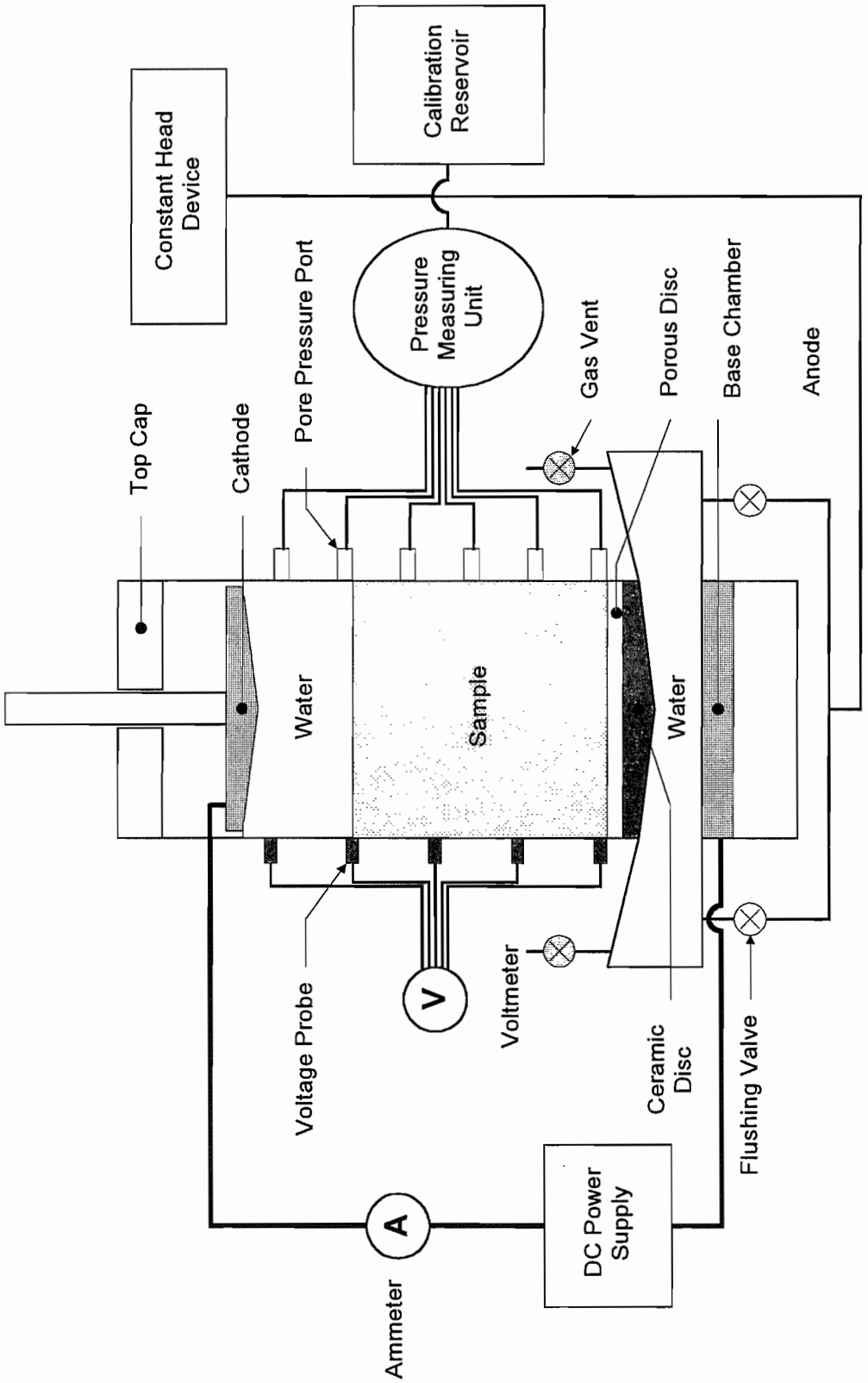

Figure 3.1 Schematic of the electrokinetic consolidation cell

of the column used in this experimental study is shown in Figure 3.2.

The pore pressure ports were let into the side of the column and connected to a pressure measuring unit (Section 3.7). A 2.5 mm thick porous plastic filter (Vyon) was set into the hole of the column wall flush with the inner surface. Voltage probes were used to measure electrical potential differences within the soil sample. These consisted of platinum rods of 0.5 mm diameter and length of 10 mm which were embedded, in contact with the soil sample, along the side of the column at regular intervals. Details of the pore pressure port and voltage probe mounting in the column wall are illustrated in Figure 3.3.

The bottom of the acrylic column was inserted into the base chamber, on which a 2.5 mm thick porous plastic disc was placed. An 'O'-ring was installed between the column and the base chamber to prevent any leakage of fluid during tests.

3.2.2 The Base Chamber

Special attention was focused on the design of the base chamber to minimize the influence of gas generated at the anode electrode. The base chamber, which is slightly wider than the cylindrical cell, accommodates a ceramic disc, a 2.5 mm thick porous plastic disc, and the anode electrode. The volume of water filling the base chamber was approximately 840 ml. A schematic diagram of the base chamber is illustrated in Figure 3.4.

A high air entry ceramic disc, fully saturated with deaired water, was installed below the ceiling of the base chamber to prevent the infiltration of gas generated at the anode electrode. The ceramic disc and inner slope of the base chamber are sloped such that floating gas bubbles move along the surface of the ceramic disc and the inner slope of the base chamber. Gas bubbles collected at the perimeter can then be released through the gas vents at frequent intervals. Flushing ports installed at the base of the chamber were used for supplying deaired water from a constant head device (see Figures 3.1 and 3.11) in order to flush the gas trapped at the perimeter. The ceiling of the base chamber is perforated with 5 mm diameter holes to maintain the uniformity of electric field, and provides mechanical support during the consolidation process as shown in Plate 3.1.

3.2.3 The Electrode

Different materials of electrodes were examined in preliminary tests; copper, aluminum, and stainless steel. However, there was a significant corrosion loss during the first experiments and, thereafter, inert graphite was chosen as the electrode material in order to avoid corrosion and the introduction of secondary products due to electrolytic reactions.

The anode was located at the bottom of the base chamber (see Figure 3.4) with the cathode mounted above the sample as shown in Figure 3.5. This arrangement allows

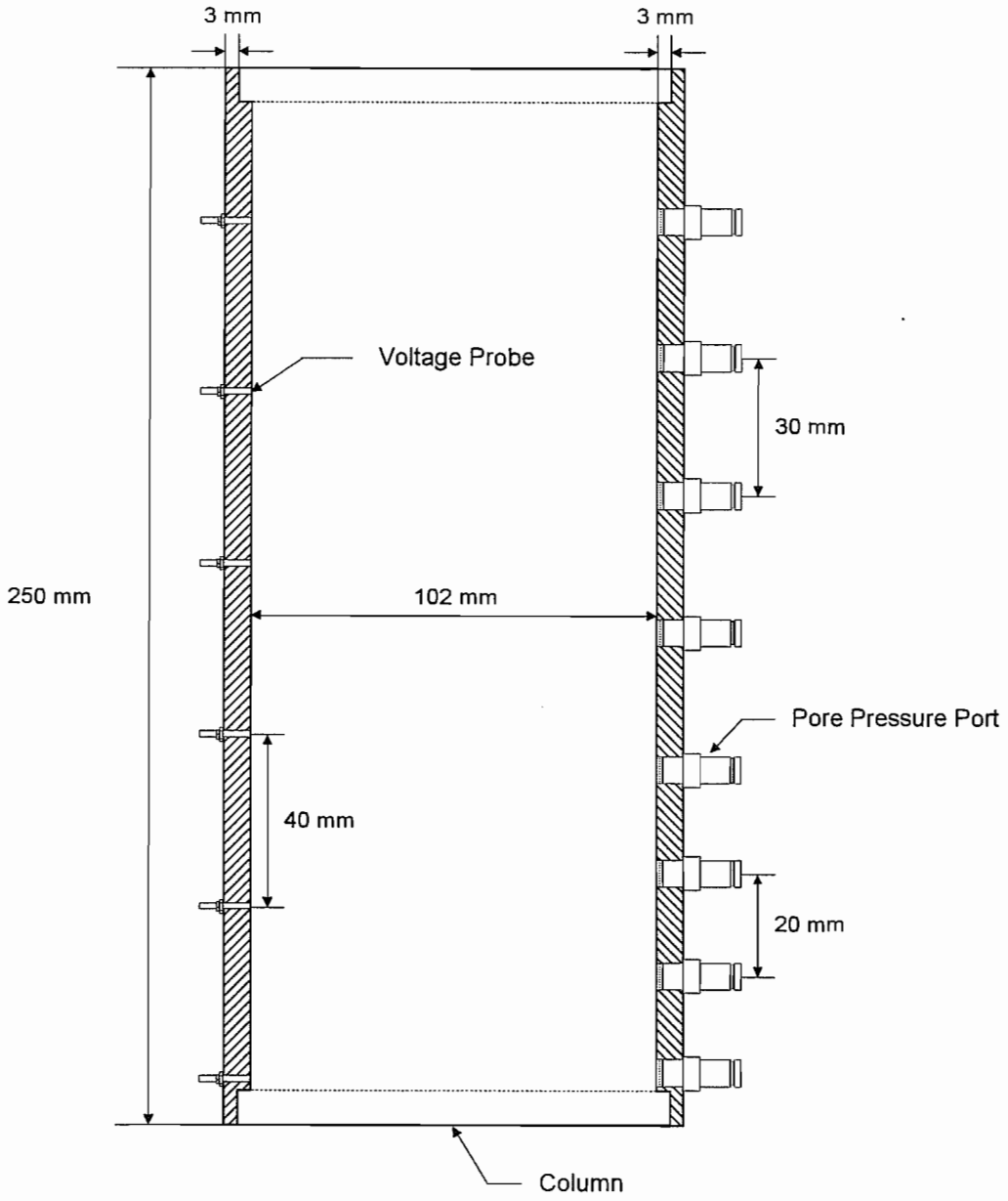

Figure 3.2 Schematic of the column used in electrokinetic consolidation tests

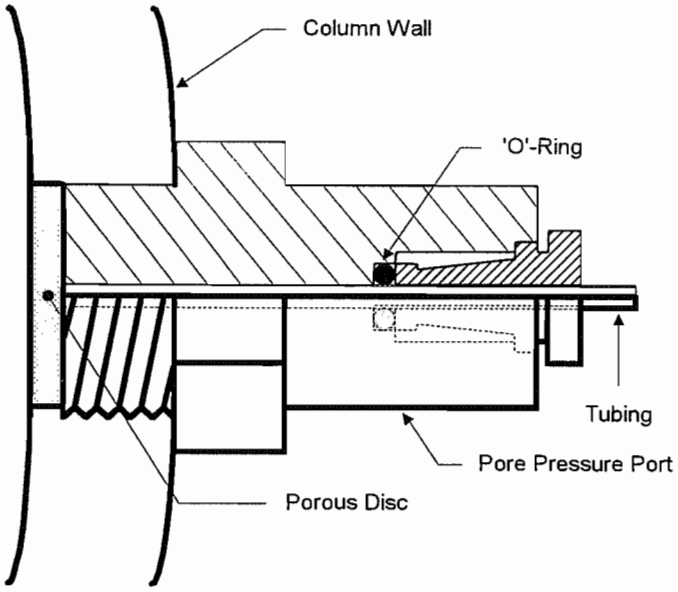

(a) Pore Pressure Port

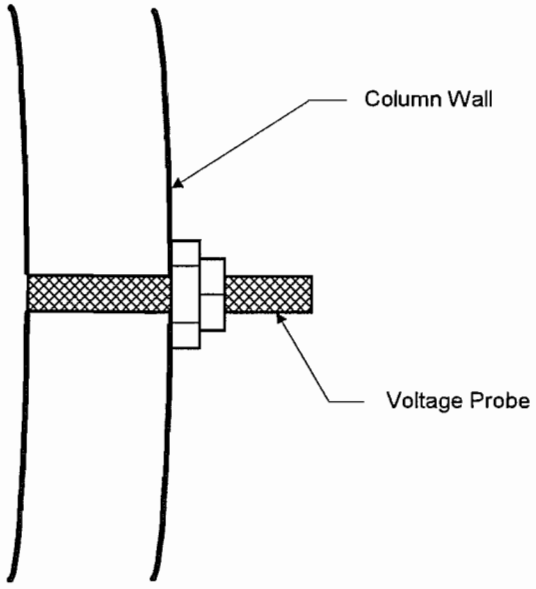

(b) Voltage Probe

Figure 3.3 Schematic of the pore pressure port and voltage probe in column wall: (a) pore pressure port; (b) voltage probe

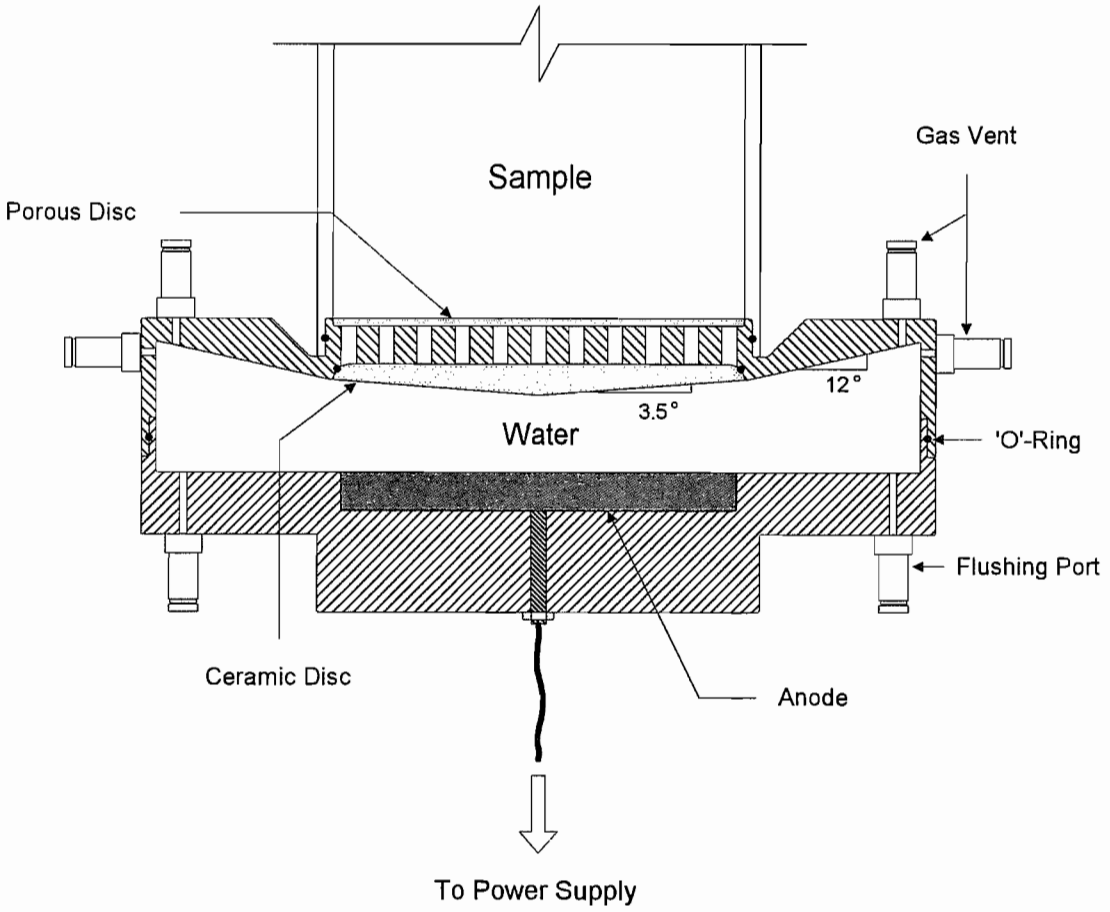

Figure 3.4 Schematic of the base chamber

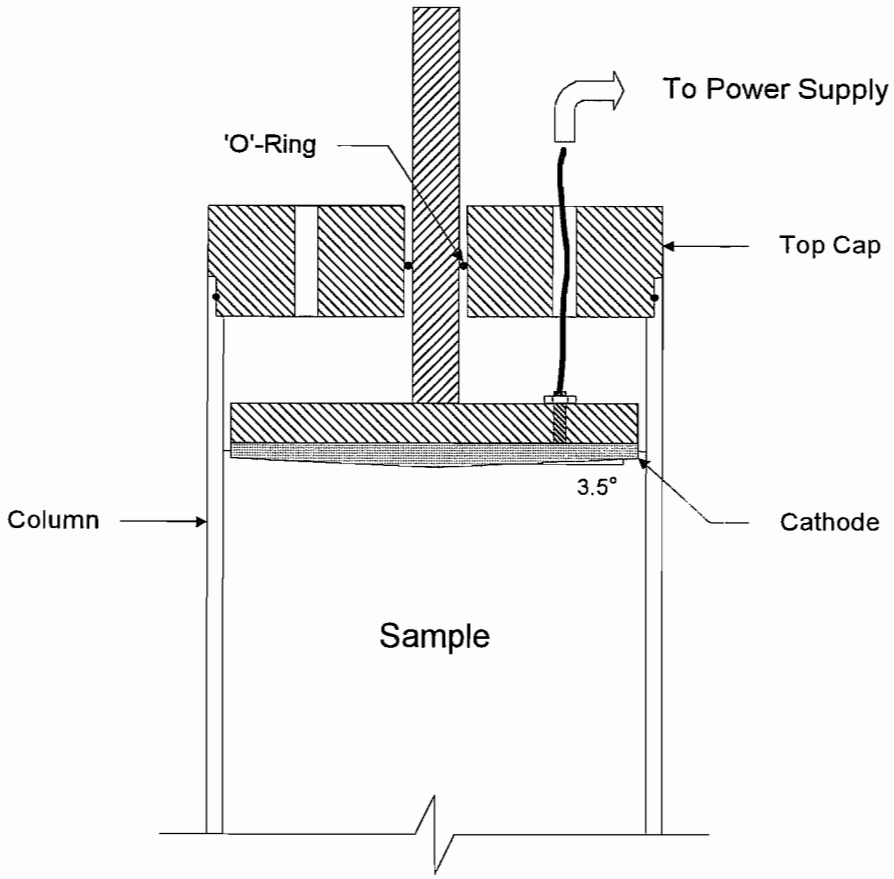

Figure 3.5 Schematic of the cathode electrode mounted on the piston

downward movement of particles due to electrophoresis and the upward movement of pore fluid by the effect of electroosmosis. Those movements of clay particles and pore fluid induced by electrokinesis are in the same direction as the movement of clay particles and pore fluid induced under gravity. The distance between the electrodes was maintained constant during the electrokinetic process.

The cathode mounted on a piston (see Figure 3.5) can be moved vertically through the centre of the top cap. Therefore, the cathode disc can be placed on top of the soil sample for any initial height. During the experiments the soil bed moved downwards away from the cathode, which remained at the level of the water surface. The gases generated at the cathode electrode moved along the surface gradient of 3.5 degrees and escaped into the atmosphere. The extended cathode electrode and the top cap are illustrated in Plate 3.2.

3.3 Electroosmotic Permeability Cell

The purpose of the electroosmotic permeability cell is to measure the water flow induced by electroosmosis and hence to calculate the electroosmotic permeability of the soil. The cell was, therefore, very similar to the electrokinetic consolidation cell (Section 3.2). However, the high air entry porous disc at the base of the cell offered considerable resistance to the water flow, so a more permeable alternative was designed. A schematic diagram of the electroosmotic permeability cell is illustrated in Figure 3.6.

In order to measure localised voltages near the soil surface at more frequent intervals within the soil sample, 20 additional voltage probes were installed. The similar shape of Vyon filter as the ceramic disc, used in the electrokinetic consolidation tests (see Figure 3.4), was installed below the ceiling of the base chamber in order to allow water flow generated by electroosmosis and also to prevent the infiltration of gas by electrolysis. As a result, the floating gas bubbles moved along the surface of the Vyon filter and the collected gas bubbles at the perimeter were released through the gas vent at frequent intervals. The ceiling of the base chamber was also perforated with 5 mm diameter holes for the same purpose described in Section 3.2.2. A schematic diagram of the base chamber for electroosmotic permeability test is shown in Figure 3.7.

3.4 Self-weight and Hydraulic Gradient Consolidation Cell

Some tests were carried out to investigate the consolidation behaviour under physical influences alone (i.e. due to self-weight and hydraulic gradient stresses). The cell in this case had a base arrangement which allowed water flow through it, and was simpler because there was no need for the electrodes. A schematic of the testing cell for self-weight and

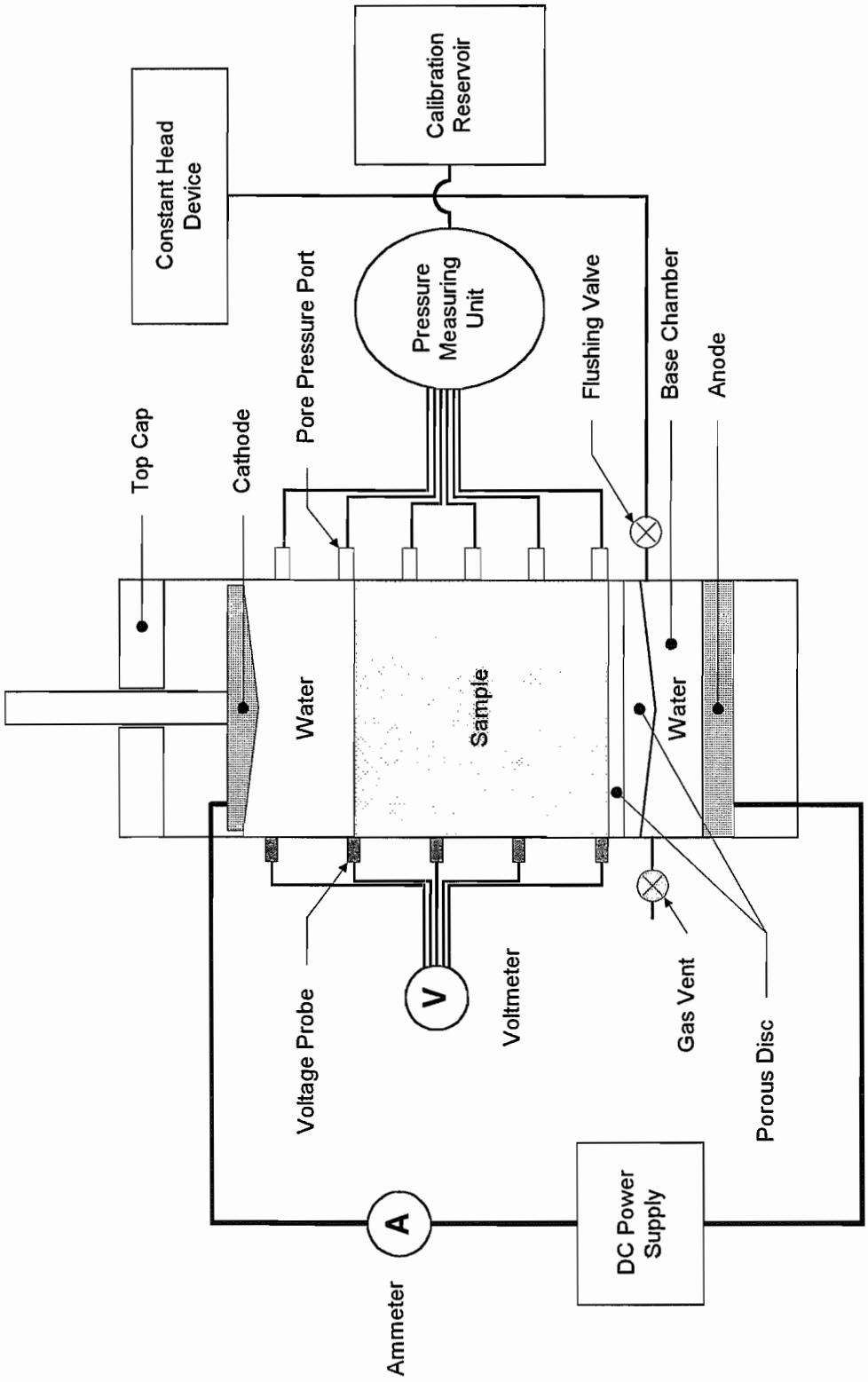

Figure 3.6 Schematic of the electroosmotic permeability cell

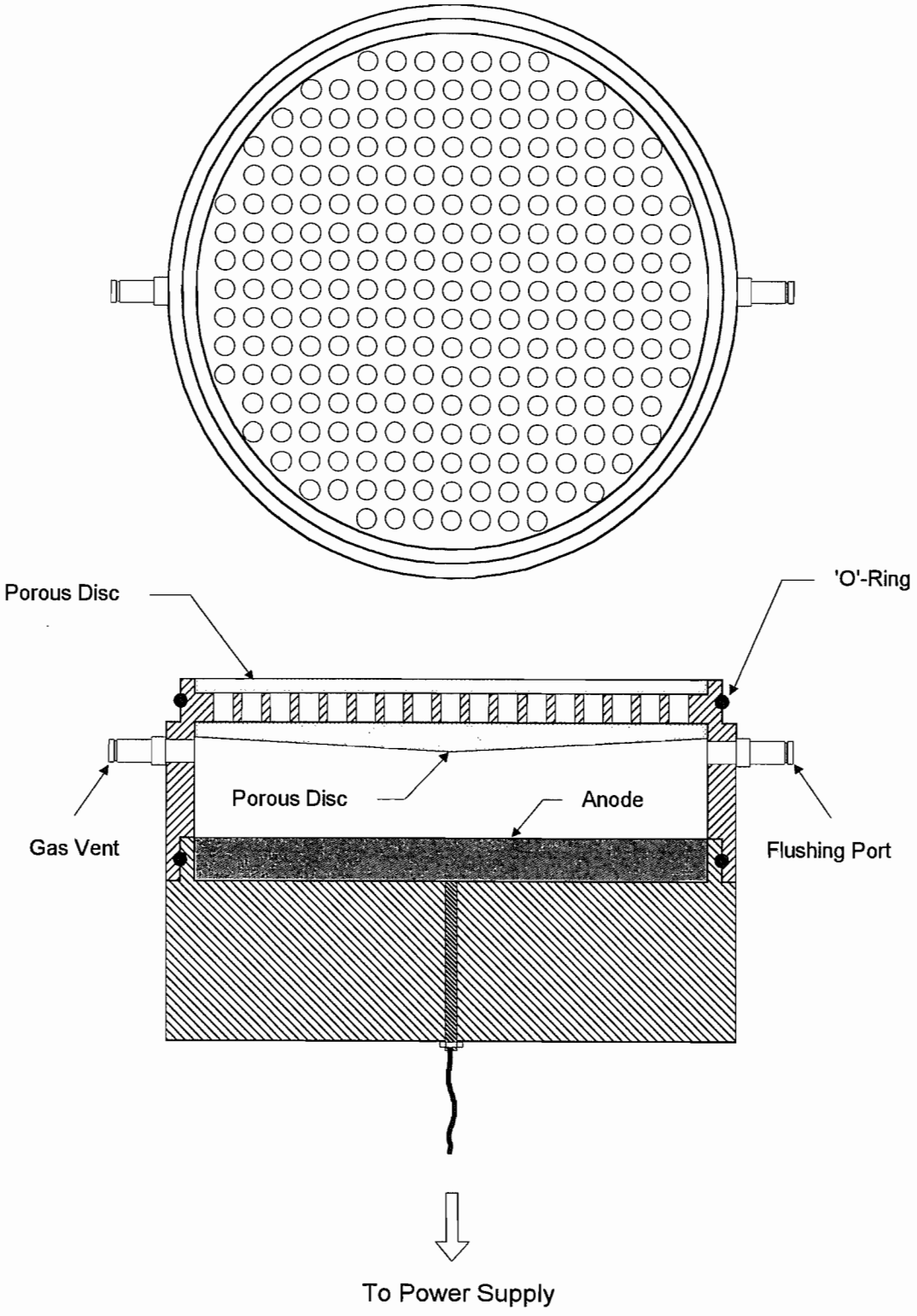

Figure 3.7 Schematic of the base chamber for electroosmotic permeability test

hydraulic gradient consolidation tests is illustrated in Figure 3.8.

The column was similar to that used in the electrokinetic cell (see Figure 3.2), with 7 pore pressure ports. Figure 3.9 shows a schematic diagram of the column used in self-weight and hydraulic gradient consolidation tests.

A base plate was designed in order to seal the end of the column. The base plate consists of two brass discs as illustrated in Figure 3.10. An 'O'-ring pressed against the column wall by screwing the face plate down to the base seals the column. The upper brass disc was designed in order to allow better drainage for water flow from the overlying porous disc into an engraved water path. The outflow of water from the soil sample was gathered in the water path and then drained through five drainage holes connected to a drainage port through the base plate.

3.5 Constant Head Device

A schematic diagram of a constant head device is presented in Figure 3.11. The constant head device consists of an outer column with outlet ports and a bleed valve, and an inner tube with open ends. In use, the constant head device is filled with deaired water with the bleed valve open as shown in Figure 3.12(a). With the lower end of the inner tube at the water level to be maintained in the sample, the level of water in the inner tube drops to the bottom end by closing the valve (A) and opening the valve (B) as shown in Figure 3.12(b). As shown by Figure 3.12(c), if the water level of the sample and that in the inner tube are the same, there is no flow of water with the valve (C) open. When the water level of the sample drops by opening the valve (D) to produce water flow through the soil, water flows from the constant head device to maintain equilibrium in the water level between the sample and the inner tube as shown in Figure 3.12(d).

3.6 X-ray Apparatus

The soil mechanics laboratory at Oxford University is equipped with a high accuracy non-destructive X-ray apparatus used for measurement of density as designed by Been (1980). The principle components of the X-ray system include; power source, X-ray tube and detector, scintillation counter, X-ray control unit, vertical lead screw and stepper motor, chart recorder, and digital height display.

The X-rays are generated in a Philips MCN 161 X-ray tube, with a maximum operating tube voltage of 160 kV. A finely collimated beam of X-rays is then passed through the testing cell, and strikes a detector unit consisting of sodium iodide crystal and photomultiplier assembly where a count rate is generated. The X-ray tube and detector are traversed

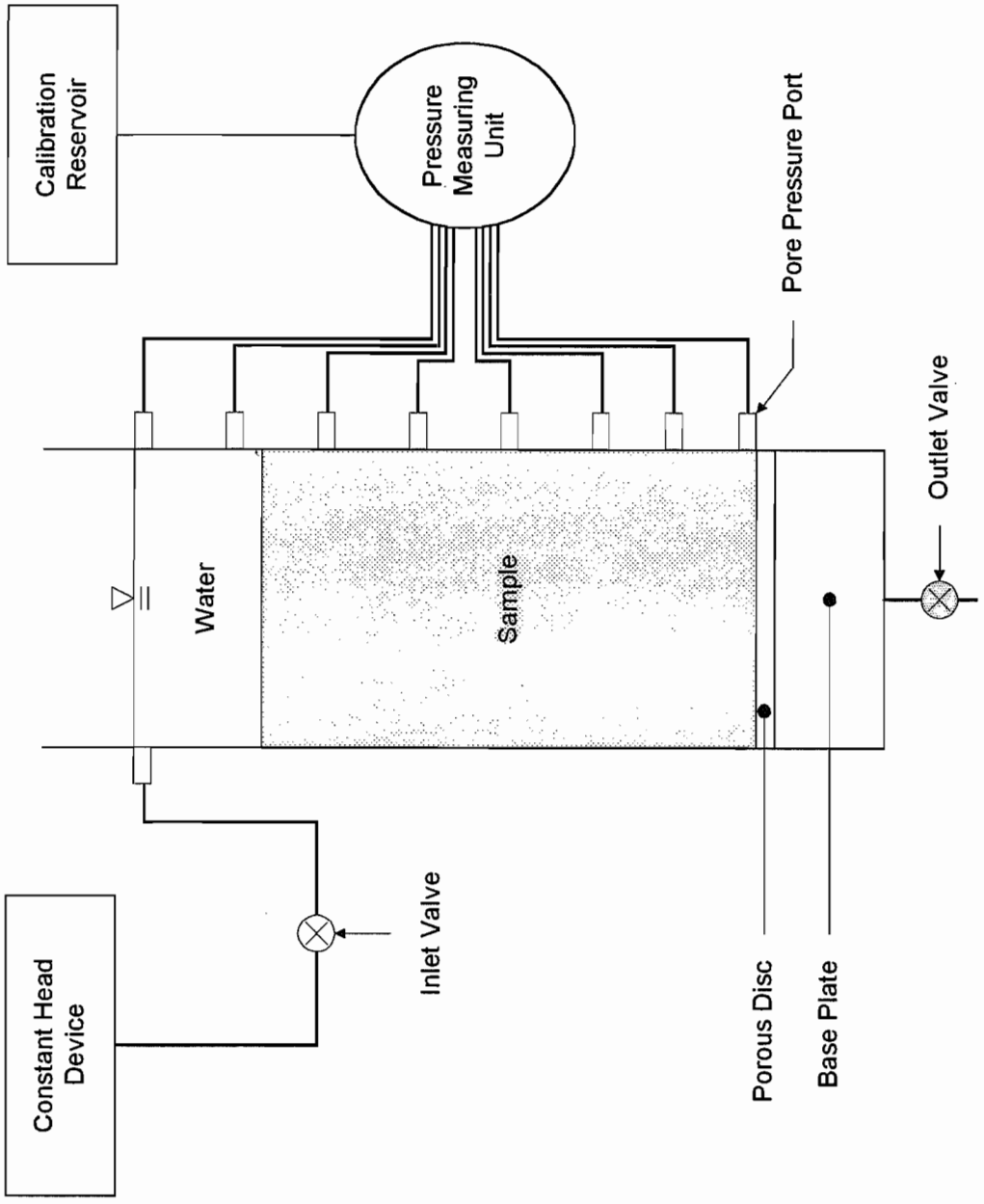

Figure 3.8 Schematic of the self-weight and hydraulic gradient consolidation cell

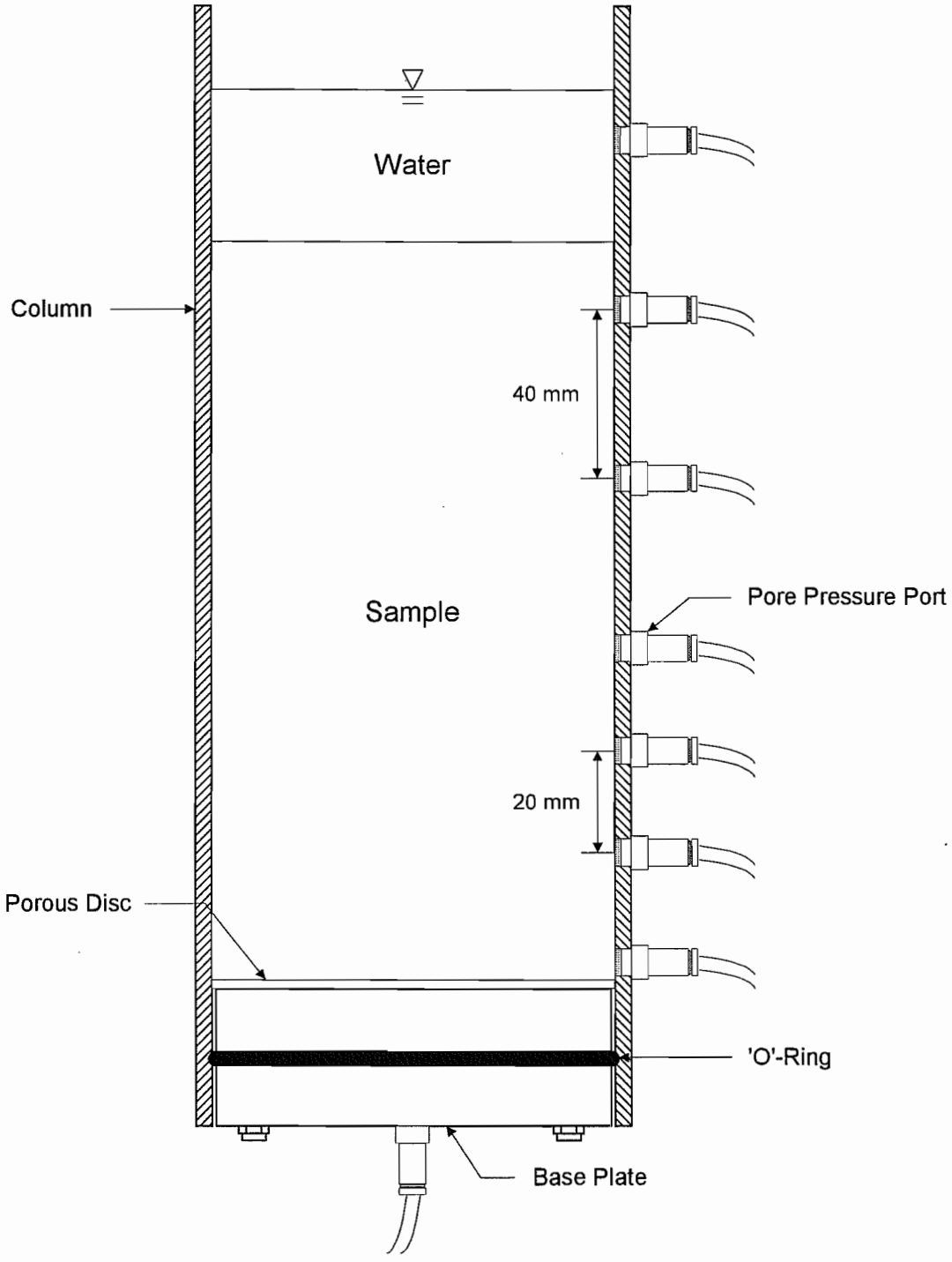

Figure 3.9 Schematic of the testing cell used for self-weight and hydraulic gradient consolidation tests

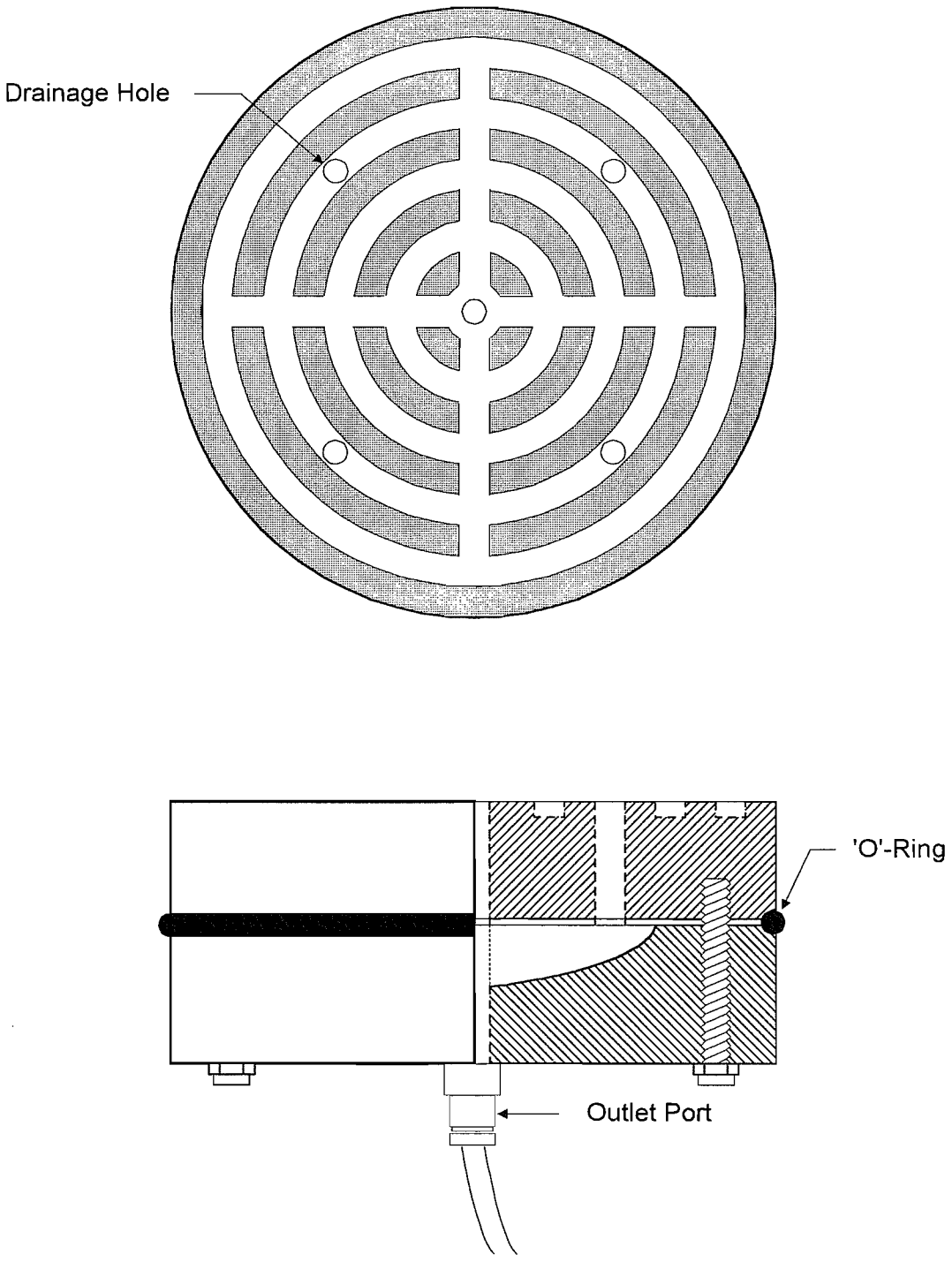

Figure 3.10 Schematic of the base plate used for self-weight and hydraulic gradient consolidation tests

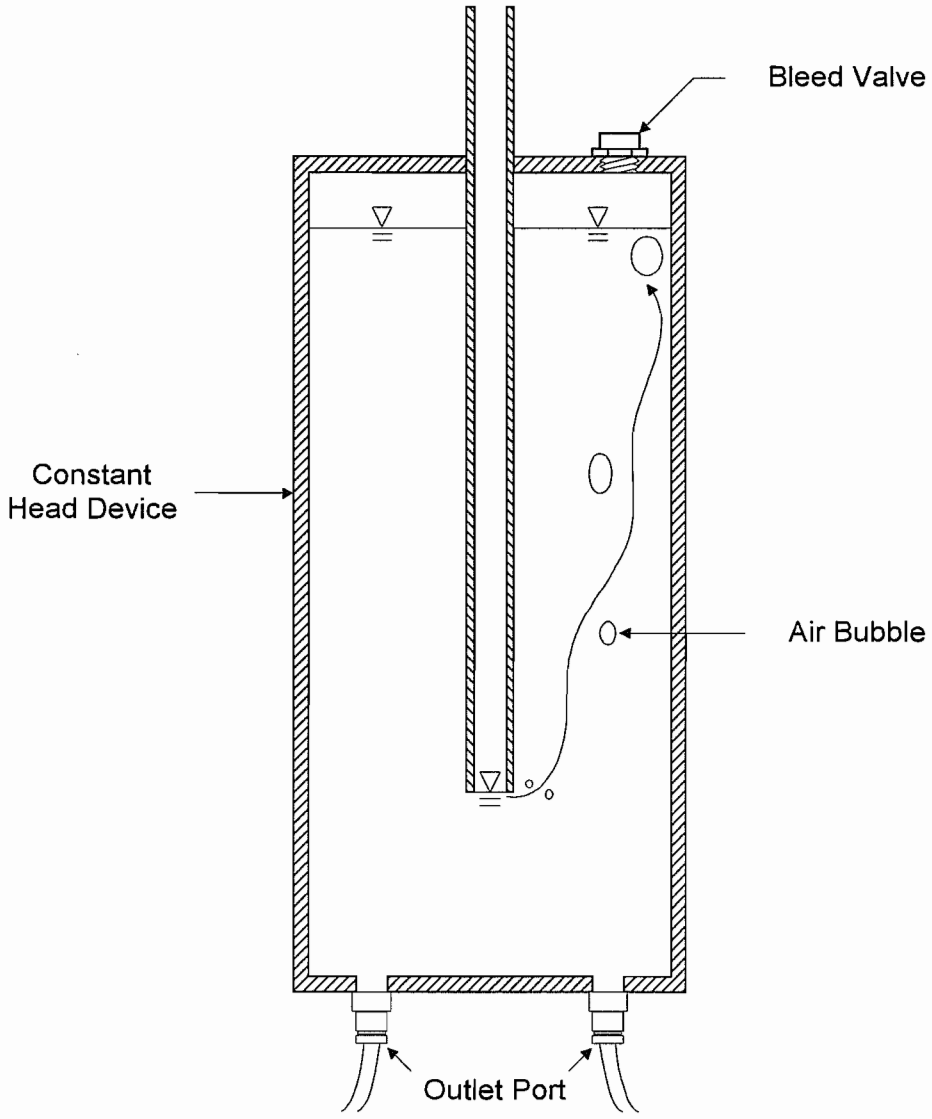

Figure 3.11 Schematic of the constant head device

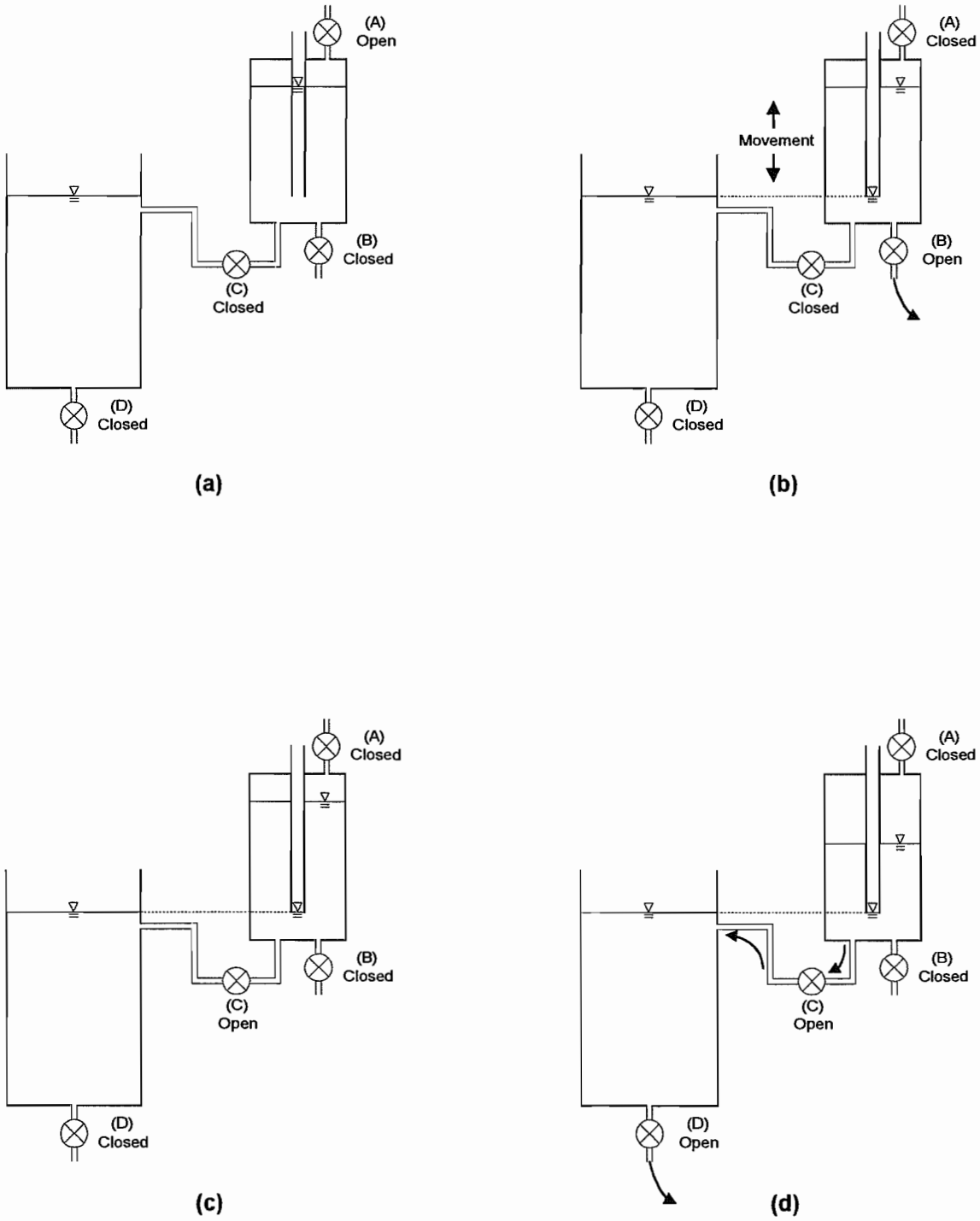

Figure 3.12 Schematic of the constant head device in use

steadily up and down the testing cell to produce a count rate profile against height; the count rate is logged automatically.

A block diagram of the X-ray system is shown in Figure 3.13. Figure 3.14 presents a schematic diagram of the X-ray apparatus.

3.6.1 Density Calibration using X-ray Attenuation Theory

An ideal narrow beam of radiation is attenuated in a homogeneous material in accordance with the following equation (Kohl *et al.*, 1961):

$$I = I_o \exp(-\mu_m \gamma x) \tag{3.1}$$

where I is the transmitted radiation intensity, I_o is the intensity corresponding to transmission in a vacuum, μ_m is the total mass absorption coefficient, γ is the density of absorbing material, and x is the absorber thickness.

Equation (3.1) can be expressed in a slightly different way as follows:

$$N = N_o e^{-k\gamma_s} \tag{3.2}$$

where N is the scintillation count rate with sample present, N_o is the scintillation count rate with no sample present, k ($=\mu_m x$) is the average attenuation constant, and γ_s is the bulk soil density.

The parameter k depends to some extent on atomic number, so that the calibration samples should be made up with the same configuration of acrylic and soil as in the experiments.

In general, if the same incident radiation intensity is applied to a slurry sample and to water in the same acrylic material, the transmitted count rates for soil and water mixture can be expressed by:

$$\gamma_s - \gamma_w = -\frac{1}{k} \ln\left(\frac{N_s}{N_w}\right) \tag{3.3}$$

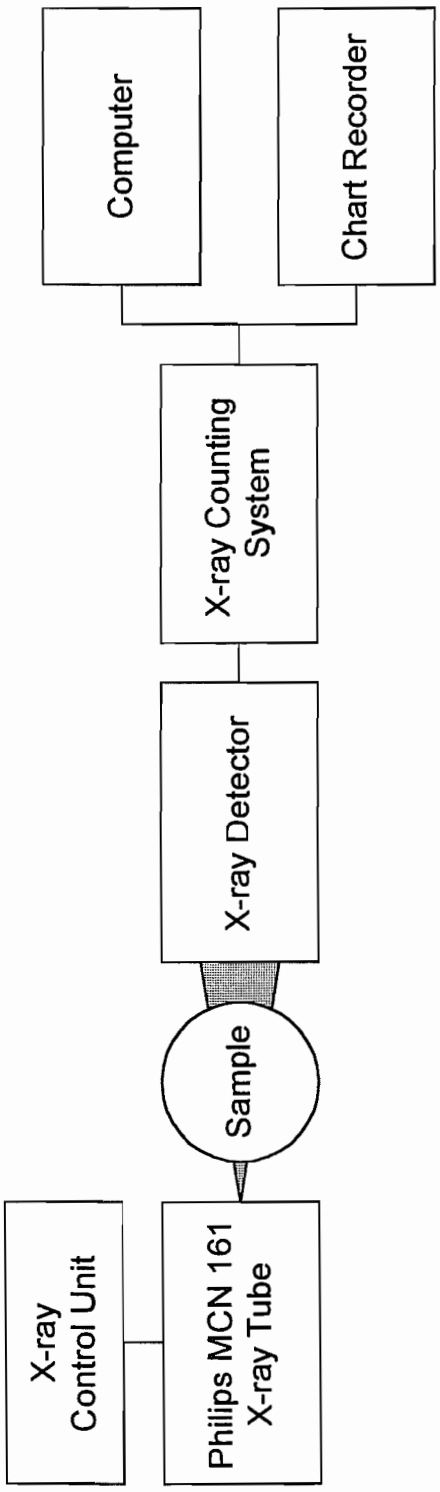

Figure 3.13 Block diagram of the X-ray system

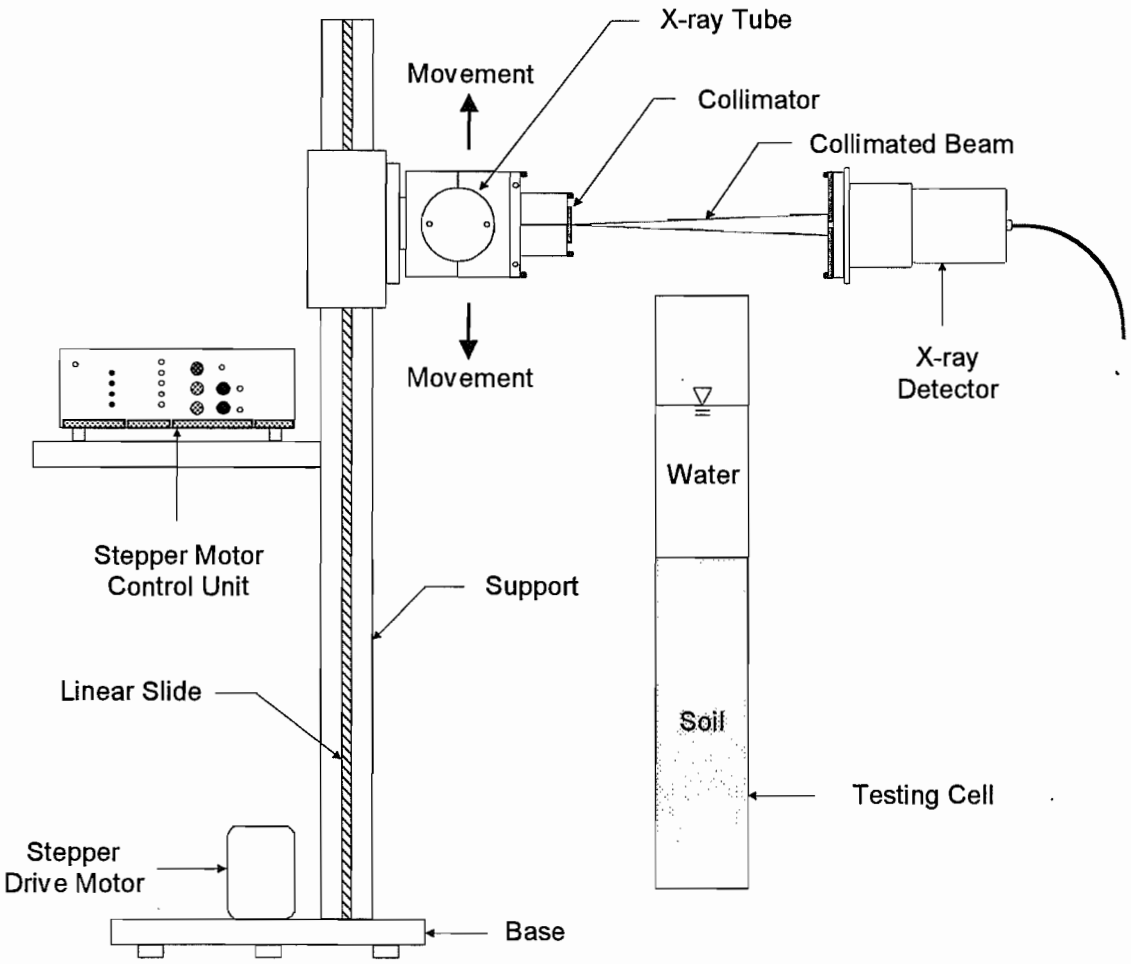

(a) Elevation

Figure 3.14 Schematic of the X-ray apparatus: (a) elevation

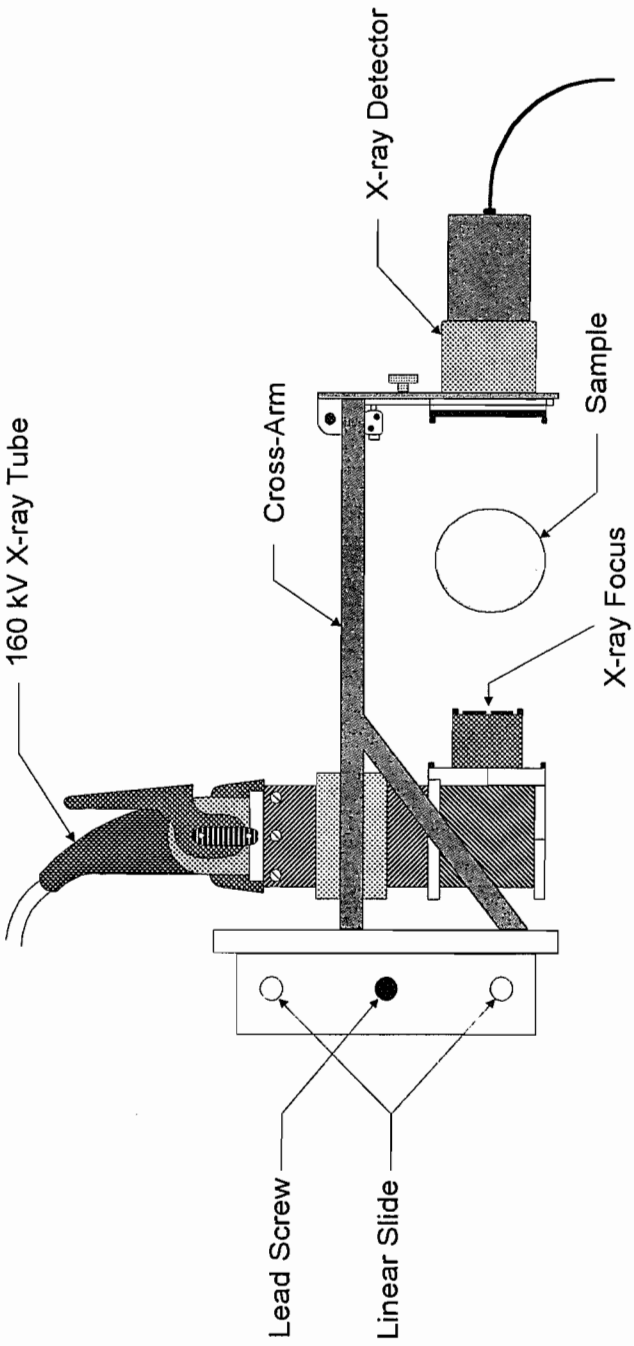

(b) Plan view

Figure 3.14 Continued: (b) plan view

where N_s is the transmitted count rate for the slurry, N_w is the transmitted count rate for water, and γ_w is the density of water.

Two independent measurements of known density are required if the two calibration constants k and N_o are to be found. One piece of information may be obtained either from the calibration water sample or the X-ray profile itself where there is overlying water whose density can be measured independently. The second calibration equation comes either from a separate sample of known density, or from the condition that the total mass of fluid and solids remains constant during an experiment.

The total vertical stress above hydrostatic at the base of a column is the sum of the buoyant weight (γ_s - γ_w) over the height of the bed:

$$\sigma_{ex} = \int_0^{h_s} (\gamma_s - \gamma_w)\, g\, dh \tag{3.4}$$

where h_s is the height of slurry surface and g is the gravitational constant. This value remains constant throughout an experiment.

Combining Equations (3.3) and (3.4), and replacing the integral by incremental summation of short linear segments gives:

$$\sigma_{ex} = -\frac{g}{2k}\left[\sum_{i=1}^{n-1} \{\ln(N_i N_{i+1})\, \Delta h_i\} - 2h_s \ln N_w\right] \tag{3.5}$$

where N_i and N_{i+1} are the count rates at consecutive elevations, and Δh_i is the difference in elevation.

The quantity σ_{ex} was determined in each experiment by measuring initial slurry density and height, and by applying Equation (3.4). Equation (3.5) was then solved to yield k. Each digitized count rate was converted to a bulk density using Equation (3.3), yielding a finely discretized profile of density versus height.

3.6.2 Density Determination using X-ray Attenuation

The continuous count rate profile was logged to a computer in 200 to 300 straight line segments. Figure 3.15 shows an example of count rate with respect to rig height data collected by X-ray. The overlying water and soil sample can be identified from count rate profile. After removal of irrelevant parts from the profile, the count rate profile was then converted to a density profile by calculating an average attenuation constant for each profile, as described in Section 3.6.1. Figure 3.16 presents an example of upwards and downwards density profiles against height converted from consecutive count rate profiles. Small variations in a density profile are due to random variations in the count rate outputs, the effect of which can be seen by comparing two profiles obtained immediately after each other.

The accuracy of density calculation is highly dependent on the traverse speed of the X-ray and to a lesser extent on the tube voltage. These were normally set at 1 mm per second and 140 kV, respectively. This standard setup provides an accuracy of density measurement of the order of ± 0.002 Mg/m^3, with a spatial resolution of around 1 mm.

3.7 Pressure Measuring Unit

Plate 3.3 shows a view of extended pressure measuring unit designed by Bowden (1988). The unit consists of two Perspex discs connected by a central bolt, with the upper disc housing a single pressure transducer (Druck PDCR 830). The upper disc can be rotated manually and the 1 mm diameter hole in front of the pressure transducer is aligned with a port in the lower disc. A schematic diagram of the assembled pressure measuring unit is presented in Figure 3.17.

In use, the pressure transducer is connected in turn to water filled tubing leading to each of the pore pressure ports and also to a calibration unit of variable head as shown in Figure 3.18. This system allows calibration of the pressure transducer immediately before the readings of sample pore pressure, thereby providing an accuracy of pore pressure measurement of the order of ± 0.01 kPa, or 1 mm head of water. An example of calibration result of pressure transducer is presented in Figure 3.19.

3.8 Experimental Procedure

3.8.1 Setup

Plate 3.4 shows a general view of the X-ray apparatus and experimental setup. The testing cell is supported by a cluster arm and a central rotatable stand. The cell is placed between an X-ray source and detector. After the cell assembly was placed in the X-ray

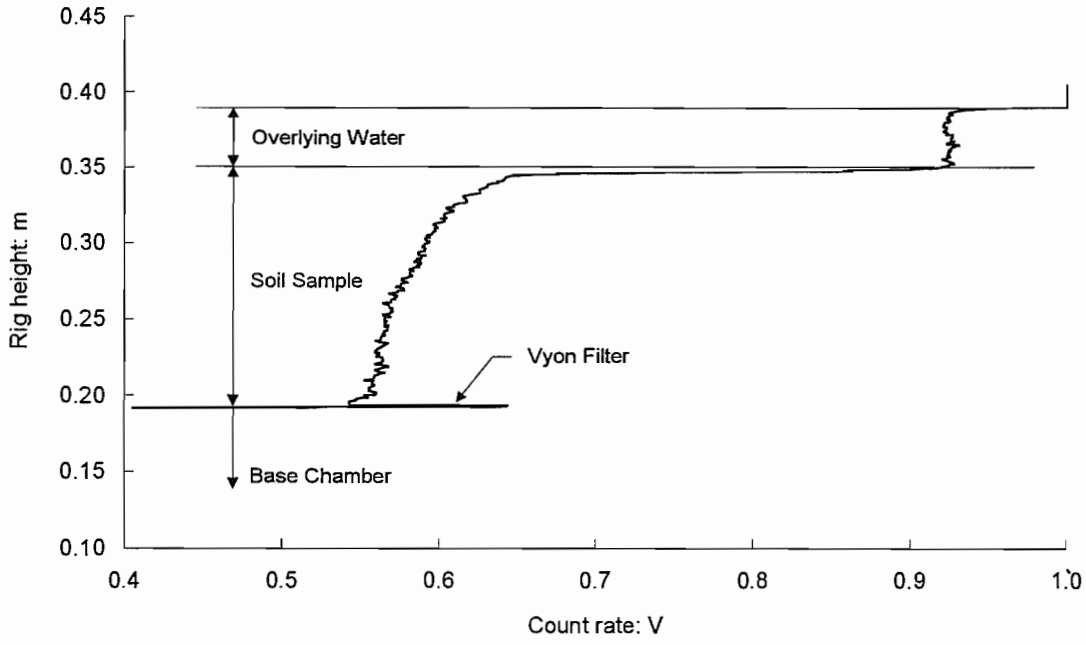

Figure 3.15 An example of X-ray count rate with respect to rig height data

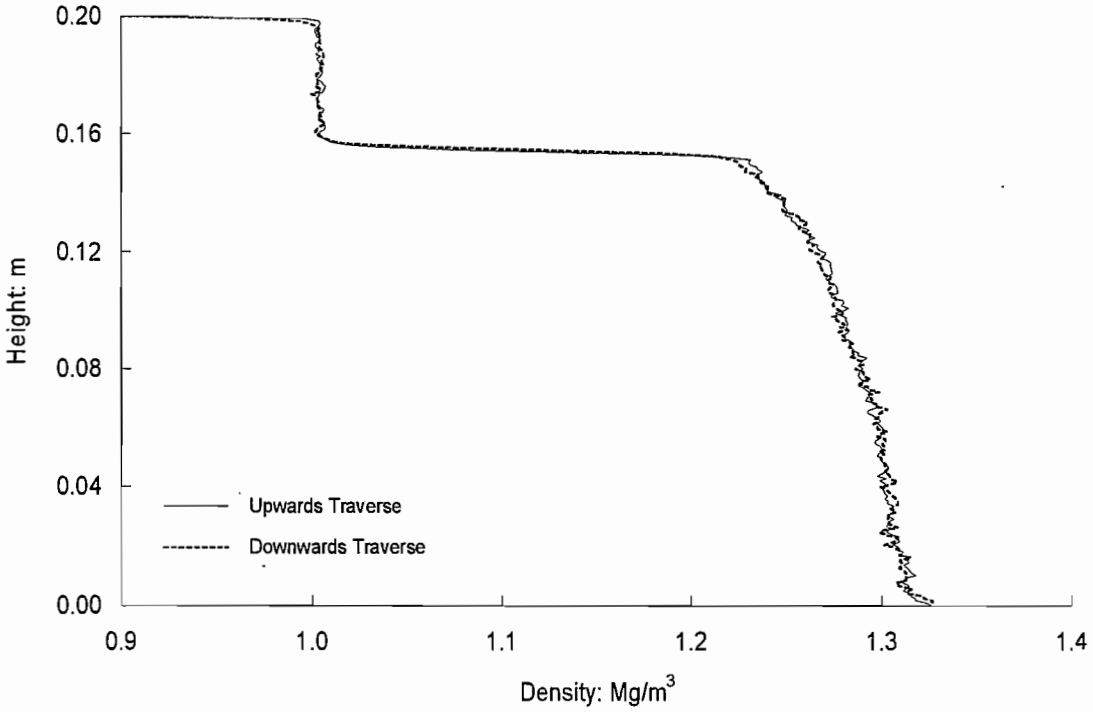

Figure 3.16 An example of upwards and downwards density profiles against height

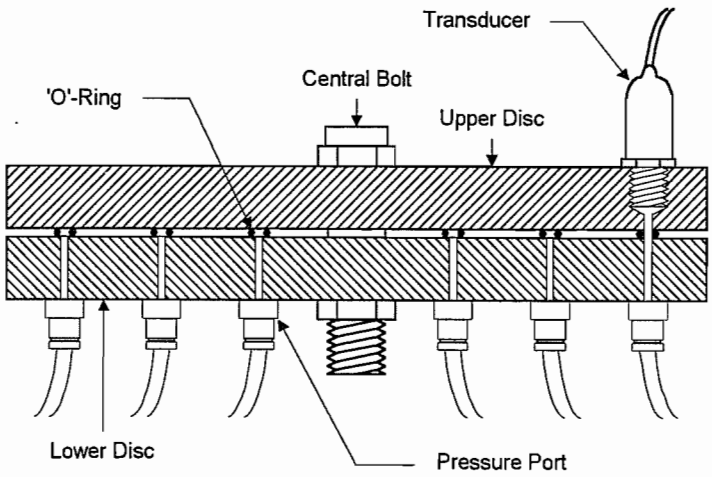

Figure 3.17 Schematic of the pressure measuring unit

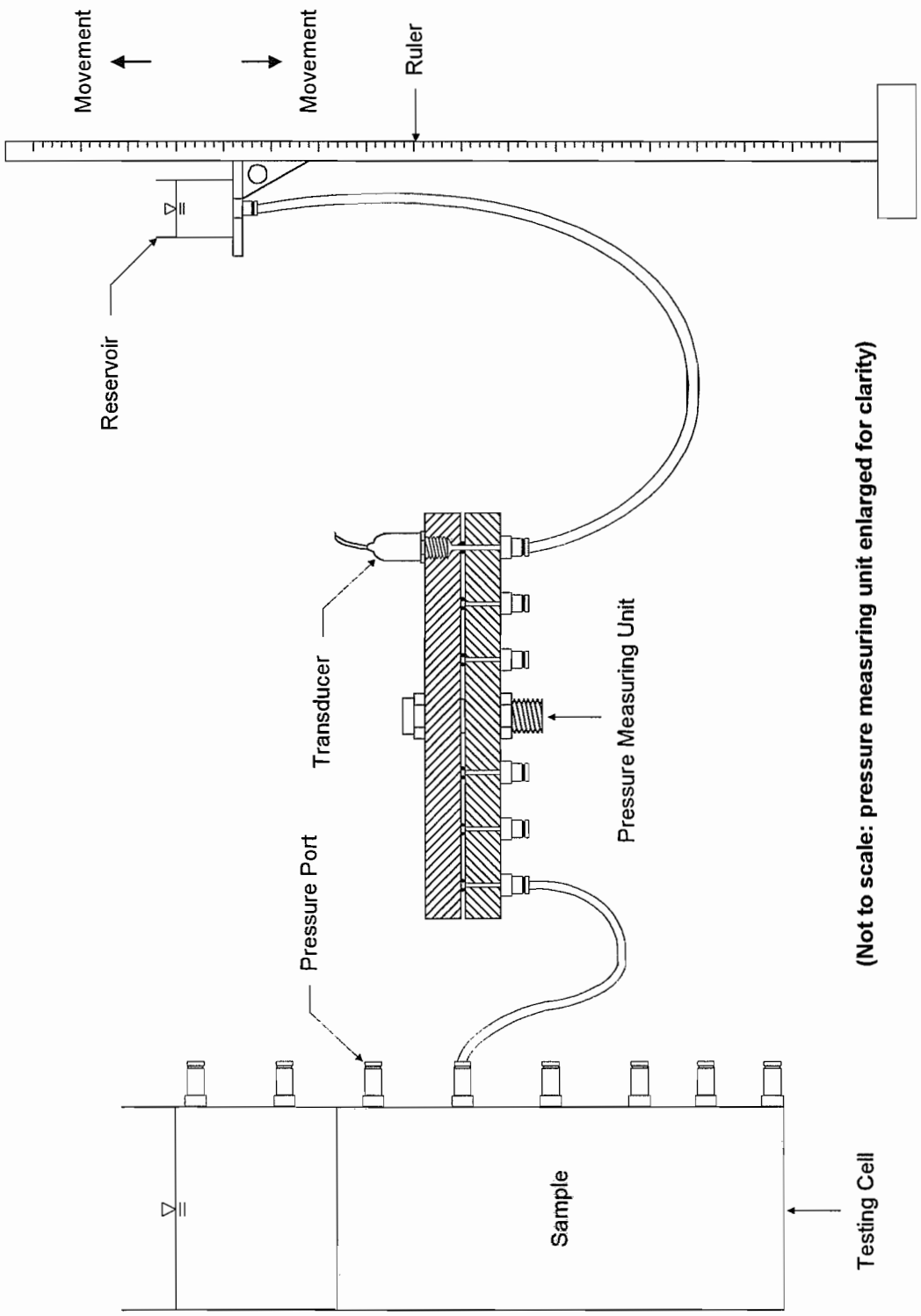

Figure 3.18 Schematic of the measurement of pore water pressure and the calibration of pressure transducer

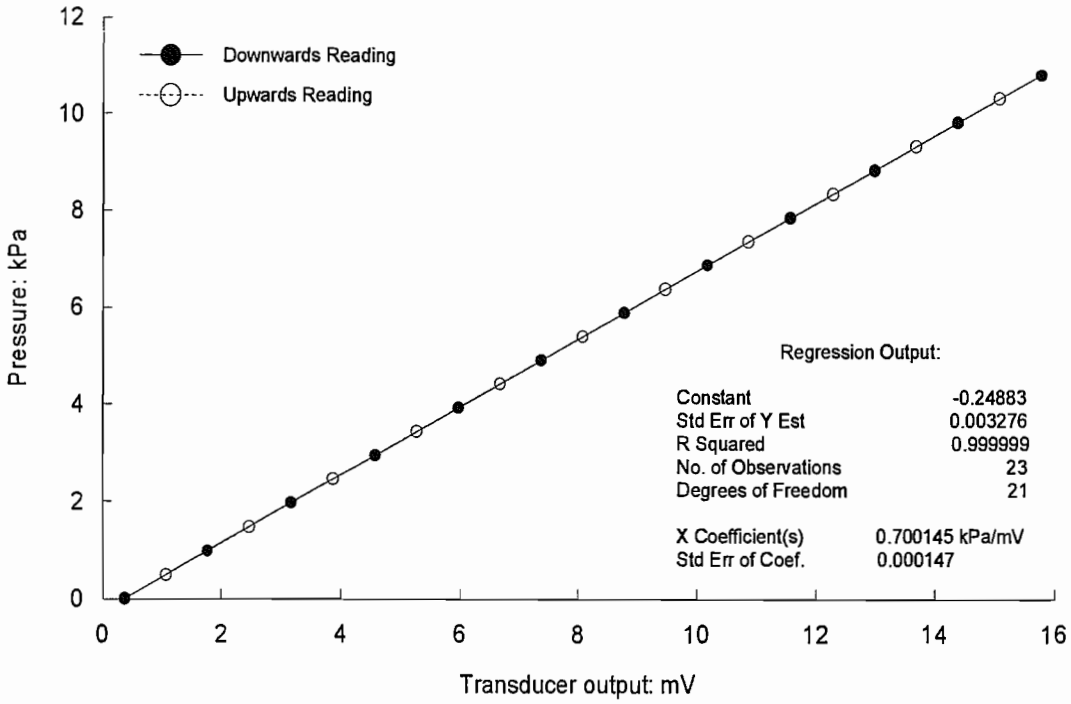

Figure 3.19 An example of calibration result of pressure transducer

laboratory, pore pressure ports on the side of the column were connected to the pressure measuring unit (Section 3.7) by 4 mm i.d. tubings. The 2.5 mm thick saturated porous disc was set on the top of the base chamber. The testing cell was then filled with deaired water, and the porous filters behind the pore pressure ports were thoroughly saturated hydraulically.

3.8.2 Sample Mixing and Placement

Initial slurry densities were prepared by mixing the required mass of soil with deaired water in an electrically operated mixer. The mixing period was generally 1 ~ 2 hours before the start of each test to promote a uniform mixture. During the mixing process, the slurry density was measured using a handheld densimeter (PAAR Density Meter DMA 35) accurate to ± 0.001 Mg/m^3.

The slurry was then introduced into the testing cell using a 21 mm i.d. tubing. Supplementary manual mixing was performed during placement in the testing cell using a spatula. The end of the tubing was initially held at the base of the column and maintained just below the rising surface of the slurry sample. The starting time was recorded and monitoring begun.

3.8.3 Surface Settlement

The height of soil sample was recorded during the experiment by using a ruler fixed on the outside of the column wall. The recorded sample heights with time were then compared with those obtained from the X-ray density profiles after the tests.

3.8.4 Density Measurement

X-ray count rates of a soil sample against height were made using the following procedures:

Step 1 After switching the X-ray power on, count rates were checked from the X-ray counting system to establish a constant X-ray generation rate.

Step 2 The X-ray source and detector were traversed twice, first down and then up, through the testing cell whilst the count rates were recorded on a chart recorder as a function of height.

Step 3 A comparison was made of the traverses in both directions recorded by the chart recorder.

Step 4 If pairs of count rate profiles differed during recording, **step 2** was repeated.

3.8.5 Pore Pressure Measurement

The transducer in the pressure measuring unit was checked and calibrated prior to each set of measurements for sample pore pressure. Calibration of the pressure transducer was made by moving a portable reservoir up and down, the elevation of which was varied relative to a fixed scale, and the pore pressure readings were derived from transducer voltage signals (see Figure 3.18). The pressure measuring system, including the calibration water reservoir, the pressure measuring unit, and a digital voltmeter, is shown in Plate 3.5.

Procedures of pore pressure measurement are as follows:

Step 1 Immediately after taking X-ray density profile, calibration of the pressure transducer was carried out and a check of the stability of data recorded.

Step 2 The pore pressure measurements were then performed one by one, rotating the pressure measuring unit to connect the transducer to each pore pressure port.

Step 3 The data recorded were converted to pressures above hydrostatic using calibration equations.

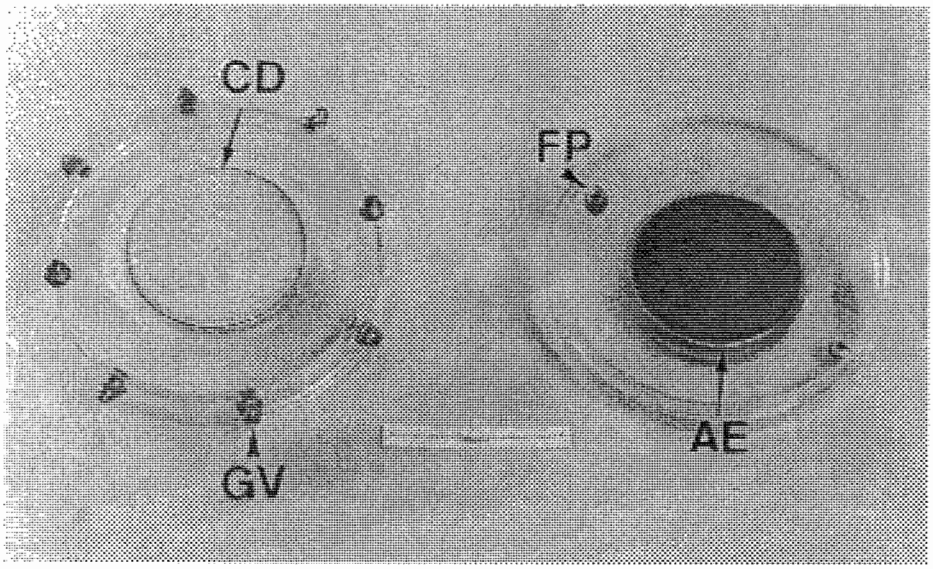

Plate 3.1 A view of the base chamber (CD: Ceramic Disc; GV: Gas Vent; AE: Anode Electrode; FP: Flushing Port)

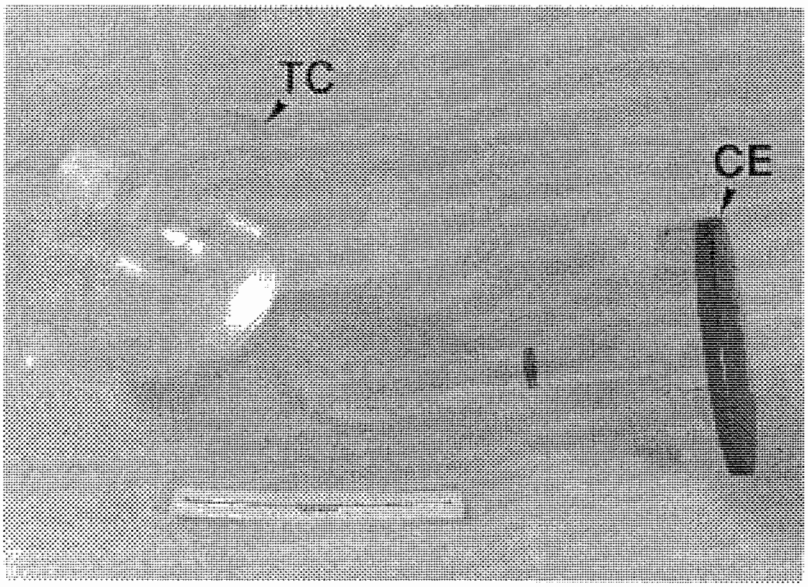

Plate 3.2 A view of the top cap and the cathode (TC: Top Cap; CE: Cathode Electrode)

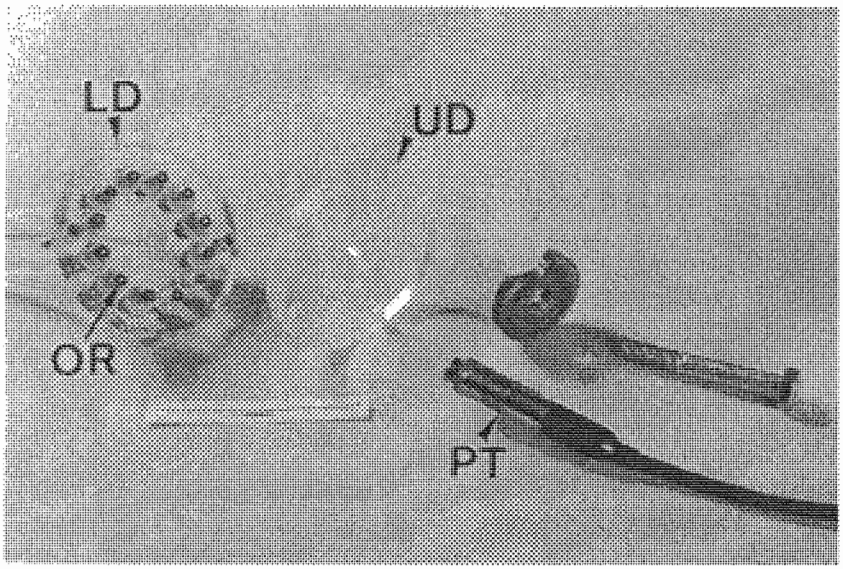

Plate 3.3 A view of the dismentled pressure measuring unit (UD: Upper Disc; LD: Lower Disc; PT: Pressure Transducer; OR: 'O'-ring)

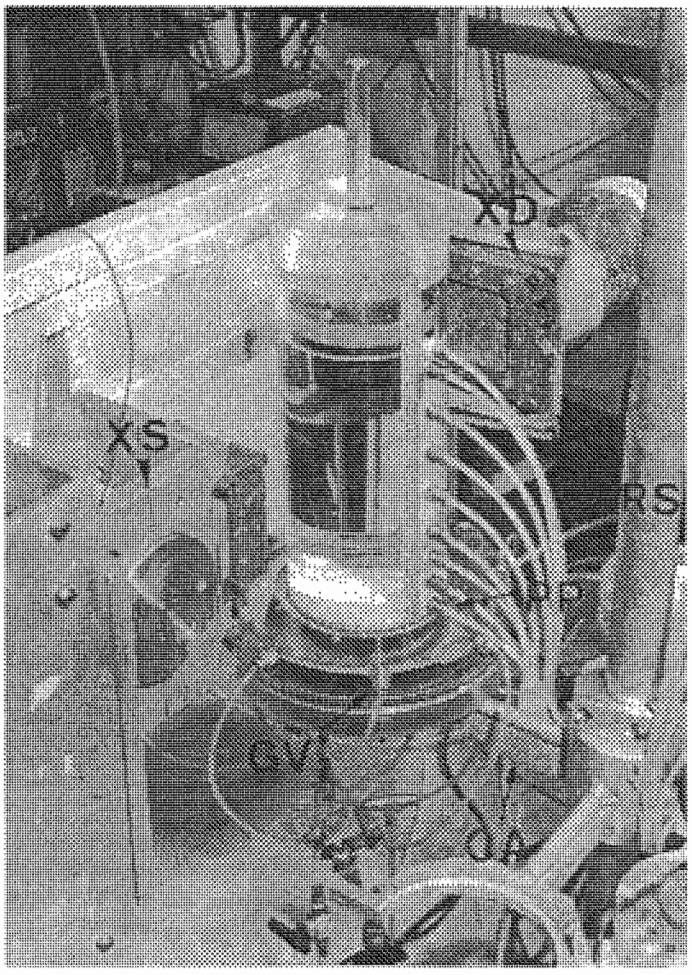

Plate 3.4 Overall view of X-ray apparatus & experimental setup (XS: X-ray Source; XD: X-ray Detector; CA: Cluster Arm; RS: Central Rotatable Stand; PP: Pressure Port; GV: Gas Vent)

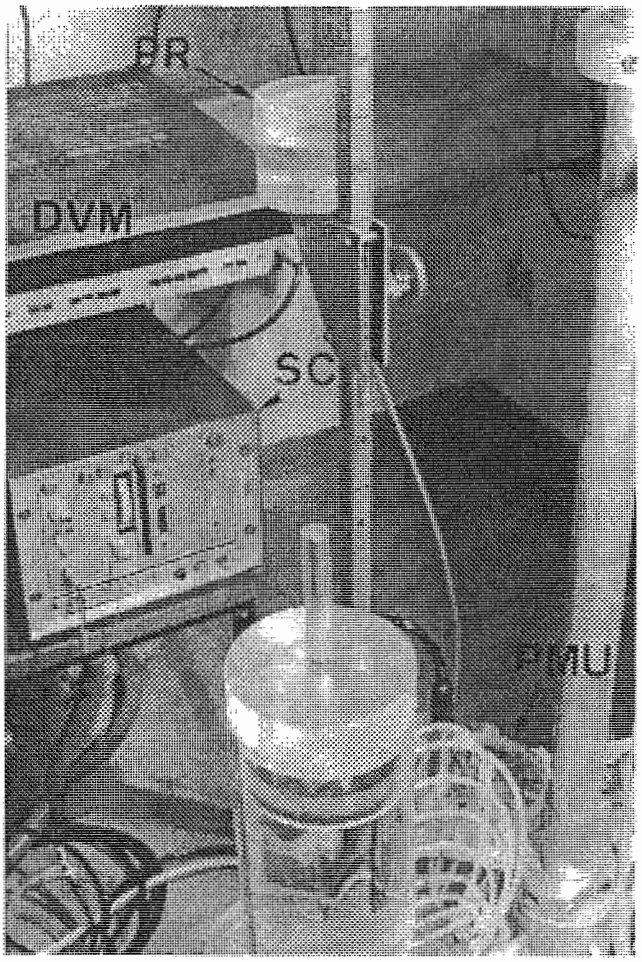

Plate 3.5 Overall view of pressure measuring system (PR: Portable Reservior; PMU: Pressure Measuring Unit; DVM: Digital Voltmeter for Pore Pressure; SC: Scintillation Counter for X-ray)

REFERENCES

Been, K. (1980). *Stress-strain behaviour of a cohesive soil deposited under water.* D.Phil. thesis, University of Oxford, UK.

Bowden, R. K. (1988). *Compression behaviour and shear strength characteristics of a natural silty clay sedimented in the laboratory.* D.Phil. thesis, University of Oxford, UK.

Kohl, J., Zentner, R. D., and Lukens, H. R. (1961). *Radioisotope applications engineering.* Van Nostrand.

CHAPTER 4 EXPERIMENTAL STUDY

4. EXPERIMENTAL STUDY

4.1 Introduction

The laboratory tests presented in this chapter investigated several aspects of soft soil behaviour under electrokinesis using kaolin clay. A number of self-weight and hydraulic gradient consolidation tests were also conducted with the same clay in order to compare the results with those obtained from electrokinetic consolidation tests. Details of the testing cells used for these tests are given in Chapter 3.

4.2 Experimental Programme

A number of experiments were undertaken with Speswhite kaolin clay with an initial density of 1.22 Mg/m^3 and height of 0.2 m under different stress conditions including self-weight, electrokinesis, and a hydraulic gradient. Each test is identified by the first letter indicating kaolin clay 'K', followed by a second letter symbolising the consolidation process ('S' for self-weight, 'E' for electrokinesis, and 'H' for hydraulic gradient), with the following digit specifying the test number within the batch (1 to 9). The test details are summarised in Table 4.1.

Tests KS1 to KS5 were devoted to an understanding of the consolidation behaviour of soft soil under self-weight condition. For tests KH1 and KH2, slurry samples were allowed to complete self-weight consolidation first, then a hydraulic gradient was applied by provision of base drainage in order to achieve higher densities and effective stresses than could occur under self-weight stresses alone.

Tests KE1 to KE6 were carried out to investigate the influence of electric field strength on the compression behaviour of soft soil. For tests KE1 to KE4, different electric field strengths of 10 to 30 V were applied to each sample before self-weight consolidation had taken place. Samples for tests KE5 and KE6 were allowed to complete self-weight consolidation and then the electric fields of 10 and 30 V were applied respectively.

Tests KE7 and KE8 were undertaken in order to examine the electroosmotic permeability of soft soil via the water flow generated by an externally applied electric field. Test KE9 was carried out to investigate variations on pH during the electrokinetic process.

The following sections contain the experimental observations and further discussion; the key measurements were surface settlement, density, and pore pressure, electric field, and soil pH as given in Table 4.2. All the tests were carried out at a constant room temperature of 25°C.

Table 4.1 Experimental conditions

Test series	Initial height (m)	Initial density (Mg/m^3)	Applied voltage (V)	Pore water (electrolyte)	Total duration (hr)	Duration of electric field (hr)
KS1 to KS5	0.2	1.22	-	Tap	-	-
KH1 & KH2	0.2	1.22	-	Tap	-	-
KE1	0.2	1.2	10	Tap	146	98
KE2	0.2	1.22	10	Tap	119	73
KE3	0.2	1.22	20	Tap	112	65
KE4	0.2	1.22	30	Tap	92	72
KE5	0.164	1.27	10	Tap	191	90
KE6	0.158	1.28	30	Tap	134	75
KE7	0.2	1.22	20	Tap	72	50
KE8	0.2	1.22	20	Deionised	68	31
KE9	0.2	1.22	30	Tap	24	20

Table 4.2 Details of measurements during laboratory tests

Test series	Settlement	Density	Pore pressure	Electric field	pH
KS1 to KS5	✓	✓	✓	-	-
KH1 & KH2	✓	✓	✓	-	-
KE1	✓	✓	✓	✓	✓
KE2	✓	✓	✓	✓	✓
KE3	✓	✓	✓	✓	✓
KE4	✓	✓	✓	✓	✓
KE5	✓	✓	✓	✓	✓
KE6	✓	✓	✓	✓	✓
KE7	✓	✓	✓	✓	✓
KE8	✓	✓	-	✓	✓
KE9	✓	-	-	-	✓

4.3 Self-Weight Consolidation Tests KS1 to KS5

Sets of self-weight consolidation tests (KS1 to KS5) were performed with an initial uniform density of 1.22 Mg/m^3 and height of 0.2 m. Surface settlement, density, and pore pressure of the soil sample were monitored during the test. The tests were stopped after the excess pore pressures had almost completely dissipated.

4.3.1 Density and Excess Pore Pressure Profiles

Density and excess pore pressure profiles for test KS1 are shown in Figure 4.1. The first density profile shown in Figure 4.1(a) presents the initial input density, and the next five show self-weight consolidation after 18, 40, 69, 115, and 214 hours. As seen, the initial slurry density was fairly uniform and the density increased upwards from the base during the self-weight stage. The initial excess pore pressure profile in Figure 4.1(b) shows that the maximum excess pore pressure developed at the base of the sample, due to the weight of soil slurry, was approximately 0.4 kPa, and this decreased linearly towards the surface of the sample. It can be seen from the 18 hour density profile that a relatively rapid increase in density occurred in the base 0.04 m of the sample. The density in the base half of the sample gradually increased whilst that in the top half remained at the initial input density by 40 hours of self-weight consolidation.

After 69 hours of self-weight consolidation, the increasing density step from the base reached the top of the soil and the density increased steadily throughout the soil. It can be seen from Figure 4.1(b) that the excess pore pressures have almost dissipated after 214 hours and the consolidation process has been completed; there was no further consolidation observed over a period of 2 days under the self-weight condition. Several density and excess pore pressure profiles for self-weight consolidation tests KS2 to KS5 are shown in Figure 4.2. A similar pattern of compression can be seen in each of these tests.

4.3.2 Surface Settlement

The simplest method of characterising consolidation process is to study the change in position of soil surface with respect to time. Surface settlements were recorded for all experiments and compared with those obtained from X-ray density profiles. Figure 4.3 presents the surface settlement with respect to time in tests KS1 to KS5. The surface settling behaviour during self-weight consolidation consists of an initial period of relatively rapid settling (for the first 100 hours or so) and a further period of slow settling at a decreasing rate. The settling rates observed from each of these tests were slightly different despite similar experimental conditions. It is likely that this is due to the initial density being

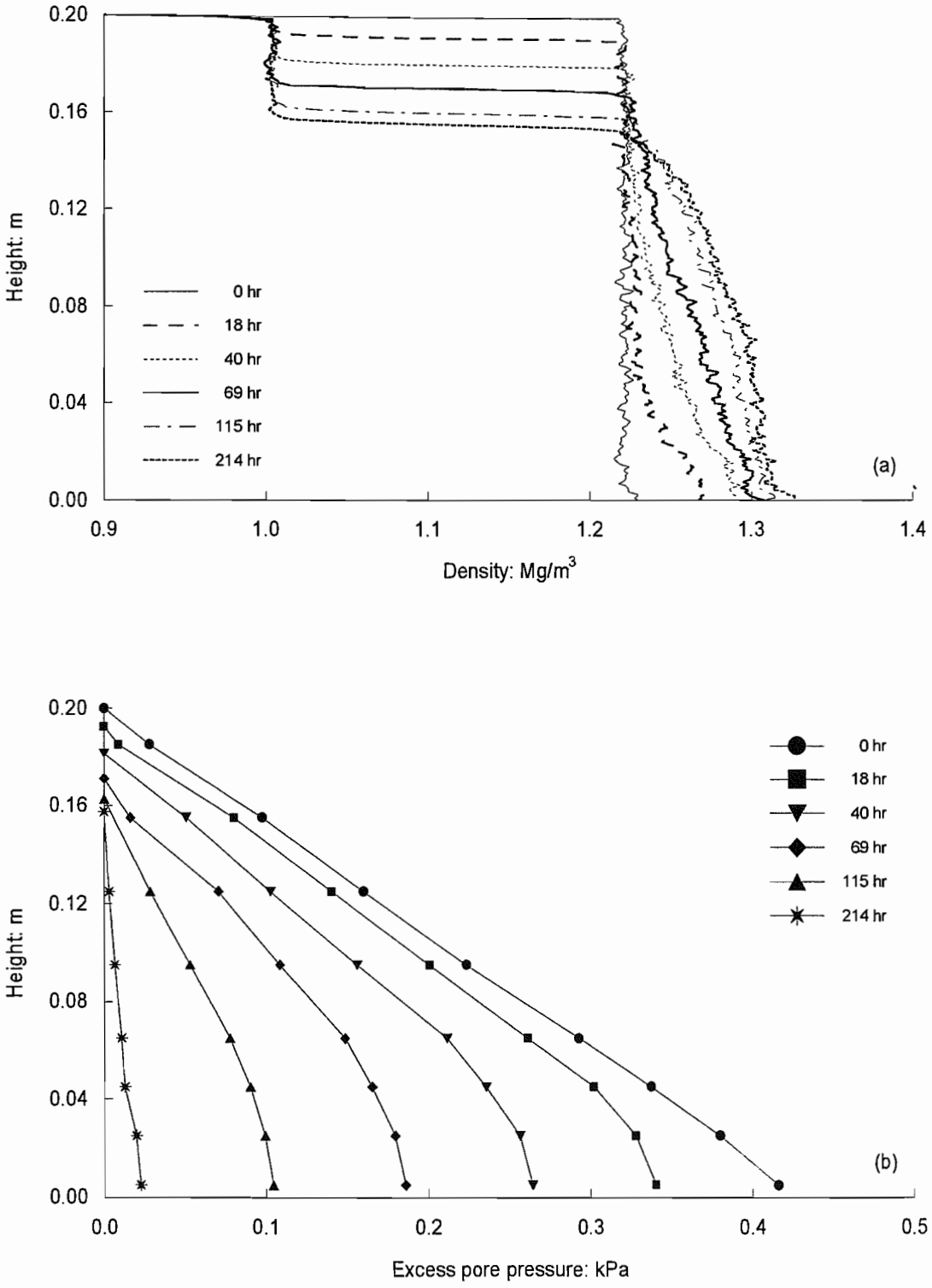

Figure 4.1 Self-weight consolidation, experiment KS1: (a) density profiles; (b) excess pore pressure profiles

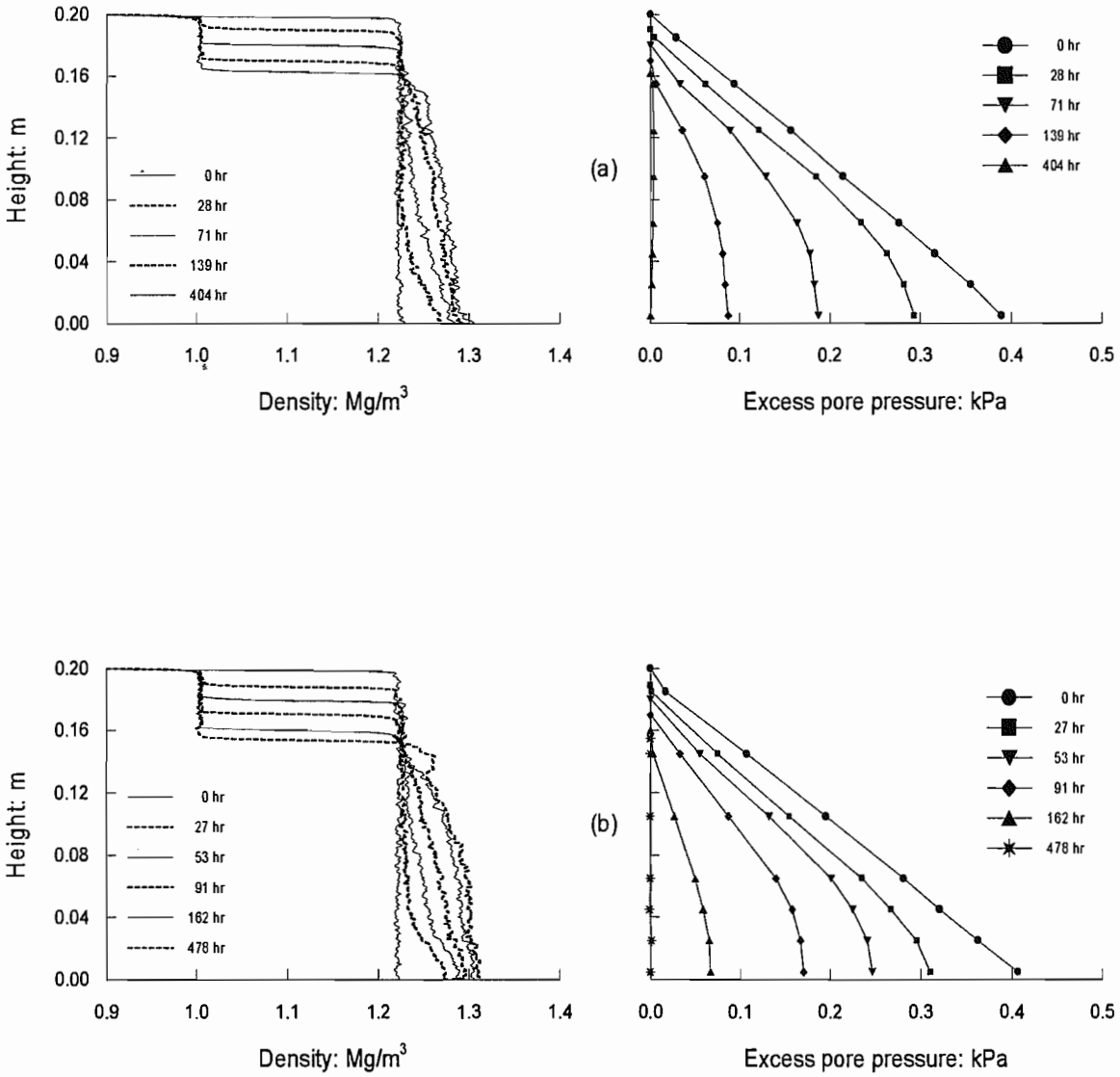

Figure 4.2 Density and excess pore pressure profiles: (a) experiment KS2; (b) experiment KS3

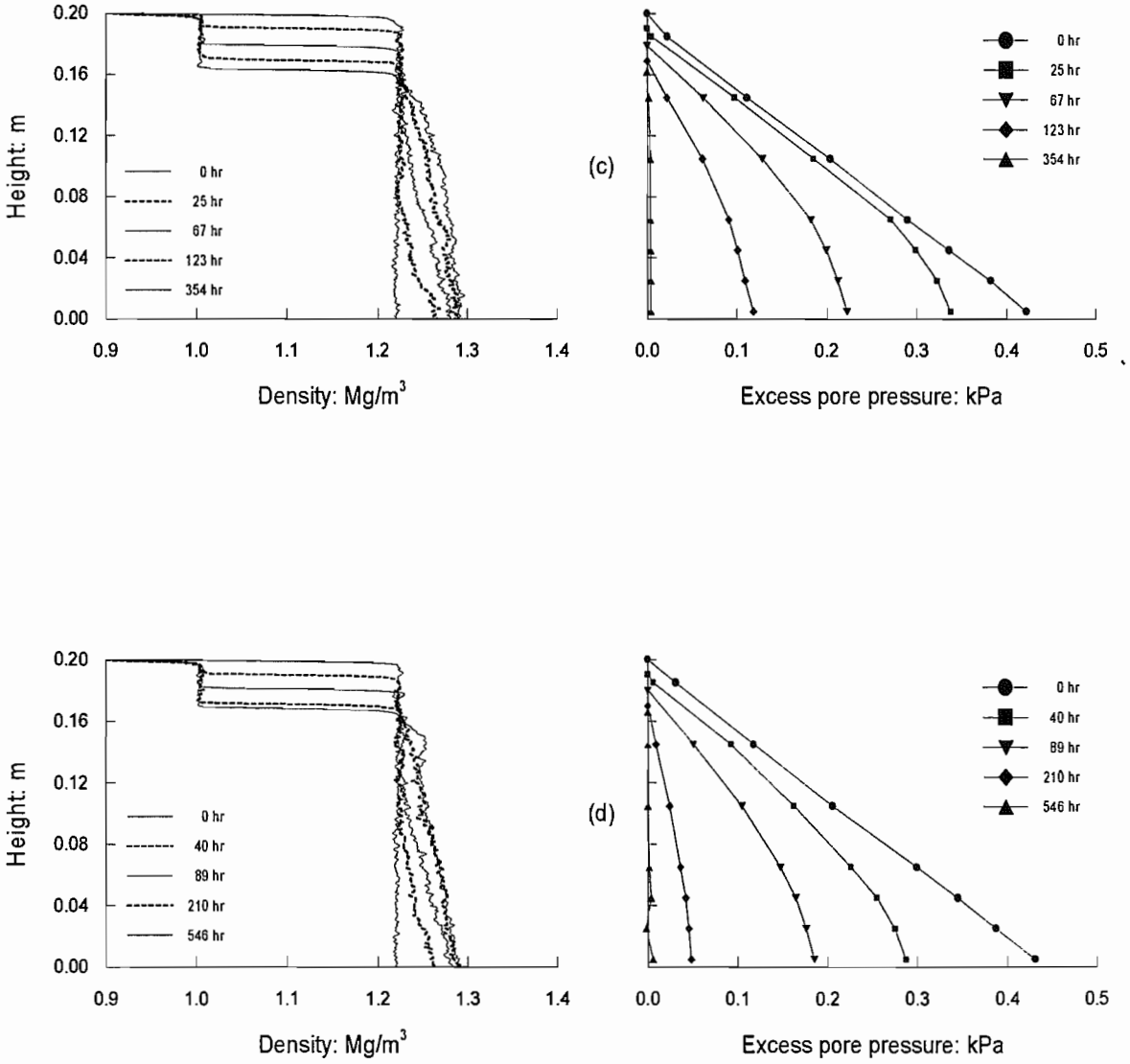

Figure 4.2 Continued: (c) experiment KS4; (d) experiment KS5

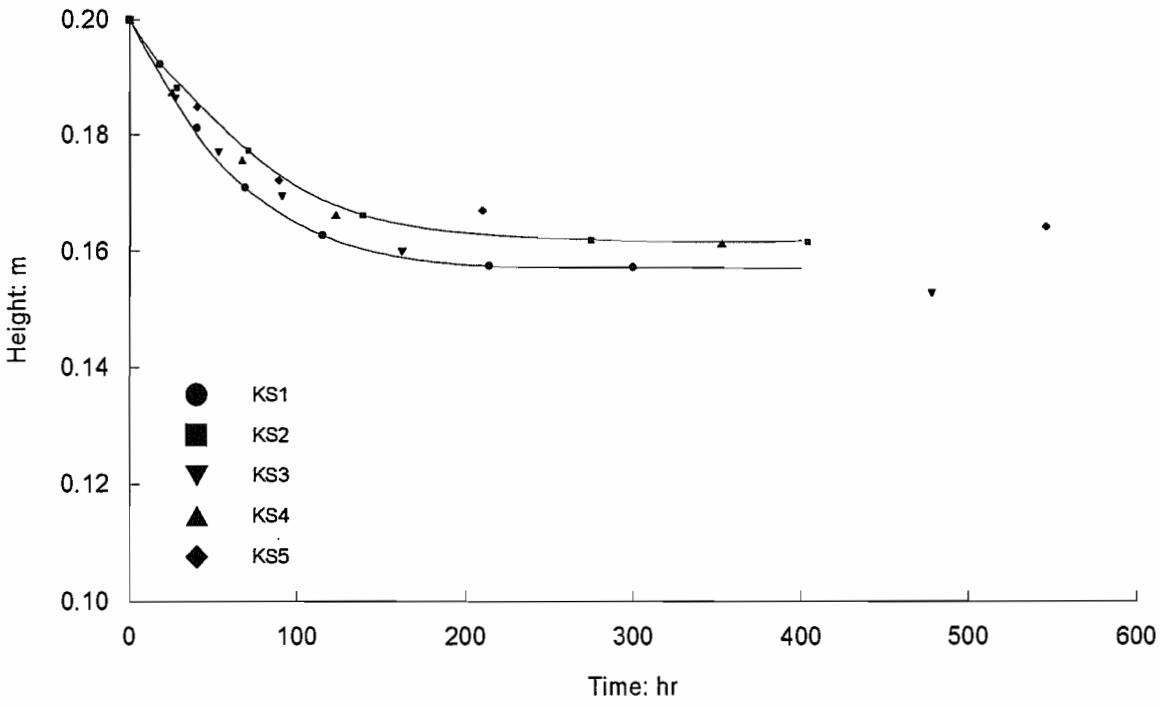

Figure 4.3 Surface settlement with respect to time results, experiments KS1 to KS5

very close to the *structural density* (Section 2.6). This could make the experiments very sensitive to the initial and uniform conditions. It appears that there may be up to 5 % difference in the surface settlement under these conditions.

4.3.3 Effective Stress and Void Ratio Relationship

The stress-strain relationship for fine-grained soils is generally represented in terms of the effective stress versus void ratio. The effective stress can be calculated by subtracting pore pressure from the total vertical stress, which can be calculated at any section in the soil by integrating the density between the section and the soil surface from the continuous density profile by X-ray. In order to calculate the effective stress at each soil element, it was assumed that the pore pressures between the measured values are linear. The void ratio can be calculated directly from the density and a value for the soil specific gravity. Thus, a relationship between effective stress and void ratio can be obtained from each pair of density and pore pressure profiles.

Figure 4.4 shows the effective stress and void ratio relationship for self-weight consolidation from test KS1. The data points lower than 0.01 kPa in effective stress are smaller than the accuracy of calculation of effective stress, and represent the initial slurry

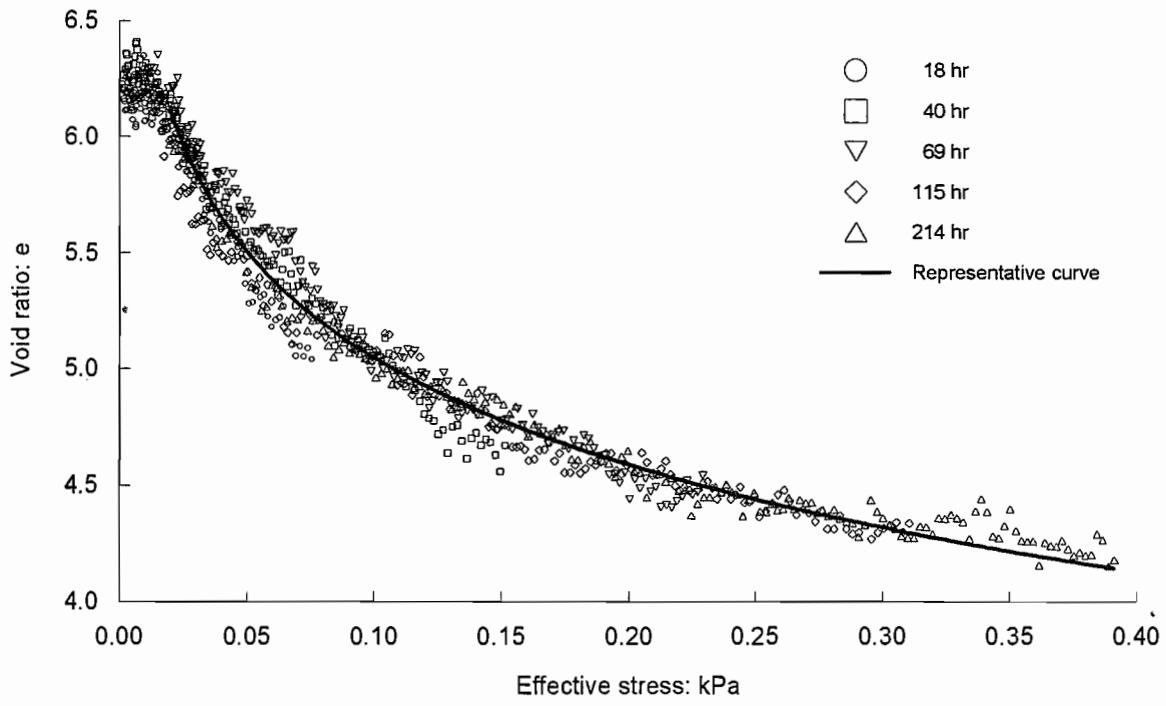

Figure 4.4 Effective stress and void ratio relationship, experiment KS1

sample. It can be seen that very small changes occurred in the initial void ratios for quite small increases in effective stresses (less than 0.02 kPa), followed by a significant reduction in void ratio as the effective stresses increased further. This result demonstrates that the data points follow a unique compression curve during self-weight consolidation with an increase in effective stresses up to 0.4 kPa and a decrease in void ratio to approximately 4. Several effective stress and void ratio relationships for self-weight consolidation tests KS2 to KS5 are presented in Figure 4.5, and a similar pattern of compression can be seen in each of these tests. A representative curve has been marked for each test, assuming a least squares best fit to a logarithmic relationship (i.e. void ratio *e* proportional to *log* σ_v'). It can be seen that there is comparatively little scatter around these representative curves.

Figure 4.6 shows all the data of the tests KS1 to KS5 plotted together along with a representative curve. It is clear that there is a wider spread of data between tests than for any single test, consistent with the different settlement curves observed. A similar range of void ratio (of the order of 0.7 at an effective stress of 0.4 kPa) has been seen by Been (1980), Elder (1985), and Bowden (1988) in experiments on a natural estuarine silty clay. The representative compression curve shown in Figure 4.6 describes the stress-strain characteristic of Speswhite kaolin clay under self-weight consolidation. From the results of these self-weight consolidation tests, some basic soil parameters for very soft soil (e.g. C_c,

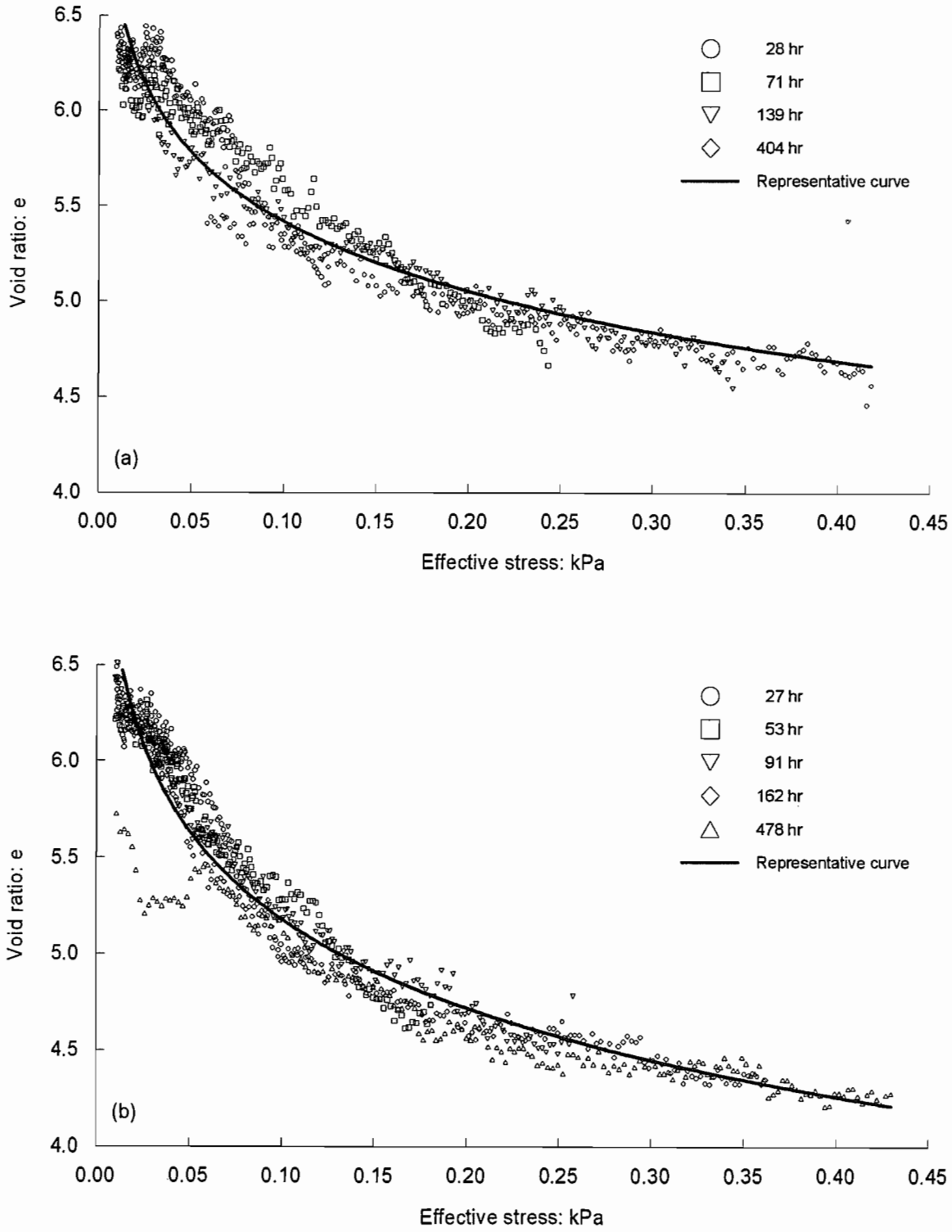

Figure 4.5 Effective stress and void ratio relationship: (a) experiment KS2; (b) experiment KS3

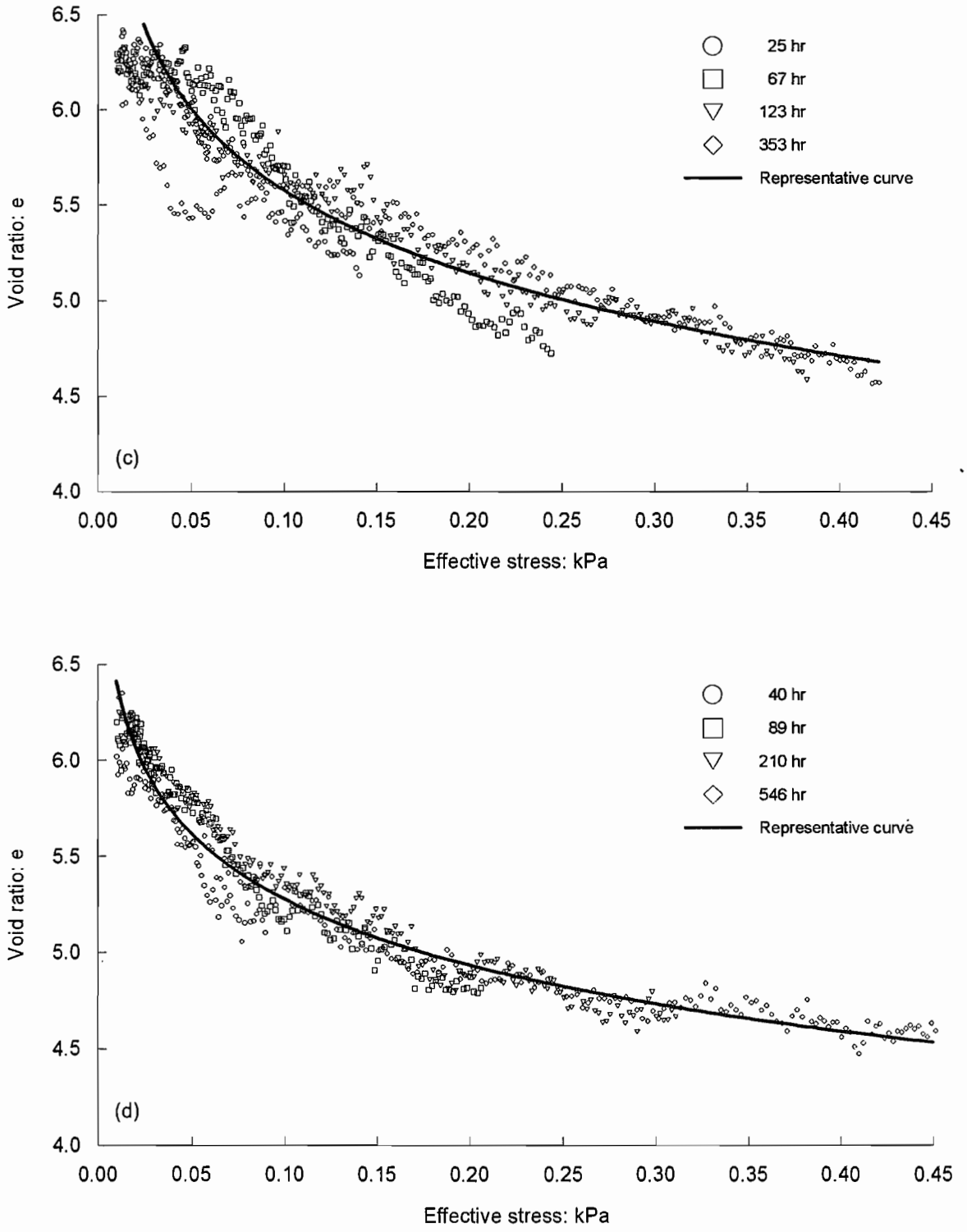

Figure 4.5 Continued: (c) experiment KS4; (d) experiment KS5

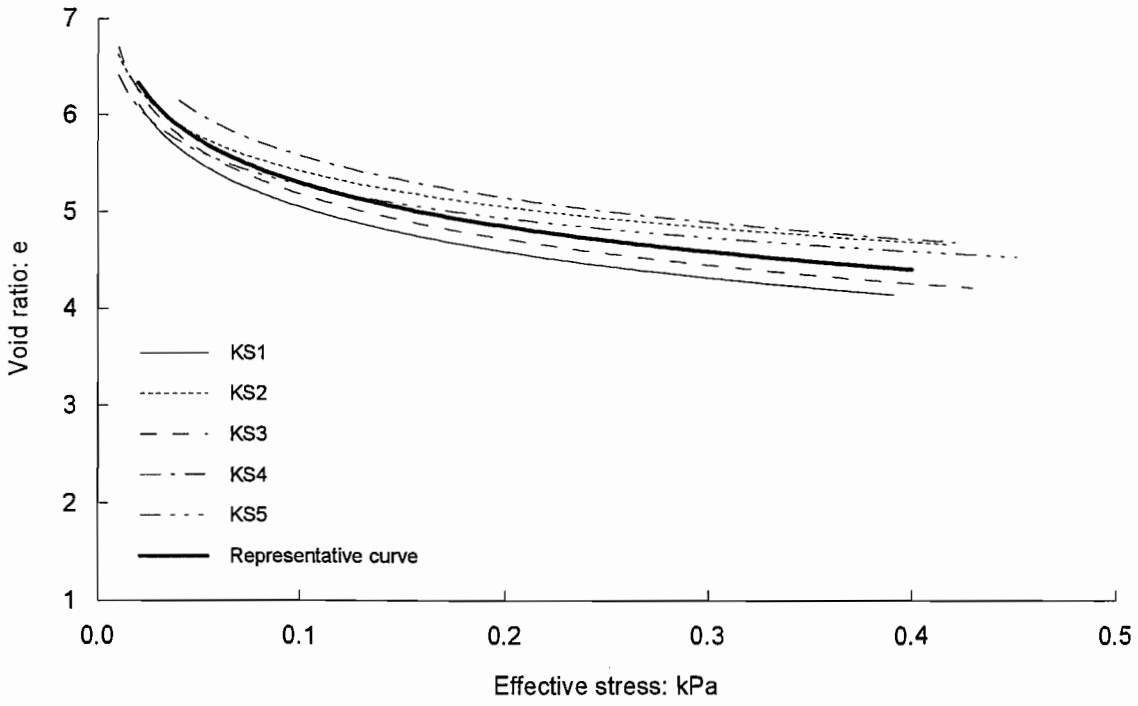

Figure 4.6 Effective stress and void ratio relationship, experiments KS1 to KS5

m_v, and k_h for Speswhite kaolin) were established in Chapter 5, which were then used to verify the applicability of the analytical model in numerical simulations given in Chapter 6.

4.4 Hydraulic Gradient Consolidation Tests KH1 and KH2

Hydraulic gradient consolidation tests KH1 and KH2 were conducted with an initial density of 1.22 Mg/m^3 and height of 0.2 m. The slurry samples were allowed to complete self-weight consolidation, then a hydraulic gradient was applied by opening a drain at the base of the testing cell. During the hydraulic gradient consolidation, the overlying water level was maintained constant by the use of a constant head device (see Figures 3.11 and 3.12). A schematic diagram of the experimental setup for the hydraulic gradient consolidation test is shown in Figure 4.7.

4.4.1 Density and Excess Pore Pressure Profiles

Figure 4.8 shows an example of density and excess pore pressure profiles obtained from hydraulic gradient consolidation test KH1. After 354 hours of self-weight consolidation process (test KS4), the excess pore pressures were almost completely dissipated under self-weight stresses (see Figure 4.2(c)). Then, the base drainage was opened (see Figure 4.7)

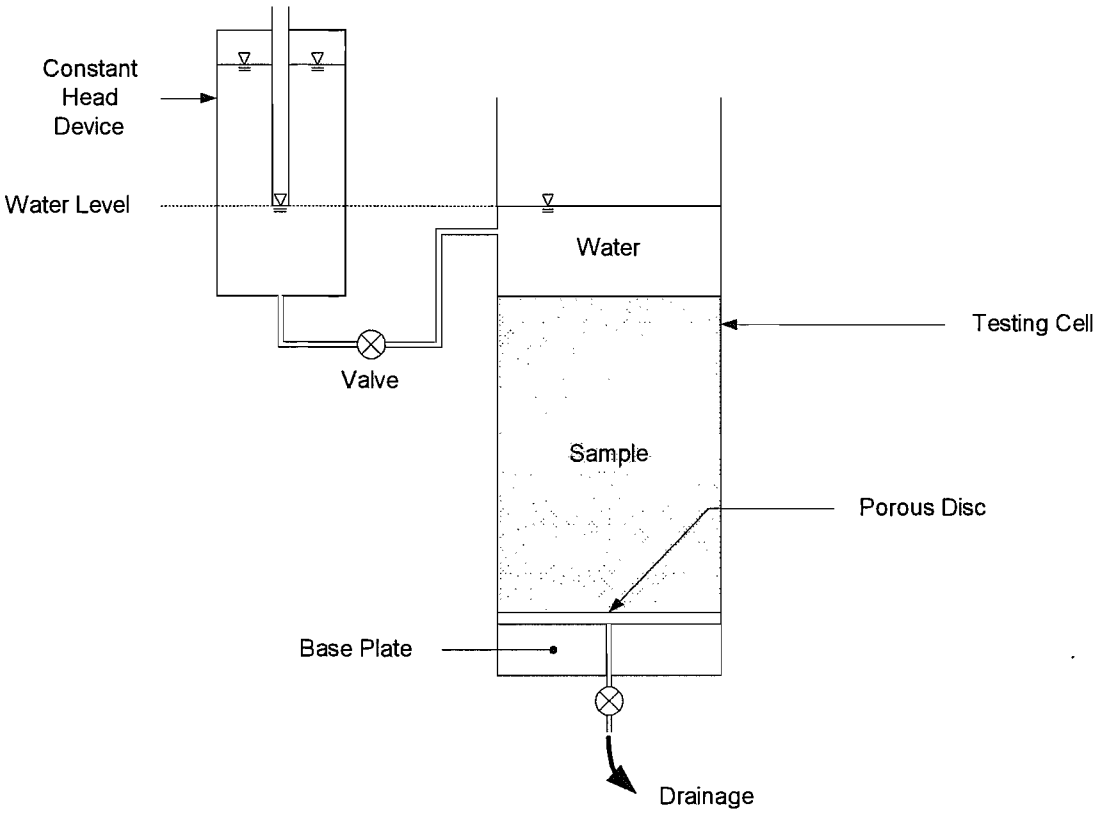

Figure 4.7 Experimental setup for hydraulic gradient consolidation test

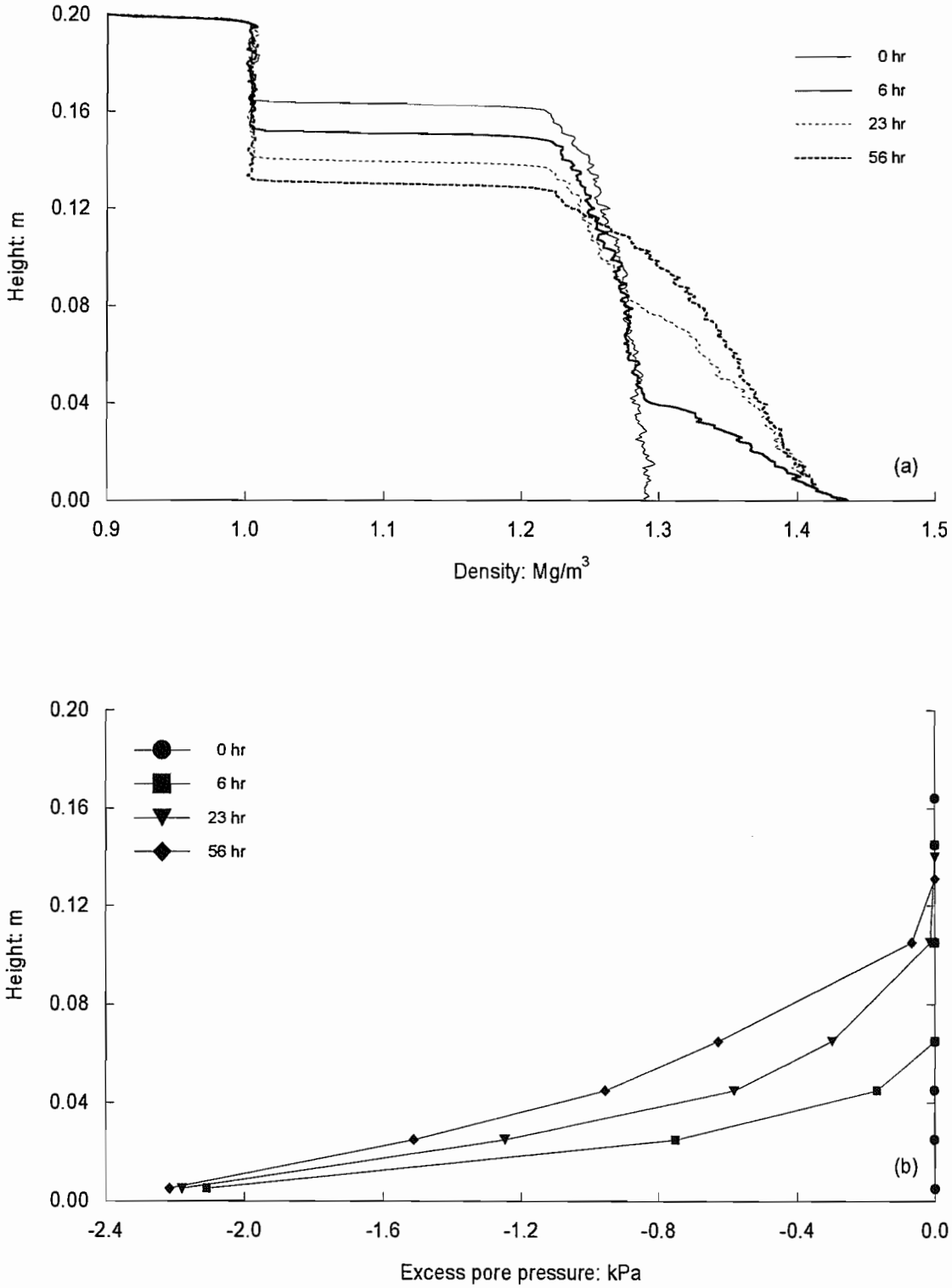

Figure 4.8 Hydraulic gradient consolidation, experiment KH1: (a) density profiles; (b) excess pore pressure profiles

and the sample was allowed to consolidate under a hydraulic gradient for about 3 days. The times marked refer to the periods elapsed following the opening of the drain. The 6 hour profile shown in Figure 4.8(b) indicates that the excess pore pressure measured at the base of the sample became negative of magnitude approximately -2.1 kPa due to the applied hydraulic gradient, consistent with the development of a density step up to about 0.04 m from the base as shown in Figure 4.8(a). The negative excess pore pressure at the base persisted until the end of the test whilst the negative values extended upwards through the bed. The density step developed under a hydraulic gradient is quite different in shape compared to that under the self-weight condition (see Figure 4.1(a)). It may be noted that the density at the base of the sample increased immediately to the maximum density on the application of a hydraulic gradient, resulting from the immediate increase in effective stress. This could cause changes in micro structure of soil sample particularly for very soft clays. This will be further discussed in the following section. A similar behaviour can also be seen in test KH2. Density and excess pore pressure profiles for test KH2 are shown in Figure 4.9.

4.4.2 Effective Stress and Void Ratio Relationship

Figure 4.10 presents typical effective stress and void ratio relationship for hydraulic gradient consolidation from tests KH1 and KH2. In contrast to the self-weight experiments, there was very high gradient of pore pressure particularly in the upper part of the sample, so that linear interpolation could give misleading results. Thus, the individual points plotted in Figure 4.10 correspond to the positions of the pore pressure ports. The 0 hour e-σ_v' points represent the soil sample after the self-weight consolidation was completed. It can be seen from the 6 hour data points in Figure 4.10(a) that the consolidation process under hydraulic gradient starts from the base of the sample, whilst the rest of the sample remains in the self-weight stage; the data points between 0.4 and 1.6 kPa in effective stresses indicate hydraulic gradient consolidation, and those less than 0.4 kPa represent the self-weight consolidation. The representative compression curves shown in Figure 4.10 include the data points obtained from hydraulic gradient consolidation only. From the representative curves, it may be noted that the stress-strain relationship under hydraulic gradient is slightly different from that under self-weight condition; the void ratio in the former case is lower than in the latter for effective stresses lower than 0.4 kPa. This pattern is consistent with a collapse of microstructure under the comparatively large effective stress gradient due to the applied water flow. Similar behaviour has been reported by Sills (Unpublished report to Rijkwaterstaat).

Those e-σ_v' points obtained from hydraulic gradient consolidation tests (KH1 and KH2) are shown in Figure 4.11, by comparison with the representative compression curve

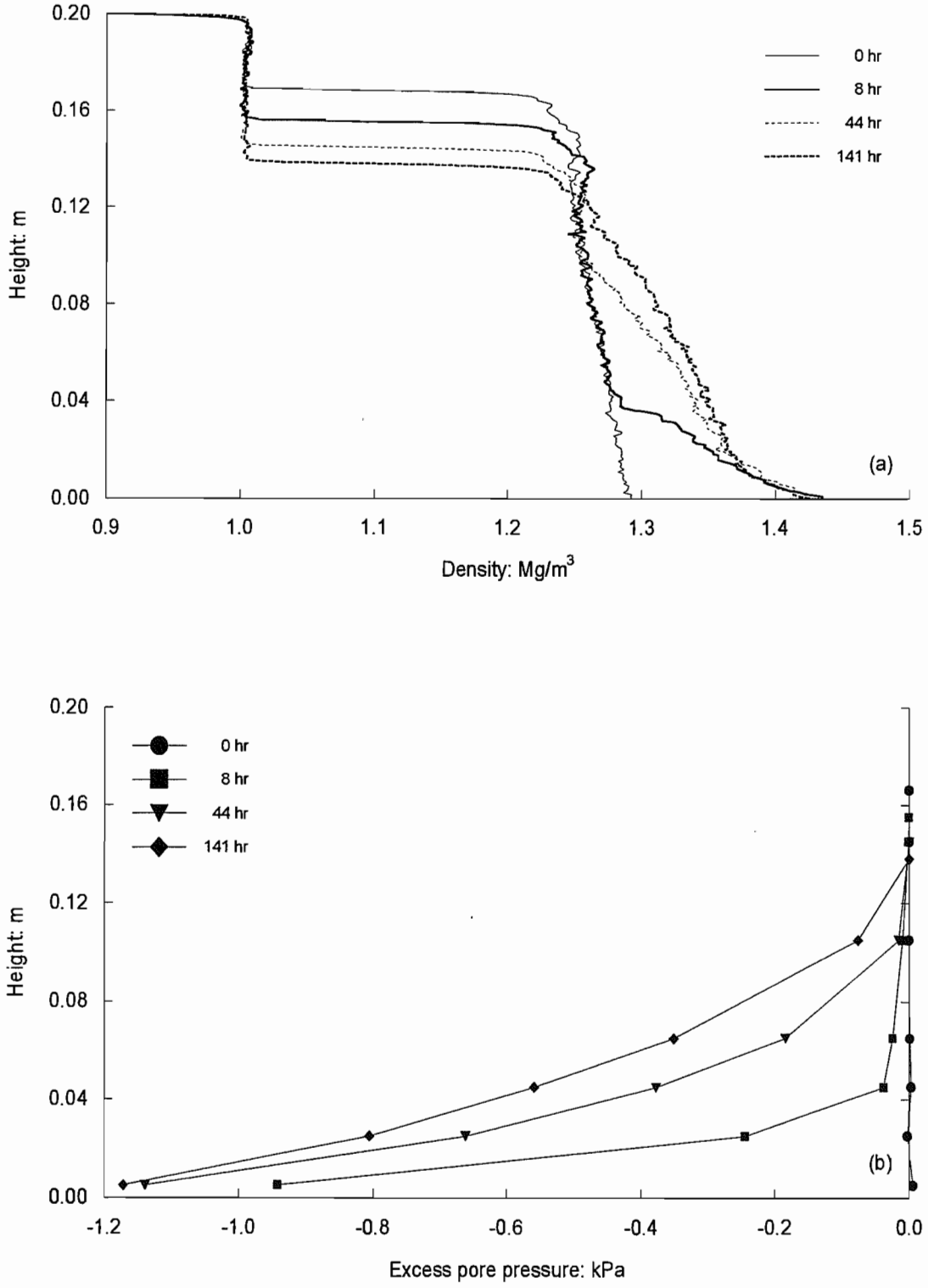

Figure 4.9 Hydraulic gradient consolidation, experiment KH2: (a) density profiles; (b) excess pore pressure profiles

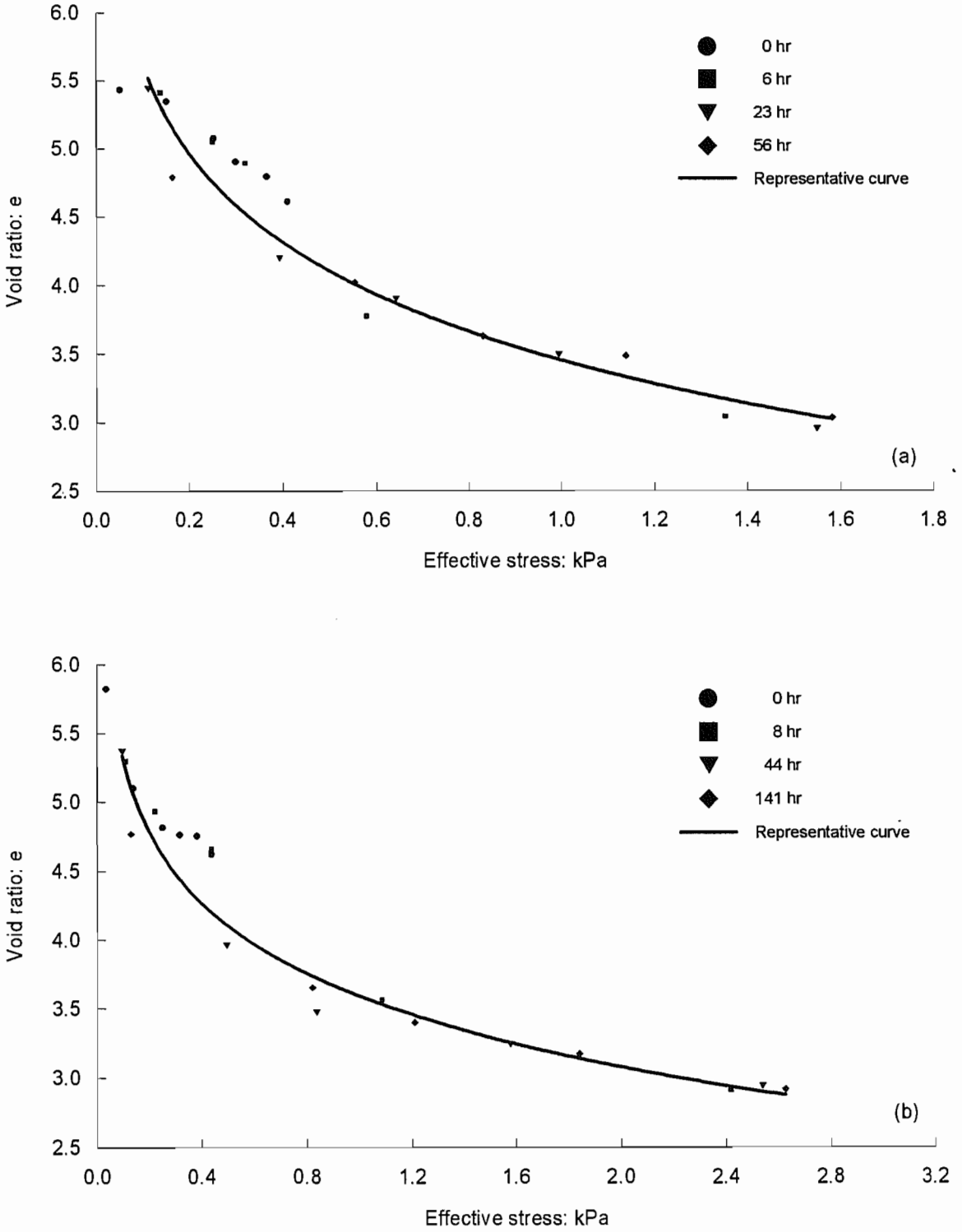

Figure 4.10 Effective stress and void ratio relationship: (a) experiment KH1; (b) experiment KH2

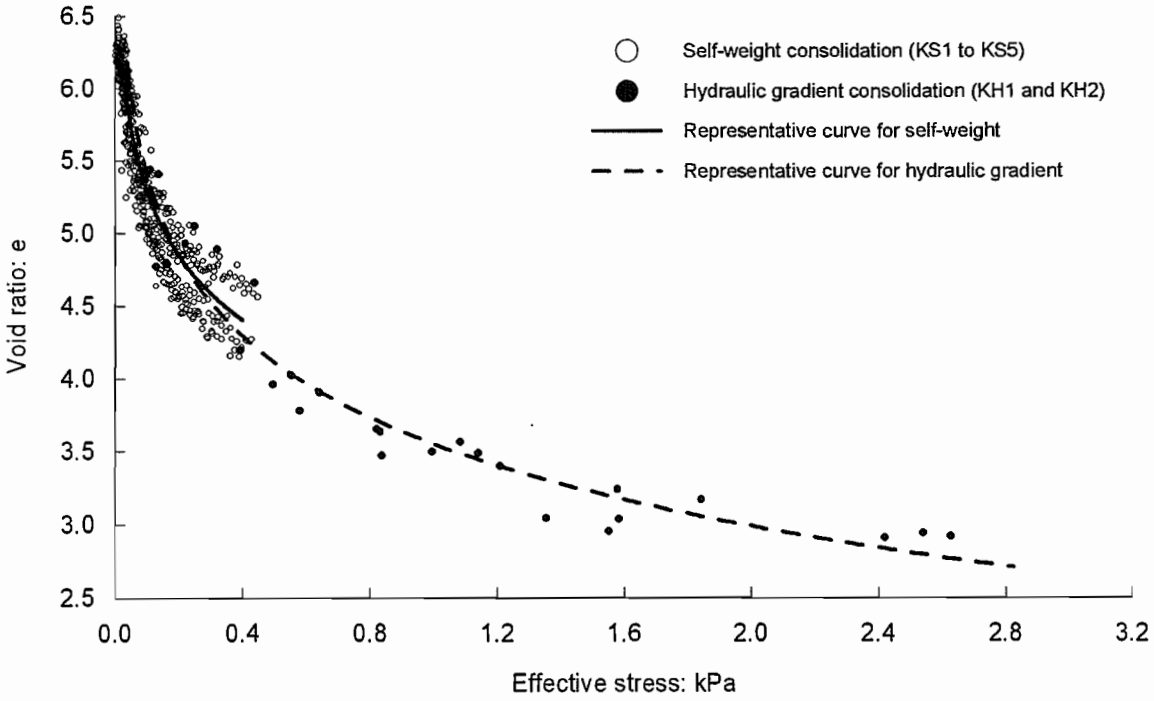

Figure 4.11 Effective stress and void ratio relationship for self-weight (KS1 to KS5) and hydraulic gradient consolidation (KH1 and KH2)

and data points obtained from self-weight consolidation tests (KS1 to KS5). It can be seen that the data points under a hydraulic gradient follow an extended consolidation curve, which is slightly steeper in gradient than the self-weight one, with an increase in effective stresses up to 2.8 kPa and a decrease in void ratio to a value less than 3.

4.5 Electrokinetic Consolidation Tests KE1 to KE4

Test KE1, conducted with an initial density of 1.2 Mg/m^3 and height of 0.2 m, was intended to check the performance of the electrokinetic cell (Section 3.2) in reducing gas penetration into the soil sample during the electrokinetic process. In order to investigate soft soil behaviour under the influence of different electric field strengths, sets of electrokinetic consolidation tests KE2, KE3, and KE4 were further carried out with an initial density of 1.22 Mg/m^3 and height of 0.2 m, and subjected to electric field strengths of 10, 20, and 30 V respectively.

4.5.1 Density and Excess Pore Pressure Profiles

Figure 4.12 shows density and excess pore pressure profiles from electrokinetic consolidation test KE1. An electric field of 10 V was applied to the sample immediately after placing in the testing cell. As shown in Figure 4.12(a), the initial slurry density with zero electrical potential was uniform throughout the soil sample. The 7 and 12 hour density profiles show that the density at the top and bottom of the sample increased rapidly after the application of electric field. The corresponding excess pore pressure profiles shown in Figure 4.12(b) demonstrate that a rapid reduction occurred in the base 0.04 m of the sample whereas the excess pore pressures in the rest of the soil decreased steadily. During this period, the applied electrical current decreased continuously (see Figure 4.24).

Several density and excess pore pressure profiles for each of tests KE2 to KE4 are shown in Figures 4.13 to 4.15. A similar pattern of consolidation can be seen in these tests with the dissipation process of excess pore pressure dependent on the applied electric field strength; the higher the applied electric field strength, the faster the dissipation of excess pore pressure.

The most surprising feature of the soil behaviour under the electric field is that the density near the soil surface (cathode region) increased considerably. It can be noted in Figure 4.12(a) that the density at the top of the soil sample significantly increased with little apparent reduction in excess pore pressure, which is in contrast to the expectation as described by Mitchell (1993). The developing denser layer near the soil surface may result from either the downward movement of clay particles by the effect of electrophoresis or the interaction between clay particles due to the change of soil pH. This will be further discussed in Section 4.9 in terms of variations of soil pH and voltage gradient. The denser layer developed at the surface also propagated towards the base of the soil, remaining at the peak density of approximately 1.26 Mg/m^3.

Another characteristic feature of electrokinetic consolidation is a rapid reduction in excess pore pressures in the top half of the sample after a certain period demonstrated by the 30 hour excess pore pressure profile shown in Figure 4.12(b). Thereafter, the excess pore pressures in the top half of the sample became even more negative than those in the base half (see the 35 hour excess pore pressure profile in Figure 4.12(d)). The same effect can be seen in the corresponding density profile where the density in the cathode region has become greater than that in the anode region as shown in Figure 4.12(c). The 30 and 35 hour density profiles indicate that the distribution of density was directly related to the corresponding negative excess pore pressures; the reduction of excess pore pressures caused the increase in density via the increase of effective stresses. The 34, 18, and 12 hour profiles for tests KE2, KE3, and KE4 also show that the excess pore pressures in the

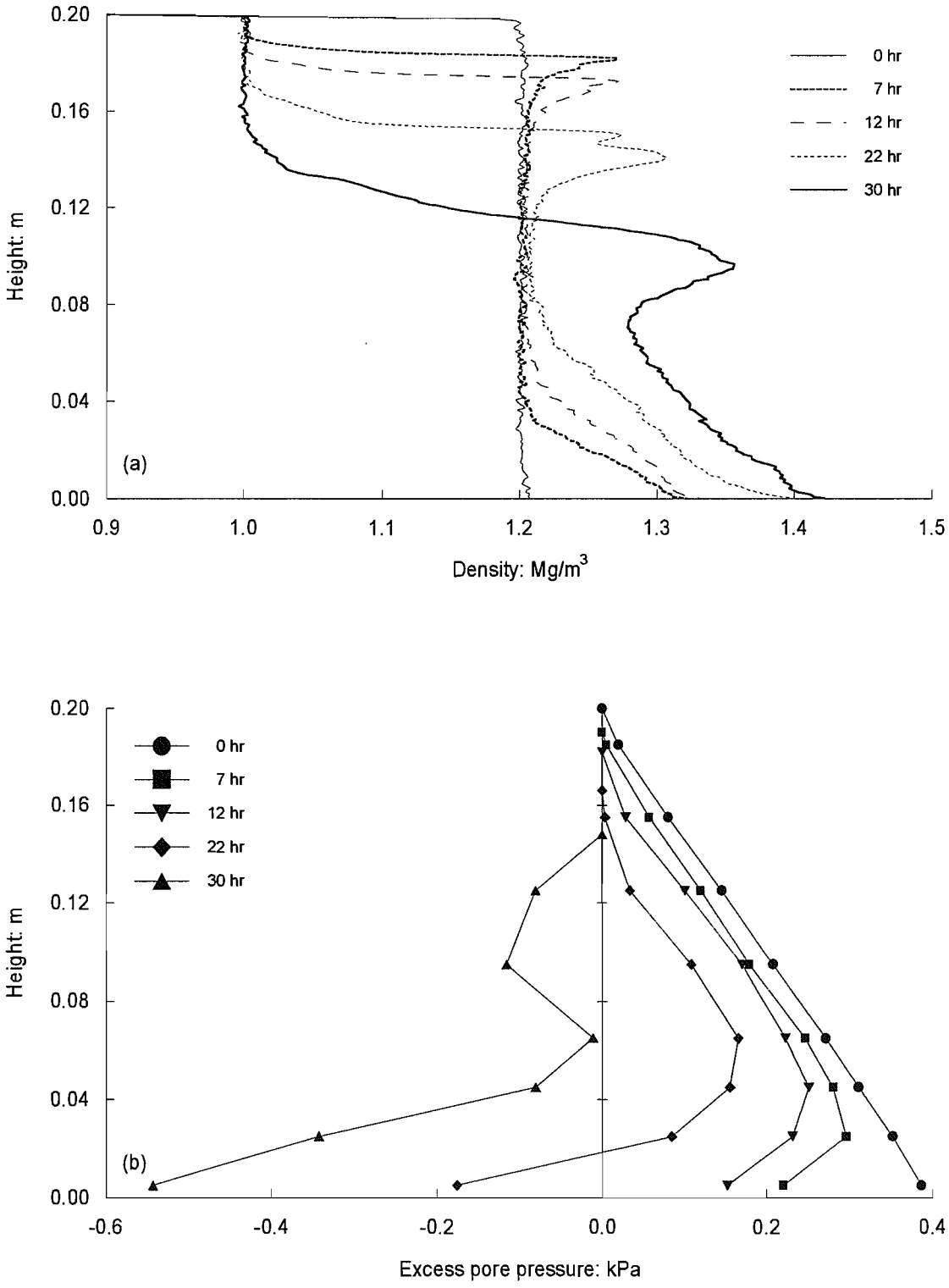

Figure 4.12 Electrokinetic consolidation, experiment KE1: (a) density profiles; (b) excess pore pressure profiles

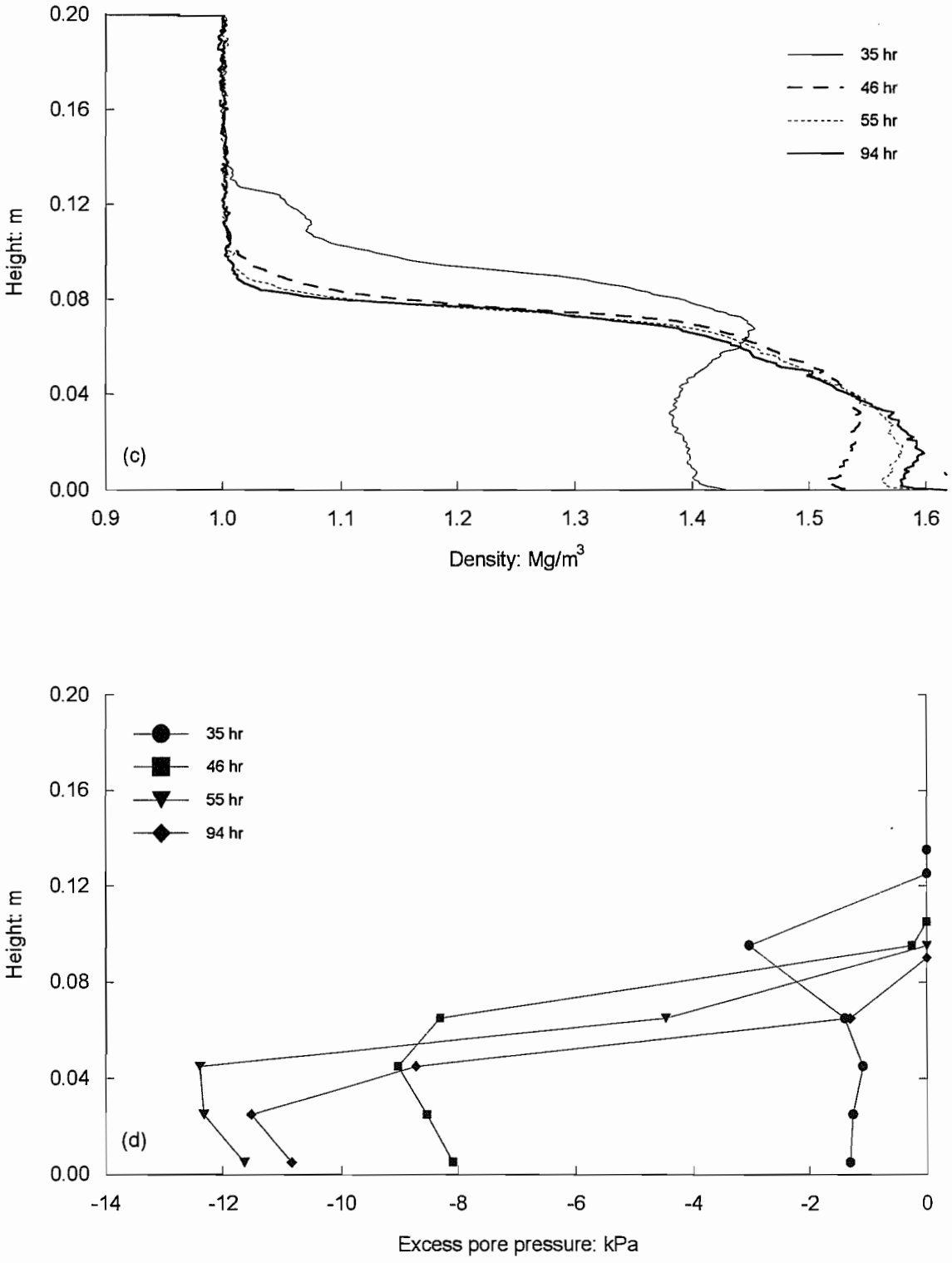

Figure 4.12 Continued: (c) density profiles; (d) excess pore pressure profiles

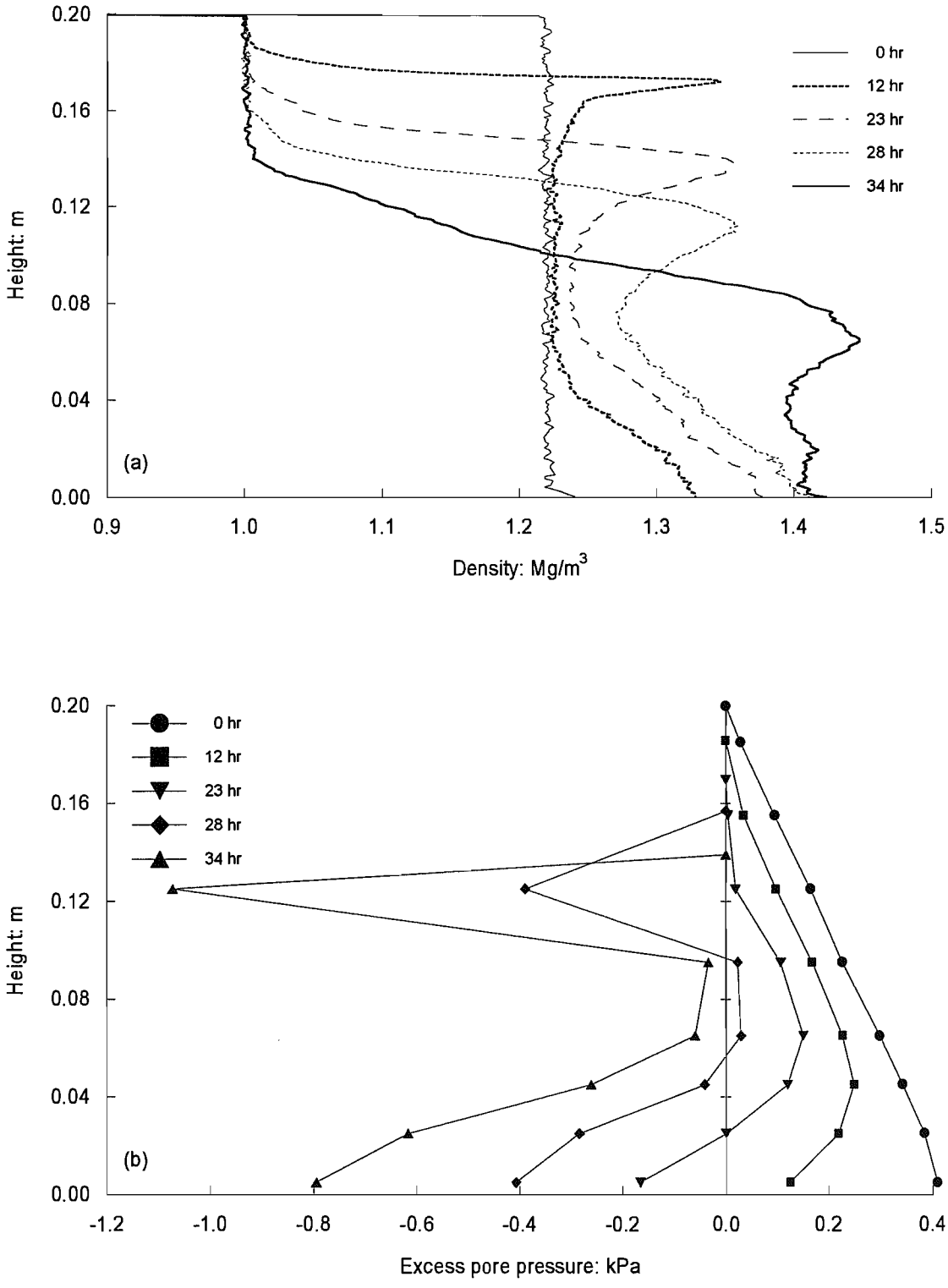

Figure 4.13 Electrokinetic consolidation, experiment KE2: (a) density profiles; (b) excess pore pressure profiles

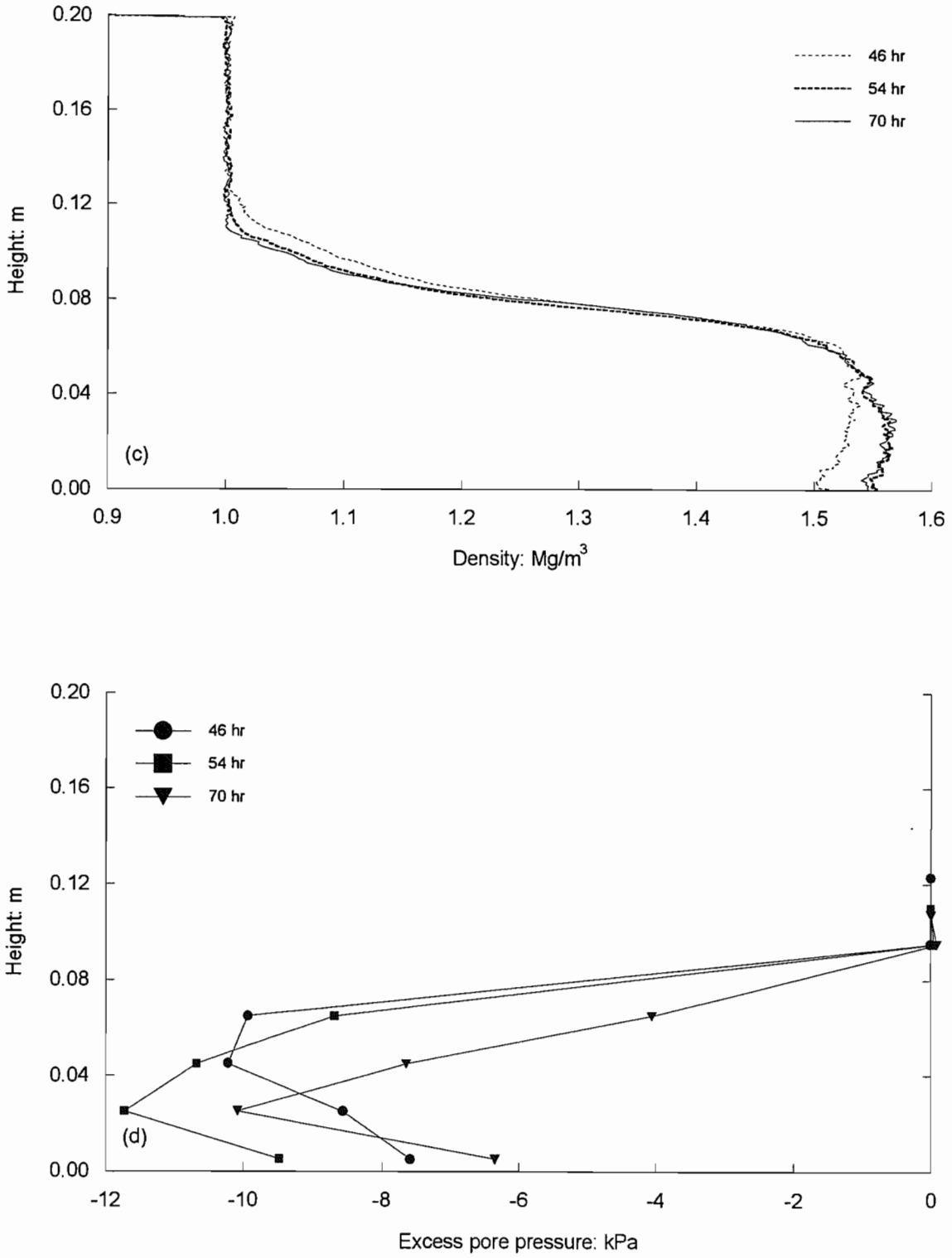

Figure 4.13 Continued: (c) density profiles; (d) excess pore pressure profiles

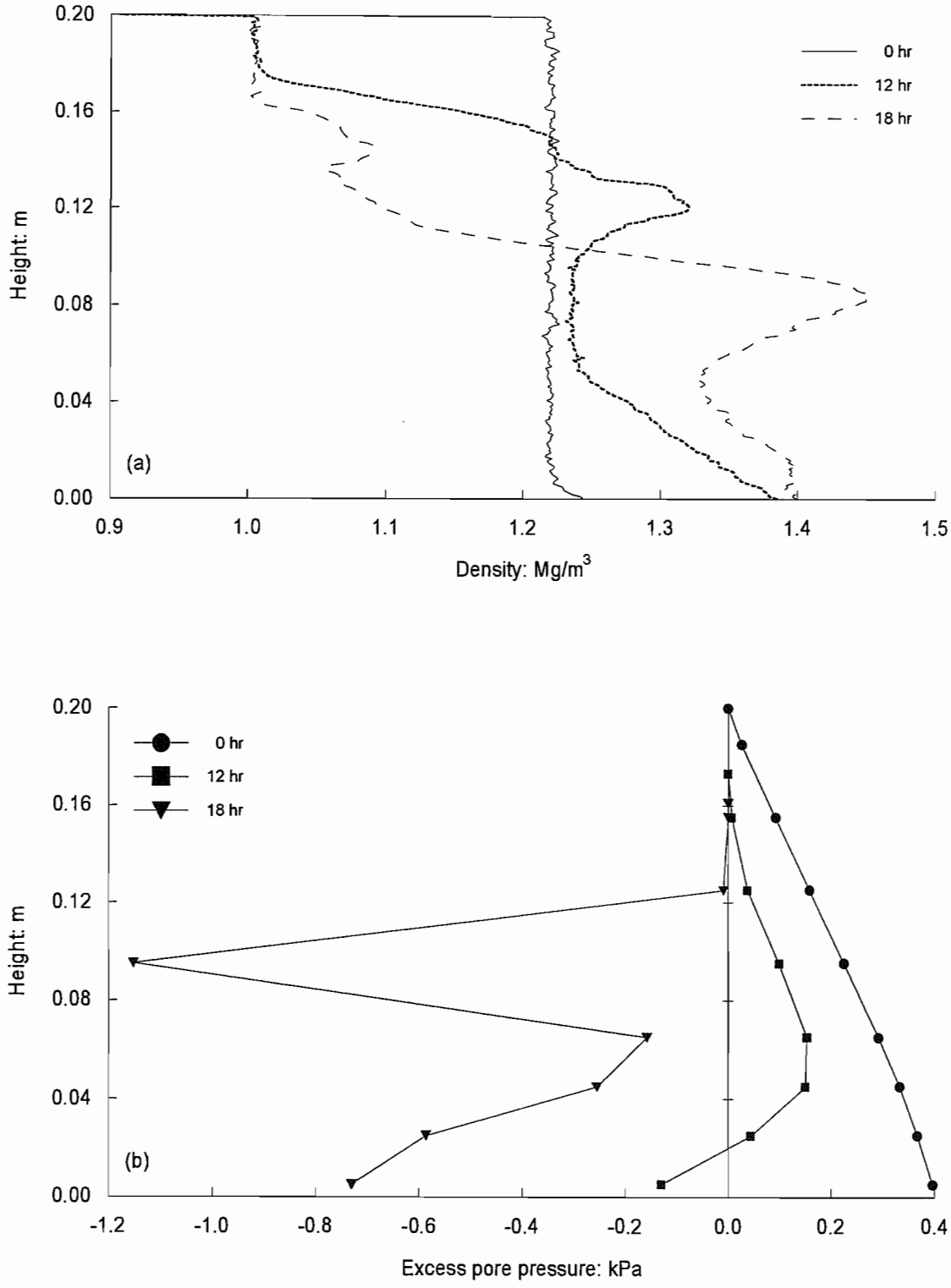

Figure 4.14 Electrokinetic consolidation, experiment KE3: (a) density profiles; (b) excess pore pressure profiles

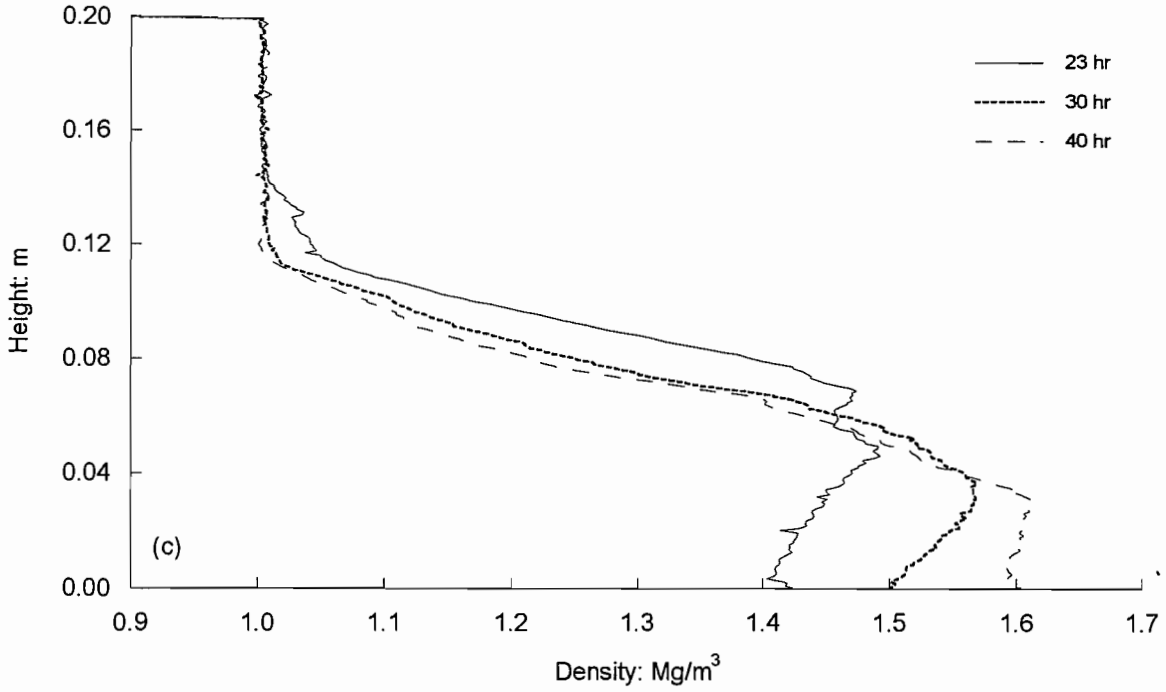

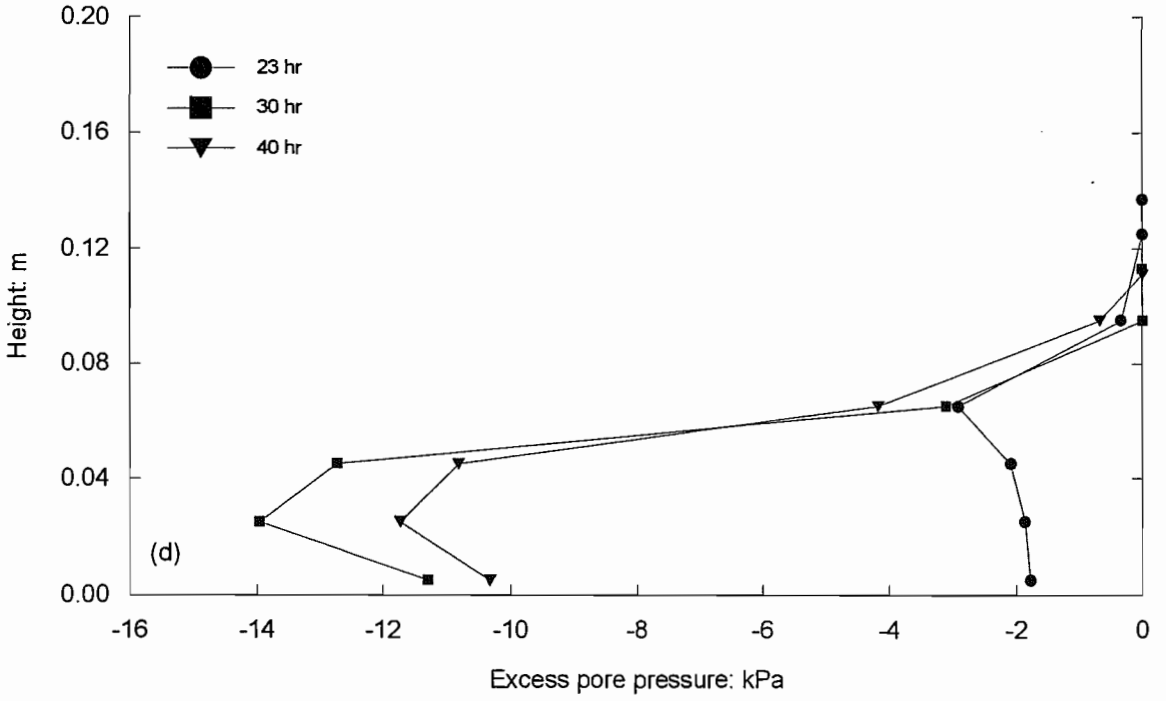

Figure 4.14 Continued: (c) density profiles; (d) excess pore pressure profiles

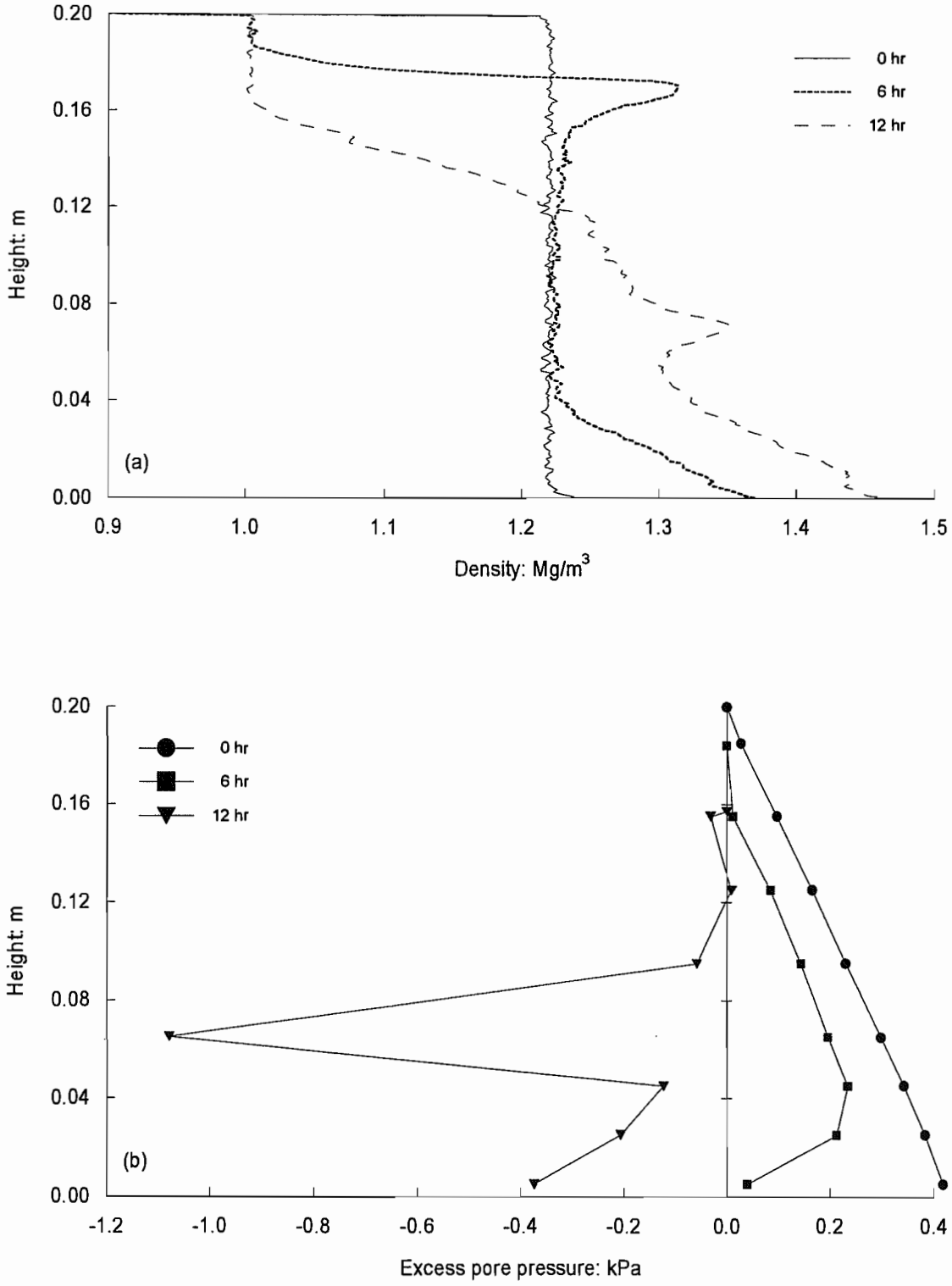

Figure 4.15 Electrokinetic consolidation, experiment KE4: (a) density profiles; (b) excess pore pressure profiles

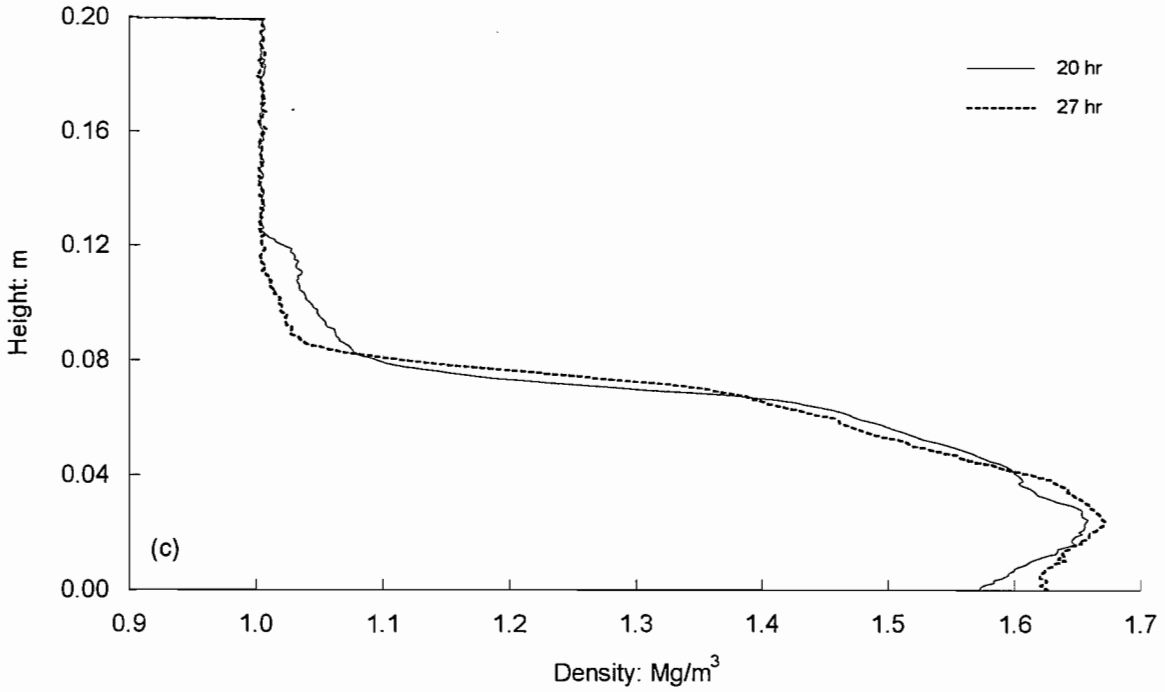

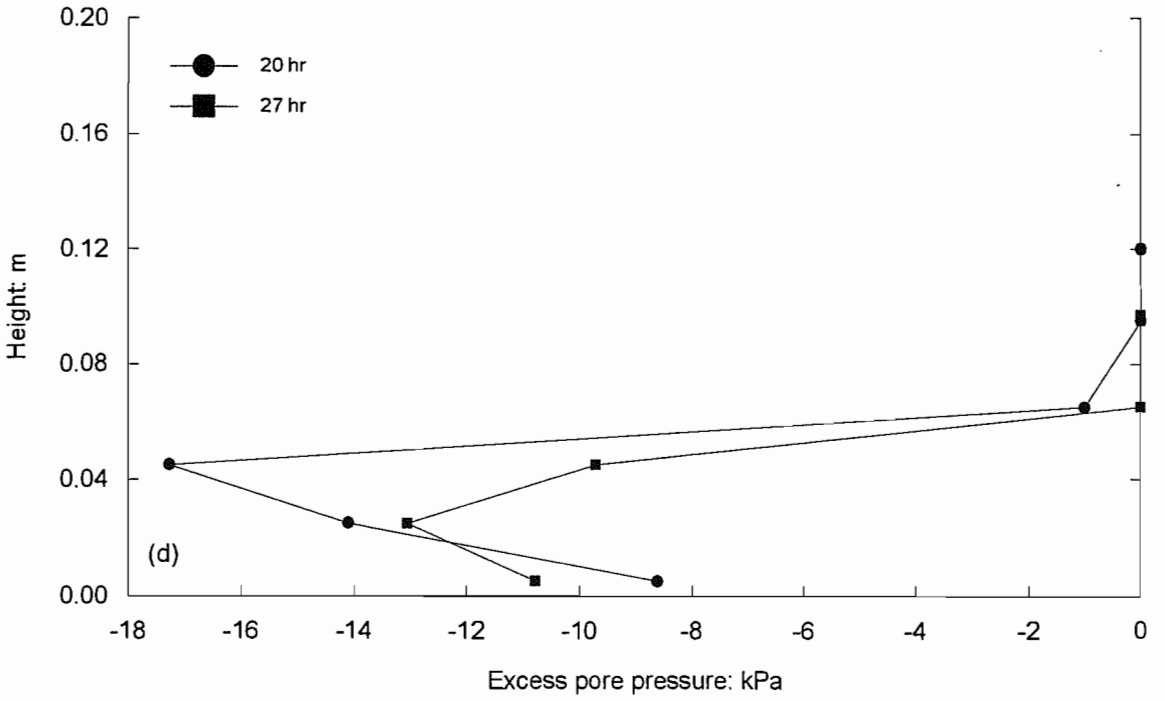

Figure 4.15 Continued: (c) density profiles; (d) excess pore pressure profiles

cathode region became more negative than those in the anode region as shown in Figures 4.13, 4.14, and 4.15, respectively.

It can be seen in Figure 4.12(d) that the negative excess pore pressures then became more negative throughout the soil bed, and extended to a maximum value of approximately -12 kPa after 55 hours of the electrokinetic process. A similar pattern can also be seen in tests KE2, KE3, and KE4; the 54, 30, and 20 hour profiles shown in Figures 4.13, 4.14, and 4.15 indicate the negative excess pore pressures extending to approximately -12, -14, and -18 kPa, respectively. It is suggested that the magnitude and developing rate of negative excess pore pressures are directly related to the applied electric field strength. The 94 hour excess pore pressure profile in Figure 4.12(d) shows that eventually the negative excess pore pressures developed by 55 hours of the electrokinetic process became slightly more positive. This change in pore pressures was caused by a reduction of the applied electrical current (see Figure 4.24). This will be further examined in Section 4.5.4 by considering the variation of electrical current.

The electric field for test KE1 was removed after 98 hours, and the final density and pore pressure measurements were taken a further 48 hours after switching off the electric field. The 146 hour excess pore pressure profile shown in Figure 4.16(b) indicates that the negative excess pore pressures became close to zero, leading to swelling throughout the soil sample as shown in Figure 4.16(a); the negative excess pore pressures had almost dissipated under gravity after the removal of electric field. A similar pattern of soil swelling occurring after the electrokinetic process in tests KE2 to KE4 can also be seen in Figure 4.17; the higher the electric field strength had been, the greater the swelling.

Final density profiles from electrokinetic consolidation tests are shown in Figure 4.18, by comparison with those obtained from self-weight and hydraulic gradient consolidation tests. The first profile shows an example of the initial input density, the second presents the density of the soil sample after the completion of self-weight consolidation (test KS1), the third shows the final density profile under a hydraulic gradient (test KH1), and the last three show density profiles after the electrokinetic process (tests KE2, KE3, and KE4). As seen, the volume change of the soil sample treated by electrokinesis was much greater than that achieved under self-weight stresses alone, with higher densities resulting from higher electric fields. The density slope at the surface (between 0.07 and 0.11 m in height) is partly due to an uneven settlement across the column, as discussed in the following section.

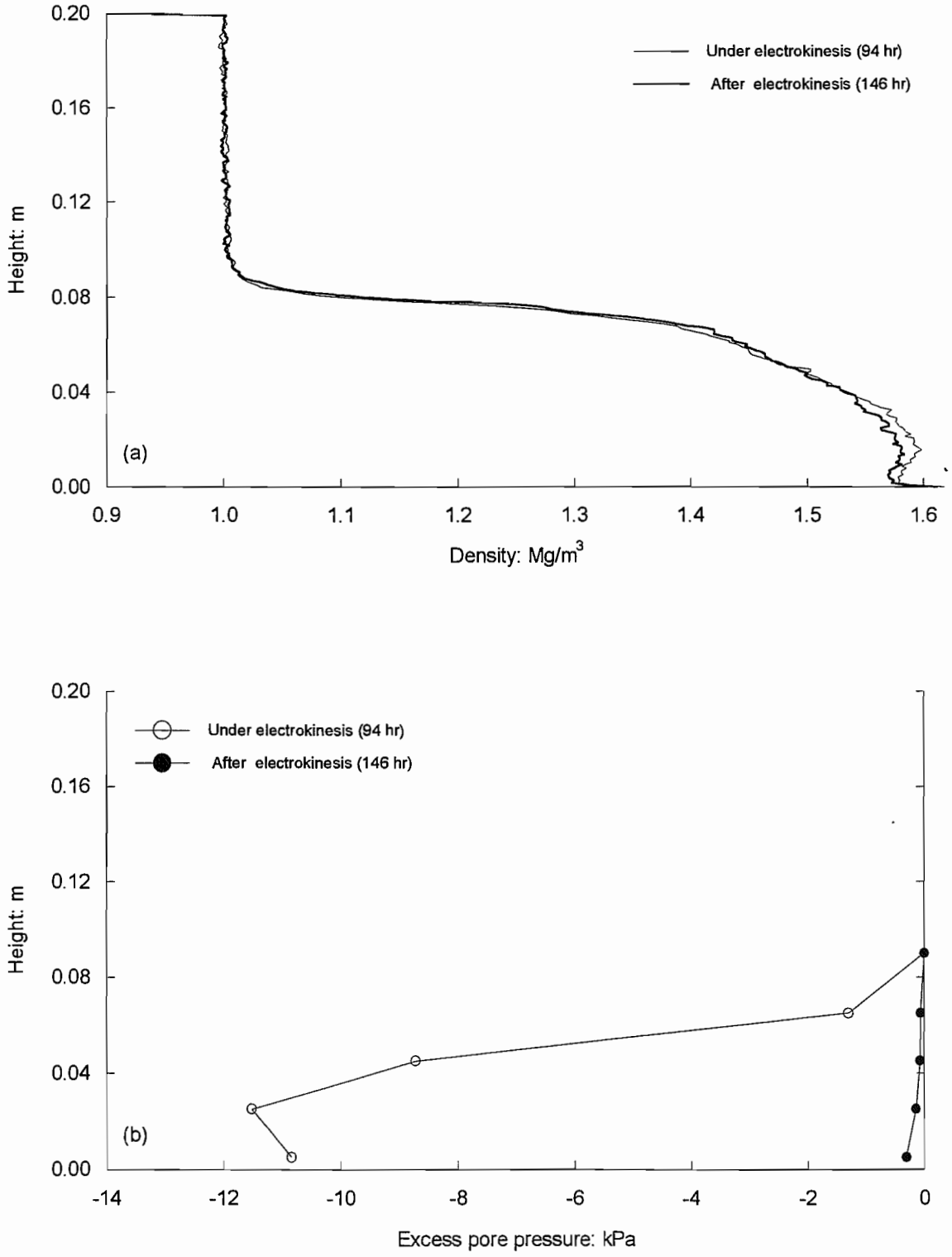

Figure 4.16 Swelling after the electrokinetic process, experiment KE1: (a) density profiles; (b) excess pore pressure profiles

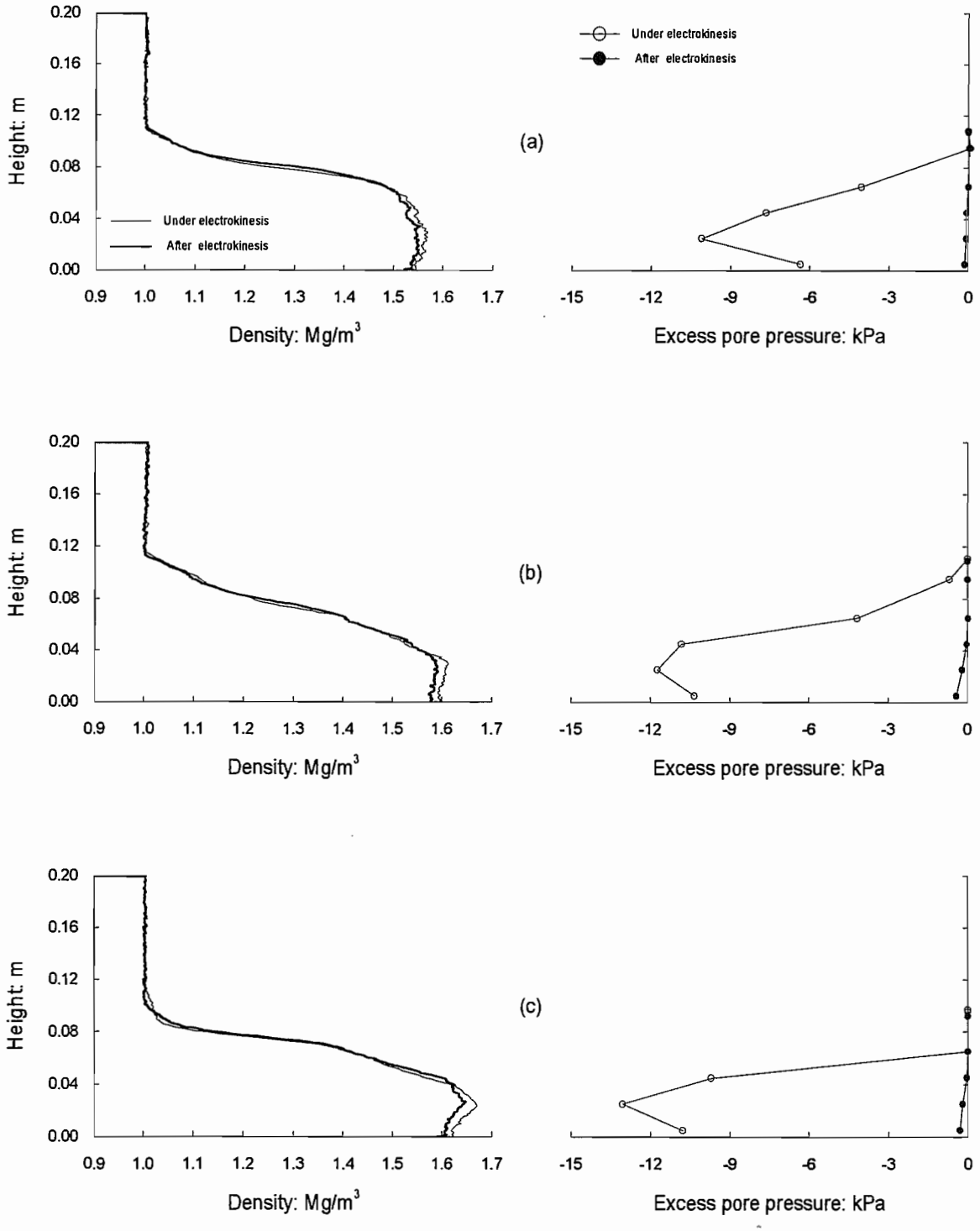

Figure 4.17 Swelling after the electrokinetic process: (a) experiment KE2; (b) experiment KE3; (c) experiment KE4

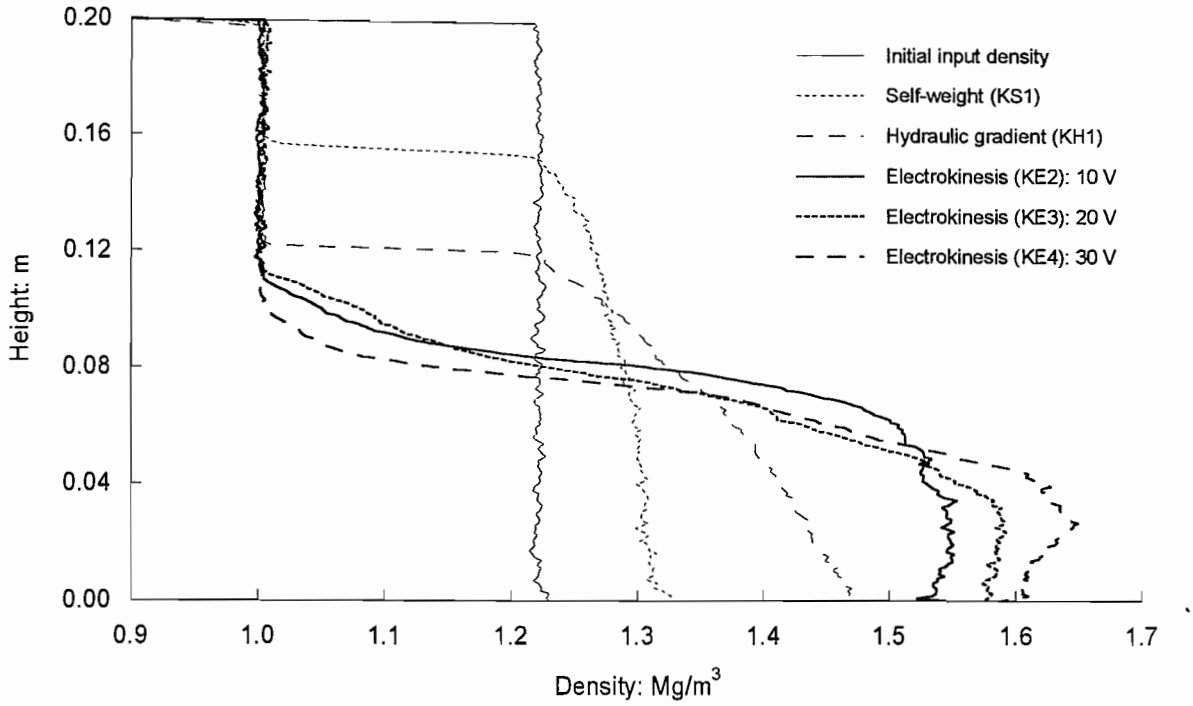

Figure 4.18 Comparison of final density profiles for self-weight, hydraulic gradient, and electrokinetic consolidation, experiments KS1, KH1, KE2, KE3, and KE4

4.5.2 Surface Settlement

It was noted that a visually different layer, a brighter white colour than the normal white of the kaolin sample, formed at the soil surface during the early stage of the electrokinetic process and disappeared in the later stage; the overlying water was colourless. Figure 4.19 shows examples of the soil appearance observed during electrokinetic consolidation test KE1.

The overlying water is illustrated as (A), the layer developed at the soil surface as (B), and the soil sample as (C). The layer (B) is most likely to be a chemical formation since the density is much lower than the initial input density as shown in Figure 4.19(a). The soil surface did not drop evenly during the electrokinetic process, resulting in a sloping surface; the surface gradient became greater with time as shown in Figure 4.19(b). In the later stage of electrokinetic process, the layer (B) disappeared and the surface gradient became smaller as shown in Figure 4.19(c). As the X-ray density profiles represent an average value at any section of the sample, the gradient indicated in density profiles (see Figures 4.19(b) and (c)) is not true density but an average of the soil and water densities.

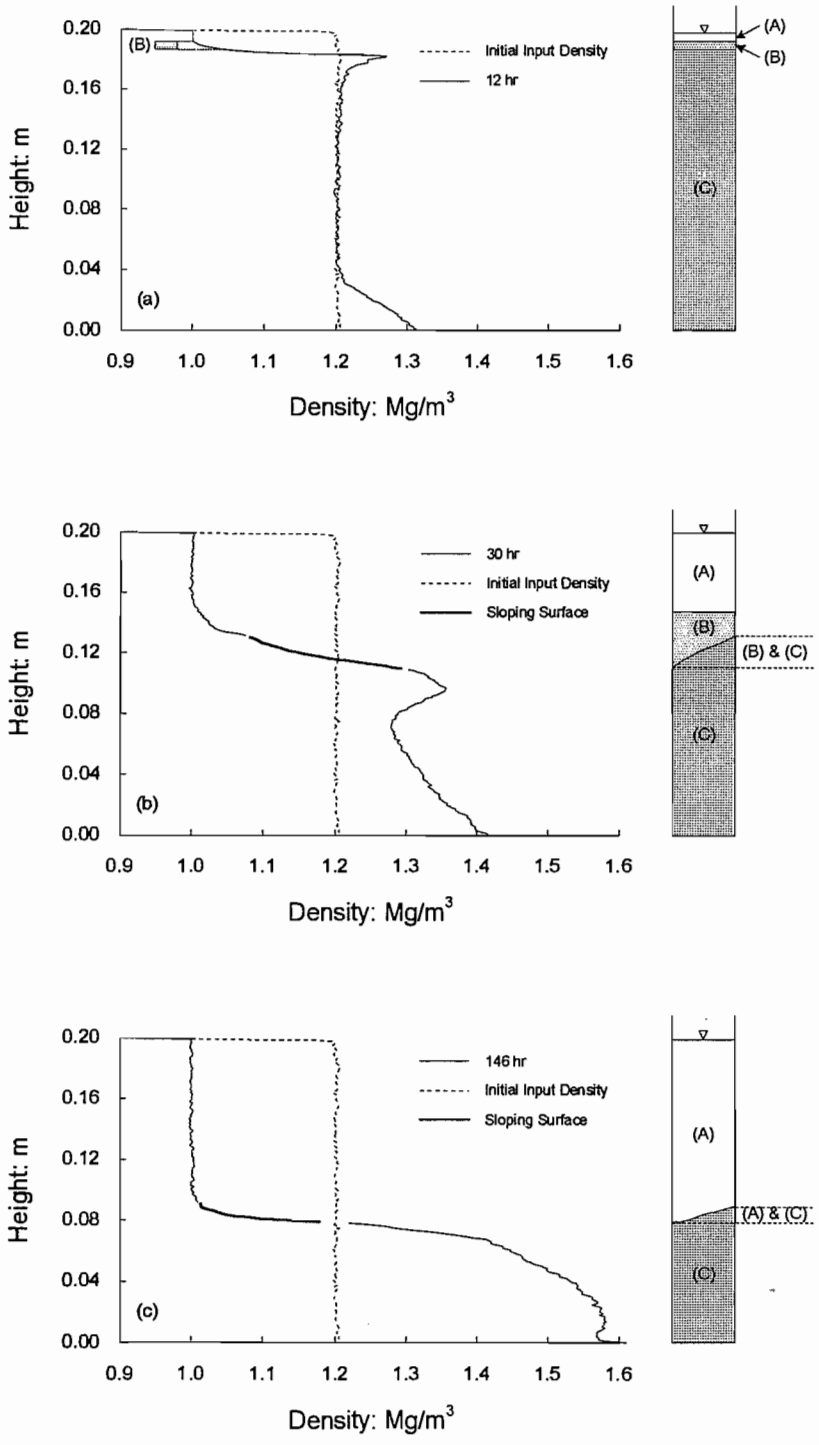

Figure 4.19 Soil appearance during the electrokinetic process, experiment KE1

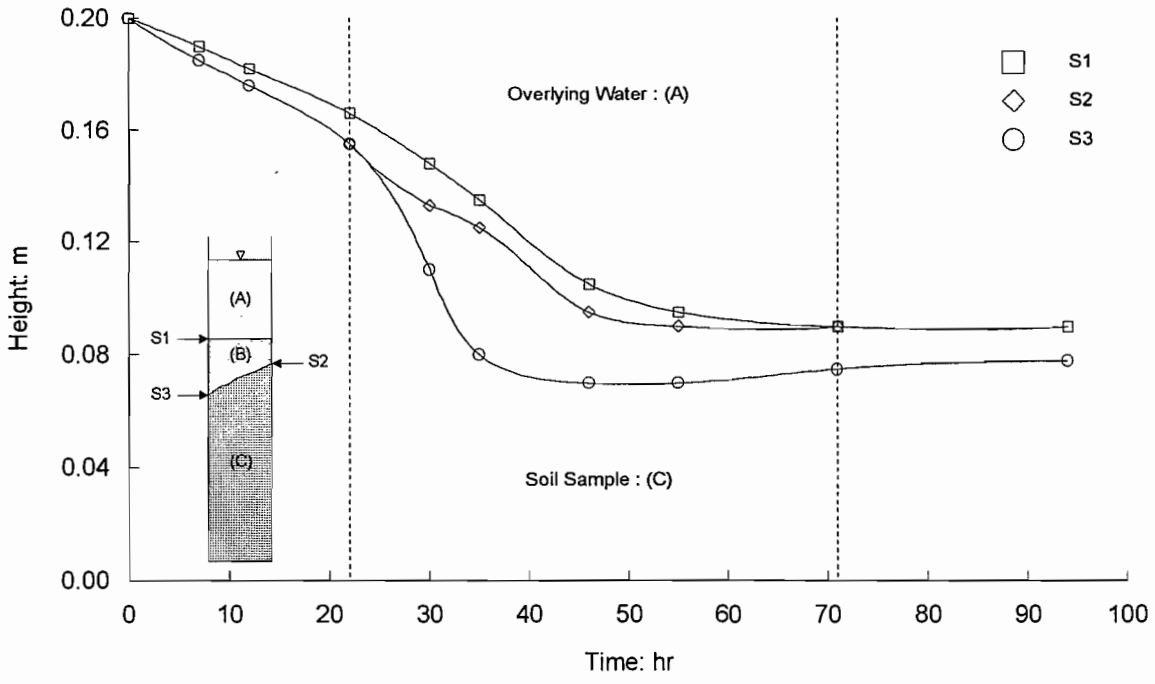

Figure 4.20 Surface settling behaviour under electrokinesis, experiment KE1

Figure 4.20 presents an example of surface settling behaviour during electrokinetic consolidation from test KE1. The surface settlement increased linearly during the first 22 hours of the electrokinetic process with the development of the layer (B). The surface settling rate increased considerably after 22 hours according to the increase of electrical current (see Figure 4.24). It can be seen that a slope developed at the soil surface and became greater with time; the slope developed at the surface is indicated by the difference between 'S2' and 'S3'. The layer (B) disappeared after 71 hours of the process, and the surface gradient became smaller (see also Figure 4.19(c)).

The surface settlement observed in tests KE2 to KE4 under the different electric field strengths are shown in Figure 4.21, by comparison with the settlement under the self-weight condition (test KS1). The surface settlements shown in Figure 4.21(a) represent the surface 'S2' and those shown in Figure 4.21(b) the surface 'S3' as given in Figure 4.20. The surface settlements under the influence of electrokinesis were faster and greater than that under the self-weight condition, as already noted from the density profiles in the previous section. It can also be seen that the settling process under higher electric field strength occurred faster.

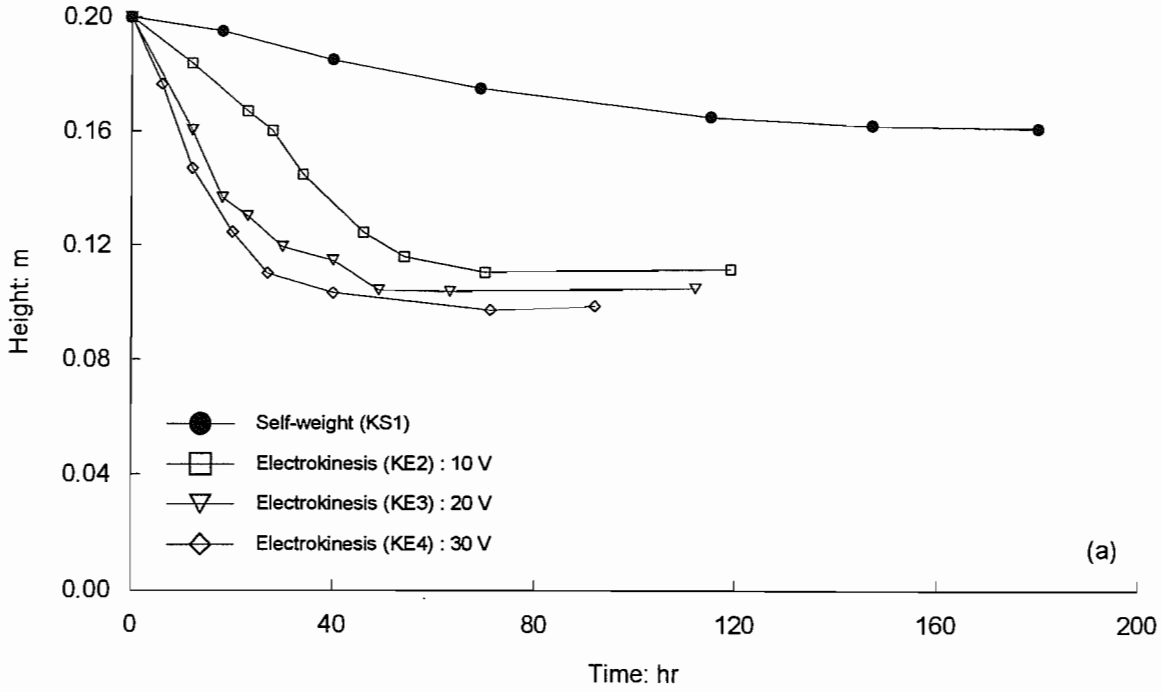

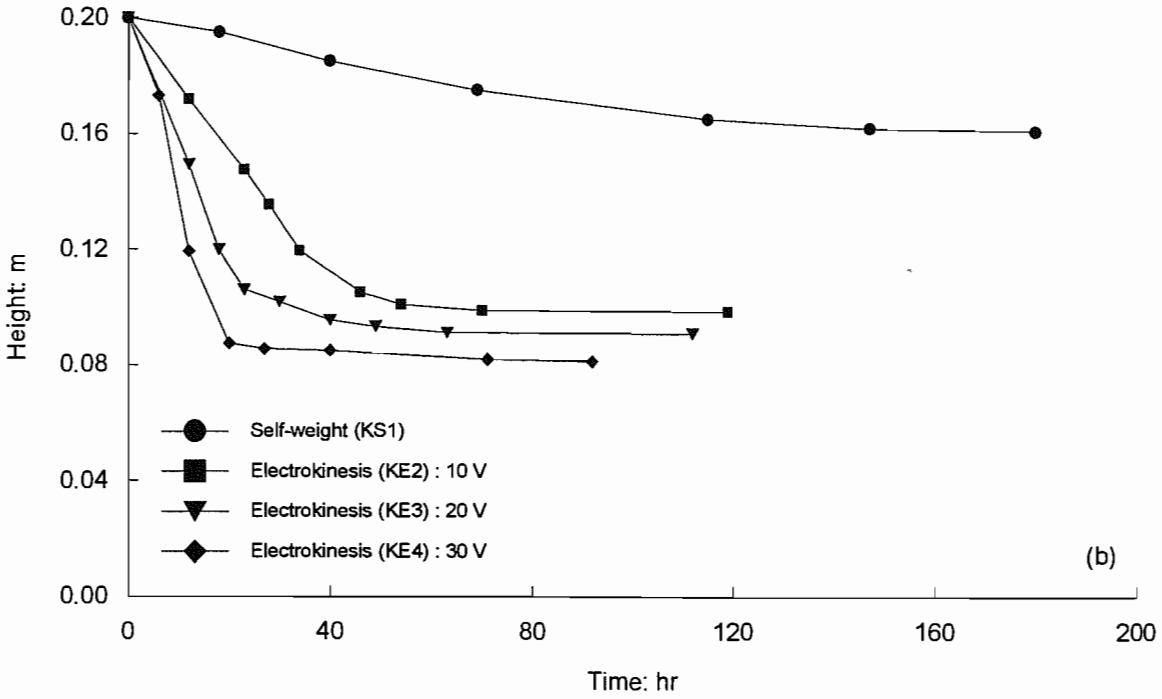

Figure 4.21 Surface settling behaviour under electrokinesis, experiments KE2 to KE4: (a) based on the upper level of soil surface; (b) based on the lower level of soil surface

4.5.3 Effective Stress and Void Ratio Relationship

Figure 4.22 shows typical effective stress and void ratio relationship for electrokinetic consolidation observed from test KE1. Note that the individual points correspond to the positions of the pore pressure ports. The solid line represents the consolidation path during the electrokinetic process whilst the dotted line indicates the subsequent swelling curve.

It can be seen that the e-σ_v' points follow a unique consolidation curve with an increase in effective stress and decrease in void ratio. This pattern of soil compression confirms that electrokinetic consolidation was controlled predominantly by the development of effective stress as for self-weight consolidation. After the removal of electric field, the 146 hour data points, the effective stresses decreased to less than 0.8 kPa and very small amounts of swelling occurred (see Figure 4.16(a)). Several effective stress and void ratio relationships for tests KE2 to KE4 are shown in Figure 4.23; a similar pattern of electrokinetic compression noted in test KE1 can also be seen in these tests.

4.5.4 Electrical Current and Voltage

Figure 4.24 shows the variation of electrical current with respect to time observed in test KE1, under a constant applied voltage of 10 V. For the first 12 hours, the electrical current continuously decreased to approximately 7 mA. The initial reduction of electrical current may result from the electrical resistance of soil slurry to the applied electric field as the initial ionic conductivity of the kaolin sample appears to be very low; the slurry sample initially acts as an insulator. As the applied electric field was fixed at 10 V, the electrical current decreased with the reduction of electrical conductivity. Although the electrical current was decreasing, consolidation process was continued as electrical current generated the water movement in the electric double layers (see Figure 4.12(a)). Thereafter, the electrical current increased to approximately 20 mA by 30 hours of the electrokinetic process.

It was observed that the initially clear water in the base chamber of the testing cell became 'Dark Yellow' between 12 and 30 hours of the electrokinetic process, and the gas generation at the electrodes became active. It appears that the water in the base chamber had become fully electrolysed. Thus, the electrical current increased as a result of the increase of electrical conductivity, resulting from the introduction of extra ions (H^+ and OH^- ions) produced by electrolysis. Consistently, the dissipation process of excess pore pressure observed during this period became relatively faster throughout the soil sample, compared to those measured for the first 12 hours of the electrokinetic process (see Figure 4.12(b)). As already noted, the excess pore pressures in the top half of the soil sample became negative during this period (see the 30 and 35 hour excess pore pressure profiles in Figures 4.12(b) and (d)).

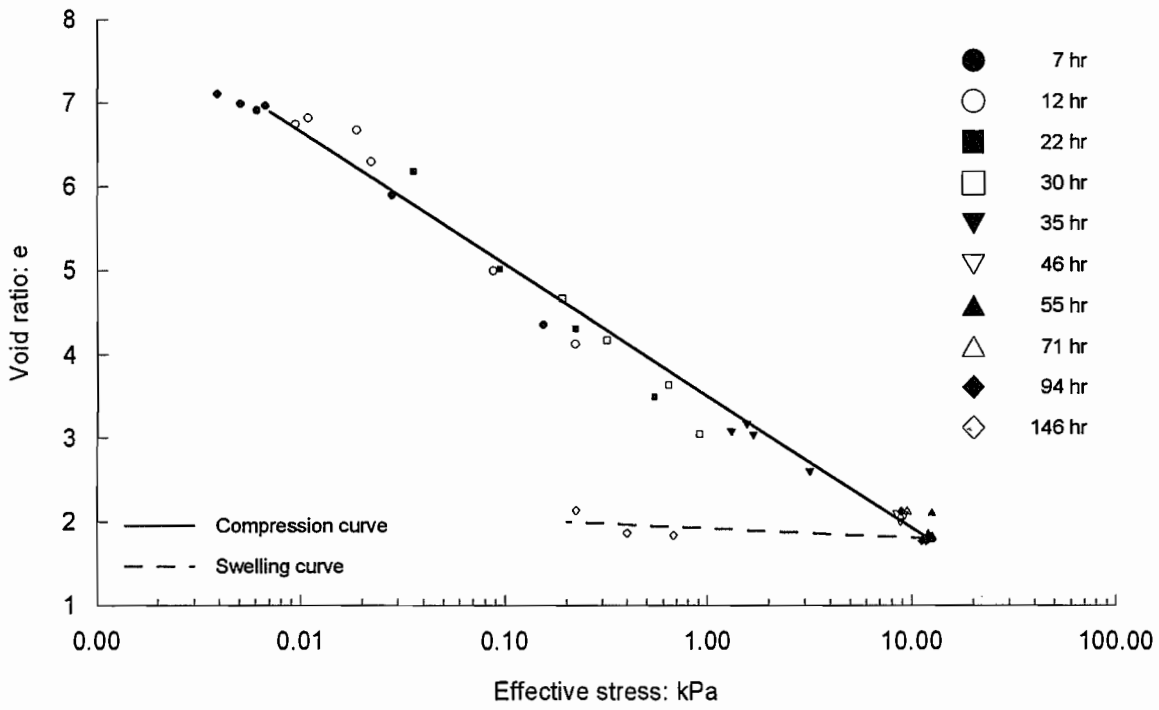

Figure 4.22 Effective stress and void ratio relationship for electrokinetic consolidation, experiment KE1

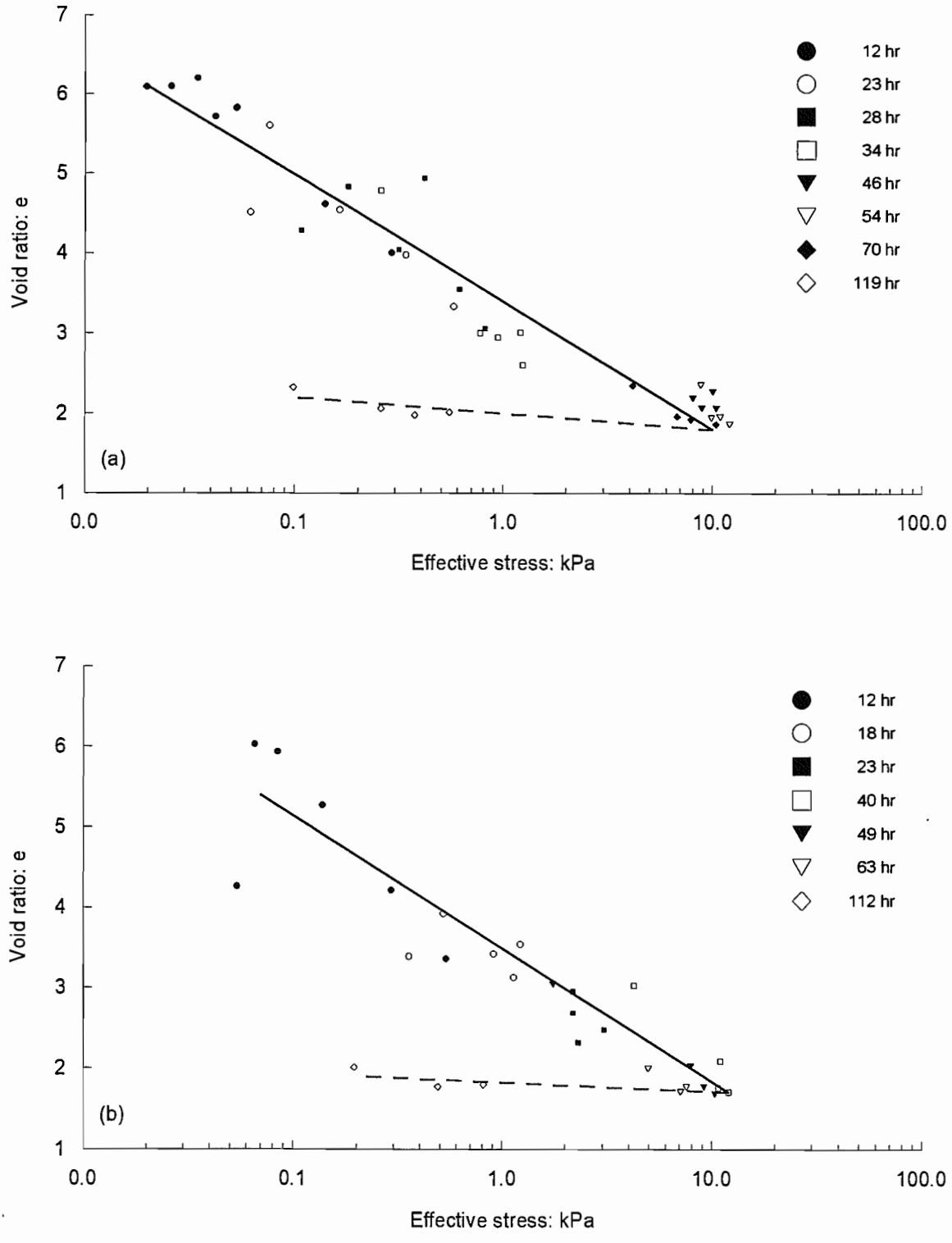

Figure 4.23 Effective stress and void ratio relationship for electrokinetic consolidation: (a) experiment KE2; (b) experiment KE3

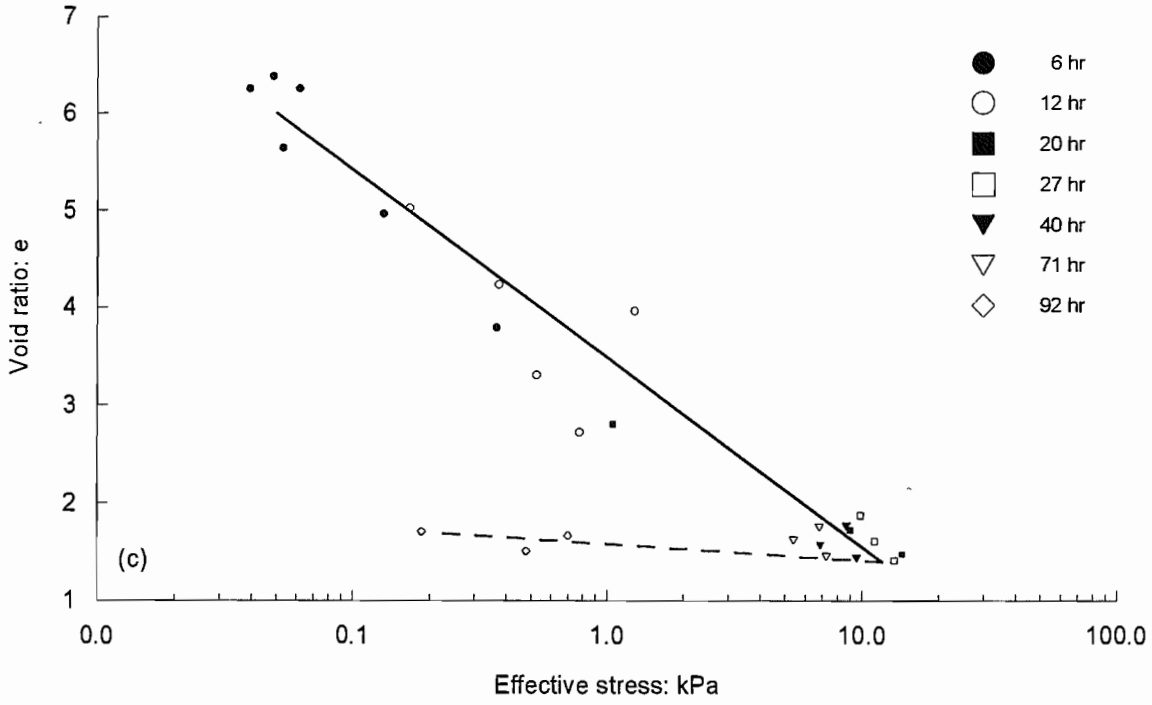

Figure 4.23 Continued: (c) experiment KE4

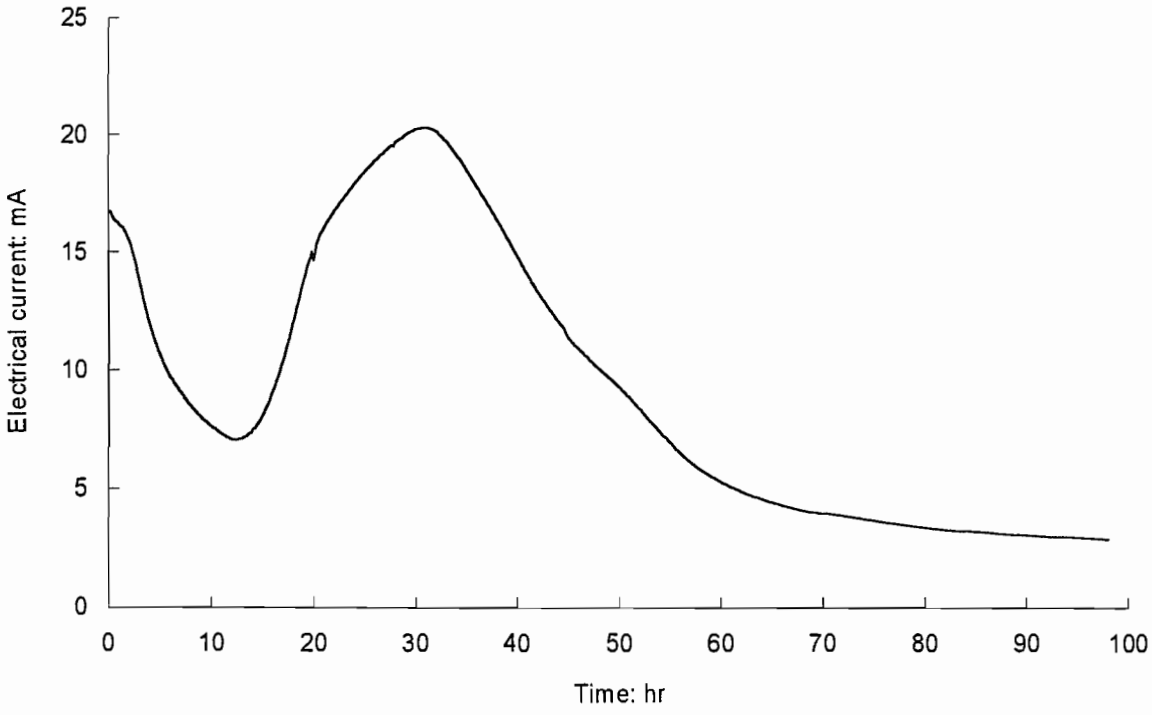

Figure 4.24 Variation of electrical current, experiment KE1

It appears that the increasing electrical current until 30 hours of the electrokinetic process induced further significant dissipation of excess pore pressures as already noted in Figure 4.12(d). It can also be seen from the 30, 35, and 46 hour density profiles shown in Figures 4.12(a) and (c) that there had been a significant increase in density due to the rapid dissipation of excess pore pressures. Subsequently, the significant increase in density resulted in an increase in soil resistance due to a depletion of ions, so that the electrical current started to drop after 30 hours of the electrokinetic process. After 55 hours, a small amount of electrical current (less than 5 mA) passed through the soil sample so that, effectively, the efficiency of electrokinesis had reduced, consistent with the negative excess pore pressures becoming more positive as already noted in Figure 4.12(d).

Figure 4.25 shows voltage profiles measured along the side of the sample for test KE1. The dotted line represents an idealised uniform voltage gradient across the electrodes. It can be seen that the voltages measured throughout the soil sample varied with time during the electrokinetic process. The voltages measured in the base half became lower than the idealised uniform voltage gradient across the electrodes (see the 1, 7, and 12 hour profiles). This variation of voltage profiles appears to be caused by the reduction of electrical current as already seen in Figure 4.24. The 7 and 12 hour profiles show that the voltages measured near the soil surface surprisingly increased. This will be further discussed in Sections 4.5.5 and 4.8 in terms of variations of soil pH. Thereafter, the voltages throughout the soil sample increased (see the 22 and 35 hour profiles) resulting from the increase of electrical current (see Figure 4.24).

It is interesting to note that the voltage gradients after 71 hours of the electrokinetic process became almost zero, which may be due to the reduction of electrical current; the electrical current passing through the soil sample became less than 5 mA by the time. The zero electrical voltage gradient implies that there is no water flow throughout the soil sample and therefore it is expected that there is no more consolidation. As already noted in Figure 4.24, the electrical current passing through the soil sample became less than 5 mA after 71 hours of the electrokinetic process. Those voltage profiles and electrical current consistently show that the electrokinetic consolidation process had been almost completed after 71 hours of the process.

The variations of electrical current for electrokinetic consolidation tests KE1 to KE4 are presented in Figure 4.26. The electrical current profiles measured in other tests under different applied electric field strengths also show a similar pattern to test KE1, and the amount and duration of the variation of electrical current was dependent on the applied electric field strength. Table 4.3 shows the maximum electrical current generated during electrokinetic consolidation tests KE1 to KE4 with the applied electric field strength and the

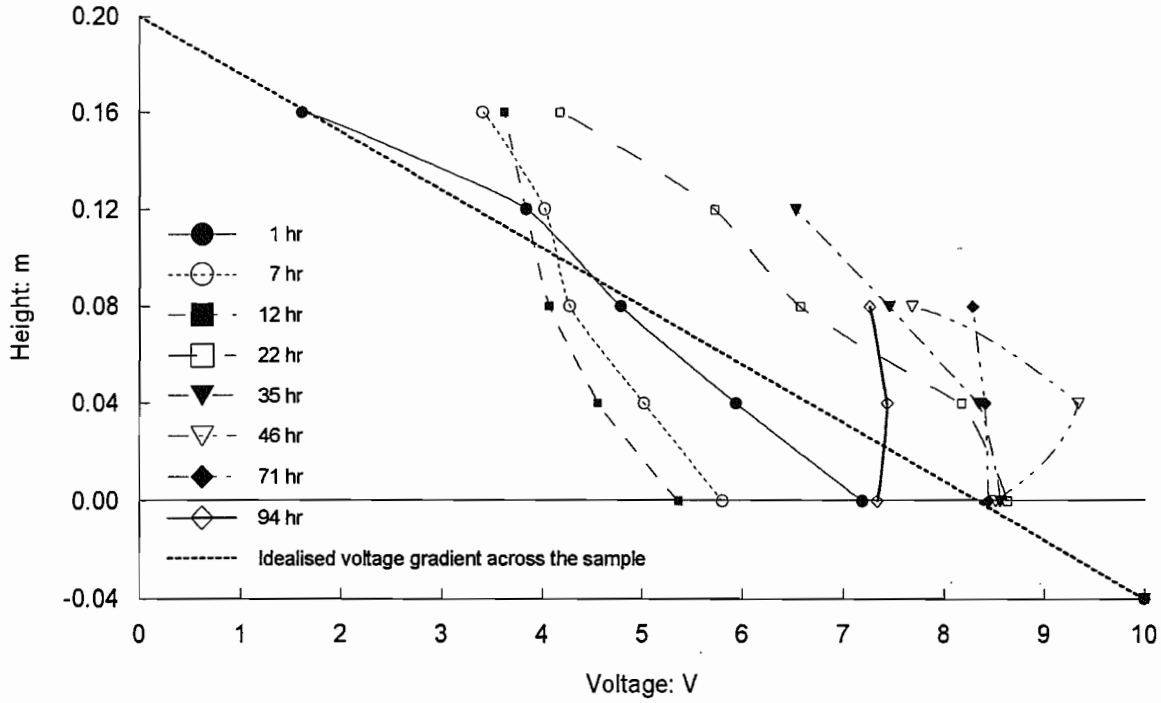

Figure 4.25 Voltage profiles, experiment KE1

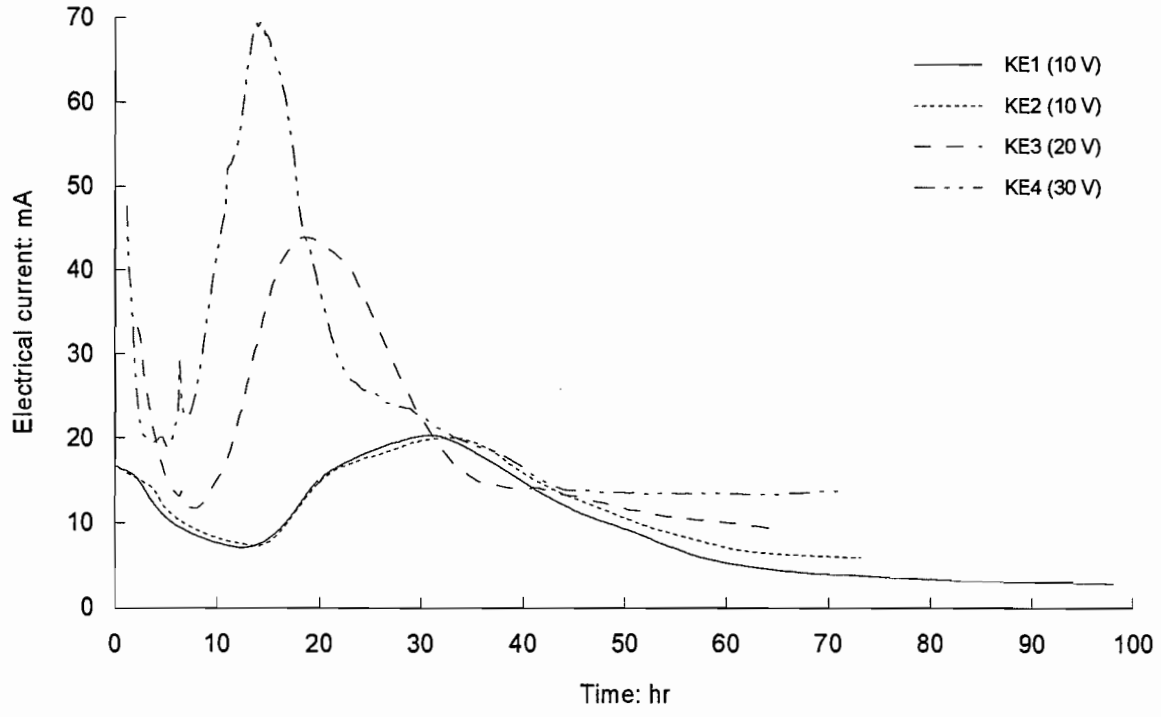

Figure 4.26 Variation of electrical current, experiments KE1 to KE4

time.

Table 4.3 Maximum electrical current generated during the electrokinetic process

	KE1	KE2	KE3	KE4
Time (Hour)	31	32	19	14
Electric field (V)	10	10	20	30
Current (mA)	20	20	44	69

4.5.5 Variation of pH

For the continuous measurements of soil density and pore pressures during the electrokinetic process, it was not possible to measure soil pH without disturbing the sample. Therefore, the pH measurements were performed after the electrokinetic consolidation tests were completed. The pH of both water above the sample (overlying water) and that in the base chamber of the electrokinetic cell was measured before the soil sample was removed from the testing cell. The pH of overlying water increased up to approximately 11, and that of the water in the base chamber of the testing cell decreased to less than 2 for tests KE1 to KE4. Then, the soil sample was carefully cut into five sections and the pH values were measured from the pore fluid extracted by centrifuge.

The pH profiles for tests KE1 to KE4, subjected to different electric field strengths and different durations of the applied field, are shown in Figure 4.27. The initial pH value for the slurry samples measured before the electrokinetic process was approximately 4.7, as indicated by the dotted line. It can be seen that the pH decreased throughout most of the soil, ranging between 2 and 4, after the electrokinetic process; the pH near the anode became less than 2.5. It appears that the H^+ ions produced in the base chamber entered into the sample and advanced half way up the soil, producing an acid front, and the base front created by OH^- ions produced at the cathode remained in the cathode region during the electrokinetic process, resulting in soil acidification occurring in the majority of the soil sample.

There is no obvious relationship between the magnitude of the applied electric field and the pH distribution, since the profile for 30 V (test KE4) is virtually identical to one of the 10 V experiments (test KE2). There is, however, a relationship with duration of the test with the shortest one (test KE3 with the electric field applied for 65 hours) showing the greatest variation through the soil bed, and the longest experiment (test KE1 with the electric field applied for 98 hours) showing the most acid conditions throughout the soil sample. The two

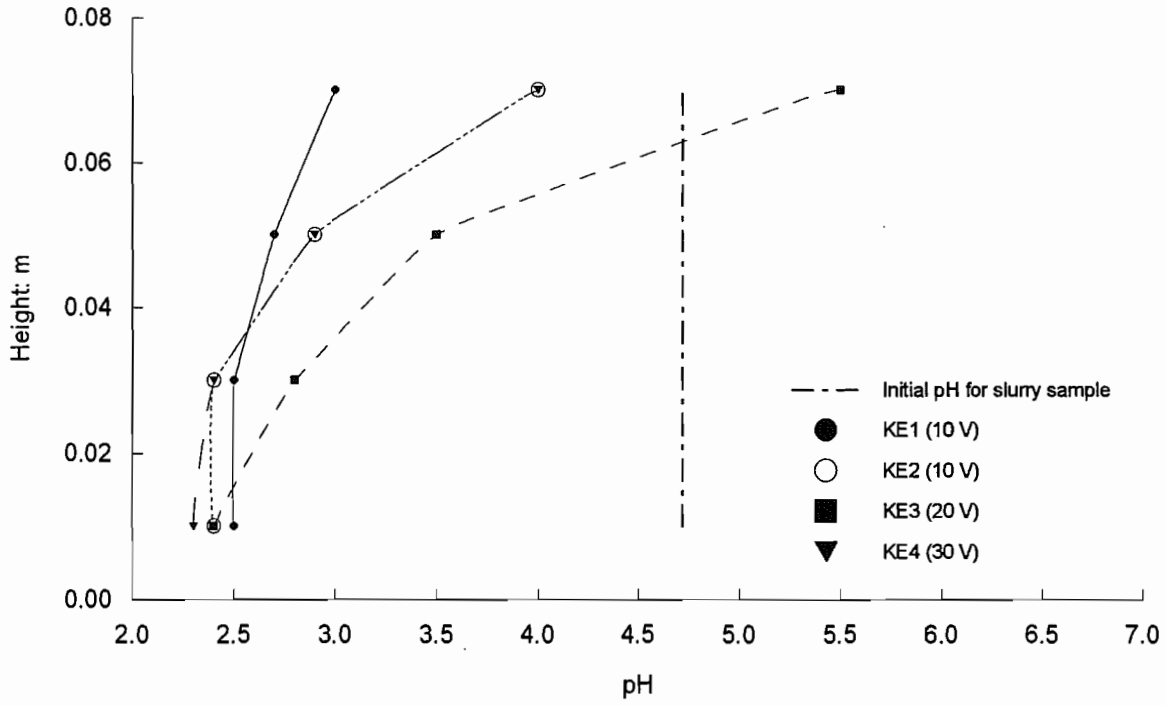

Figure 4.27 pH profiles after the electrokinetic process, experiments KE1 to KE4

tests KE2 and KE4, respectively lasting for 73 and 72 hours, have an intermediate pH distribution (see also Figure 4.26). West and Stewart (1995) suggested that the relatively high mobility of the acid front may be due to the water flow by electroosmosis from the anode to the cathode reinforcing the migration of hydrogen ions but retarding hydroxyl ions. It may also be noted that in the present experiments the consolidating soil was moving away from the advancing base front, and this would have reduced its penetration into the bed.

4.6 Electrokinetic Consolidation Tests KE5 and KE6

Electrokinetic consolidation tests KE5 and KE6 were further carried out to investigate the effect of electrokinesis on the behaviour of soft soil at slightly higher stress level. The important difference between these tests and previous ones (tests KE1 to KE4) was that the soil sample used was normally consolidated under the self-weight condition before applying electric fields.

4.6.1 Density and Excess Pore Pressure Profiles

Figure 4.28 presents density and excess pore pressure profiles obtained from test KE5. The first profile shown in Figure 4.28(a) shows the initial input density and the second

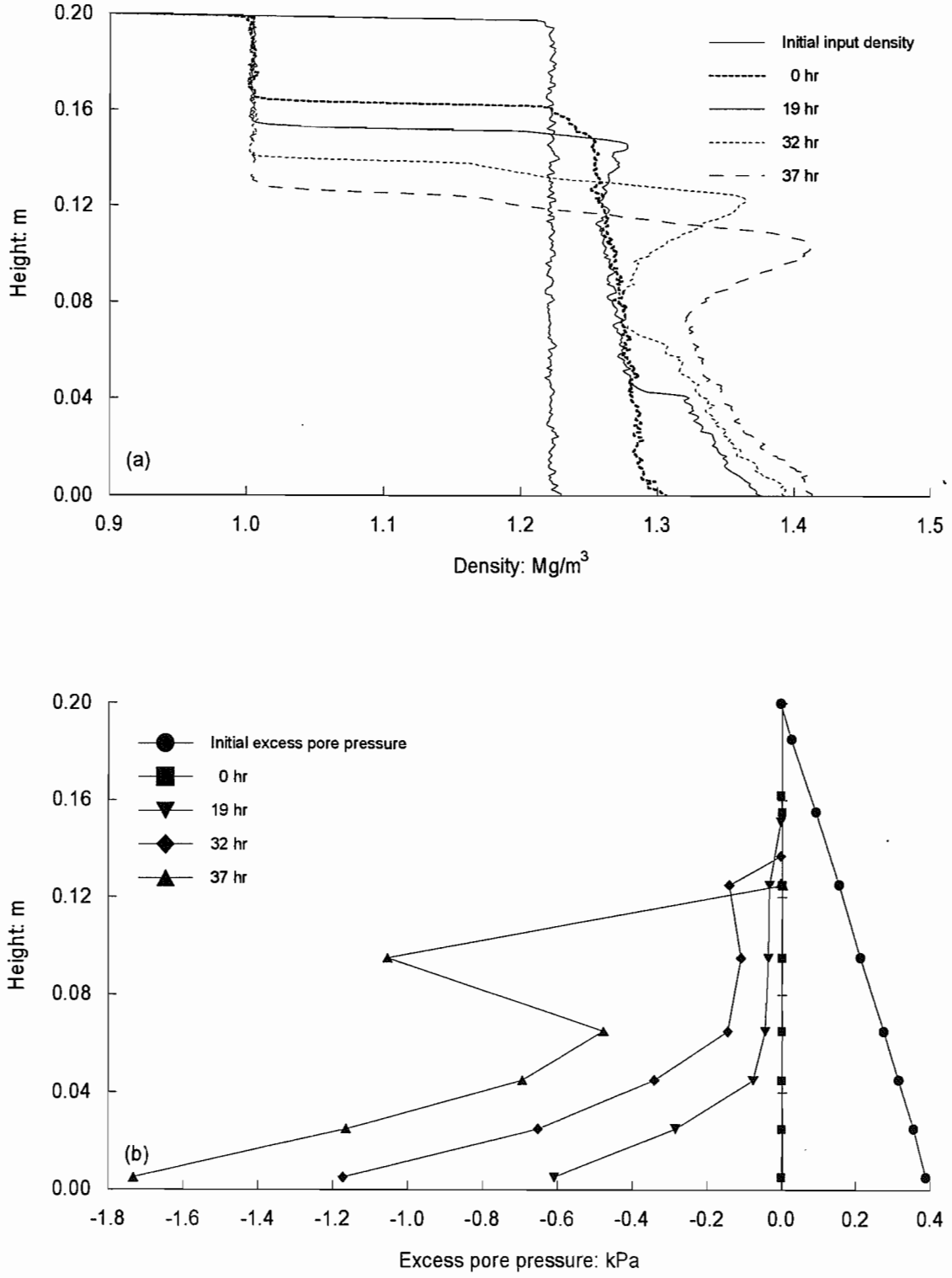

Figure 4.28 Electrokinetic consolidation, experiment KE5: (a) density profiles; (b) excess pore pressure profiles

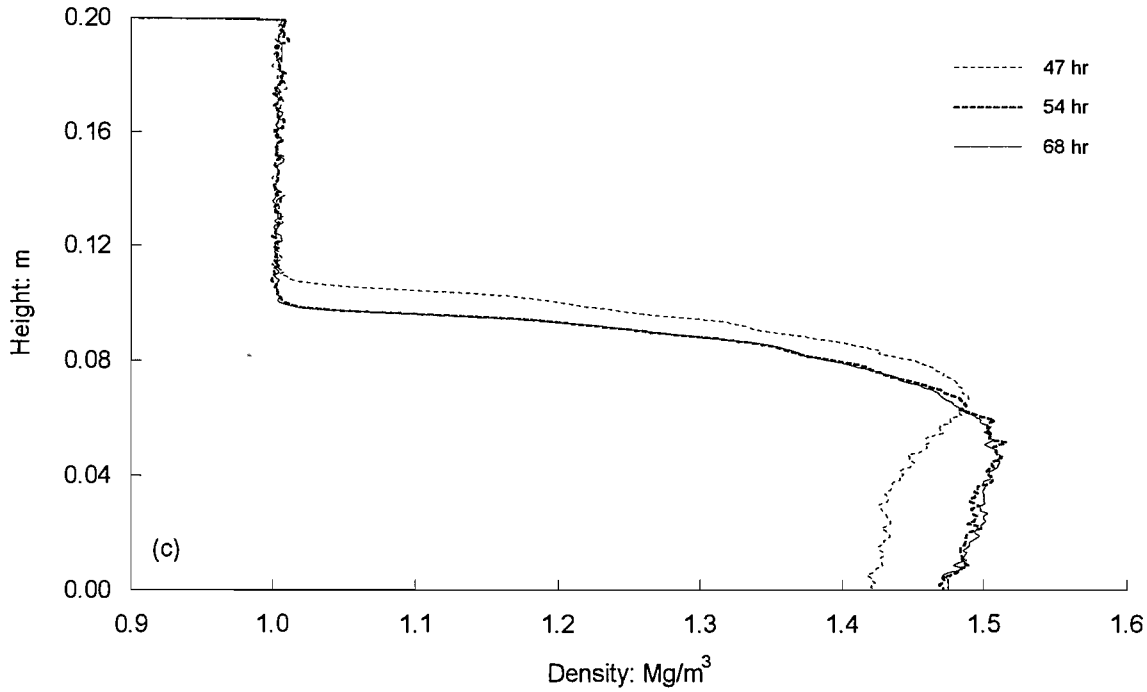

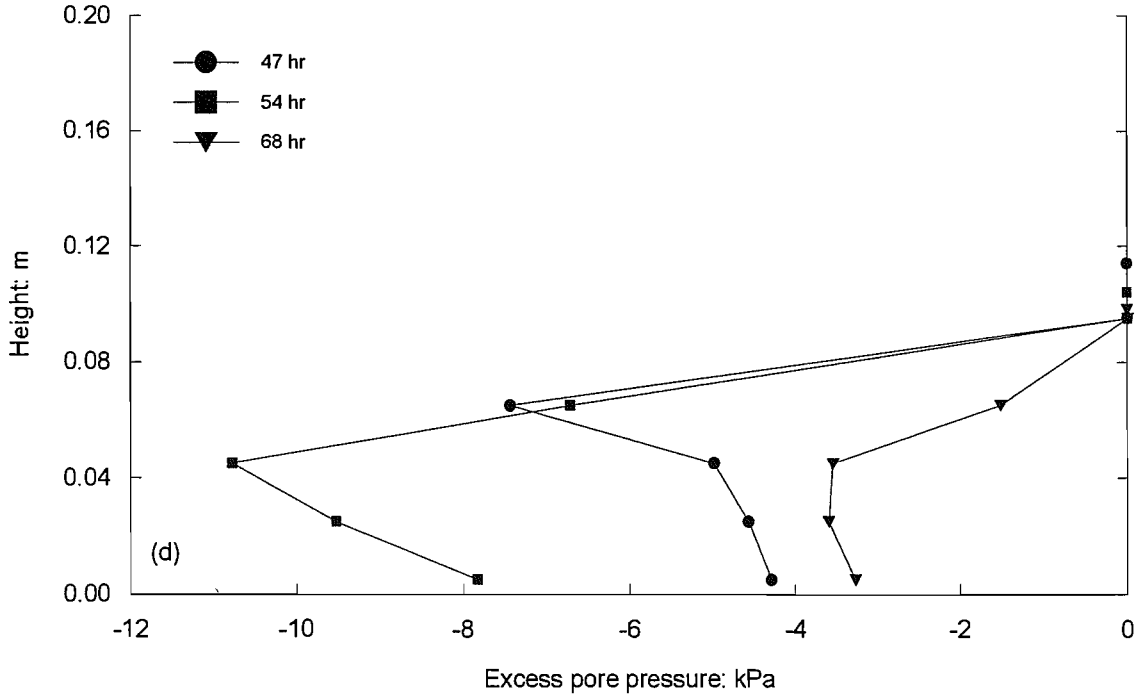

Figure 4.28 Continued: (c) density profiles; (d) excess pore pressure profiles

presents the soil density after 404 hours of self-weight consolidation as test KS2 (Figure 4.2(a)). The corresponding excess pore pressure profiles in Figure 4.28(b) show that the excess pore pressures had almost completely dissipated under the self-weight condition. An electric field of 10 V was then applied to the soil sample, and the subsequent times shown are measured from this time.

As seen, after 19 hours of the electrokinetic process, excess pore pressures became negative throughout the sample. The 19 hour density and excess pore pressure profiles show that a rapid reduction of excess pore pressures occurred in the base 0.04 m, consistent with the increase in density from the base. It can also be seen that the density in the top 0.03 m of the sample increased slightly. After 32 hours of the electrokinetic process, the density near the soil surface increased considerably with small negative excess pore pressures being developed in that region; the peak density near the soil surface was almost as high as that at the bottom of the soil bed. The 37 hour excess pore pressure profile shown in Figure 4.28(b) indicates that the negative excess pore pressure in the cathode region significantly decreased as already noted in the previous tests KE1 to KE4; the excess pore pressure below the denser layer developed at the soil surface became more negative.

As would be expected from the previous tests, the negative excess pore pressure in the cathode region became even more negative than those in the anode region after 47 hours of the electrokinetic process (see Figure 4.28(d)). The density profiles in Figure 4.28 show that the consolidation process is directly related to the development of negative excess pore pressure in the later stage of electrokinetic process. The negative excess pore pressures continued to become more negative by 54 hours of the process, extending to approximately -11 kPa in the middle of the sample (see Figure 4.28(d)). Thereafter, they had become more positive by 68 hours of the electrokinetic process due to the reduction of electrical current to be discussed later with respect to Figure 4.33.

Figure 4.29 shows density and excess pore pressure profiles from electrokinetic consolidation test KE6, subjected to an electric field of 30 V. Test KE6 is very similar to test KE5. The 4 hour density profile shown in Figure 4.29(a) demonstrates that a density step had not developed yet at the soil surface whereas the density increased from the base of the soil sample. This suggests that the electrokinetic consolidation occurred first in the anode region predominantly by the effect of electroosmosis then additional compression process observed in the top half of the sample occurred as a result of the change in pH. This will be further discussed in Sections 4.6.4 and 4.8.

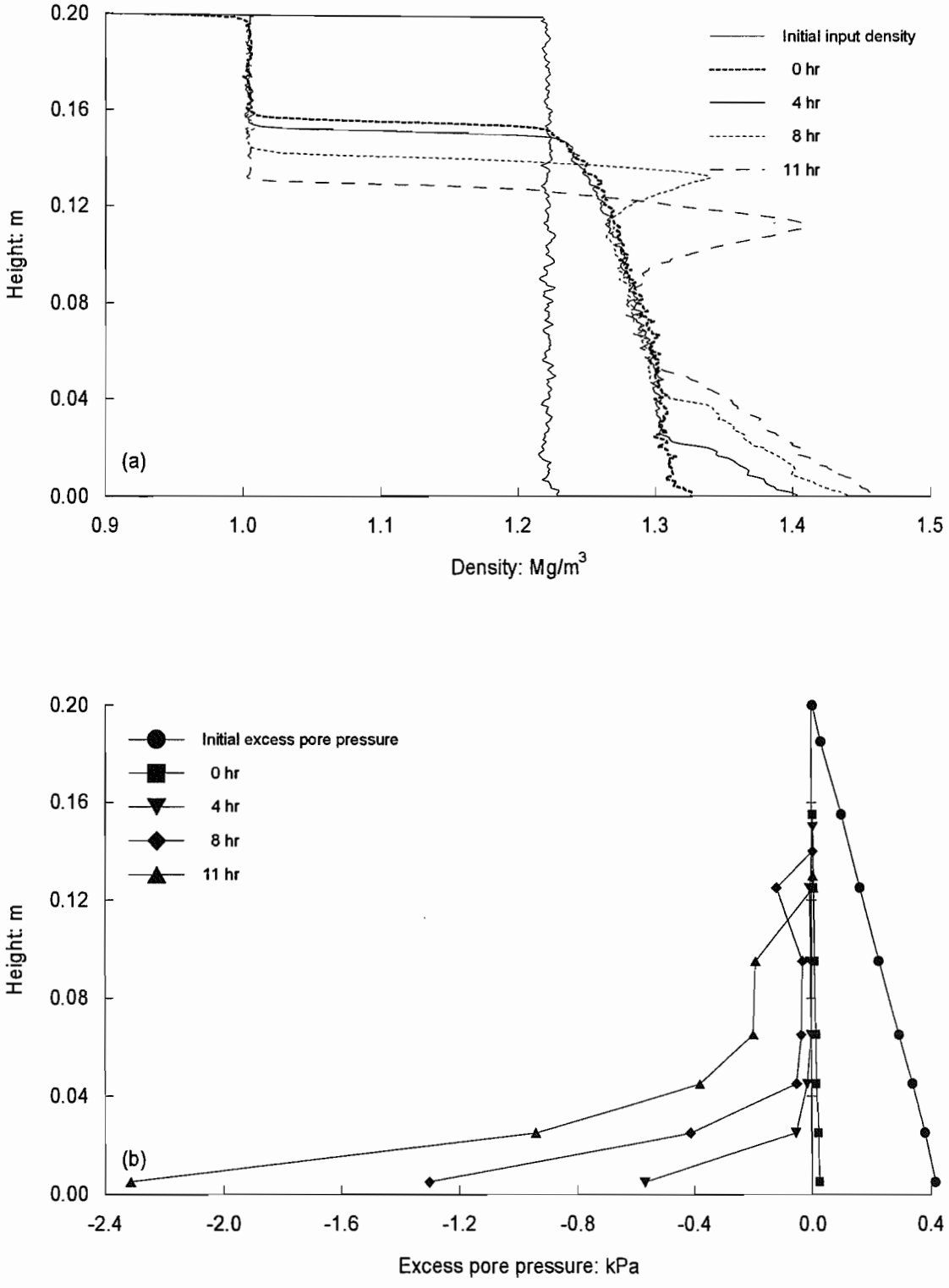

Figure 4.29 Electrokinetic consolidation, experiment KE6: (a) density profiles; (b) excess pore pressure profiles

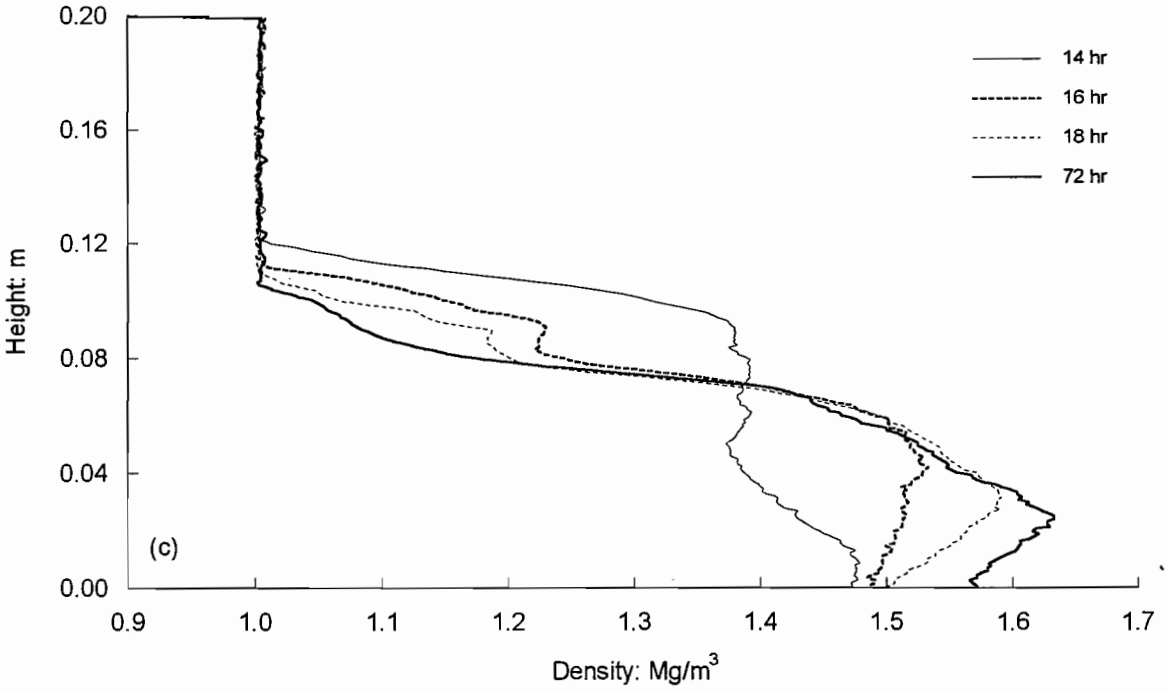

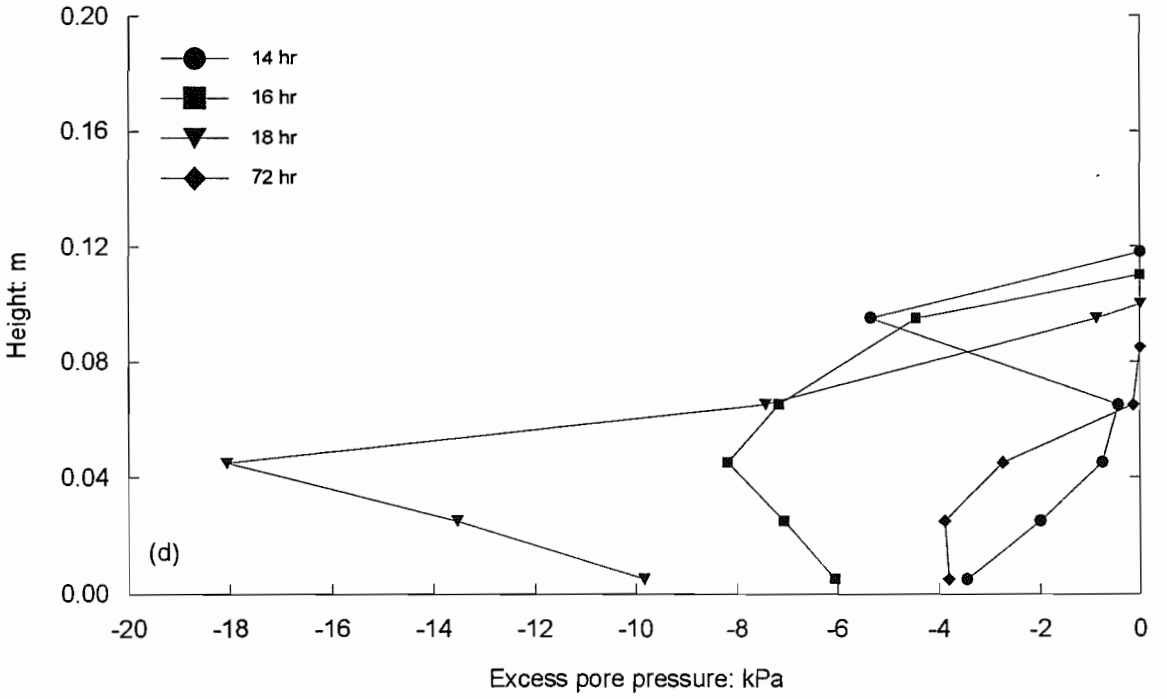

Figure 4.29 Continued: (c) density profiles; (d) excess pore pressure profiles

4.6.2 Effective Stress and Void Ratio Relationship

Effective stress and void ratio relationship for electrokinetic consolidation test KE5 is shown in Figure 4.30. The 0 hour e-σ_v' points represent the soil sample after the self-weight consolidation completed. As seen, the e-σ_v' points continuously follow a unique consolidation curve during the electrokinetic process; the solid line is representative curve for consolidation path during the electrokinetic process whilst the dotted line represents swelling curve after the electrokinetic process. It can be noted that the overall pattern appears to be quite similar to the previous tests KE1 to KE4. As the applied electrical current decreased in the later stage of electrokinetic process (see Figure 4.33), the effective stresses developed by electrokinesis decreased following the swelling curve (see the 68 hour e-σ_v' points in Figure 4.30). The effective stress and void ratio relationship for test KE6 is presented in Figure 4.31. The compression is slightly steeper than in test KE5, but overall behaviour is quite similar.

A number of representative compression curves for electrokinetic consolidation tests (KE2 to KE6) are plotted in Figure 4.32. As seen, the maximum range in void ratio over the different tests is approximately unity. The representative compression curve plotted as a solid single line is taken as the stress-strain characteristic of kaolin clay under electrokinesis, covering a range of applied electric field strengths and initial stress conditions for soil samples, and will be used as an input parameter for numerical simulations reported in Chapter 6.

4.6.3 Electrical Current

Figure 4.33 shows electrical current with respect to time results measured from tests KE5 and KE6, by comparison with those from tests KE2 and KE4. Tests KE2 and KE5 were performed under the similar applied electric field strength of 10 V, and tests KE4 and KE6 under 30 V. As seen, the variations of electrical current under the same applied electric field strength are quite similar. It can be noted from Figures 4.28 and 4.29 that the development of negative excess pore pressure is directly related to the applied electric field strength; the higher the applied electric field strength the greater the negative excess pore pressure and degree of consolidation. Moreover, similar magnitudes of negative excess pore pressure developed at similar times under similar applied electric field strengths (see Figures 4.13(d), 4.15(d), 4.28(d), and 4.29(d)). These are summarised in Table 4.4.

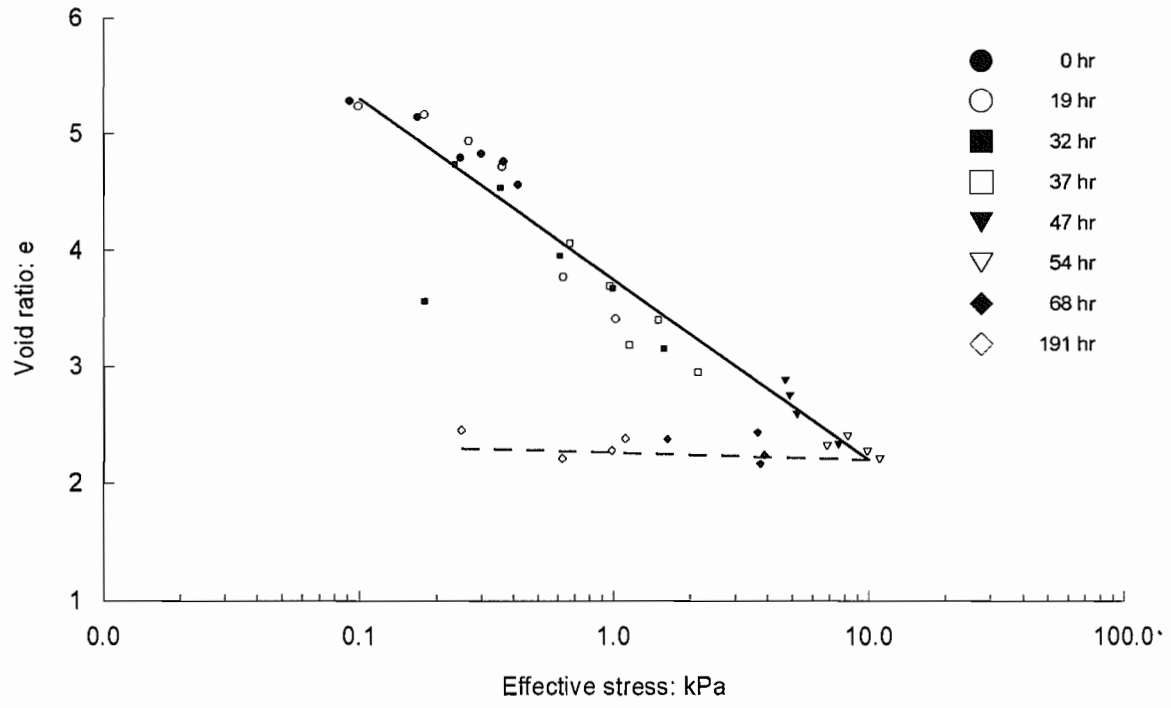

Figure 4.30 Effective stress and void ratio relationship for electrokinetic consolidation, experiment KE5

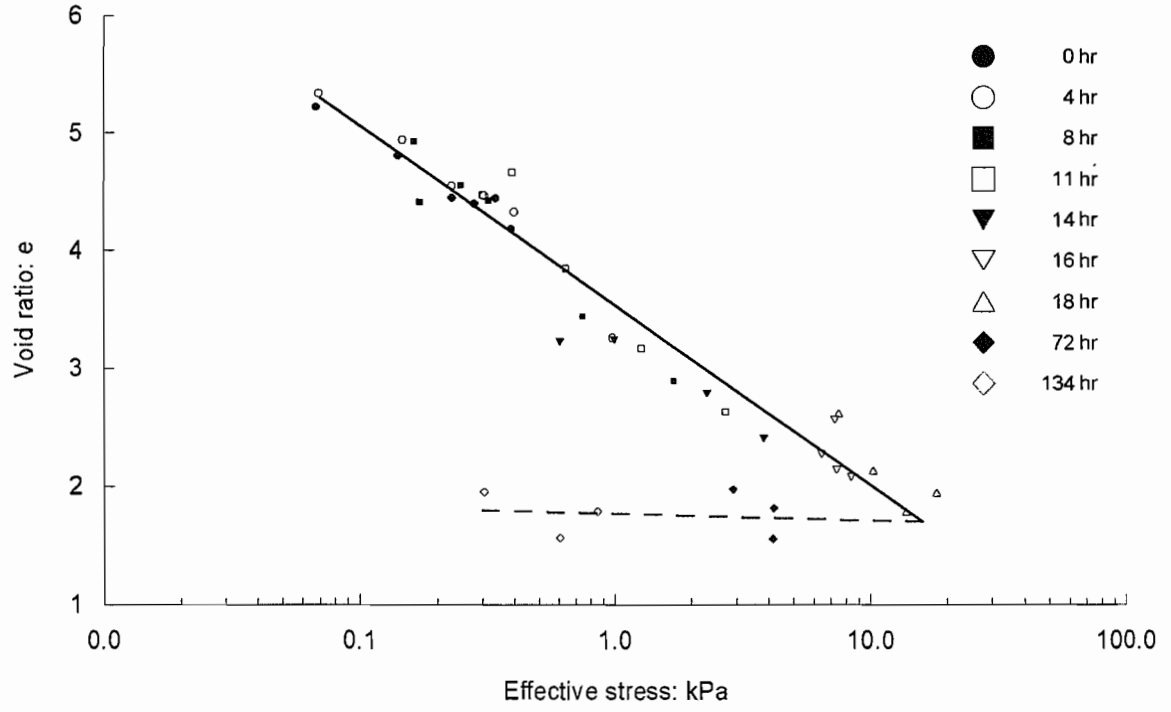

Figure 4.31 Effective stress and void ratio relationship for electrokinetic consolidation, experiment KE6

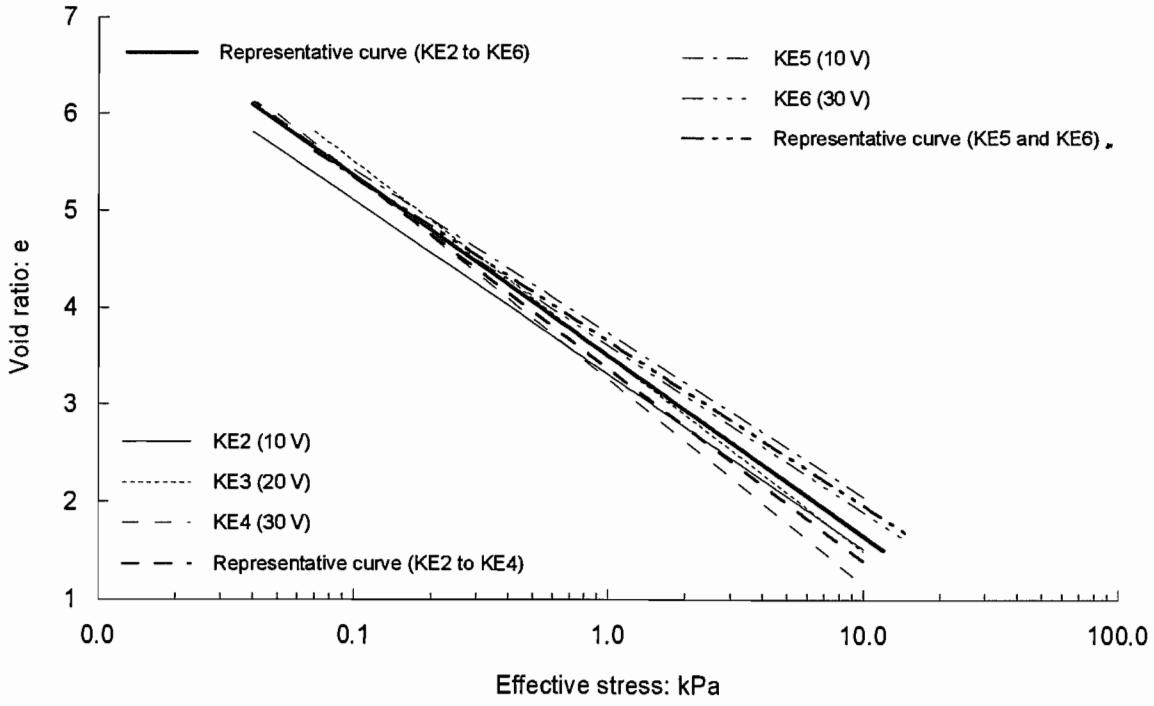

Figure 4.32 Effective stress and void ratio relationship for electrokinetic consolidation, experiments KE2 to KE6

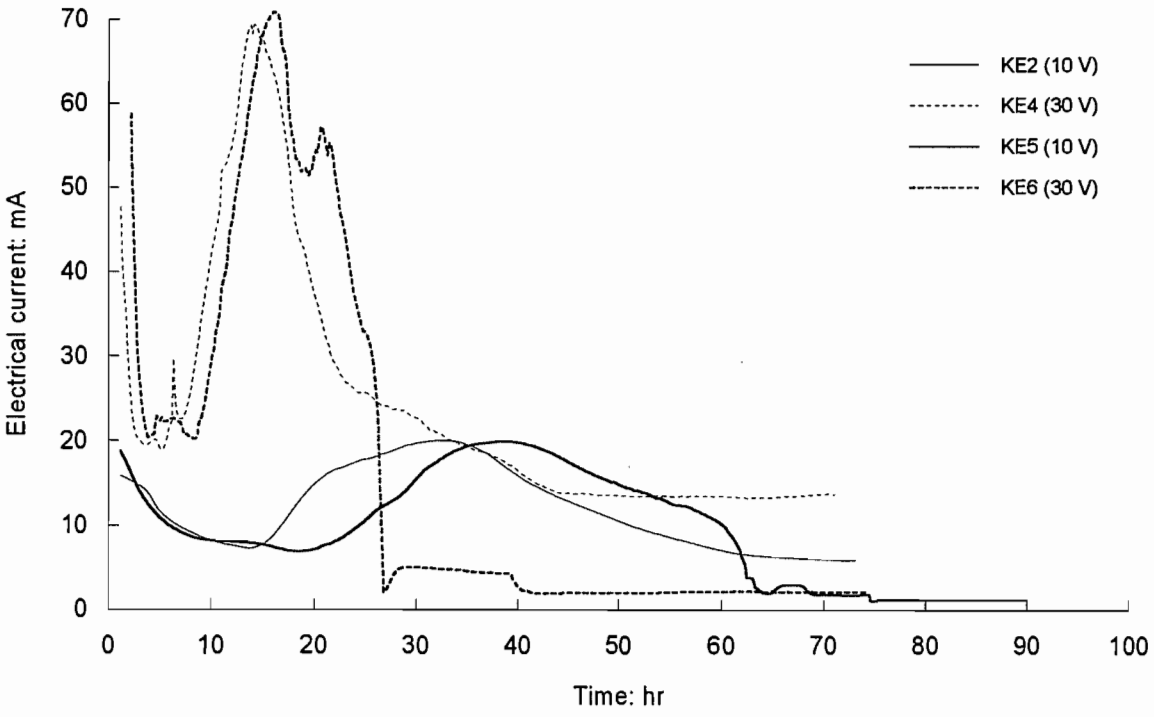

Figure 4.33 Variation of electrical current, experiments KE2, KE4, KE5, and KE6

Table 4.4 Negative excess pore pressure and electric field strength

	KE2	KE4	KE5	KE6
Time (Hour)	54	20	54	18
Electric field (V)	10	30	10	30
Pore pressure (kPa)	-12	-18	-11	-18

4.6.4 Variation of pH

In these tests, the pH values of overlying water and that the water in the base chamber of the testing cell were found to be very similar to those measured in the previous tests (Section 4.5.5); the pH values of overlying water and the water in the base chamber were 11 and 2 respectively. The initial pH value for the slurry samples measured before the electrokinetic process was also approximately 4.7.

The pH profiles for tests KE5 and KE6 are shown in Figure 4.34. It can also be seen from these pH profiles that the soil pH decreased to less than 4 in the most of soil sample and the relationship with duration of the experiment. Test KE5, subjected to the electric field for 90 hours, shows more acid conditions throughout the soil bed than test KE6 with the electric field applied for 75 hours. These results show a similar pattern to the previous electrokinetic consolidation tests KE1 to KE4.

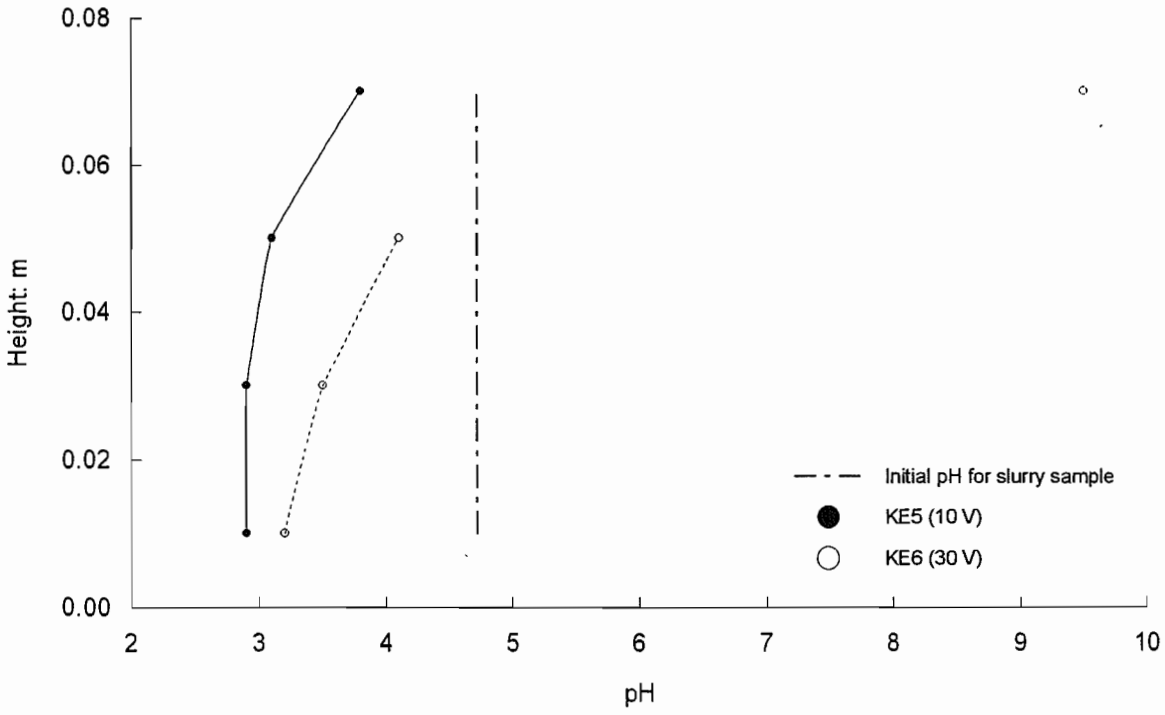

Figure 4.34 pH profiles after the electrokinetic process, experiments KE5 and KE6

4.7 Electroosmotic Permeability Tests KE7 and KE8

Tests KE7 and KE8 were carried out to determine the coefficient of electroosmotic permeability from laboratory experiments. In order to maintain continuous water flow through the soil sample during electroosmotic permeability test, it was necessary to modify the base chamber of electrokinetic cell. Design details of the electrokinetic cell for electroosmotic permeability tests are given in Section 3.3.

Electroosmotic permeability tests KE7 and KE8 were performed with the similar initial density of 1.22 Mg/m^3 and height of 0.2 m as those chosen for electrokinetic consolidation tests. The slurry sample for test KE7 was saturated with tap water as for the soil samples used in the previous electrokinetic consolidation tests. However, in test KE8, the clay sample was mixed and saturated with deionised water in order to examine the effects of a different electrolyte solution on the electrokinetic process. During the electrokinetic process, flow volume induced by electroosmosis, electrical current and voltage, density and pore pressure of the soil sample were monitored. The test was stopped after the electrical current became almost zero.

4.7.1 Electroosmotic Flow

Figure 4.35 shows the volume of fluid outflow collected in a burette during test KE7. There was no measurable flow for the first 2 hours of the electrokinetic process, and thereafter the water flow increased slowly until 13 hours. Subsequently, the water flow increased rapidly and then nonlinearly decreased in time. It was noted through the testing column that channels appeared between the sample and the column at this time. The visual appearance of this channelling is that of several pipes, 0.5 to 1 mm in diameter, rising almost vertically through the mud carrying water upwards relatively fast. Therefore, the water supplied from the constant head device (Section 3.5) was flowing through those channels after about 12 hours of the electrokinetic process. Therefore, the water flow rate measured for the first 9 hours of the electrokinetic process was considered for the calculation of electroosmotic permeability (Section 5.4.1).

A similar pattern of electroosmotic flow was observed in test KE8 as shown in Figure 4.36. The volume of water flow increased linearly during the first 20 hours of the electrokinetic process, and thereafter the flow rate became fast. The electroosmotically induced water flow is slightly different in amount depending on the electrolyte solution used, so that the coefficient of electroosmotic permeability is expected to be different for different electrolyte solutions.

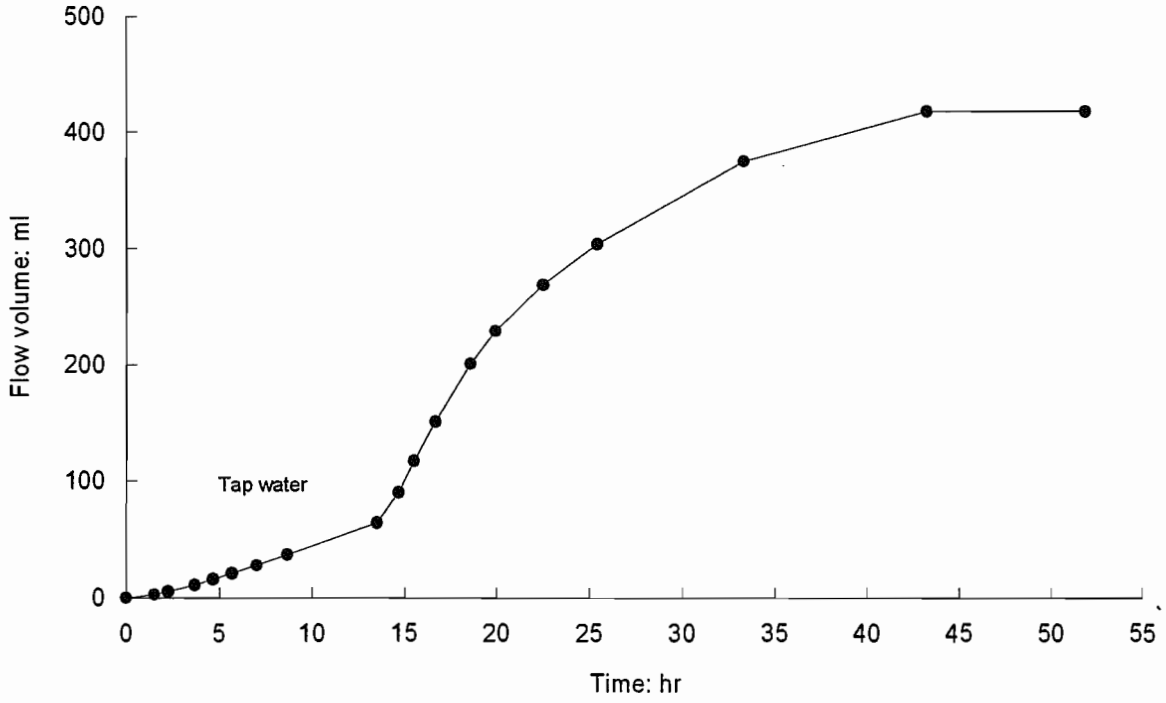

Figure 4.35 Electroosmotic flow volume with respect to time, experiment KE7

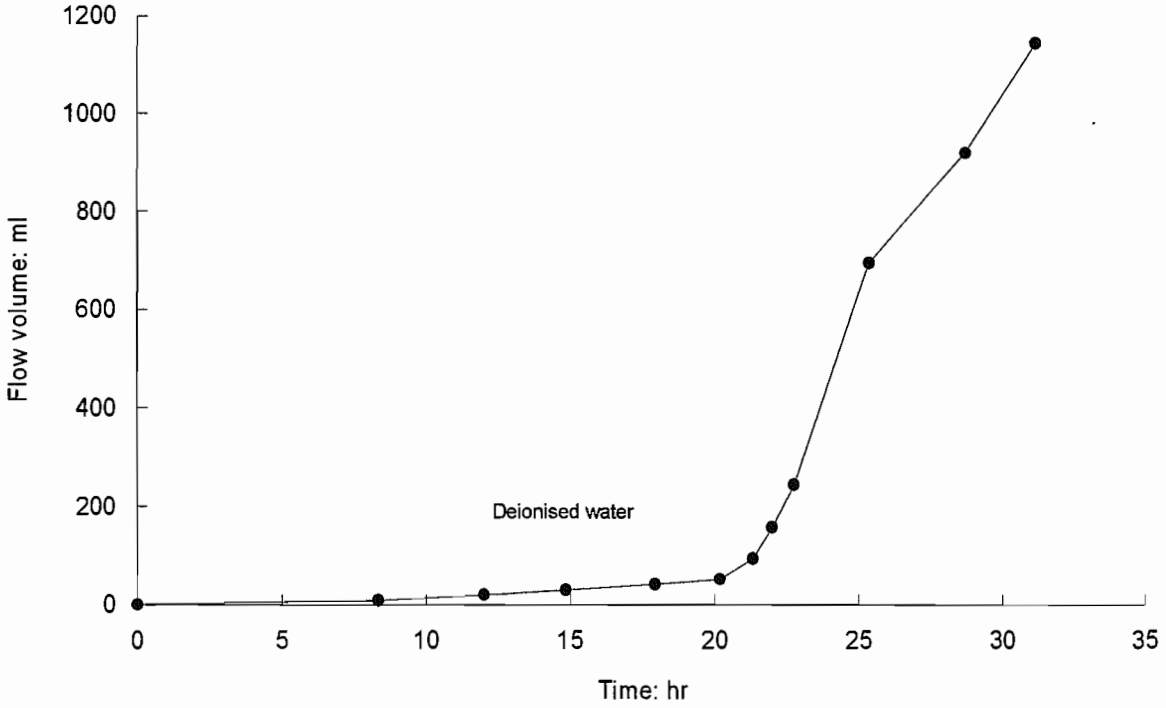

Figure 4.36 Electroosmotic flow volume with respect to time, experiment KE8

4.7.2 Density and Excess Pore Pressure Profiles

Figure 4.37 shows density and excess pore pressure profiles from test KE7. The first density profile shown in Figure 4.37(a) is the initial input density and the second is the density profile after 26 hours of self-weight consolidation. Then, the electric field of 20 V was applied and this profile is marked 0 hours.

An open boundary condition for horizontal flow (Section 2.5.3) is not expected to generate negative excess pore pressure during the electrokinetic process (Esrig, 1968). However, in this experiment, excess pore pressures existed throughout the bed at the start of the test, and the distribution was changed by opening the base to hydrostatic pressure as shown in Figure 4.37(b). The excess pore pressures through the soil did not change much during the first few hours, but they have dropped considerably by 7 hours of the electrokinetic process. The period after 14 hours, when the flow rate increased significantly, corresponds to negative excess pore pressures in the soil. The reductions in excess pore pressure would imply corresponding increases in effective stress and density.

Figure 4.38 presents density profiles observed from test KE8. In this electroosmotic permeability test, density profiles were frequently taken in the early stage of electrokinetic process in order to investigate the development of denser layer at the soil surface under the open boundary condition. As seen, the density near the soil surface increased rapidly after 3 hours of the electrokinetic process as already noted in electrokinetic consolidation tests (Sections 4.5 and 4.6). The pattern of consolidation is also similar to test KE7.

Considering the density profiles observed in electrokinetic consolidation test KE3 (see the 18 and 23 hour density profiles in Figure 4.14(a) and (c)), it appears that the denser layer may also have developed during the early stage of electroosmotic permeability test KE7 (see Figure 4.37(a)) and disappeared by 19 hours of the electrokinetic process when the first density profile was taken.

4.7.3 Electrical Current and Voltage

Figure 4.39 presents variations of electrical current and voltage profiles for test KE7. The electrical current and the voltage profiles measured from test KE7 in Figures 4.39(a) and (b) show a similar trend to that already seen in electrokinetic consolidation tests; the electrical current decreased between 0 and 2 hours, as the resistance increased near both the anode and cathode, consistent with the significant increase in voltage drop occurring in these regions. Between 2 and 12 hours the current increased, consistent with reductions in the voltage gradients at the electrodes. Thereafter, the soil has consolidated and the current drops. In this experiment, in contrast to the earlier ones, the voltage drop at the anode increased steadily. The overall variation in electrical current for test KE7 is slightly faster

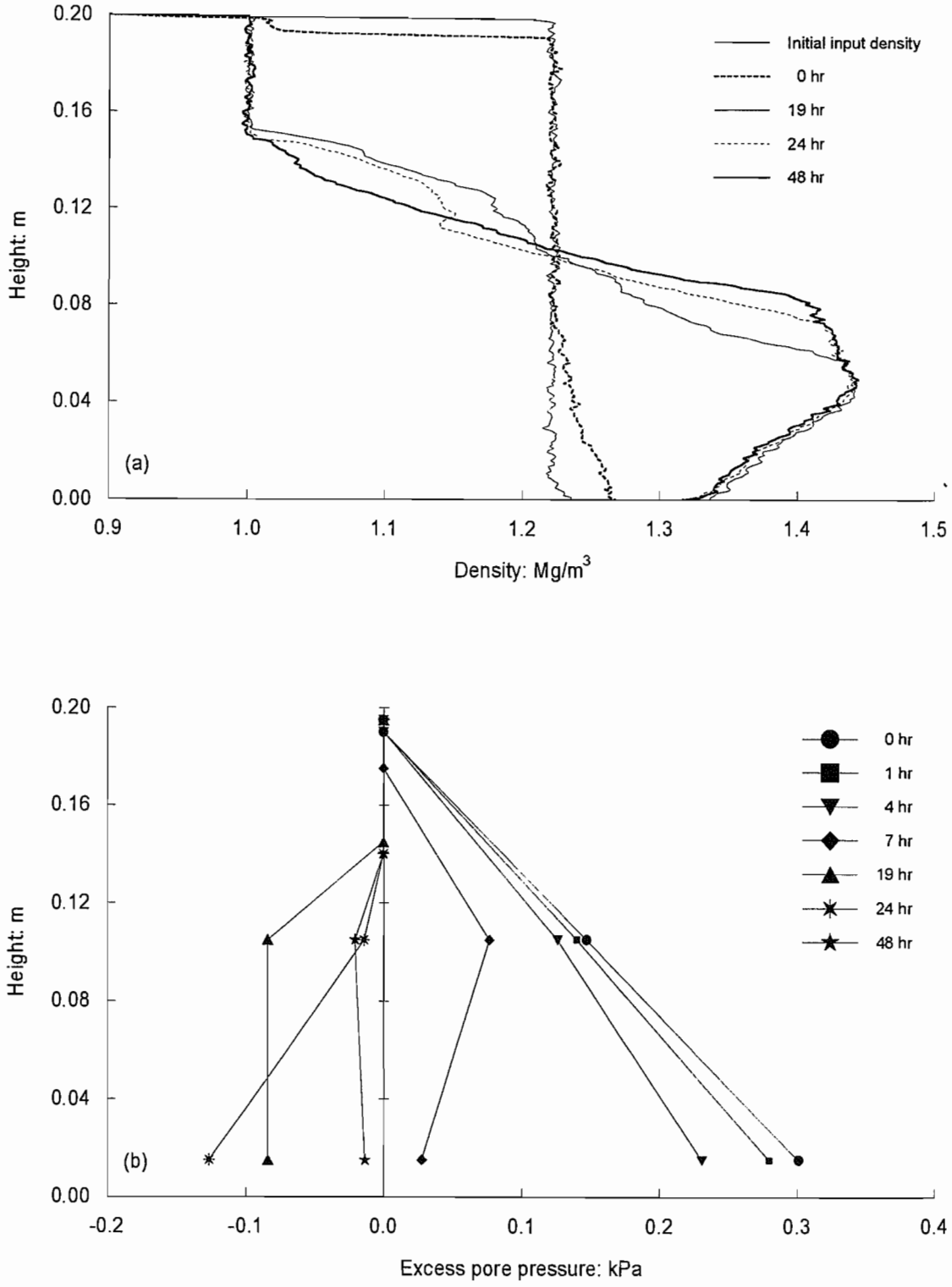

Figure 4.37 Electroosmotic permeability test KE7: (a) density profiles; (b) excess pore pressure profiles

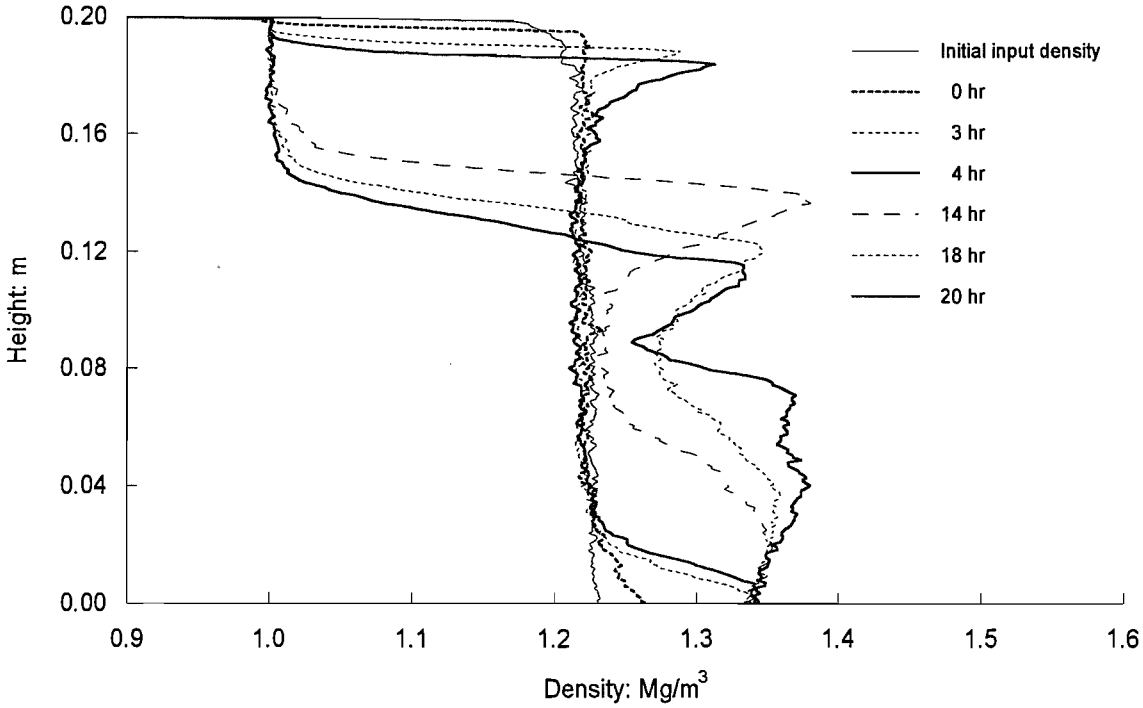

Figure 4.38 Density profiles from electroosmotic permeability test KE8

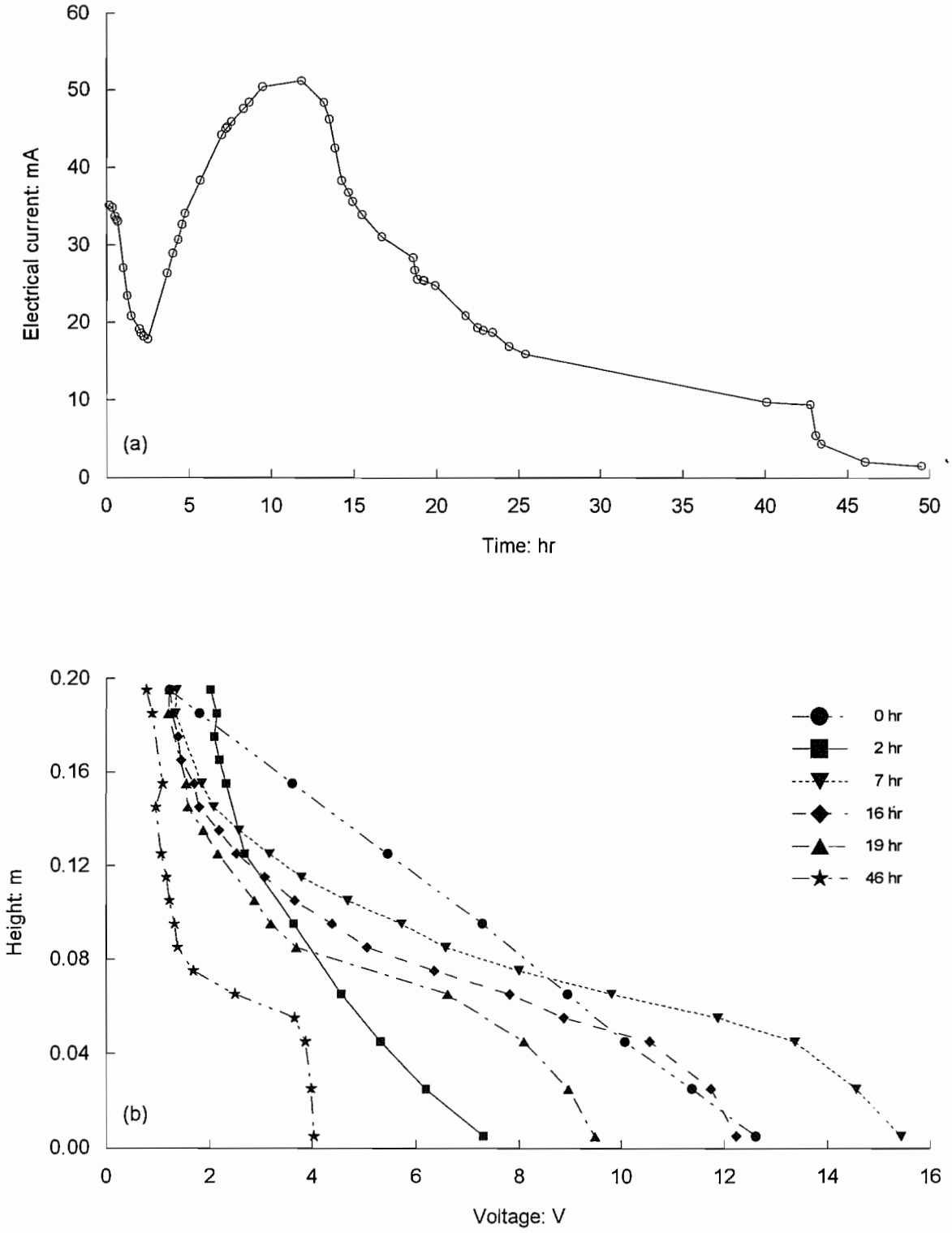

Figure 4.39 Variation of electric field, experiment KE7: (a) electrical current; (b) voltage profiles

than that observed in test KE3 under the similar applied electric field strength of 20 V (see Figure 4.26). However, it can be seen that the general pattern of variation in electrical current for test KE7 is similar to test KE3. It can be seen from the 46 hour voltage profile that the voltage gradient in the base half of the sample became almost zero. The same effect was already seen in electrokinetic consolidation test KE1 (see the 71 and 94 hour profiles in Figure 4.25).

Figure 4.40 shows electrical current and voltage profiles for test KE8, conducted with deionised water as electrolyte solution. As seen, the variation of electrical current for this test is quite different in shape compared to those tests conducted with tap water. The electrical current continuously increased until 20 hours of the electrokinetic process, and thereafter decreased significantly becoming almost zero. It can be noted that the maximum electrical current observed during test KE8 was less than 18 mA, which is almost similar value measured after 2 hours of the electrokinetic process in test KE7 (see Figure 4.39(a)). As expected, the variation of electrical current depends on the electrolyte solution used in the base chamber of testing cell; deionised water requires more time to be electrolysed. However, it can be noted that the voltages measured near the soil surface in the early stage of the process became relatively high, which is quite similar to those already observed in other electrokinetic tests (see Figures 4.25 and 4.39). The overall pattern in the variation of voltage profiles is also similar to test KE7.

4.7.4 Variation of pH

The outflow of water from the overlying water was collected and pH measurements were made during electroosmotic permeability tests KE7 and KE8. Figure 4.41 shows effluent pH profiles for tests KE7 and KE8. On the application of electric field, the effluent pH collected at the cathode immediately rose up to approximately 9 due to the electrolytic reaction at the cathode. After 10 hours of the electrokinetic process, both the effluent pH of tests KE7 and KE8 became approximately 12, and remained relatively constant until 20 hours of the process. Thereafter, the pH decreased with further processing due to the acid front from the anode.

It is interesting to note that the decrease in pH was accompanied by the decrease in electrical current. As the electrical current reduced, there may be fewer ions being produced by electrolysis and the migrating cations creating the acid front continuously move towards the cathode, resulting in the decrease of pH in overlying water after 20 hours of the electrokinetic process.

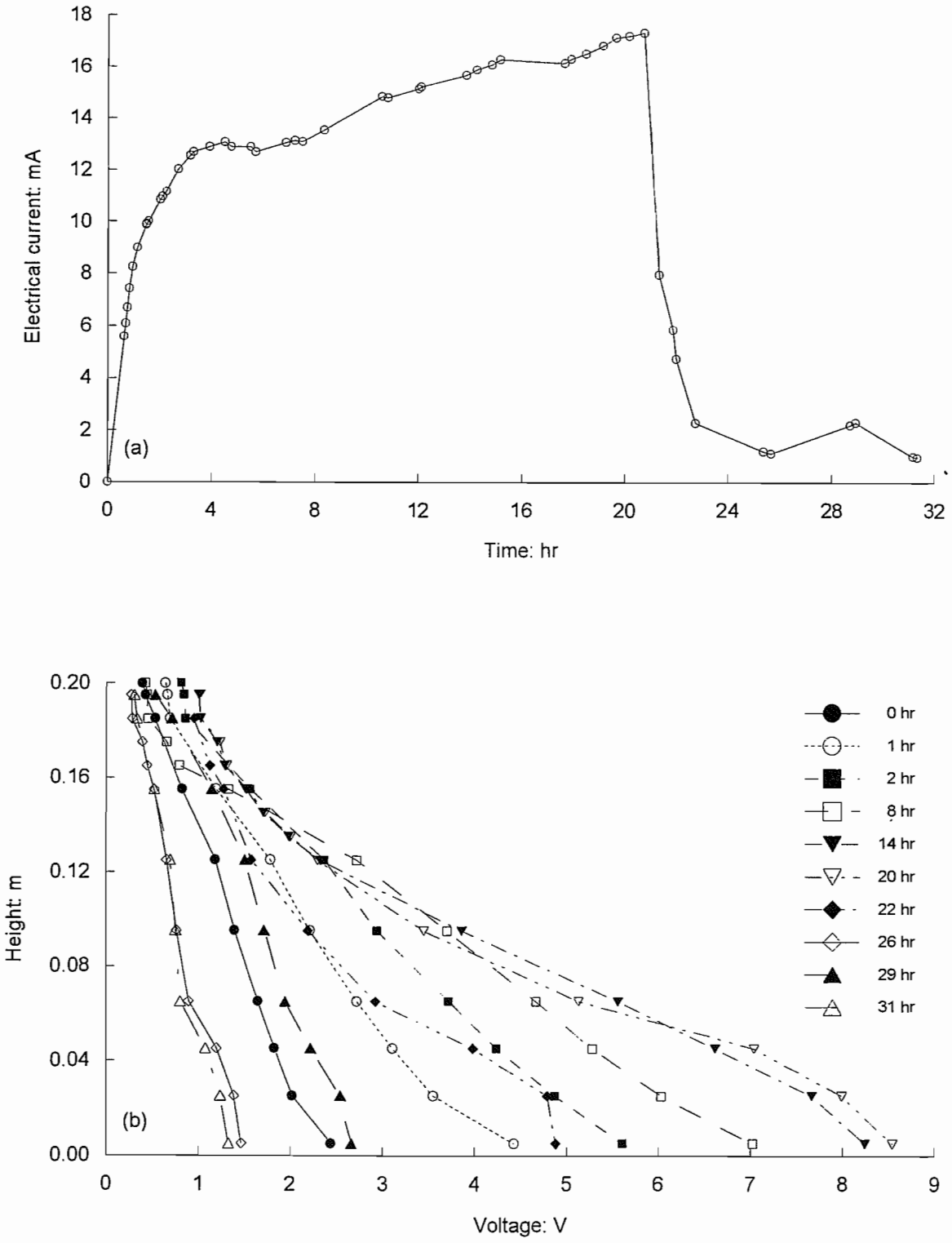

Figure 4.40 Variation of electric field, experiment KE8: (a) electrical current; (b) voltage profiles

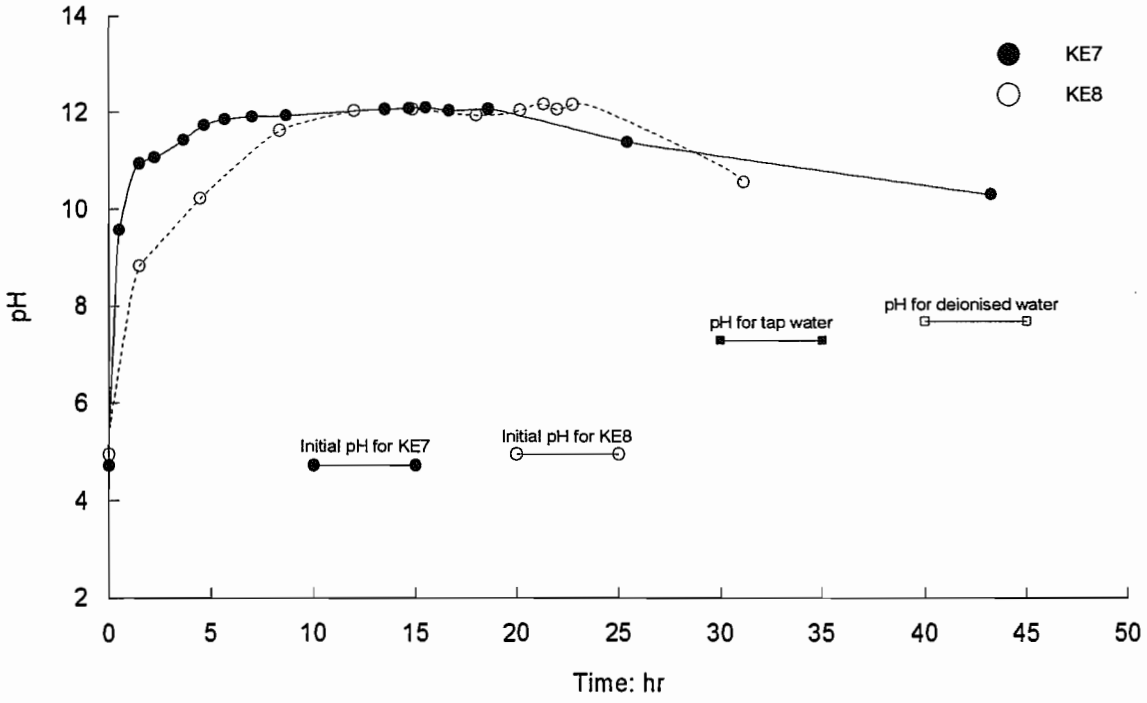

Figure 4.41 Effluent pH profiles during the electrokinetic process, experiments KE7 and KE8

4.8 pH Test KE9

Test KE9 was conducted with a similar initial condition to that of test KE4, an initial density of 1.22 Mg/m^3 and height of 0.2 m subjected to electric field strength of 30 V, in order to investigate the variation of soil pH during the electrokinetic process. As it was not possible to measure soil pH by directly inserting a pH probe into the sample during the electrokinetic process, the pH measurements were made on the pore fluid extracted from the sample, via syringes, through pH ports.

Figure 4.42 shows the effluent pH profiles for test KE9. The initial pH of water in the base chamber was approximately 7 as tap water was used for the electrolyte solution. As seen, the pH in the anode chamber decreased rapidly on the application of electric field and became almost 2 after 12 hours of the electrokinetic process. The pH profile from overlying water indicates the similar pattern to that observed in test KE7 (see Figure 4.41); the pH of the initial slurry sample was approximately 4.7 and the effluent pH increased up to approximately 9 after 30 minutes of the electrokinetic process.

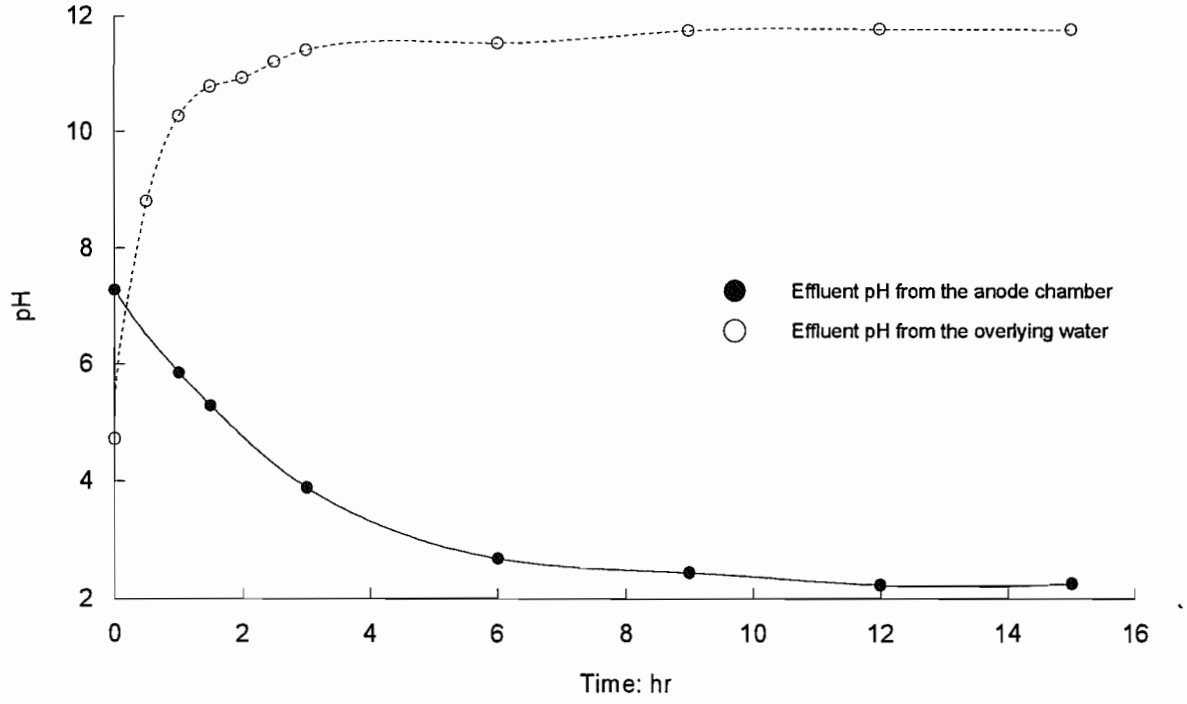

Figure 4.42 Effluent pH profiles during the electrokinetic process, experiment KE9

In practice, it was found that clay blocked the needle preventing the extraction of pore fluid as electrokinetic consolidation proceeded, so that it was not possible to extract enough fluid in the base half of the sample for pH analysis during the electrokinetic process. Figure 4.43 shows pH profile measured from slurry samples extracted by syringe near the soil surface, by comparison with the surface settlement for test KE9; the pH profile represents the pH value of approximately 7. As seen, the pH near the soil surface, in the top 0.01 m, increased higher than 7 after 3 hours of the electrokinetic process. As already noted in Figure 4.42, the pH of overlying water increased up to approximately 11 after 3 hours of electrokinetic process. Therefore, the base front generated from the cathode should have advanced gradually towards the anode with time.

The pH of base front appears to be approximately 11 from the effluent pH, and the advancing base front increases the soil pH with time. Therefore, it is suggested that there may be a zone of neutralisation (pH 7) one step behind the base front. However, the acid front migrating from the anode is generally much faster than the base front, so that the zone of neutralisation may remain near the surface of the sample in the later stage of the electrokinetic process. It can be noted that the pH at the soil surface became almost 7 after 12 hours of the electrokinetic process; the acid front may have migrated and reached the top of the sample after 12 hours of the process. The acid front could not be clearly identified as

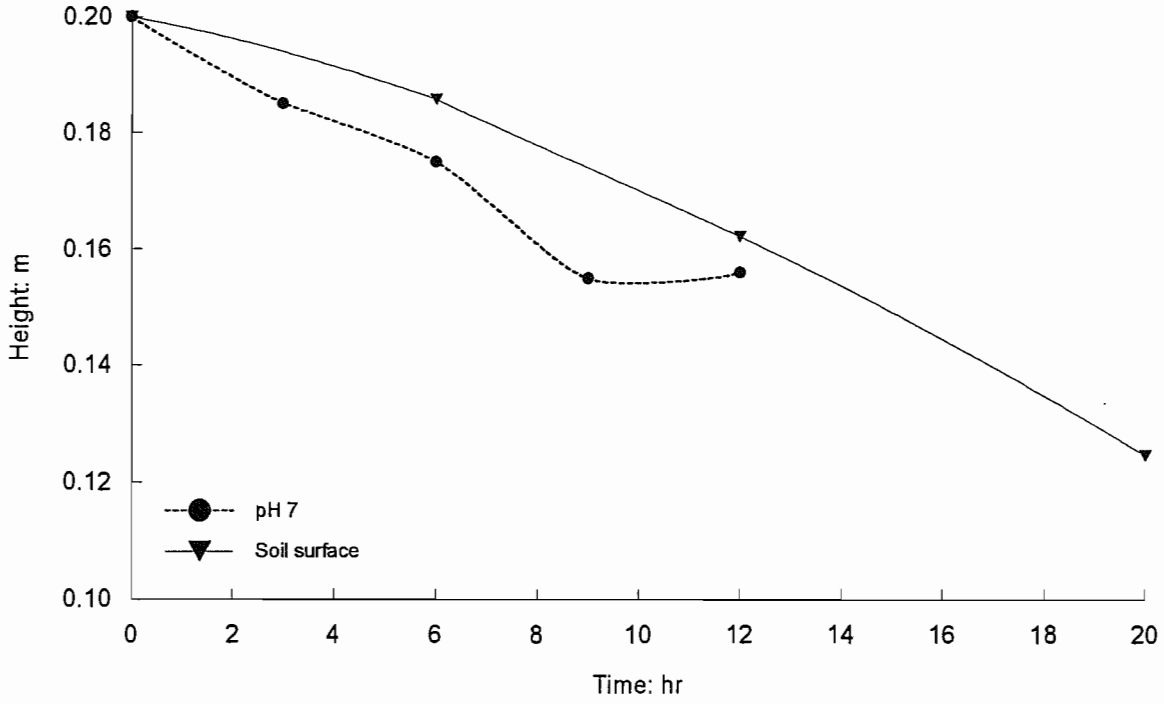

Figure 4.43 Variation of soil pH during the electrokinetic process, experiments KE9

it was not possible to measure the pH of soil sample after 12 hours of the process, however it can be expected that the soil pH could possibly become less than 7 in the most part of the sample, and become lower as the electrokinetic process proceeds (see Figures 4.27 and 4.34).

4.9 Summary of Test Results and Discussion

The application of electric field on a soil mass generates a net water flow from the anode towards the cathode, resulting from the movement of hydrated water carried by existing positive ions in the soil (Mitchell, 1993). As the initial distribution of ions in kaolin slurry is supposed to be uniform throughout, the initial water flow by electroosmosis is also expected to be uniform at any section in the slurry sample. For the configuration of a closed anode, the water flow generated by electroosmosis will lead to a reduction in the excess pore pressures. This reduction occurred first at the anode and produced a rapid increase in density. On the other hand, there was no significant change in density and excess pore pressure in the rest of the soil bed. It appears that the volume of water removed by the effect of electroosmosis in the middle part of the sample was replaced by a similar amount of water carried away from the anode region; the continuous movement of pore fluid did not cause

consolidation in the early stages.

It was noted that the density at the soil surface increased considerably on the application of electric field. It may be seen that the density step developed at the soil surface was much sharper than that developed at the base of the soil. There are two possible explanations for this. The first is electrophoresis, which occurs only if the density is low enough for soil particles to be moved under the electric field. It is unlikely that electrophoresis occurs at densities greater than the structural density. In this case, the initial density was very close to the structural density, and some increase in density could be due to the particle movement. However, if this was the case, the increased density might have been expected to occur over a larger depth of the bed rather than just at the surface. An alternative explanation links this increased density with electrochemical reactions as a result of the change in ion concentration (H^+ and OH^- ions) due to electrolysis and migration of ions. As discussed in Section 4.5.5, hydroxyl ions produced by electrolysis would be introduced from the cathode into the soil sample, and would increase the pH at the soil surface with which the cathode was initially in contact. It was already noted that the pH of overlying water increased up to approximately 9 within a few hours of the start of the electrokinetic process. It appears that the cations adsorbed in electric double layers would try to diffuse away from the surface of clay particles to make equal concentration throughout, resulting in an increase of zeta potential. The increase of zeta potential in a zone close to the cathode, due to the increase of pH, has been reported by several researchers (Eykholt & Daniel, 1994; West & Stewart, 1995; Yeung *et al.*, 1997). At present, the effects of changes in zeta potential on the magnitude of electrokinetic water flow is not well established. This increase, as described in Section 2.3.4, could cause an increase of electroosmotic permeability and contribute to the development of the density step in the cathode region.

Another possible explanation for the rapid increase in density near the soil surface is an increase in voltage gradient in the region due to neutralisation. This could be caused in the region close to the cathode where the base conditions interact with the acid soil. This would be particularly marked in these experiments where the initial pH of the soil was only 4.7. These neutral conditions would give rise to a reduction in electrical conductivity. On the application of electric field free ions within the soil sample would start to migrate towards the electrodes of opposite charge and, in addition, extra ions produced during the electrokinetic process (H^+ and OH^- ions) also migrate towards the opposite poles. The acid front created by migrating cations would advance towards the cathode, and would meet the base front in a region close to the cathode at the soil surface.

The nonlinearlity of voltage gradient already seen in Sections 4.5.4 and 4.7.3 affected the observed excess pore pressures. The increase of voltage gradient near the soil surface

would generate substantially greater electroosmotic flow in that region than that in the anode region, resulting in the development of suction in the vicinity to balance the demand of water flow due to low hydraulic permeability. Such suction development in the cathode region was not observed in the initial stage of electrokinetic consolidation. This may be attributed to the lack of experimental data points near the soil surface due to the limited number of pore pressure ports, but it is also possible that the increase in surface density initially was due to some mechanism other than an increase in effective stress.

Acar and Alshawabkeh (1996) also reported that significant reduction of pore pressure occurred in the region close to the cathode where the electrical potential gradient was maximum. Thereafter, in the later stage of the electrokinetic process, the negative excess pore pressure close to the anode was less negative than those immediately above. This would be caused by a reverse flow from the cathode to the anode due to the variations of zeta potential; the zeta potential increased in the cathode region and decreased in the anode region resulting from the electrolytic reactions. These relative contributions of zeta potential on the electrokinetic flow have been witnessed by several researchers (Eykholt & Daniel, 1994; Stewart & West, 1996; Acar & Alshawabkeh, 1996). After the removal of electric field, the negative excess pore pressures developed during the process became close to the hydrostatic pressures and slight swelling occurred. This pattern was evident in all the electrokinetic tests given in this chapter.

In summary, a number of processes affect the excess pore pressures. These processes include changes in pH and zeta potential, and electroosmotic flow under a potential gradient. The excess pore pressures then change the effective stresses. The results show that there is a consistent correlation of void ratio with effective stress, indicating that ultimately the increase of density in a soil under the influence of electrokinesis is controlled by the development of effective stress.

REFERENCES

Acar, Y. B. and Alshawabkeh, A. N. (1996). Electrokinetic remediation. I: pilot-scale tests with lead-spiked kaolinite. *J. Geotech. Engng. ASCE*, 122(3), 173-185.

Been, K. (1980). *Stress-strain behaviour of a cohesive soil deposited under water.* D.Phil. thesis, University of Oxford, UK.

Bowden, R. K. (1988). *Compression behaviour and shear strength characteristics of a natural silty clay sedimented in the laboratory.* D.Phil. thesis, University of Oxford, UK.

Elder, D. McG. (1985). *Stress strain and strength behaviour of very soft sediment.* D.Phil. thesis, University of Oxford, UK.

Esrig, M. I. (1968). Pore pressures, consolidation, and electrokinetics. *J. Soil Mech. Fdns. Div. ASCE*, 94(4), 899-921.

Eykholt, G. R. and Daniel, D. E. (1994). Impact of system chemistry on electroosmosis in contaminated soil. *J. Geotech. Engng. ASCE*, 120(5), 797-815.

Mitchell, J. K. (1993). *Fundamentals of soil behaviour.* 2nd Ed. New York: Wiley.

Stewart, D. I. and West, L. J. (1996). Electrokinetic soil decontamination - effect of local resistivity variations. *Proc. 2th Int. Congress on Environmental Geotechnics, Osaka*, 10, 1101-1106.

West, L. J. and Stewart, D. I. (1995). Effect of zetal potential on soil electrokinesis. *Geoenvironment 2000, Geotechnical Special Publication 46*, 1535-1549.

Yeung, A. T., Hsu, C., and Menon, R. M. (1997). Physicochemical soil-contaminant interactions during electrokinetic extraction. *J. Hazardous Materials* 55, 221-237.

CHAPTER 5 MATERIAL PROPERTIES

5. MATERIAL PROPERTIES

5.1 Introduction

The clay chosen for the experimental study was Speswhite kaolin. Kaolin is commercially marketed by ECC International Ltd as Speswhite kaolin which is excavated in Cornwall. For many reasons kaolin has been an ideal material for soil research. It is very homogeneous and can be obtained in large quantities. Kaolinite is relatively inert compared to the other active clay minerals. The small specific surface area of kaolinite reduces the effect on secondary processes creep or and it is therefore often used for modelling primary consolidation behaviour. Moreover, the electrochemical and mechanical properties of kaolinite are well known. The grading curve for Speswhite kaolin is shown in Figure 5.1.

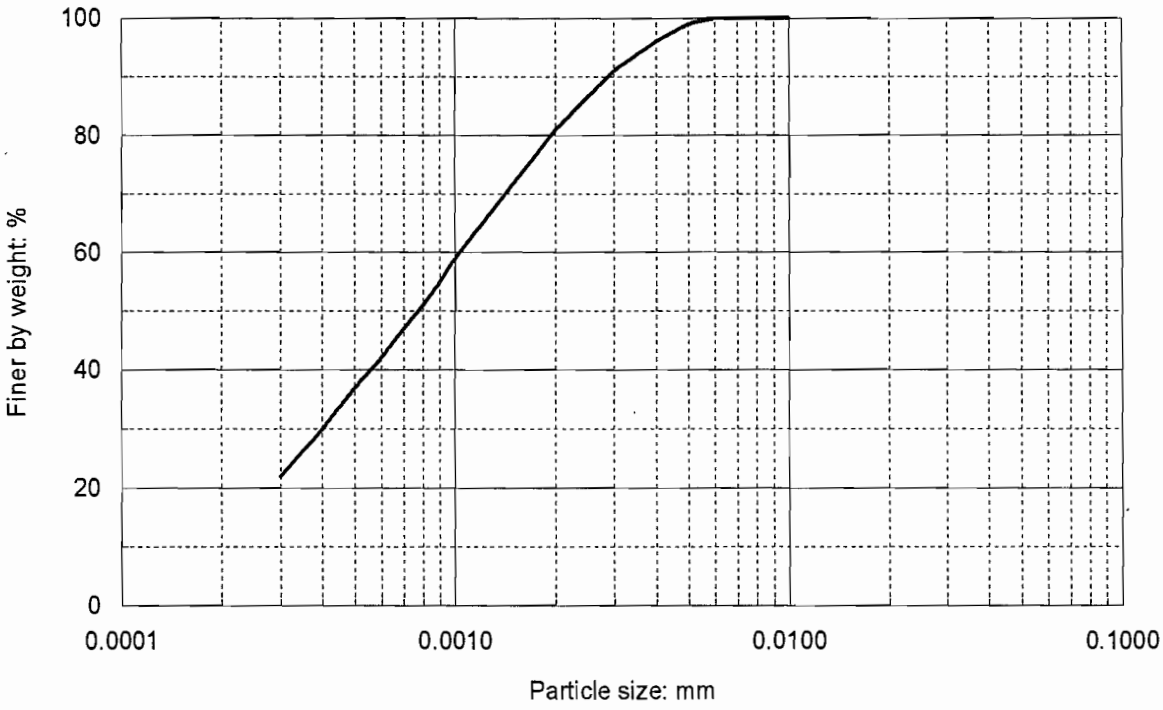

Figure 5.1 Grading curve for Speswhite kaolin (After ECC International Ltd 1993)

The chemical content, specifications, and typical properties are presented in Table 5.1, 5.2, and 5.3 respectively.

Table 5.1 Chemical content of Speswhite kaolin clay (After ECC International Ltd, 1999)

Chemical	Content (%)
SiO_2	47.2
Al_2O_3	37.9
Fe_2O_3	0.68
TiO_2	0.02
CaO_2	0.06
MgO	0.24
K_2O	1.59
Na_2O	0.12
loss on ignition	12.3

Table 5.2 Specification of Speswhite kaolin clay (After ECC International Ltd, 1999)

Specification	Value
Brightness	85.5 ± 0.7
300 mesh residue	0.02 % max.
+ 10 microns	0.5 % max.
- 2 microns	80 ± 3 % max.
moisture content	1.5 % max.
pH	5.0 ± 0.5
Typical Properties	**Value**
Yellowness	4.7
Specific gravity	2.6
Surface area	14 m^2/g
Oil absorption	42 g/100g
Water soluble salts content	0.2 %

Table 5.3 Review of some Speswhite kaolin properties

Reference	LL (%)	PI (%)	G_s
Stewart & West (1996)	80	38	2.60
Nyirenda (1989)	66	31	2.64
Fannin (1986)	62	31	2.61
Atkinson & Evans (1985)	63	34	-
Gue (1984)	65	31	2.60
Atkinson *et al.* (1984)	65	35	2.65
Francescon (1983)	69	31	2.61

5.2 Compressibility

The compressibility relationship for Speswhite kaolin under different stress conditions was investigated in the previous chapter. Figure 5.2(a) shows representative effective stress and void ratio relationships for self-weight, hydraulic gradient, and electrokinetic consolidation on a linear plot. These relationships are also shown on logarithmic scale for effective stresses in Figure 5.2(b). Slightly different gradients can be seen in each of the linear representative compression curves under different stress conditions. Table 5.4 presents the compression index for Speswhite kaolin. These values obtained from the laboratory tests will be used as input parameters in Chapter 6 in order to predict surface settlement, degree of consolidation, and density change during self-weight, hydraulic gradient, and electrokinetic consolidations.

5.3 Hydraulic Permeability

A relationship between hydraulic permeability and void ratio for Speswhite kaolin clay can be derived from the density and excess pore pressure profiles given in Section 4.3.1.

The general form of Darcy's law during consolidation process can be written as:

$$-n v_r = k_h i_h \tag{5.1}$$

where v_r is the relative velocity of pore fluid to soil particles, k_h is the hydraulic permeability, and i_h is the hydraulic gradient.

If both pore fluid and soil particles are assumed to move separately, continuity requires the net flow of pore fluid and soil particles to be zero; the total volume below any fixed section in the column must necessarily remain constant, so that:

$$(1-n) v_s + n v_f = 0 \tag{5.2}$$

where v_s is the velocity of soil particles and v_f is the velocity of pore fluid with respect to a fixed plane in the column.

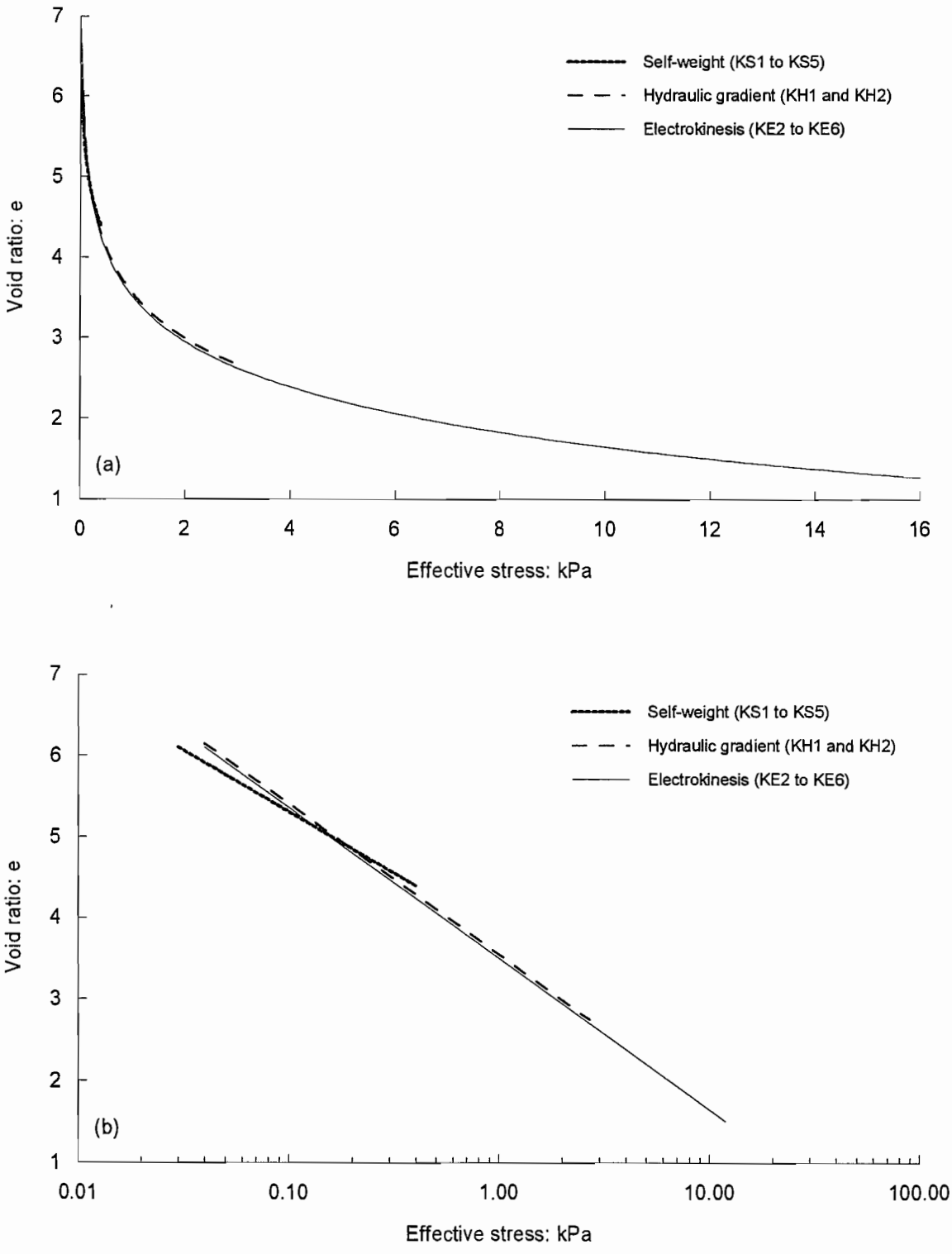

Figure 5.2 Effective stress and void ratio relationship for self-weight, hydraulic gradient, and electrokinetic consolidation: (a) linear scale; (b) logarithmic scale

Table 5.4 Compression index for Speswhite kaolin under different stress condition

Type of consolidation	C_c
Self-weight consolidation	1.51
Hydraulic gradient consolidation	1.81
Electrokinetic consolidation	1.82

Therefore, the relative velocity is given by:

$$v_r = v_f - v_s = -\frac{v_s}{n} \tag{5.3}$$

where the negative sign indicates the relative velocity opposite to the direction of the velocity of soil particles.

Combining Equations (5.1) and (5.3), the hydraulic permeability is found as:

$$k_h = -\frac{v_s}{ni} \tag{5.4}$$

The average velocity of soil particles for an element of the soil for the time between taking two density profiles is simply the change in height of that soil element divided by the time between the profiles. Porosity and an average hydraulic gradient can be calculated directly from density and excess pore pressure profiles respectively. Thus, an average hydraulic permeability for a soil element is found.

Figure 5.3 shows an example plot of hydraulic permeability calculated in this way versus void ratio for test KS1. Hydraulic permeabilities at the base cannot be calculated as the solids are not moving, and in many instances the soil near the base was also moving too slowly to be measured. Scatter in the permeability values is inevitable because measurement of both the hydraulic gradient and the position of a particular soil element is rather inaccurate. Nevertheless the plots are remarkably consistent. Hydraulic permeabilities range from 4×10^{-8} to 7×10^{-7} m/sec in all five tests KS1 to KS5 and all showed approximately the similar trend of the logarithm of permeability with void ratio.

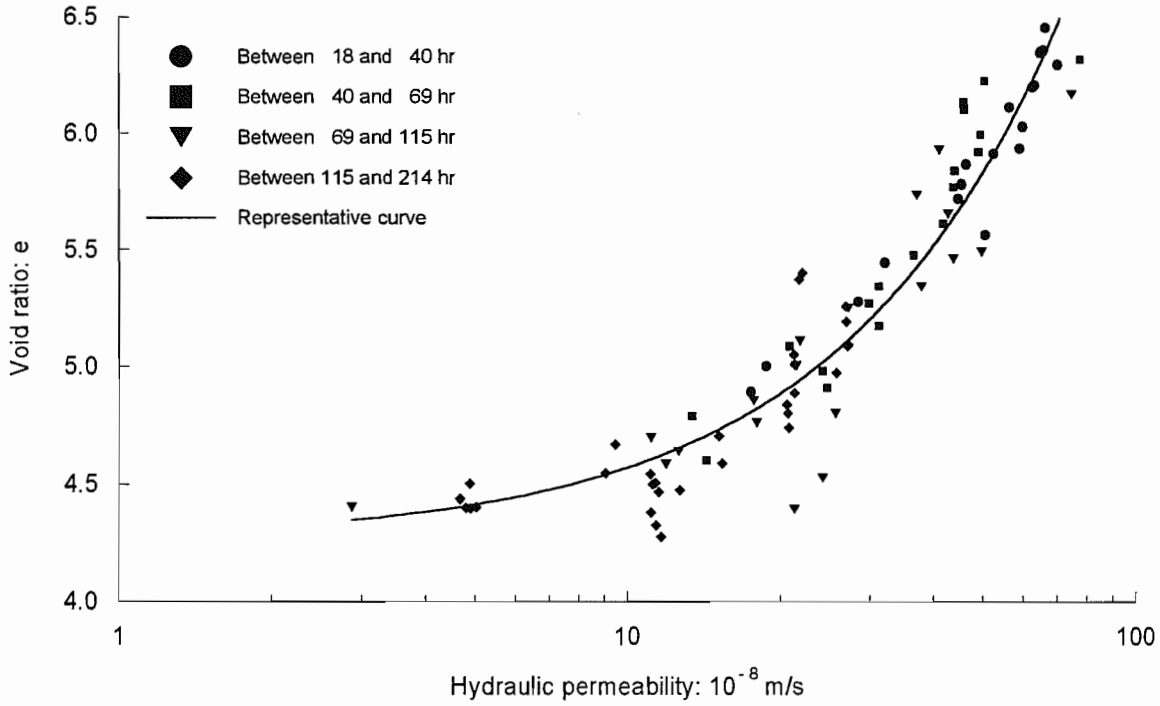

Figure 5.3 Hydraulic permeability and void ratio relationship, experiment KS1

5.4 Electroosmotic Permeability

5.4.1 Experimental Determination of Electroosmotic Permeability

For the experimental determination of electroosmotic permeability, sets of laboratory tests were carried out using Speswhite kaolin saturated with both deionised and tap water. Experimental details for the electroosmotic permeability tests are given in Section 4.7. The tests were carried out at constant room temperature in an electroosmotic permeability testing cell (Section 3.3).

As already noted in Figure 4.35, the electroosmotic water flow in test KE7 occurred for the first 12 hours before channelling started (Section 4.7.1). During electroosmotic permeability tests under the open boundary condition, negative excess pore pressures were developed with time resulting in soil consolidation (see Figure 4.37). The overlying water produced by the consolidation process is part of the water flow out of the soil, so that it should be included in the calculation of electroosmotic permeability. Figure 5.4 presents the flow volume against time for the sum of overflow of water collected in a burette and overlying water produced by the consolidation process. It can be seen that the flow volume induced

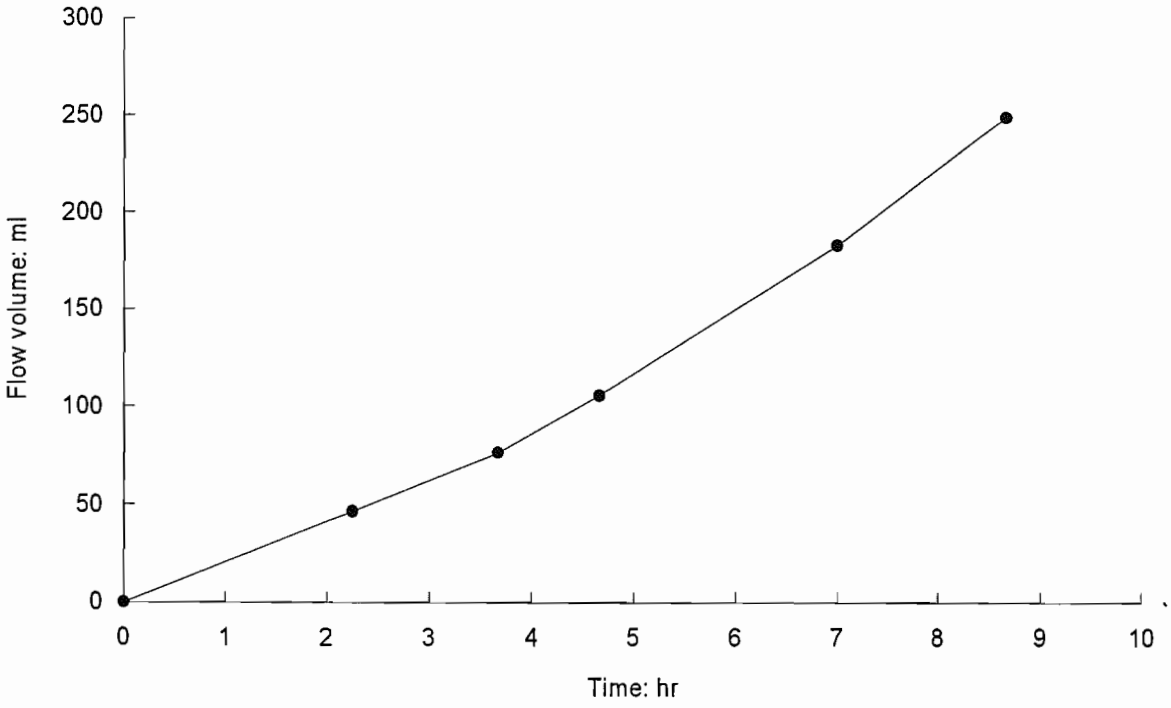

Figure 5.4 Electroosmotic flow volume (overflow + consolidation) with respect to time, experiment KE7

by electroosmosis increased approximately linearly for the first few hours, followed by a second stage with a slightly higher flow rate.

The electroosmotic permeability is the gradient of flow rate against electrical gradient as shown in Equation (2.5). Therefore, in order to calculate average values, representative voltage gradients across the soil sample for each time should be determined. Figure 5.5 shows the representative voltage gradient profiles estimated from Figure 4.39. As seen, the voltage gradients increased with time from an initial value of about 0.6 to 0.9 V/cm. This range corresponds to the first two stages of the flow rate against time as shown in Figure 5.4. The voltage gradient of 0.6 V/cm existed during the first 4 hours, whilst the excess pore pressures remained high as shown in Figure 4.37(b). The voltage gradient then increased as the excess pore pressures reduced and the flow rate increased slightly. The electroosmotic flow rates are plotted in Figure 5.6 against the electrical gradients to determine the coefficient of electroosmotic permeability. Figure 5.6 shows two possible interpretations of the data, one considering just the first 4 hours, and the other for 9 hours. The values of the coefficient of electroosmotic permeability are 1.18×10^{-8} $m^2/V \cdot sec$ and 1.32×10^{-8} $m^2/V \cdot sec$, respectively. This corresponds to approximately 10 % difference between the two values. Nevertheless, they are both within the range of values encountered

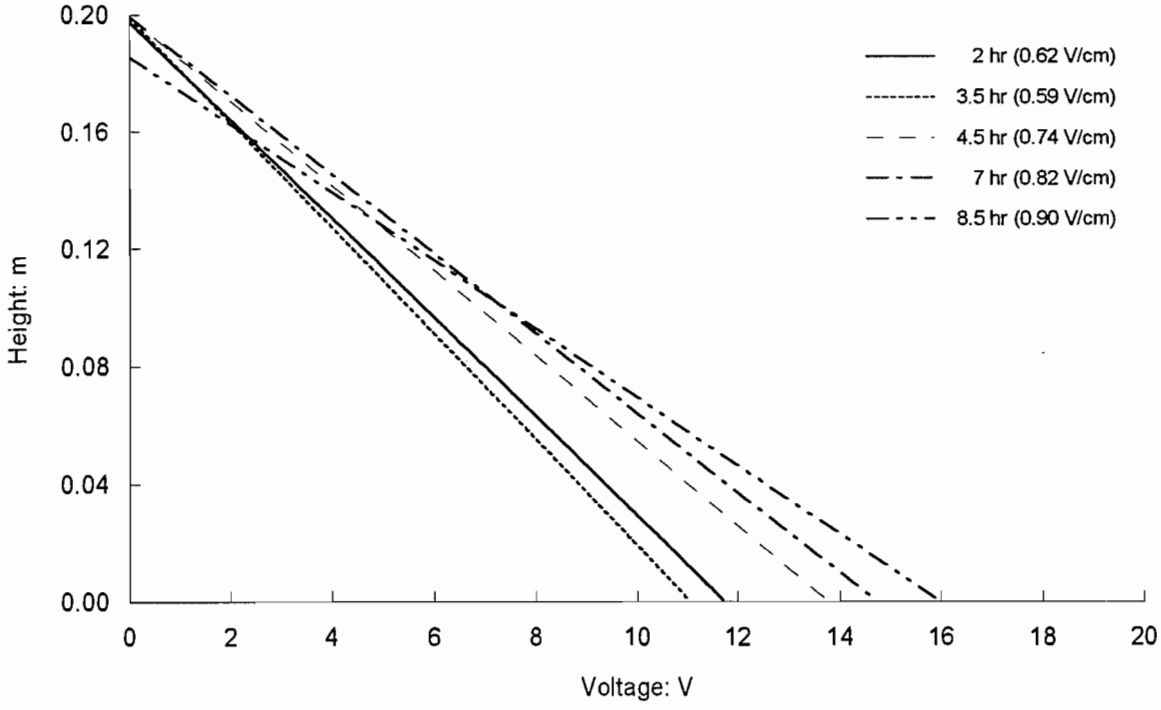

Figure 5.5 Representative voltage gradient profiles across the soil sample, experiment KE7

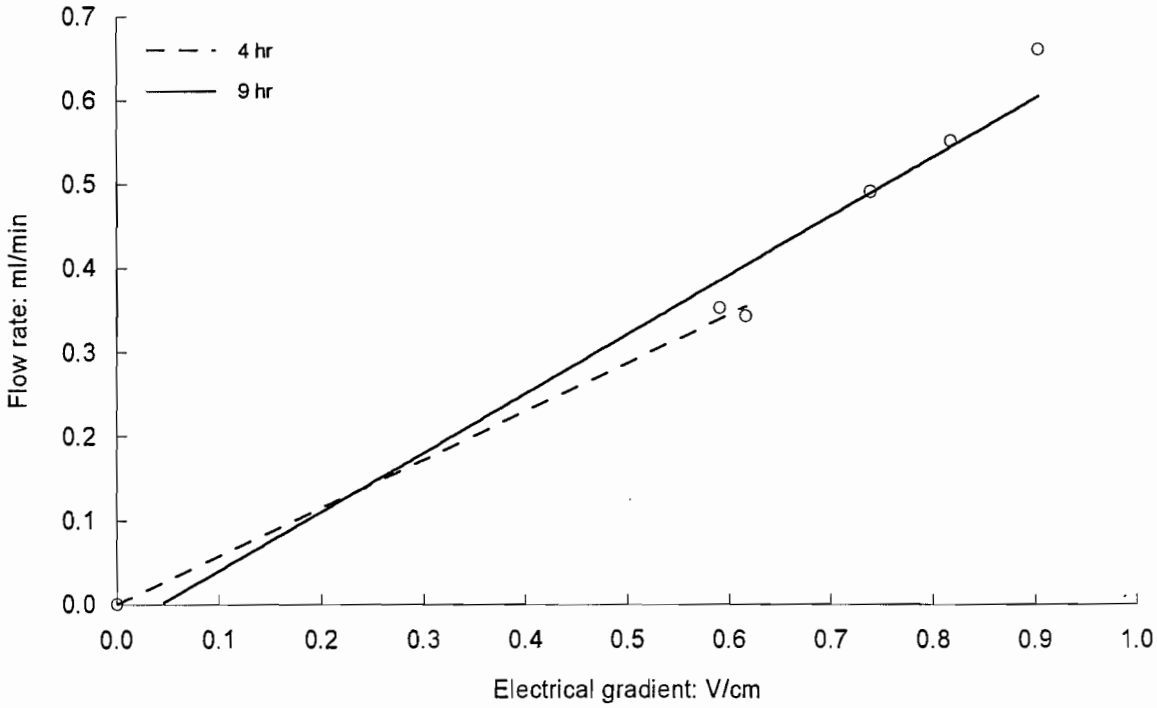

Figure 5.6 Electroosmotic permeability, experiment KE7

in the literature.

The electroosmotic permeability for test KE8, conducted with deionised water, was also calculated in the similar manner described above. The value for test KE8 with deionised water was found to be 2.44×10^{-8} $m^2/V \cdot sec$, which is higher than the value for test KE7 with tap water. The difference appears to be mainly due to the concentration of ions. If the concentration of ions increases, the zeta potential will decrease due to the compression of the electric double layer (Section 2.3.4), which in turn results in a decrease in electroosmotic permeability.

5.4.2 Theoretical Determination of Electroosmotic Permeability

The electroosmotic permeability is directly dependent on porosity, relative permittivity and zeta potential, and inversely related to viscosity as defined in Equation (2.6). Therefore, an alternative method of evaluation is to combine these values.

5.4.2.1 Porosity

The porosity can be calculated directly from the values of specific gravity and density of soil samples used in this study by following equation:

$$n = \frac{G_s \gamma_w - \gamma_s}{(G_s - 1)\gamma_w} \tag{5.5}$$

where G_s is the specific gravity of soil, γ_w is the unit weight of water, and γ_s is the unit weight of slurry.

The changes in porosity during electroosmotic permeability tests estimated by the density profiles range from 0.72 to 0.86 approximately.

5.4.2.2 Viscosity

As the laboratory tests reported in Chapter 4 were conducted at room temperature, the value of viscosity at 25°C for water was necessary in order to provide values for the theoretical predictions of electroosmotic permeability.

5.4.2.3 Permittivity

Static electrical permittivity is defined as follows:

$$\varepsilon = \varepsilon_o D \tag{5.6}$$

where ε_o is the vacuum permittivity and D is the relative permittivity.

Relative permittivity, often called *dielectric constant*, is the ratio of the capacity of an electric condenser in a vacuum and in a given material, but with a vacuum between the plates (Tan, 1993). Only static permittivity is considered further as it is used in double layer theory.

Therefore, Equation (2.6) can be expressed as follows:

$$k_e = \frac{n\varepsilon_o D\zeta}{\eta} \tag{5.7}$$

The dynamic viscosity, vacuum permittivity, and relative permittivity of water at 25°C are given in Table 5.5.

5.4.2.4 Zeta Potential

Zeta potential of a particular soil can be determined from electrophoretic mobility measurements of particles using a flat cell micro-electrophoresis with a zetameter (West & Stewart, 1995), which was not available at Oxford University. The Speswhite kaolin used in this study is chemically similar to the Speswhite kaolin used by West and Stewart and should therefore have similar zeta potential values. Therefore, the value of zeta potential for slurry sample of Speswhite kaolin used in this study was estimated to -20 mV for the pore fluid pH of 4.7 from the measured zeta potential values for Speswhite kaolin clay by West and Stewart (1995).

5.4.2.5 Coefficient of Electroosmotic Permeability

The input parameters used for the theoretical prediction of electroosmotic permeability of Speswhite kaolin clay are given in Table 5.5. The coefficient of electroosmotic permeability calculated from Equation (5.7) ranges from 3.92×10^{-9} to 2.01×10^{-8} $m^2/V \cdot sec$. The representative value of electroosmotic permeability calculated based on the initial condition for the porosity of 0.83 and the zeta potential of -20 mV at pH of 4.7

was 1.29 × 10^{-8} $m^2/V \cdot sec$. The values of the electroosmotic permeability obtained from laboratory electroosmotic permeability tests (Section 5.4.1) were 1.18 × 10^{-8} $m^2/V \cdot sec$ and 1.32 × 10^{-8} $m^2/V \cdot sec$. These results are clearly all in the same range.

Table 5.5 Input parameters for calculation of electroosmotic permeability

Parameter	Value
Vacuum permittivity (ε_o)	8.85 × 10^{-12} (C^2/Jm)
Static electrical permittivity (ε)	6.93 × 10^{-10} (C^2/Jm)
Relative permittivity (D)	78.3
Porosity (n)	0.72 ~ 0.86
Zeta potential (ζ)	7 ~ 30 (mV)
Dynamic viscosity (η)	0.89 × 10^{-3} (Ns/m^2)

REFERENCES

Atkinson, J. H., Evans, J. S., and Ho, E. W. L. (1984). Non-uniformity of triaxial samples due to consolidation with radial drainage. *Geotechnique* 34(3), 353-355.

Atkinson, J. H. and Evans, J. S. (1985). Discussion. *Geotechnique* 35(3), 378-380.

Fannin, R. J. (1986). *Geogrid reinforcement of granular layers on soft clay - a study at model and full scale*. D.Phil. thesis, University of Oxford, UK.

Francescon, M. (1983). *Model pile test in clay - stresses and displacements due to installation and axial loading*. Ph.D. thesis, University of Cambridge, UK.

Gue, S. S. (1984). *Ground heave around driven piles in clay*. D.Phil. thesis, University of Oxford, UK.

Nyirenda, Z. M. (1989). *The piezocone in lightly over consolidated clay*. D.Phil. thesis, University of Oxford, UK.

Stewart, D. I. and West, L. J. (1996). Electrokinetic soil decontamination - effect of local resistivity variations. *Proc. 2th Int. Congress on Environmental Geotechnics, Osaka*, 10, 1101-1106.

Tan, K. H. (1993). *Principles of soil chemistry*. 2nd Ed. Marcel Dkker, Inc.

West, L. J. and Stewart, D. I. (1995). Effect of zetal potential on soil electrokinesis. *Geoenvironment 2000, Geotechnical Special Publication 46*, 1535-1549.

CHAPTER 6 THEORETICAL STUDY

6. THEORETICAL STUDY

6.1 Introduction

This chapter introduces the solutions for the dissipation of excess pore pressure of self-weight and electrokinetic consolidation under particular initial and boundary conditions. Consolidation settlement and density changes due to the changes in excess pore pressure have been investigated using the concept of mass conservation, and compared with laboratory experimental results.

6.2 Solution for Self-weight Consolidation

The differential equation governing Terzaghi's one-dimensional consolidation (Section 2.7.2) gives:

$$\frac{\partial u_e}{\partial t} = C_v \frac{\partial^2 u_e}{\partial z^2} \tag{6.1}$$

where

$$C_v = \frac{k_h}{m_v \gamma_w} \tag{6.2}$$

The general solution to the one-dimensional consolidation Equation (6.1) can be expressed as (Appendix):

$$u_e = (A_1 cosBz + A_2 sinBz) A_3 \exp(-B^2 C_v t) = (A_4 cosBz + A_5 sinBz) \exp(-B^2 C_v t) \tag{6.3}$$

where $A_1 \sim A_5$, and B are constants.

6.2.1 Initial and Boundary Conditions

The values of the constants in Equation (6.3) depend on the drainage boundary conditions and initial distribution of excess pore pressure, so that they can be evaluated from the initial and boundary conditions as shown in Figure 6.1. The initial and boundary conditions for self-weight consolidation (one-way drainage) are as follows:

$$z = 0: \quad 0 \le t \le \infty; \quad u_e = 0$$
$$z = H: \quad 0 \le t \le \infty; \quad \frac{\partial u_e}{\partial z} = 0$$
$$t = 0: \quad 0 \le z \le H; \quad u_e = u_{ei}$$

where z is the distance from the soil surface measured positively downwards, H is the height of soil, and u_{ei} is the initial excess pore pressure.

The first boundary condition dictates that A_4 is 0, and therefore:

$$u_e = A_5 \sin Bz \exp(-B^2 C_v t) \tag{6.4}$$

From the second boundary condition:

$$\frac{\partial u_e}{\partial z} = A_5 B \cos Bz \exp(-B^2 C_v t) = 0 \tag{6.5}$$

and

$$A_5 \cos BH = 0 \quad or \quad BH = \frac{(2n-1)\pi}{2} \tag{6.6}$$

where n is an integer.

From the above, a general solution of Equation (6.3) can be given in the form:

$$u_e = \sum_{n=1}^{n=\infty} A_n \sin \frac{(2n-1)\pi z}{2H} \exp\left(\frac{-(2n-1)^2 \pi^2 T_v}{4} \right) \tag{6.7}$$

where

$$T_v = \frac{C_v t}{H^2} \tag{6.8}$$

and T_v is the dimensionless time factor.

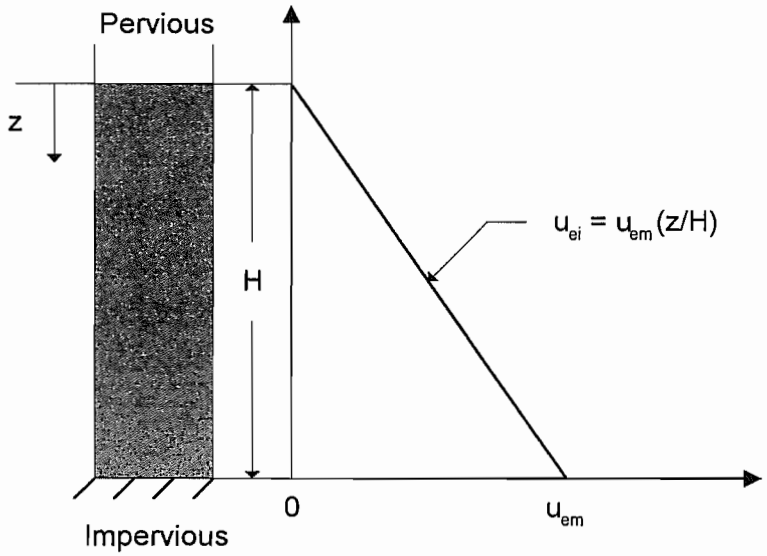

Figure 6.1 Distribution of the initial excess pore pressure for self-weight consolidation

The value of the constant A_n can be found by considering the distribution of excess pore pressure at $t = 0$:

$$u_{ei} = \sum_{n=1}^{n=\infty} A_n \sin\frac{(2n-1)\pi z}{2H} \tag{6.9}$$

Equation (6.9) is a *Fourier sine series*, and A_n can be given by:

$$A_n = \frac{2}{H}\int_0^H u_{ei} \sin\frac{(2n-1)\pi z}{2H} dz \tag{6.10}$$

Combining Equations (6.7) and (6.10) gives:

$$u_e = \sum_{n=1}^{n=\infty}\left(\frac{2}{H}\int_0^H u_{ei} \sin\frac{(2n-1)\pi z}{2H} dz\right) \sin\frac{(2n-1)\pi z}{2H} \exp\left(\frac{-(2n-1)^2\pi^2 T_v}{4}\right) \tag{6.11}$$

If the value of initial excess pore pressure can be given, Equation (6.11) can be solved.

6.2.2 Linear Variation of Initial Excess Pore Pressure

The linear variation of initial excess pore pressure under self-weight condition, as shown in Figure 6.1, can be written as:

$$u_{ei} = u_{em}\frac{z}{H} \tag{6.12}$$

where u_{em} is the maximum excess pore pressure at the base of soil.

Substitution of the above relation for u_{ei} into Equation (6.11) yields:

$$u_e = \sum_{n=1}^{n=\infty}\left(\frac{2}{H}\int_0^H \frac{u_{em}z}{H}\sin\frac{(2n-1)\pi z}{2H}dz\right)\sin\frac{(2n-1)\pi z}{2H}\exp\left(\frac{-(2n-1)^2\pi^2 T_v}{4}\right) \tag{6.13}$$

therefore

$$u_e = \frac{8u_{em}}{\pi^2}\sum_{n=1}^{n=\infty}\frac{(-1)^{n+1}}{(2n-1)^2}\sin\frac{(2n-1)\pi z}{2H}\exp\left(\frac{-(2n-1)^2\pi^2 T_v}{4}\right) \tag{6.14}$$

Equation (6.14) is the analytical solution for the dissipation of excess pore pressure under self-weight condition. The solution for Equation (6.14) is shown in Figure 6.2 with dimensionless height.

The average degree of consolidation for the entire layer is given by:

$$U_{av} = \frac{\frac{1}{H}\int_0^H u_{ei}dz - \frac{1}{H}\int_0^H u_e dz}{\frac{1}{H}\int_0^H u_{ei}dz} \tag{6.15}$$

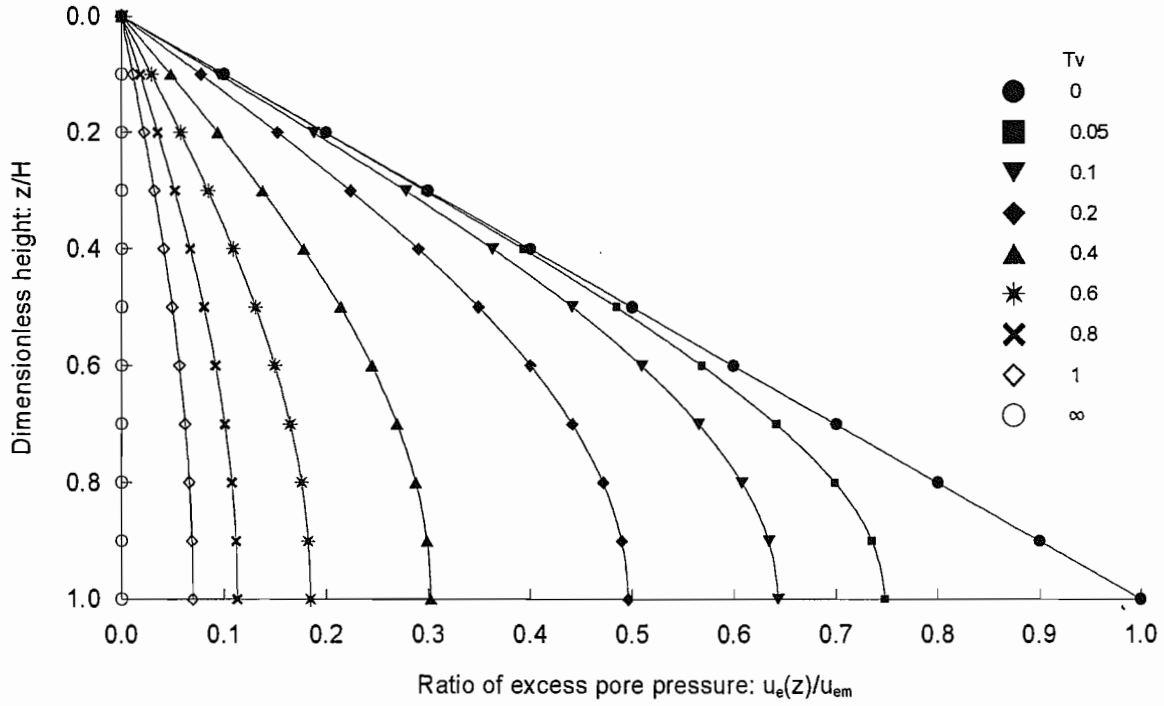

Figure 6.2 Isochrones of excess pore pressure as a function of dimensionless time and distance for one-dimensional self-weight consolidation with drainage through the upper surface only

Combining Equations (6.14) and (6.15) gives:

$$U_{av} = 1 - \frac{32}{\pi^3} \sum_{n=1}^{n=\infty} \frac{(-1)^{n+1}}{(2n-1)^3} \exp\left(\frac{-(2n-1)^2 \pi^2 T_v}{4} \right) \tag{6.16}$$

The average degree of consolidation curve from Equation (6.16) is shown in Figure 6.3 as a function of the dimensionless time factor.

6.3 Solution for Electrokinetic Consolidation

The differential equation governing one-dimensional electrokinetic consolidation reviewed in Section 2.7.2 is:

$$C_v \frac{\partial^2 \xi}{\partial z^2} = \frac{\partial \xi}{\partial t} \tag{6.17}$$

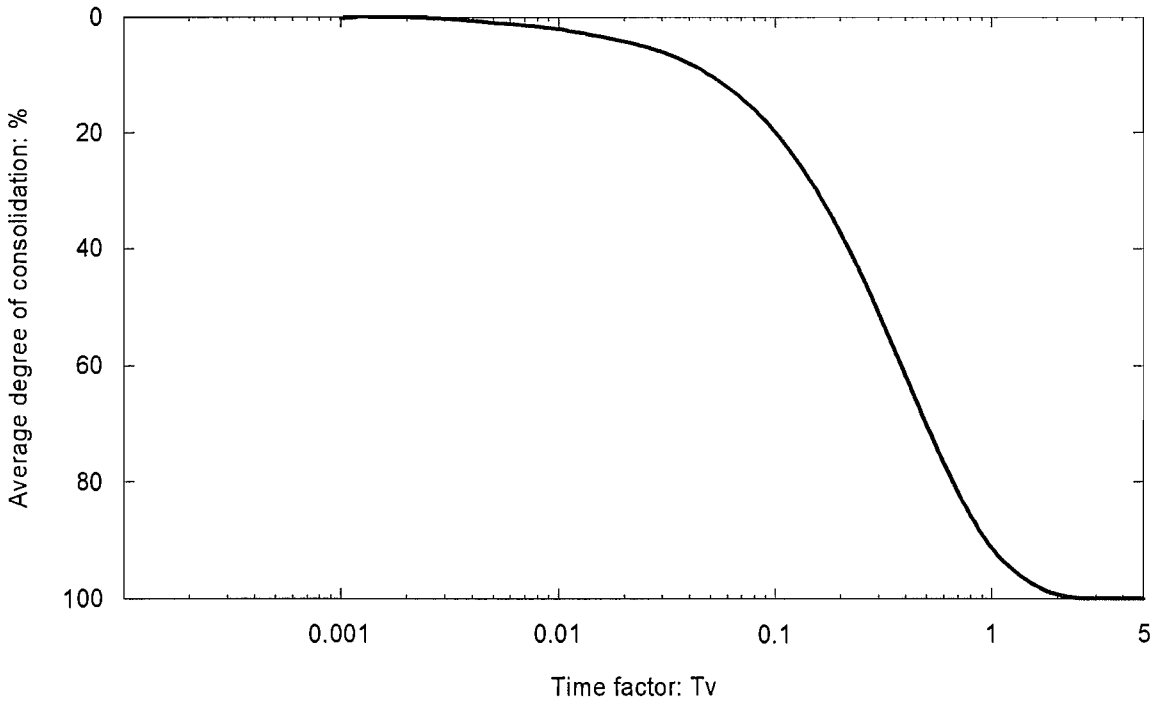

Figure 6.3 Average degree of consolidation versus dimensionless time for one-dimensional self-weight consolidation

where the dummy variable is given as:

$$\xi = \frac{k_e \gamma_w}{k_h} E + u_e \tag{6.18}$$

6.3.1 Linear Variation of Electrical Potential Gradient

One of the assumptions for the theoretical prediction of electrokinetic flow process is that the electrical voltage gradient between electrodes is linear and constant during the electrokinetic process. The linear variation of the applied electric field, as shown in Figure 6.4, may be written as:

$$E = E_m \frac{z}{H} \tag{6.19}$$

where E is the applied voltage, E_m is the maximum applied voltage at the anode, z is the distance from the cathode, and H is the distance between electrodes.

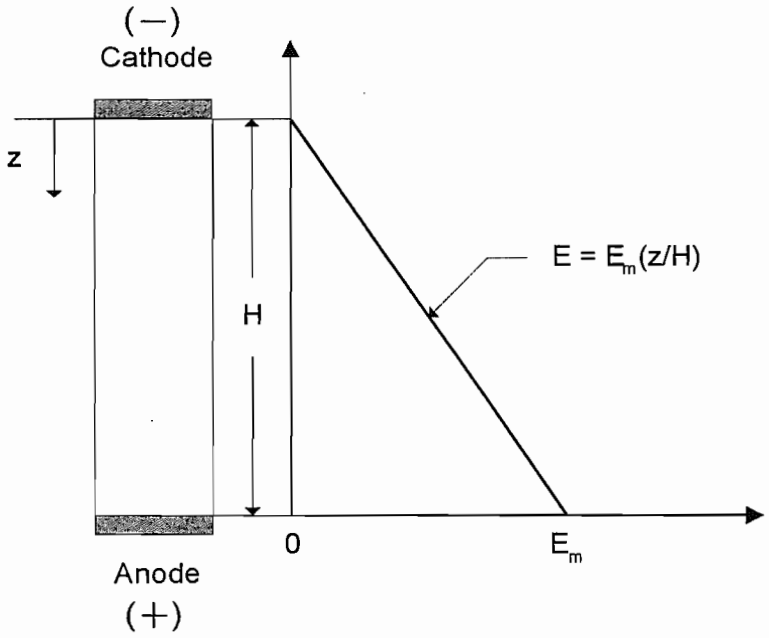

Figure 6.4 Linear variation of the voltage gradient across the electrodes

6.3.2 Initial and Boundary Conditions

Electroosmotic flow generated by the applied electric field will flow from the closed anode towards the open cathode during electrokinetic consolidation (Section 2.5.3). If the anode is positioned at the bottom of the soil mass and the cathode at the top, the boundary conditions in this case are exactly the same as in one-dimensional self-weight consolidation. The boundary conditions are as follows:

$$\textit{Cathode}\,(z=0):\quad 0 \le t \le \infty;\quad u_e = 0;\quad E = 0;\quad \xi = 0$$

$$\textit{Anode}\,(z=H):\quad 0 \le t \le \infty;\ \textit{zero flow};\quad \frac{\partial \xi}{\partial z} = 0$$

By use of the preceding boundary conditions, the solutions for Equation (6.17) can be given following the same procedures reported in the previous section and Appendix:

$$\xi = \sum_{n=1}^{n=\infty} A_n \sin\frac{(2n-1)\pi z}{2H} \exp\left(\frac{-(2n-1)^2\pi^2 T_v}{4}\right) \tag{6.20}$$

The initial boundary condition can be expressed as follows:

$$t = 0: \quad 0 \le z \le H; \quad \xi = \xi_i$$

To satisfy the initial boundary condition at $t = 0$, the value of the constant A_n may be found as follows:

$$\xi_i = \sum_{n=1}^{n=\infty} A_n \sin\frac{(2n-1)\pi z}{2H} \tag{6.21}$$

Equation (6.21) is a *Fourier sine series*, and A_n can be given by:

$$A_n = \frac{2}{H}\int_0^H \xi_i \sin\frac{(2n-1)\pi z}{2H} dz \tag{6.22}$$

Combining Equations (6.20) and (6.22) gives:

$$\xi = \sum_{n=1}^{n=\infty}\left(\frac{2}{H}\int_0^H \xi_i \sin\frac{(2n-1)\pi z}{2H} dz\right)\sin\frac{(2n-1)\pi z}{2H}\exp\left(\frac{-(2n-1)^2\pi^2 T_v}{4}\right) \tag{6.23}$$

6.3.3 Zero Initial Excess Pore Pressure

If the initial excess pore pressure is zero, ξ_i is given by Equations (6.18) and (6.19) as:

$$\xi_i = \frac{k_e \gamma_w}{k_h} E = \frac{k_e \gamma_w E_m}{k_h}\frac{z}{H} \tag{6.24}$$

Substitution of the above relation for ξ_i into Equation (6.23) yields:

$$\xi = \sum_{n=1}^{n=\infty}\left[\frac{2}{H}\left(\frac{k_e \gamma_w E_m}{k_h}\right)\int_0^H \frac{z}{H}\sin\frac{(2n-1)\pi z}{2H} dz\right]\sin\frac{(2n-1)\pi z}{2H}\exp\left(\frac{-(2n-1)^2\pi^2 T_v}{4}\right) \tag{6.25}$$

where

$$\frac{2}{H}\int_0^H \frac{z}{H}\sin\frac{(2n-1)\pi z}{2H}dz = \frac{8(-1)^{n+1}}{(2n-1)^2\pi^2} \tag{6.26}$$

hence

$$\xi = \frac{8k_e\gamma_w E_m}{k_h\pi^2}\sum_{n=1}^{n=\infty}\frac{(-1)^{n+1}}{(2n-1)^2}\sin\frac{(2n-1)\pi z}{2H}\exp\left(\frac{-(2n-1)^2\pi^2 T_v}{4}\right) \tag{6.27}$$

From Equation (6.18), u_e can be expressed as follows:

$$u_e = -\frac{k_e\gamma_w}{k_h}E(z) + \frac{8k_e\gamma_w E_m}{k_h\pi^2}\sum_{n=1}^{n=\infty}\frac{(-1)^{n+1}}{(2n-1)^2}\sin\frac{(2n-1)\pi z}{2H}\exp\left(\frac{-(2n-1)^2\pi^2 T_v}{4}\right) \tag{6.28}$$

Equation (6.28) is the analytical solution to predict the dissipation of excess pore pressure during the electrokinetic process. The solution for Equation (6.28) is shown in Figure 6.5.

The average degree of electrokinetic consolidation for the entire layer can also be given by Equation (6.15). Combining Equations (6.15) and (6.28) gives:

$$U_{av} = 1-\frac{32}{\pi^3}\sum_{n=1}^{n=\infty}\frac{(-1)^{n+1}}{(2n-1)^3}\exp\left(\frac{-(2n-1)^2\pi^2 T_v}{4}\right) \tag{6.29}$$

This equation for the average degree of consolidation under electrokinesis is identical to Equation (6.16), which was for the case of self-weight consolidation, and so the same curve as shown in Figure 6.3 can be used.

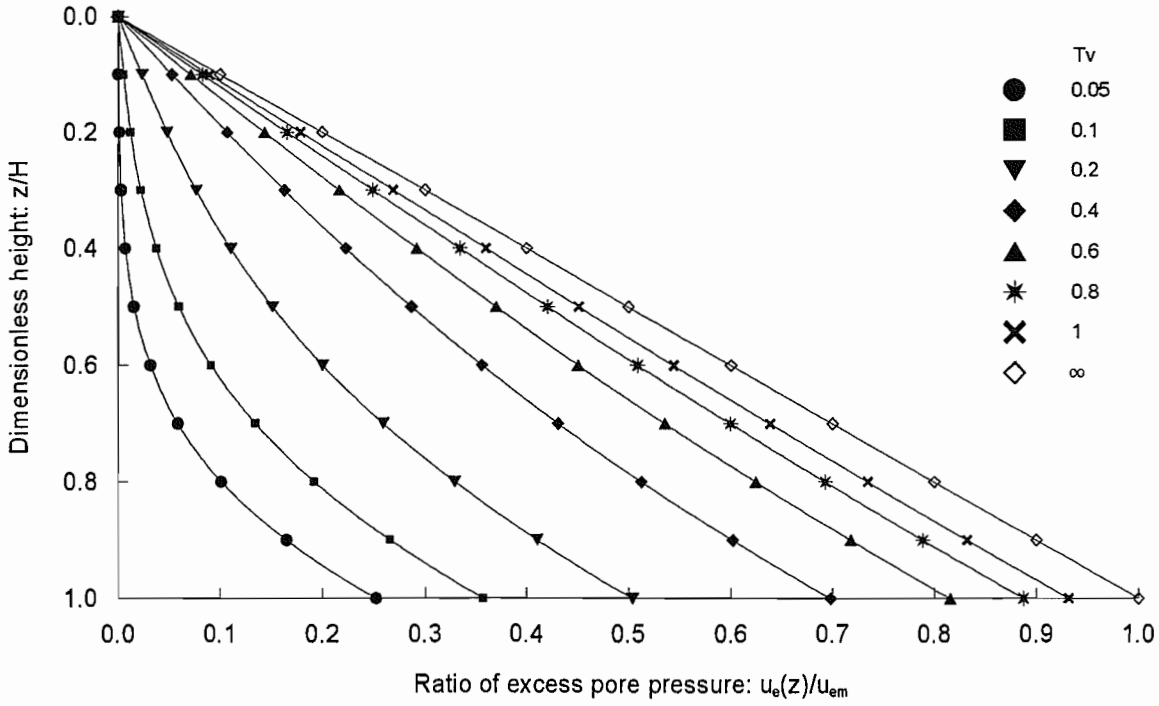

Figure 6.5 Isochrones of excess pore pressure as a function of dimensionless time and distance for one-dimensional electrokinetic consolidation with drainage through the upper surface (cathode)

6.3.4 Linear Variation of Initial Excess Pore Pressure

If the initial excess pore pressure varies linearly as shown in Figure 6.6, ξ_i may be written as:

$$\xi_i = \left(\frac{k_e \gamma_w}{k_h} E_m + u_{em} \right) \frac{z}{H} \tag{6.30}$$

Substitution of the above relation for ξ_i into Equation (6.23) yields:

$$\xi = \frac{8}{\pi^2} \left(\frac{k_e \gamma_w}{k_h} E_m + u_{em} \right) \sum_{n=1}^{n=\infty} \frac{(-1)^{n+1}}{(2n-1)^2} \sin \frac{(2n-1)\pi z}{2H} \exp\left(\frac{-(2n-1)^2 \pi^2 T_v}{4} \right) \tag{6.31}$$

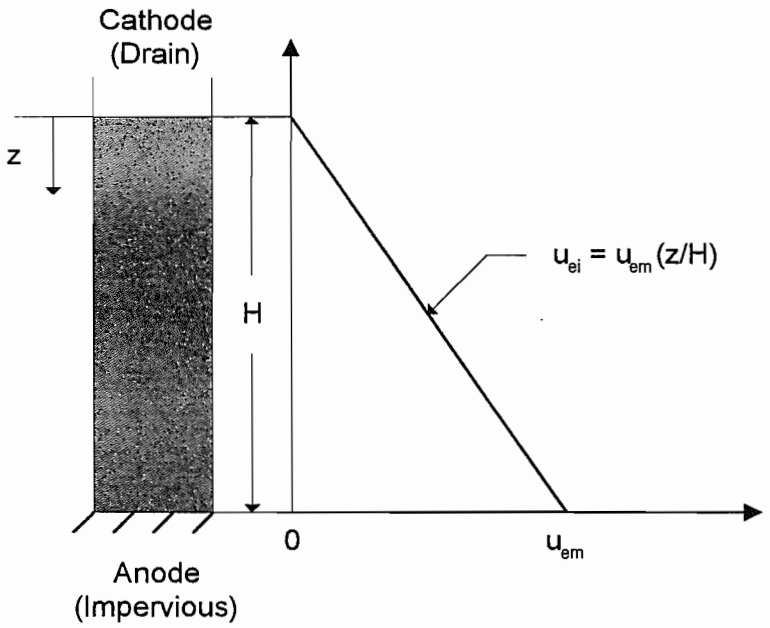

Figure 6.6 Distribution of the initial excess pore pressure for electrokinetic consolidation

therefore, from Equation (6.18), u_e can be given by:

$$u_e = -\frac{k_e \gamma_w}{k_h} E(z) + \frac{8}{\pi^2}\left(\frac{k_e \gamma_w}{k_h} E_m + u_{em}\right) \sum_{n=1}^{n=\infty} \frac{(-1)^{n+1}}{(2n-1)^2} \sin\frac{(2n-1)\pi z}{2H} \exp\left(\frac{-(2n-1)^2 \pi^2 T_v}{4}\right) \tag{6.32}$$

The average degree of consolidation can also be obtained by solving Equations (6.15) and (6.32):

$$U_{av} = 1 - \frac{32}{\pi^3} \sum_{n=1}^{n=\infty} \frac{(-1)^{n+1}}{(2n-1)^3} \exp\left(\frac{-(2n-1)^2 \pi^2 T_v}{4}\right) \tag{6.33}$$

This is also identical to Equations (6.16) and (6.29), which was for the case where the excess pore pressure is zero with depth, and so the same curve as shown in Figure 6.3 can be used.

6.4 Calculation of Surface Settlement and Density Profile

This section introduces calculations of consolidation settlement and changes in density throughout the soil induced by the dissipation of excess pore pressure.

6.4.1 Surface Settlement

At the end of consolidation, pore pressures will be hydrostatic below the surface of the soil mass. As the total vertical stress is simply a function of depth in the soil mass, the increase in effective stress is equal to the decrease in excess pore pressure. Values of excess pore pressure can be calculated directly from the analytical solutions given in the previous sections, and subtracted from the total vertical stress to give the vertical effective stress. By dividing the soil mass into small elements as shown in Figure 6.7(a), the increase in effective stress at the centre of the element, or the average of the increase in effective stress at the top and at the bottom of the layer may be estimated.

Assuming that strains are one-dimensional and small (i.e. that the boundary position remains constant), the changes in void ratio for each layer can be estimated from Equation (6.34) by calculation of a representative increase in effective stress for each layer as shown in Figure 6.7(b).

$$e_f = e_i - C_c \log(\sigma'_{vf} / \sigma'_{vi}) \tag{6.34}$$

where C_c is the compression index, e_i and e_f are the initial and final void ratios, and σ_{vi}' and σ_{vf}' are the initial and final vertical effective stresses respectively.

The calculated final void ratio from Equation (6.34) can then be converted to the final consolidation settlement ρ_f in each of the elements by following equation:

$$\rho_f = \frac{C_c \log(\sigma'_{vf} / \sigma'_{vi})}{1 + e_i} h \tag{6.35}$$

where h is the thickness of soil element.

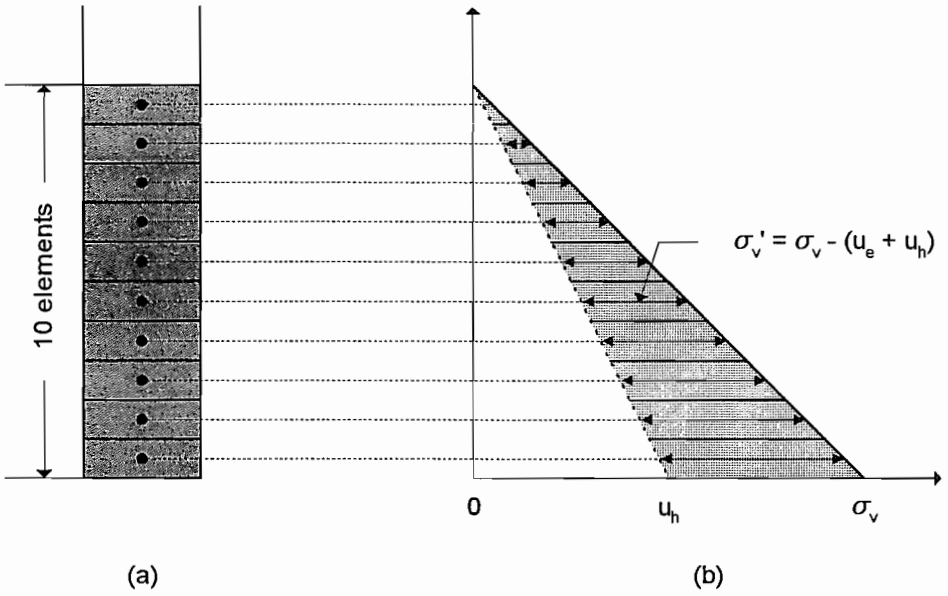

Figure 6.7 Estimation of final consolidation settlement with small strain assumption: (a) soil elements; (b) stress distribution (σ_v': vertical effective stress; σ_v: total vertical stress; u_e: excess pore pressure; u_h: hydrostatic pressure)

Then, the settlement at the soil surface can be estimated by adding together the settlement of each layer. The consolidation settlement at any time *t* can then be calculated from Equation (6.16). The dimensionless settlement as a function of time factor for consolidation is presented in Figure 6.8.

6.4.2 Excess Pore Pressure Profile

Normalised excess pore pressure as a function of dimensionless height *z/H* and time factor T_v can be calculated from appropriate equations (Sections 6.2 and 6.3). These profiles for one-dimensional self-weight consolidation from Figure 6.2 have been plotted in Figure 6.9. In the small strain approach followed so far, the boundary of the soil remains at *z/H = 0*. However, the calculated settlement provides an estimate of the changing location of the surface, and this has been incorporated into the excess pore pressure profiles as shown in Figure 6.9.

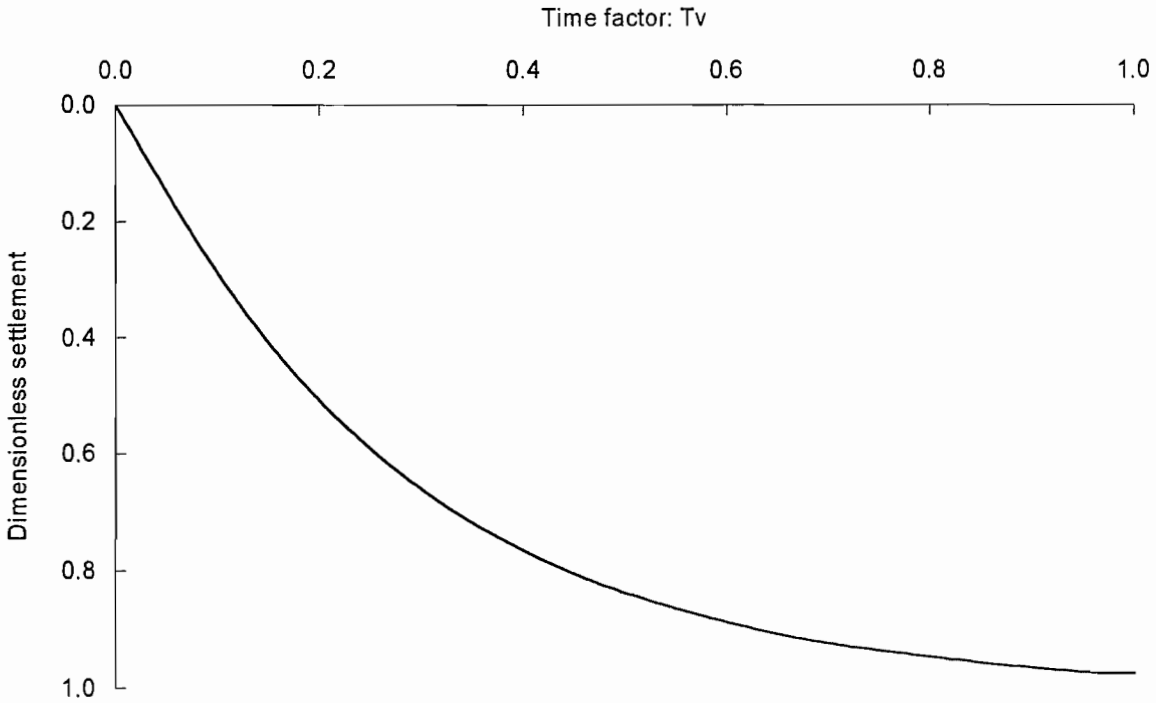

Figure 6.8 Dimensionless consolidation settlement as a function of dimensionless time factor

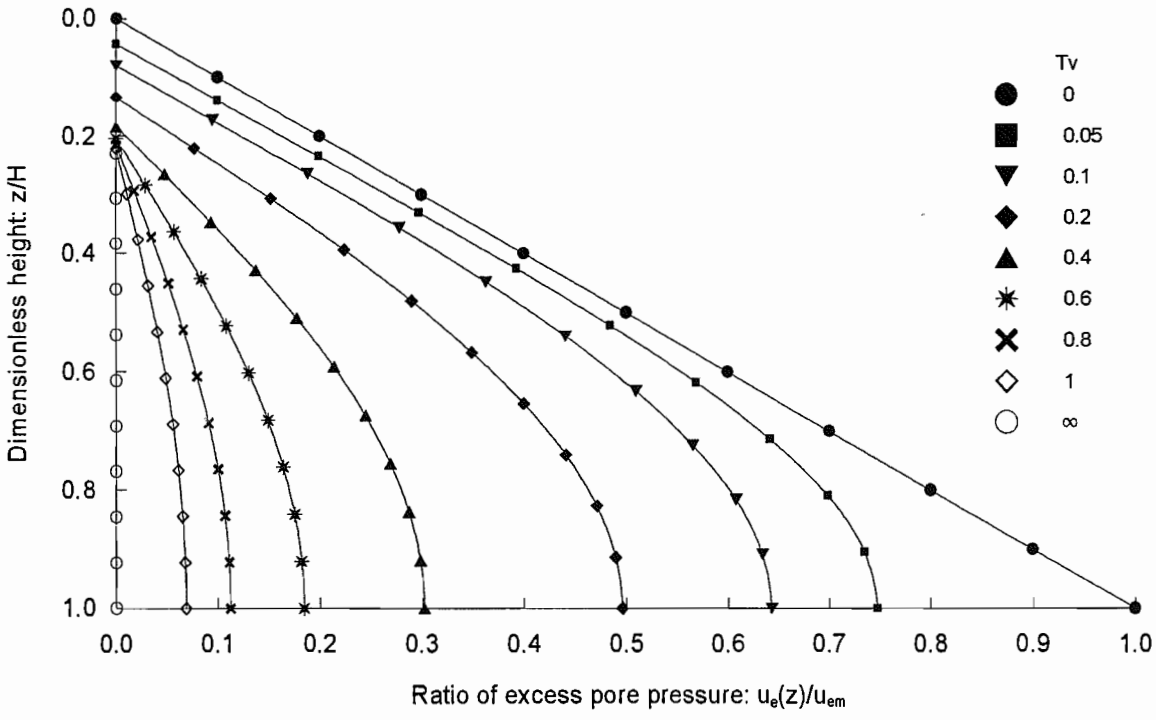

Figure 6.9 Normalised excess pore pressure profiles with dimensionless surface settlement and respect to time factor

6.4.3 Density Profile

As the changes in sample height at any time t can be calculated (Section 6.4.1), the corresponding vertical effective stress can also be estimated from the excess pore pressures calculated independently (Section 6.4.2). Following the similar procedure as reported in Section 6.4.1, the changes in void ratio for each layer can be calculated from the vertical effective stress from Equation (6.34). Thus, the changes in density for each layer can be estimated by the following equation:

$$\gamma_s = \frac{G_s + e}{(1 + e)} \gamma_w \tag{6.36}$$

where G_s is the specific gravity of soil, γ_w is the unit weight of water, and γ_s is the unit weight of slurry.

6.5 Numerical Simulations for Self-weight Consolidation

In order to assess material parameters for the soil sample used in the laboratory tests and to validate the analytical models for electrokinetic consolidation described in Section 6.3, numerical simulations were carried out on the evaluation of soil behaviour under self-weight condition. If there is no electric field applied across the soil mass, voltage E and the coefficient of electroosmotic permeability k_e in Equation (6.32) should be zero. The analytical solution for electrokinetic consolidation then becomes exactly the same as Equation (6.14) for self-weight consolidation. Therefore, self-weight consolidation behaviour can be simulated using the analytical model for electrokinetic consolidation by giving the values of electroosmotic permeability and applied electric field as zero.

6.5.1 Choice of Soil Parameters and Initial Conditions

Self-weight consolidation tests were performed with the initial density of 1.22 Mg/m^3 and height of 0.2 m, and measured overlying water density during the test was 1.001 Mg/cm^3 (Chapter 4). The specific gravity of Speswhite kaolin clay was chosen from literature as 2.61.

The effective stress and void ratio relationship from Figure 4.4 for test KS1 has been plotted in Figure 6.10 on a logarithmic scale. Initial void ratio at zero effective stress can be calculated directly from the known initial slurry density as 6.32. As shown by Figure 6.10, the range of effective stress for initial slurry sample is so wide and the accuracy of pore pressure measurement is the order of ±0.01 kPa (Chapter 3). Therefore, the value of initial void ratio used for numerical simulation has been determined as 6.1 at the effective stress of 0.02 kPa.

The value of void ratio at the end of self-weight consolidation was 4.14 at the effective stress of 0.38 kPa. Given the void ratio and corresponding effective stress values, compression index C_c and the coefficient of compressibility m_v can be calculated by following equations:

$$C_c = \frac{e_i - e_f}{\log(\sigma_f' / \sigma_i')} \tag{6.37}$$

$$m_v = \frac{1}{1 + e_i}\left(\frac{e_i - e_f}{\sigma_f' - \sigma_i'}\right) \tag{6.38}$$

where e_i and σ_i' are the void ratio and effective stress at the beginning of consolidation, and e_f and σ_f' are those at the end of consolidation respectively.

6.5.2 Determination of the Coefficient of Consolidation

The time factor T_v consists of the coefficient of consolidation, C_v, real time, t, and the sample height, H (Equation (6.8)). Two soil parameters, the hydraulic permeability, k_h, and the coefficient of compressibility, m_v, are embodied in the coefficient of consolidation, C_v (Equation (6.2)). Therefore, two of the three parameters of hydraulic permeability, coefficient of compressibility, and coefficient of consolidation must be specified in order to generate a solution to the equations for prediction of excess pore pressures described in Sections 6.2 and 6.3.

The compression index and the coefficient of compressibility have been determined in the previous section as 1.53 and 0.77 respectively. As already shown by Figure 5.3 (Section 5.3), the void ratio and hydraulic permeability relationship calculated from density and pore pressure profiles gives a wide range of hydraulic permeability values covering the changes in void ratio throughout the soil sample. Therefore, a direct estimate of the coefficient of consolidation is obtained by finding the best fit between calculated and measured excess pore pressure at some instant. In this case, the 69 hour excess pore pressure profile was chosen.

The excess pore pressure profile calculated after 69 hours of self-weight consolidation process is shown in Figure 6.11 as a solid line with the real measurement as dots. The coefficient of consolidation determined for this best fit result is 4.12×10^{-8} m/sec.

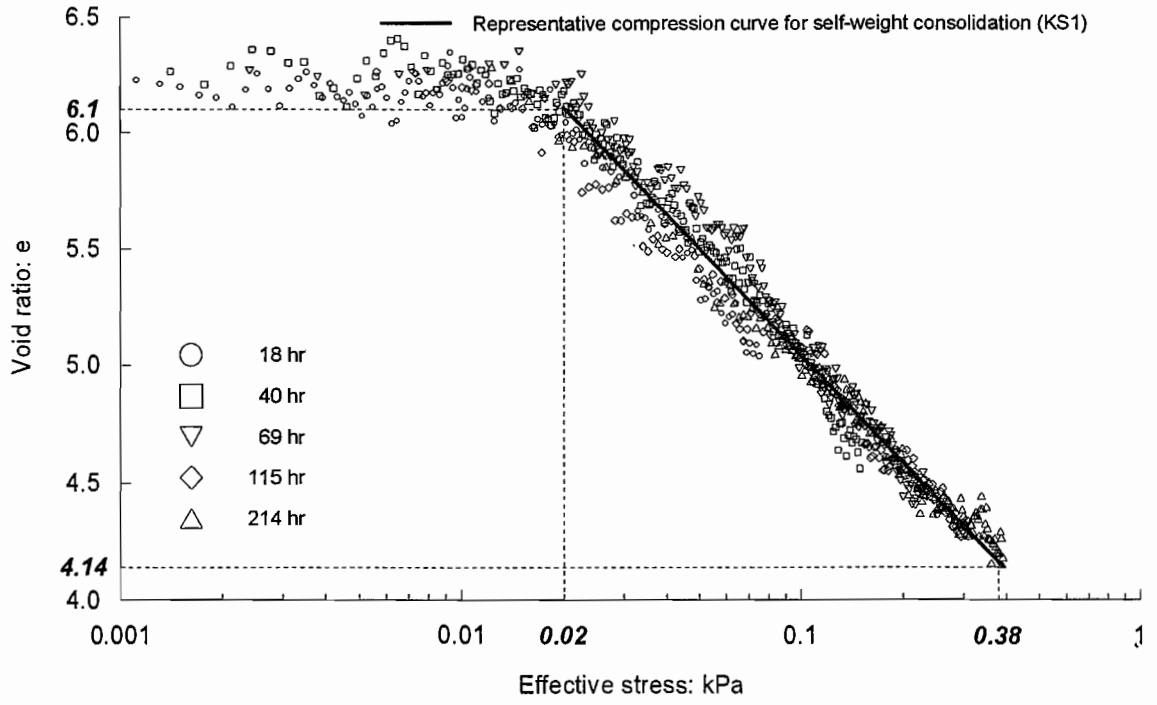

Figure 6.10 Determination of compression index and compressibility from effective stress and void ratio relationship, experiment KS1

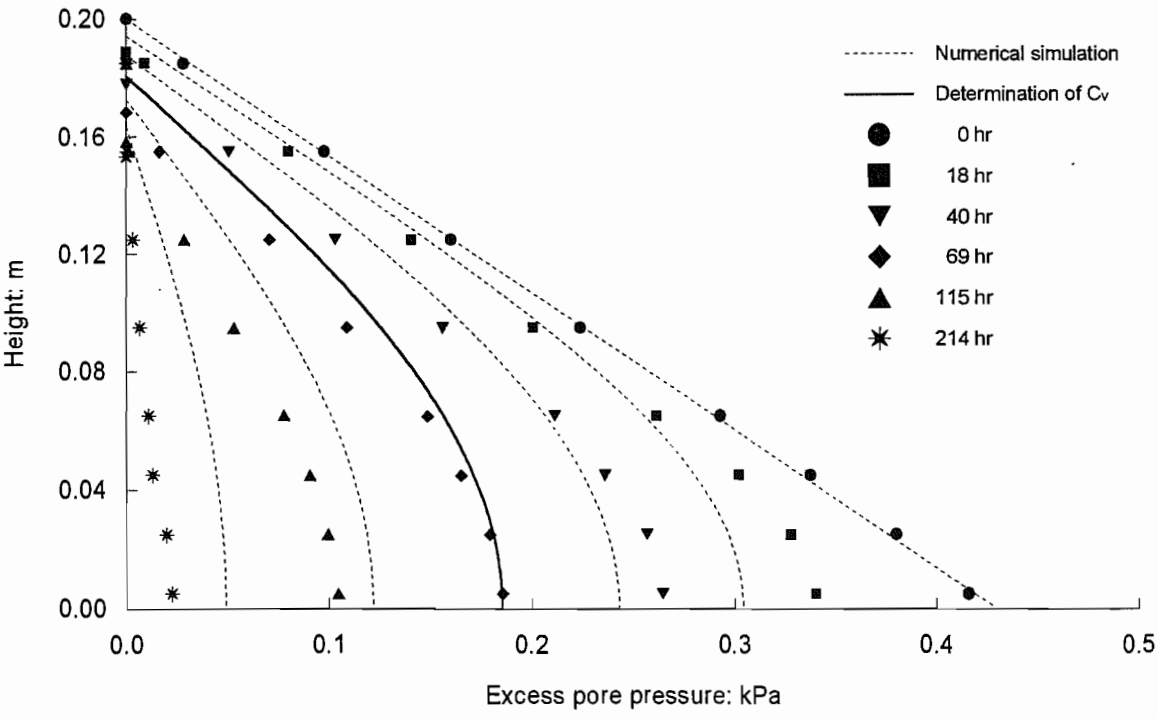

Figure 6.11 Determination of the coefficient of consolidation from excess pore pressure distributions, experiment KS1

All the other excess pore pressure profiles were then calculated using this value of the consolidation coefficient, and theoretical and experimental values are plotted in Figure 6.11 as dotted lines and points respectively.

6.5.3 Numerical Simulations with Small Strain Assumption

In this section, the value of consolidation coefficient determined from test KS1 is therefore used as an input parameter in the analytical model in order to compare simulated surface settlement, density and excess pore pressure profiles within the layer of soil sample to actual measurements. The parameters used for numerical simulations are given in Table 6.1.

Some of calculated density and excess pore pressure profiles for self-weight consolidation test KS1 are shown in Figure 6.12 with measured profiles. As seen, calculated excess pore pressure profiles fit the real profiles reasonably well. This is expected as the value of consolidation coefficient for the simulation was partly based on the measured excess pore pressure profile (Section 6.5.2). However, it can be noted that the calculated density profiles are slightly larger than measured profiles. As there is no change in the total stress during self-weight consolidation, the total stress at any particular level in soil sample should be equal to the integral of the density above that level. However, numerical simulations with small strain assumption did not satisfy this condition.

Table 6.1 Material parameters from test KS1 for numerical simulation

Parameter	Value
Initial height (m)	0.2
Initial slurry density (Mg/m^3)	1.22
Overlying water density (Mg/m^3)	1.001
Specific gravity	2.61
Void ratio at zero effective stress	6.32
Void ratio at the beginning of consolidation	6.1
Void ratio at the end of consolidation	4.14
Effective stress at the beginning of consolidation (kPa)	0.02
Effective stress at the end of consolidation (kPa)	0.38
Compression index	1.53
Coefficient of compressibility (m^2/kN)	0.77

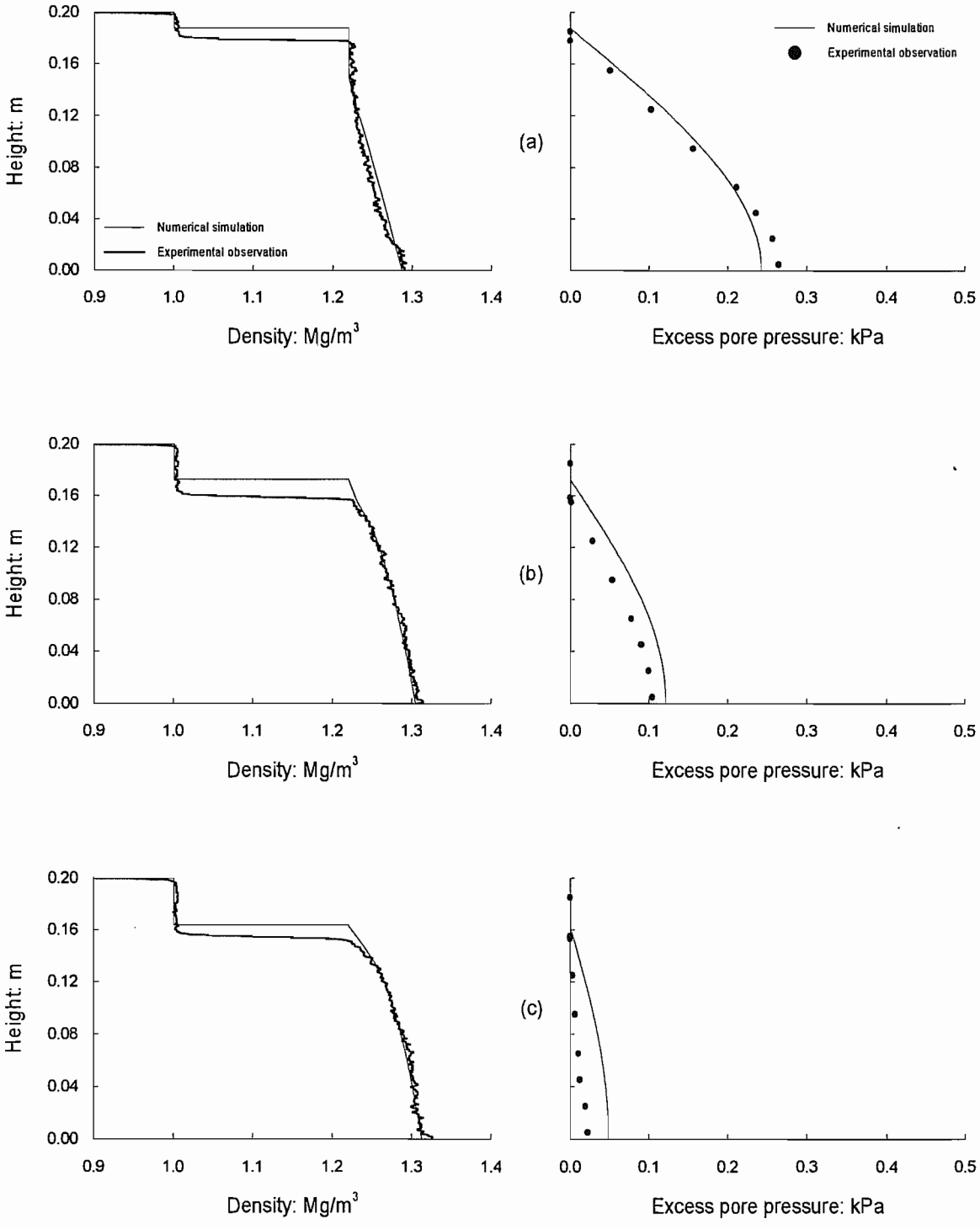

Figure 6.12 Numerical simulation of density and excess pore pressure profiles correspond to small strain assumption, experiment KS1: (a) 40 hr; (b) 115 hr; (c) 214 hr

6.5.4 Corrections of Surface Settlement and Density Profile

Figure 6.13 illustrates this requirement in the simple case by starting from the assumption that a soil bed of uniform density increases by consolidation to another bed of uniform higher density. A simplified block diagram of the procedure for determination of new total stress distribution is given in Figure 6.14. The surface settlement is calculated as already described in Section 6.4.1. The total vertical stress at the base remains unchanged at σ_v, and the effective stress, the difference between the total stress curve and pore pressure, leads to a new void ratio and density distribution. This then gives use to a new total stress variation (no longer linear) through the bed combined with a new settlement to be consistent with the new void ratio (see Figure 6.13(c)). The condition of constant area beneath the density profile is checked, and the surface position and densities are adjusted by a process of iteration until this area no longer changes. Thus, when a density profile is achieved which is consistent with the pore pressures and total stresses and for which mass is conserved, this must be the correct solution for the soil parameters used.

Figure 6.15(a) shows an example of density profile calculated under the small strain assumption by comparison with the profile simulated based on the conservation of mass. As seen, the density profile estimated under the small strain assumption gives bigger total stress than that calculated based on the conservation of mass due to the overestimated effective stresses throughout the soil sample (see also Figures 6.13(b) and (c)). Figure 6.15(b) shows an example of density profiles with time interval calculated based on the conservation of mass. The area of overlying water, indicated as (A), after a certain period of consolidation process shows the reduction of total vertical stress becoming hydrostatic pressure. Therefore, the reduction of total vertical stress in overlying water should be the same as the integral of the increased soil density, indicated as (B), due to the consolidation process, so that there is no change in the total vertical stress.

6.5.5 Numerical Simulations with Conservation of Mass

Figure 6.16 shows measured surface settlement for test KS1 as dots with calculated settlement as solid line plotted on the same axes. As seen, the numerical simulation incorporating the conservation of mass gives good agreement with the measured settlement. Simulated density and excess pore pressure profiles are also compared in Figure 6.17 with measured profiles. Calculated excess pore pressure profiles are similar as those shown in Figure 6.12 because those can be calculated directly from appropriate equations given in Sections 6.2 and 6.3. It can be seen that simulated density profiles based on the mass conservation fit very closely to the measured profiles observed in the laboratory experiment. The input parameters for this simulation are the effective stress and void ratio relationship

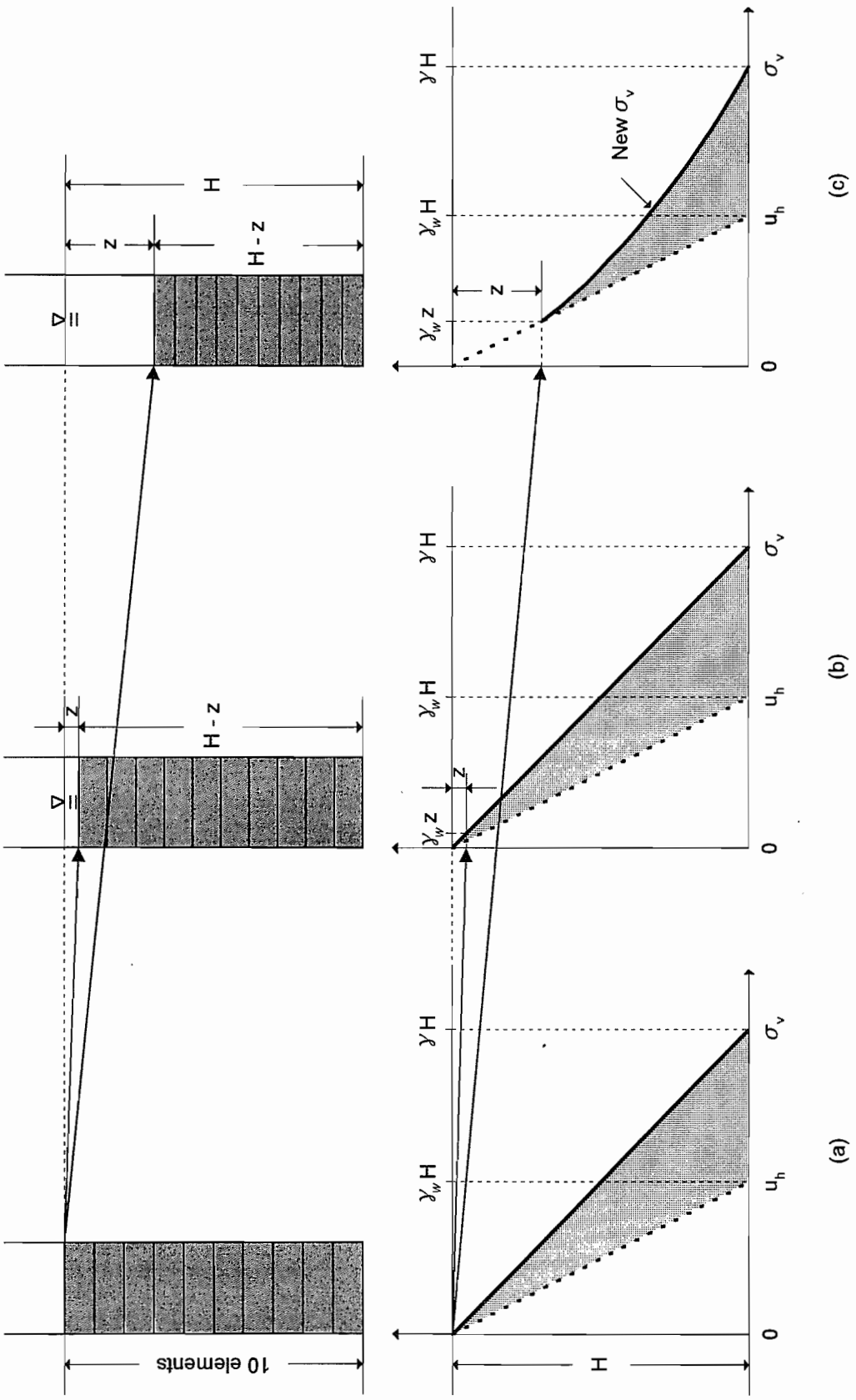

Figure 6.13 Correction of total stress distribution with consolidation settlement: (a) initial condition; (b) small strain approach; (c) mass conservation approach

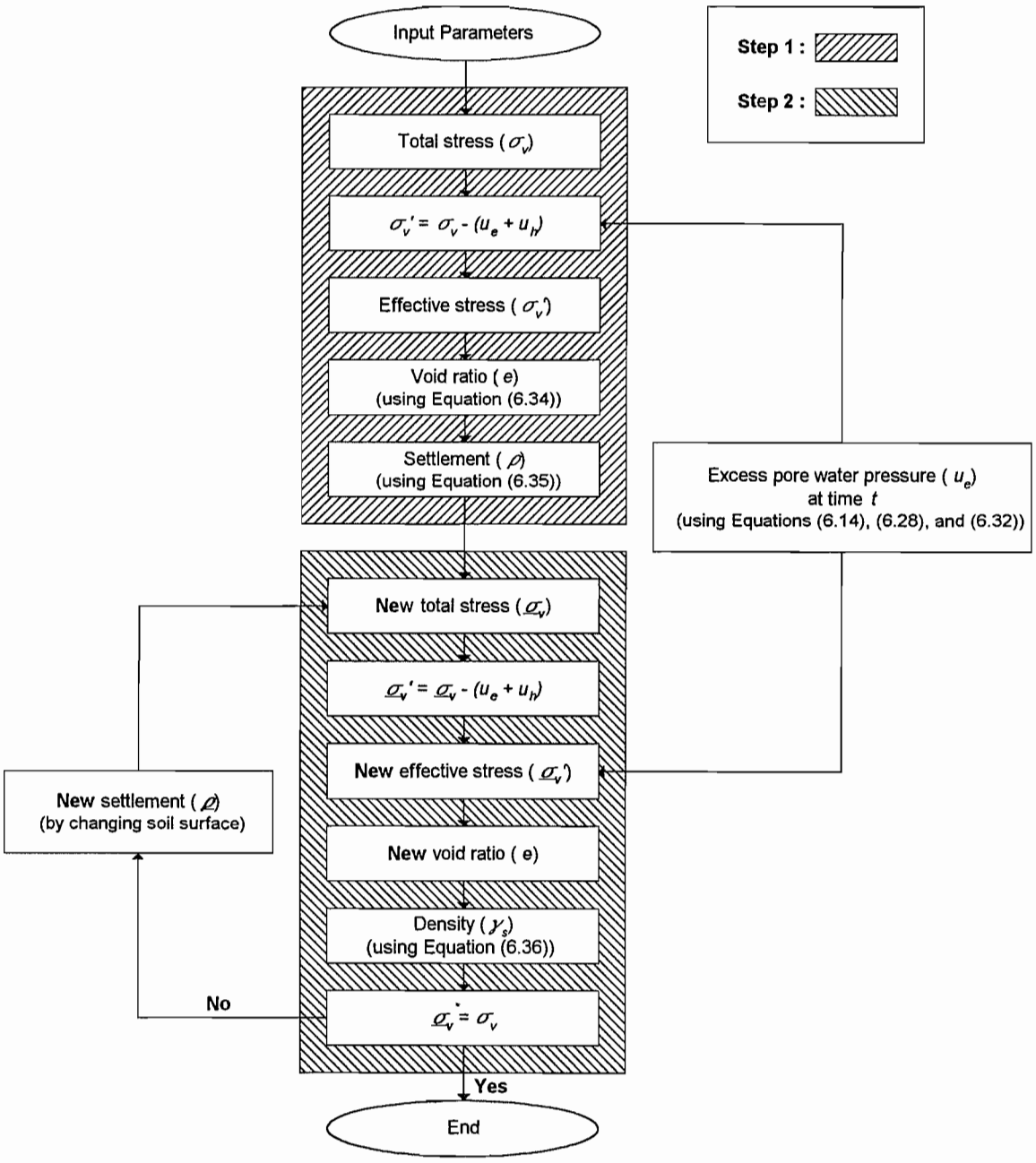

Figure 6.14 Block diagram of the procedure for determination of surface settlement based on conservation of mass

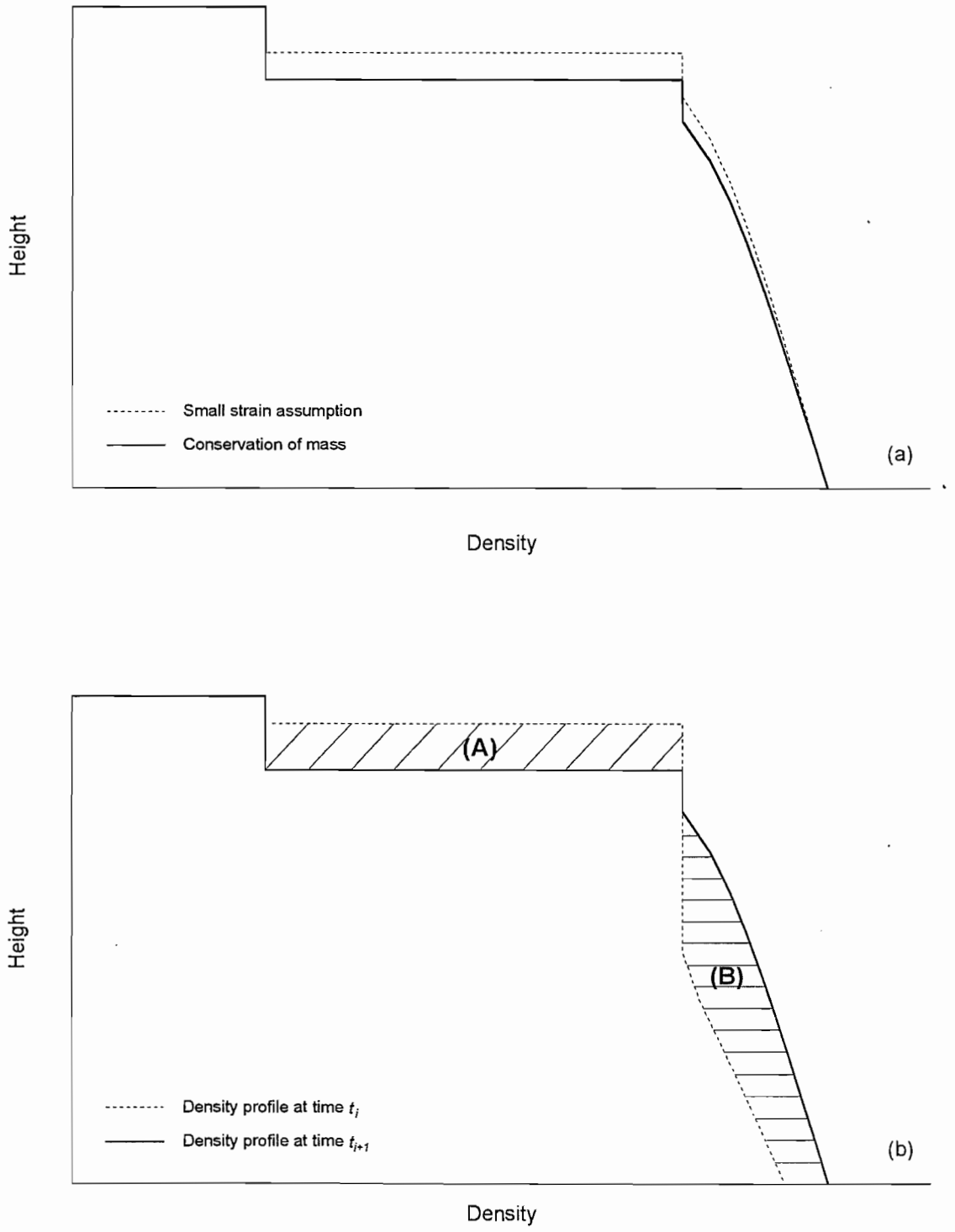

Figure 6.15 Calculation of density profile: (a) comparison between small strain assumption and mass conservation; (b) example of density profiles with time interval

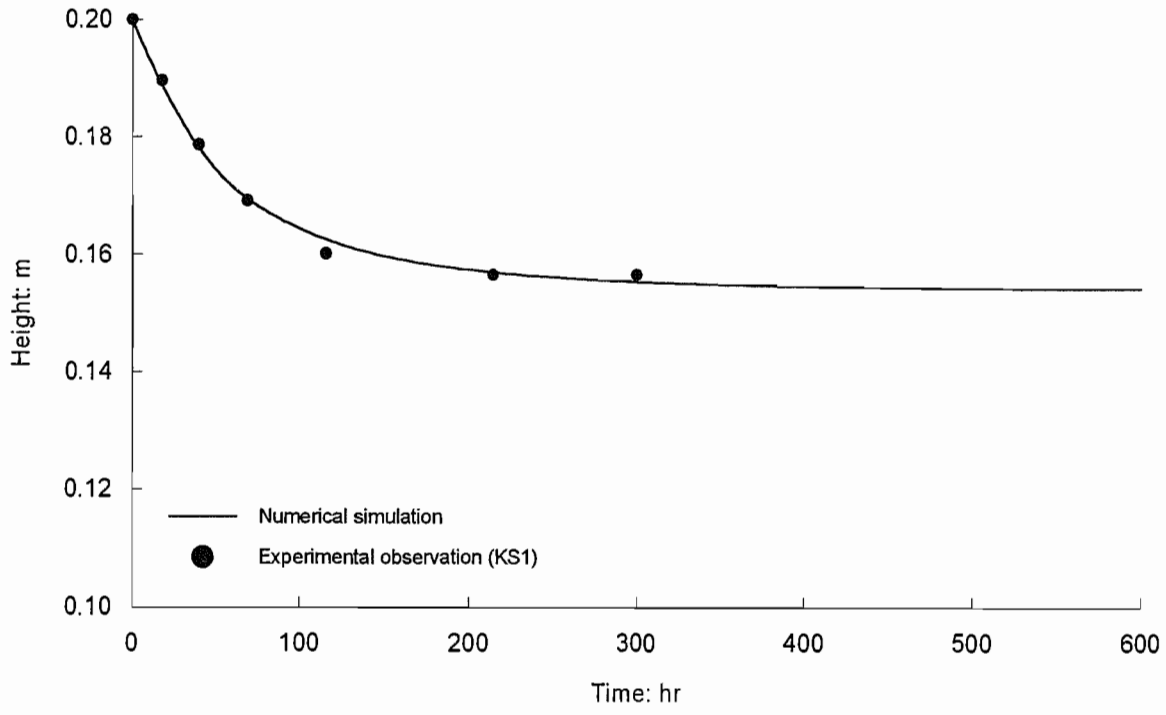

Figure 6.16 Numerical simulation of surface settlement with respect to time result, experiment KS1

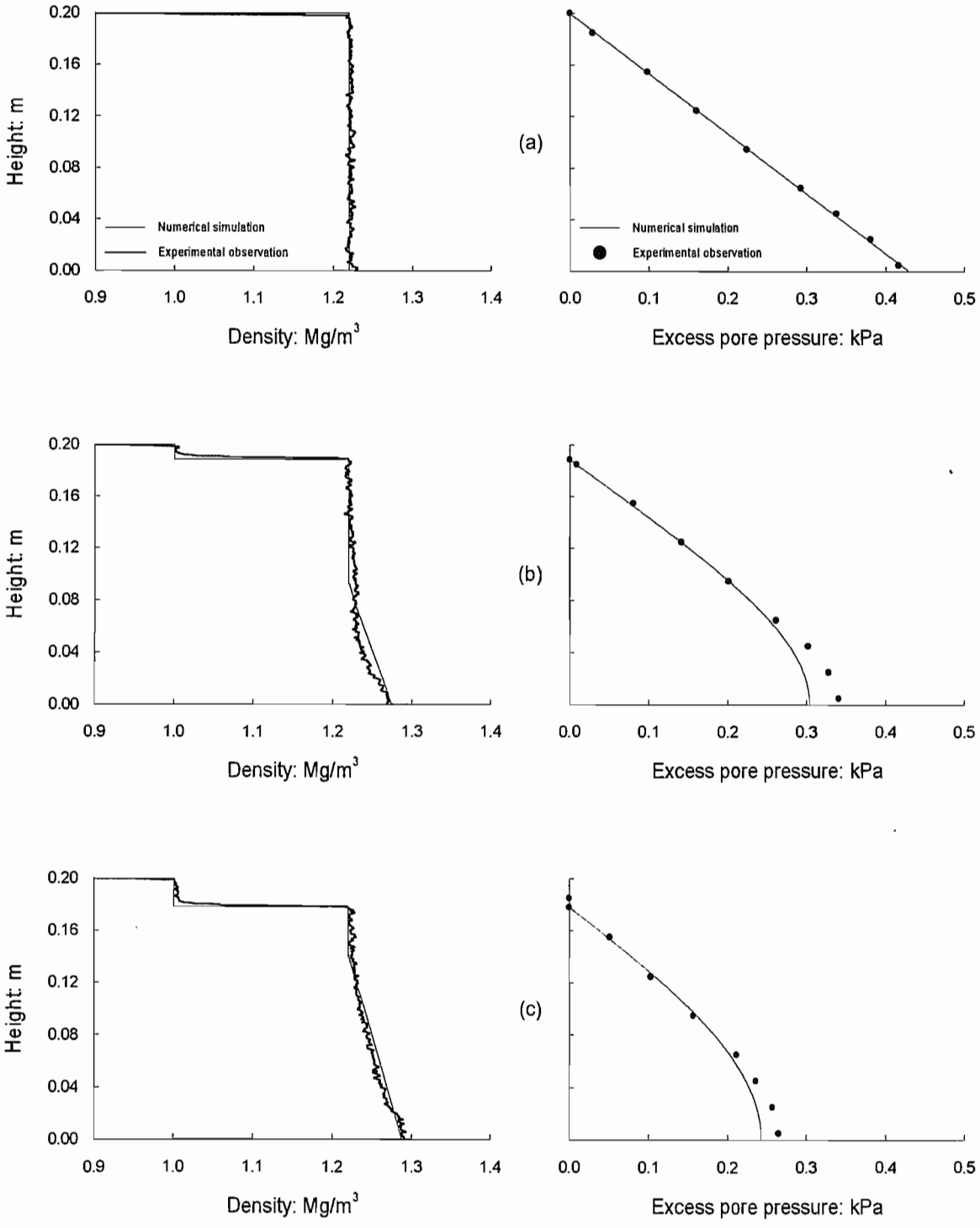

Figure 6.17 Numerical simulation for density and excess pore pressure profiles, experiment KS1: (a) 0 hr; (b) 18 hr; (c) 40 hr

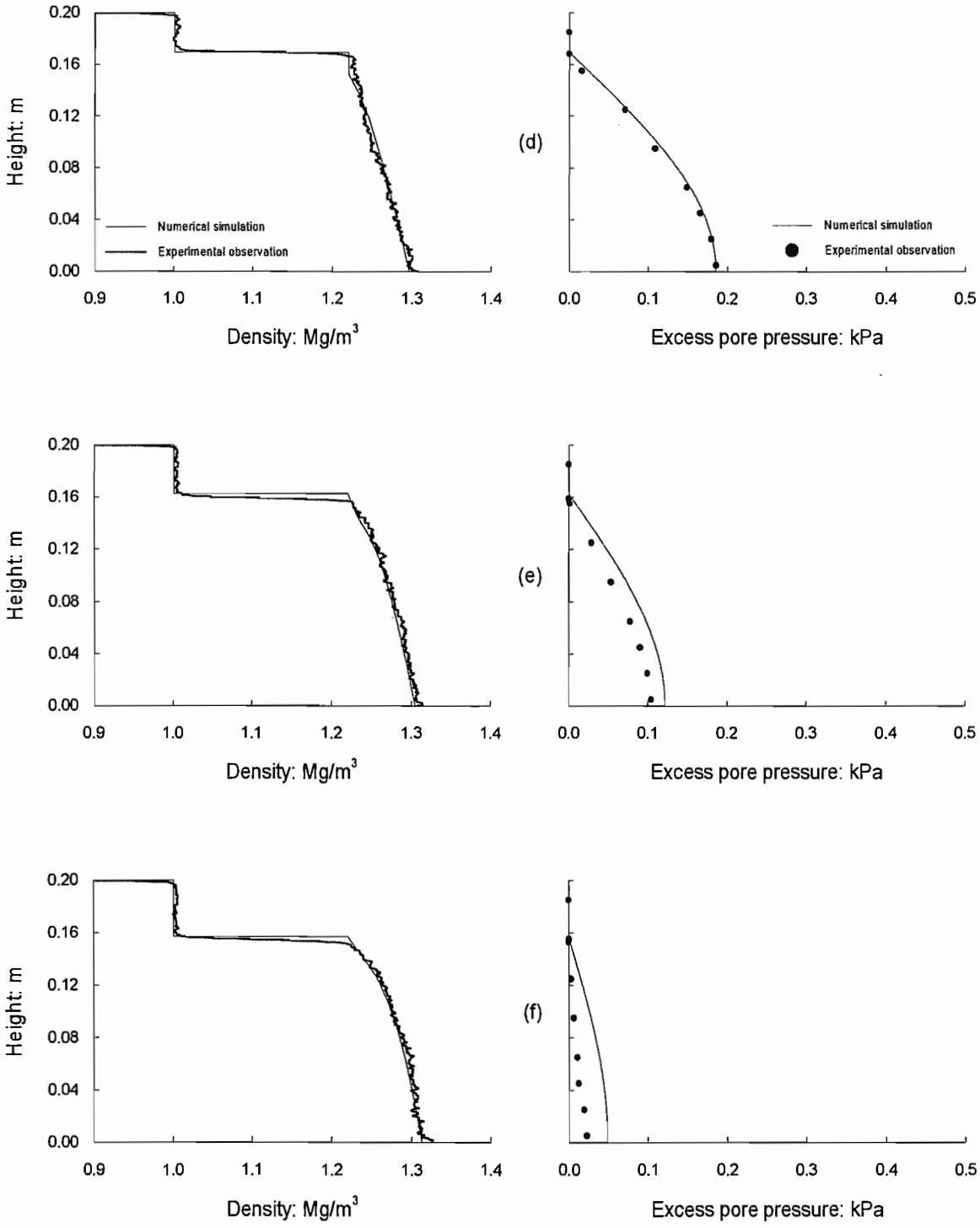

Figure 6.17 Continued: (d) 69 hr; (e) 115 hr; (f) 214 hr

for the soil, along with value of C_v obtained by matching one pore pressure profile in the middle of the consolidation process. It has then been possible to model the whole self-weight consolidation process, achieving a very close match between the density profiles and pore pressure profiles at each stage.

Figure 6.18 presents numerical simulations of excess pore pressure profiles with the real profiles observed in tests KS2 to KS5 using the soil parameters calculated from test KS1. There are differences between simulated and experimental results. However, these are due to the variations in experiments which had all started with identical initial conditions. This comparison, therefore, provides an indication of the accuracy with which a numerical prediction can be made.

6.6 Numerical Simulations for Electrokinetic Consolidation

Comparisons between numerical simulations based on the conservation of mass for electrokinetic consolidation and the experimental data from electrokinetic consolidation tests are presented in the following sections.

6.6.1 Simulations using C_v from Self-weight Consolidation Test

As reported in Chapter 5, effective stress and void ratio relationships were slightly different under the conditions of self-weight, hydraulic gradient, and electrokinesis (see Figure 5.2). Assuming that there is no change in material properties during the electrokinetic process, numerical simulations were performed using material parameters for Speswhite kaolin clay under very low effective stress conditions obtained from self-weight consolidation test as input parameters in order to predict the soil behaviour under electrokinesis. The coefficient of electroosmotic permeability determined from laboratory experiments, which was theoretically evaluated in Section 5.4.2.5, was used in numerical simulations as an input parameter. The values of input parameters governing the consolidation process are presented in Table 6.2.

6.6.1.1 Surface Settlement

Figure 6.19 presents numerical simulation of surface settlement for electrokinetic consolidation tests. Calculated surface settlements based on the conservation of mass are shown as solid line with measured surface height as dots on the same axes. Note that the measured settlements were chosen based on the upper level of soil surface (see Figure 4.21(a)). In general, numerical simulations show reasonable agreement with the laboratory experimental data although the simulated surface settlements are slightly slower than the

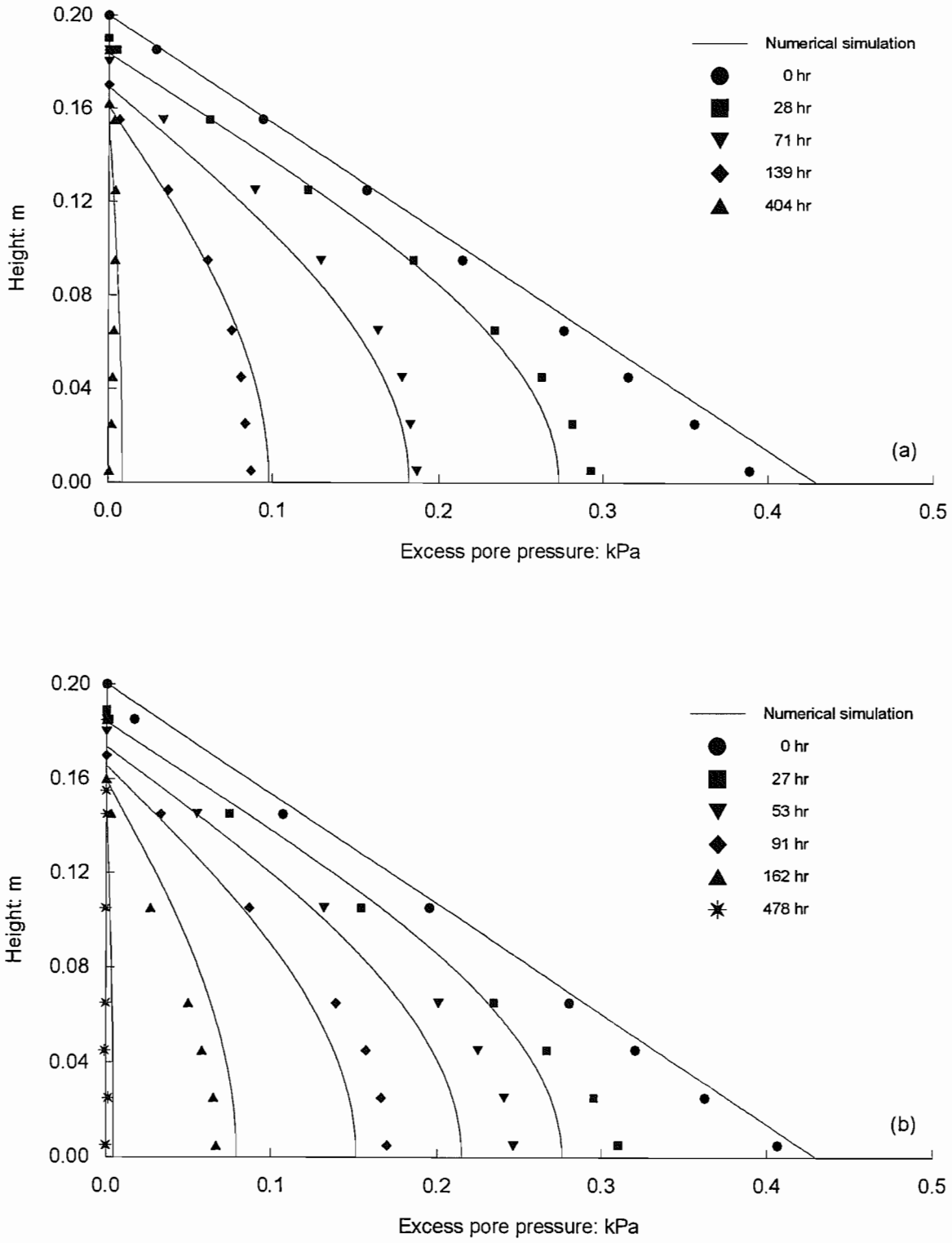

Figure 6.18 Numerical simulation of excess pore pressure: (a) experiment KS2; (b) experiment KS3

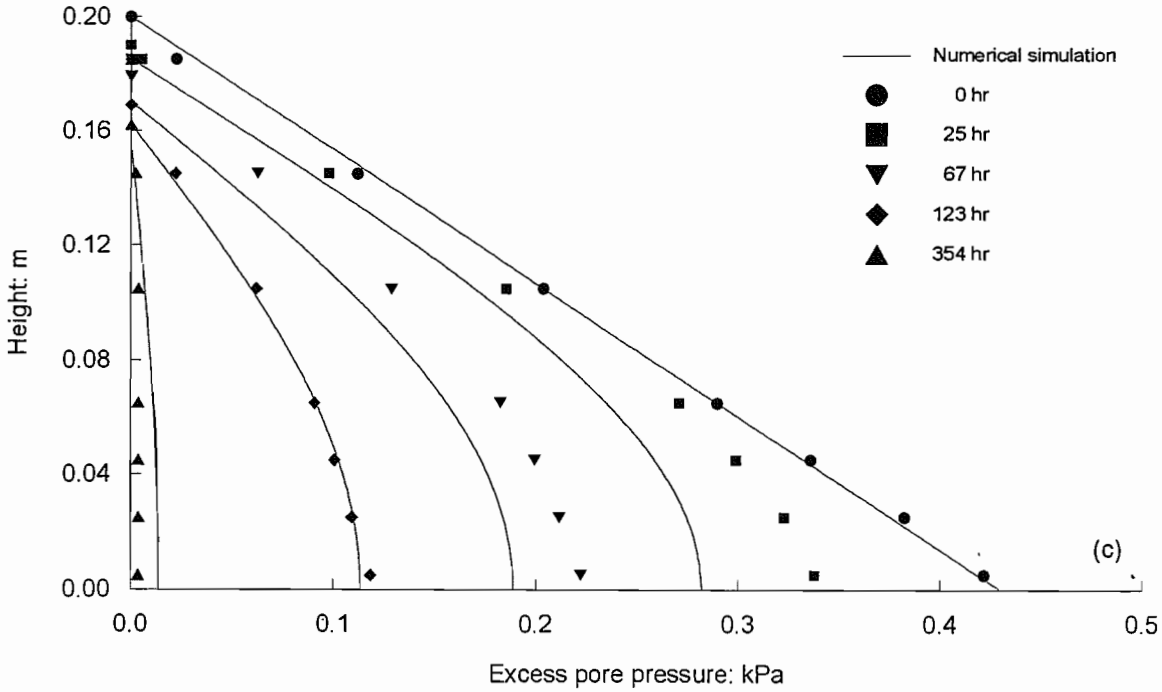

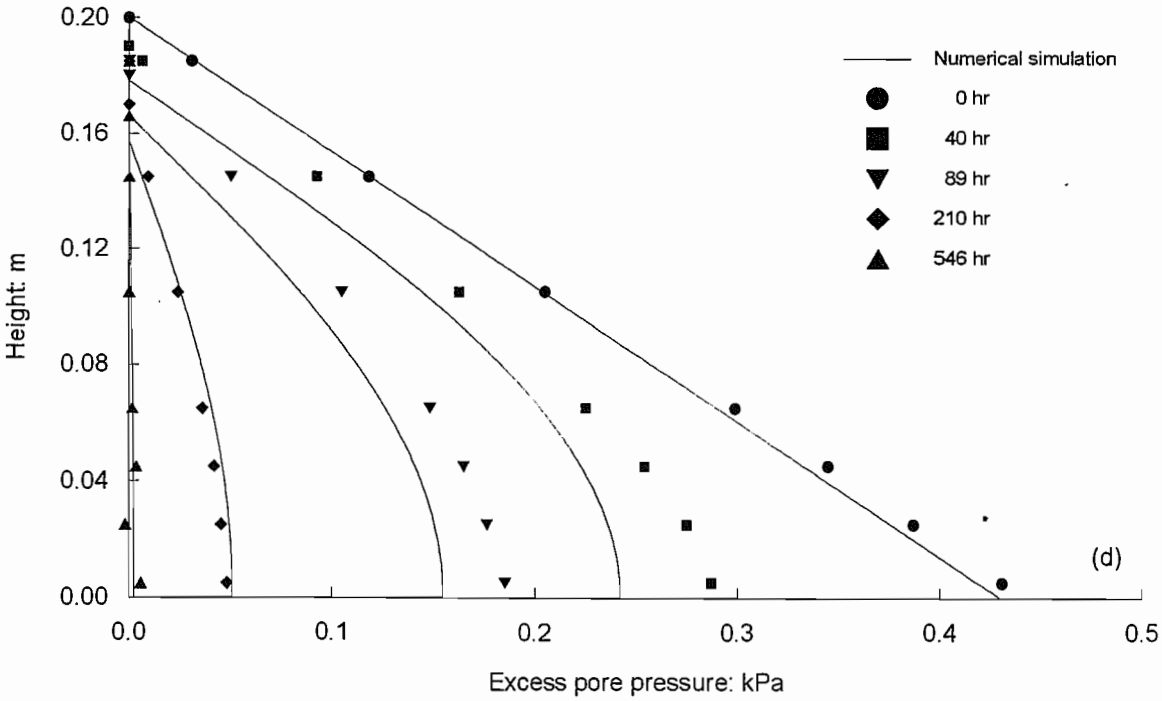

Figure 6.18 Continued: (c) experiment KS4; (d) experiment KS5

Table 6.2 General input parameters for electrokinetic consolidation

Parameter	Value
Initial height (m)	0.2
Initial slurry density (Mg/m^3)	1.22
Overlying water density (Mg/m^3)	1.001
Specific gravity	2.61
Duration (hr)	590
Void ratio at zero effective stress	6.32
Void ratio at the beginning of consolidation	6.1
Effective stress at the beginning of consolidation (kPa)	0.02
Compression index	1.53
Coefficient of compressibility (m^2/kN)	0.77
Hydraulic permeability (m/sec)	3.11×10^{-7}
Coefficient of consolidation (m^2/sec)	4.12×10^{-8}
Electroosmotic permeability ($m^2/V \cdot sec$)	1.32×10^{-8}

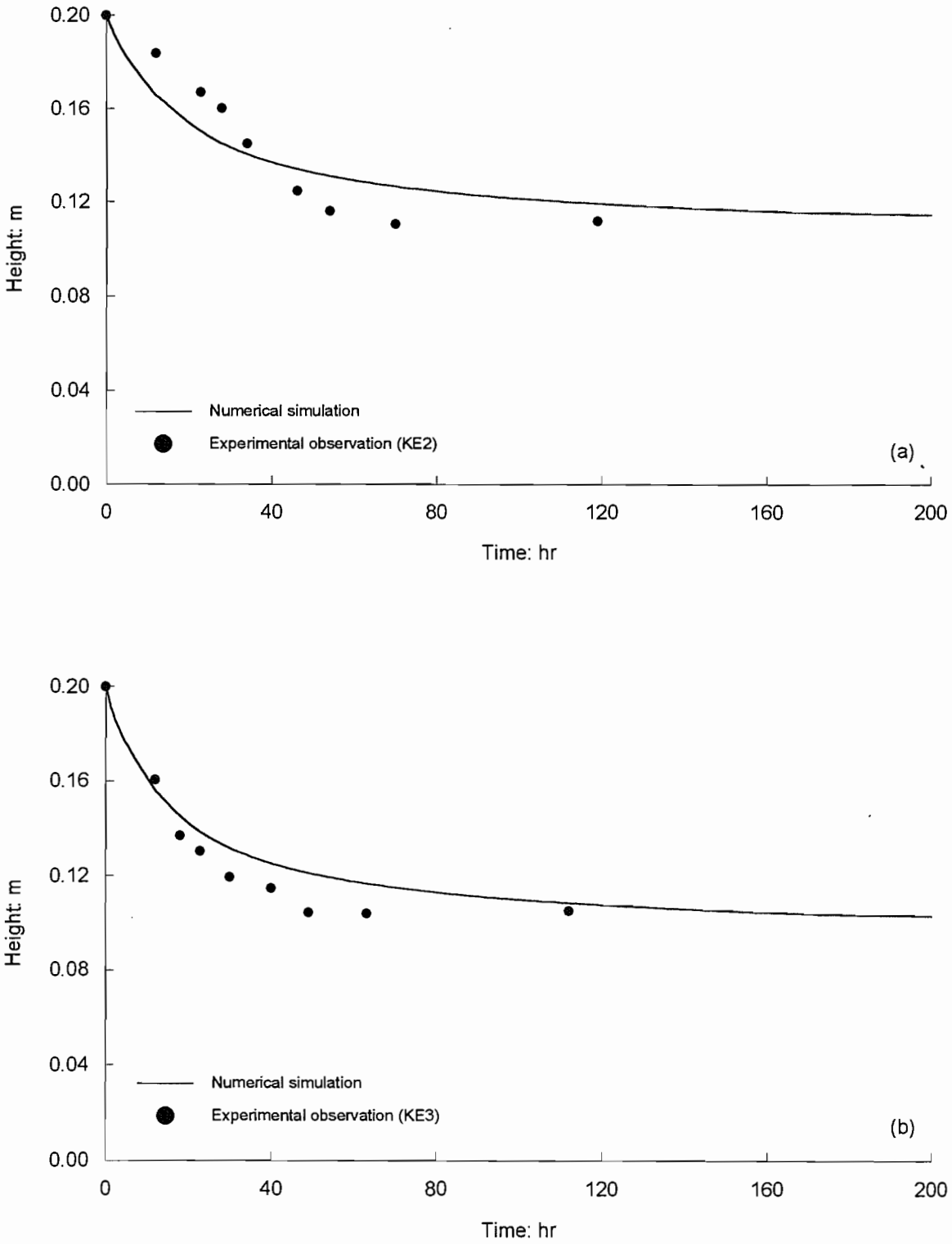

Figure 6.19 Numerical simulation of surface settlement with respect to time result: (a) experiment KE2; (b) experiment KE3

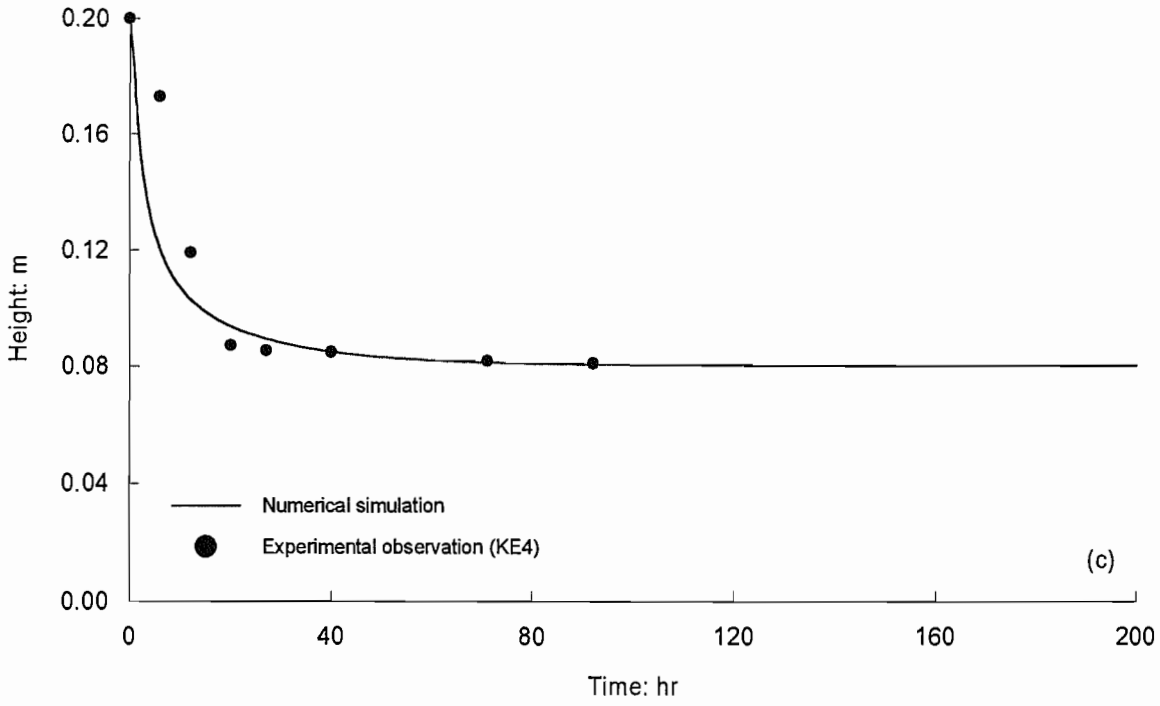

Figure 6.19 Continued: (c) experiment KE4

measured values in the intermediate stage. It can also be noted that the higher the applied electric field strength the better the numerical predictions. Both simulated and observed surface settlement results are summarised in Table 6.3.

Table 6.3 Comparison of measured and simulated surface height.

Test Series	Measured sample height (m)		Simulated sample height (m)	
KE2	0.107 (70 hr)†	0.109 (119 hr)‡	0.115*	0.111§
KE3	0.104 (63 hr)†	0.105 (112 hr)‡	0.103*	0.099§
KE4	0.097 (71 hr)†	0.099 (92 hr)‡	0.096*	0.092§

Note: † indicates observed surface height in the final stage of electrokinetic process,

‡ indicates observed surface height after the electrokinetic process,

* indicates calculated surface height of 83% of consolidation (200 hours),

§ indicates calculated surface height of 100% of consolidation (590 hours).

As shown in Table 6.3, 590 hours of electrokinetic process was required in numerical simulations in order to complete consolidation using the material parameters obtained from self-weight consolidation test (Table 6.2). However, as seen, electrokinetic consolidation

tests were completed within 100 hours depending on the applied electric field strength. This discrepancy is mainly due to the use of the coefficient of consolidation obtained from self-weight consolidation tests. It appears that an appropriate C_v value for electrokinetic consolidation should be found for better simulations, and this will be examined in Section 6.6.2.

6.6.1.2 Density and Excess Pore Pressure Profiles

The simulated settlement curve shown in the previous section was obtained by calculation of the average void ratio changes in the soil bed, and the real settlement was an upper level of soil surface measured in the laboratory experiments (see Figure 4.21(a)). In this section the parameters obtained from self-weight consolidation test are used in the analytical model in order to compare simulated density and excess pore pressure profiles within the layer to actual density and excess pore pressure profiles.

Figures 6.20 to 6.22 show measured density and excess pore pressure profiles for tests KE2 to KE4 with simulated profiles. Overall, the numerical simulation was not able to predict soil behaviour under electrokinesis such as the development of denser layer and negative pore pressure near the soil surface in the early stage of electrokinetic process. During the early stage of the consolidation process, simulated pore pressure profiles were more negative than the real measurements, resulting in a greater degree of consolidation in the base half of the soil sample. This can be seen for the first 23, 12, and 6 hours for tests KE2, KE3, and KE4 respectively. Consistent with the good fit with the real measurements in excess pore pressures, there is better agreement in density profiles at 28, 18, and 12 hours for tests KE2, KE3, and KE4 respectively. Thereafter, in the later stage of electrokinetic process, simulated excess pore pressure profiles were less negative than the real profiles and therefore the density profiles were correspondingly underestimated; 46, 30, and 20 hours of density and excess pore pressure profiles for tests KE2, KE3, and KE4 respectively.

6.6.2 Simulations using C_v from Electrokinetic Consolidation Test

Numerical simulations of settlement, density and pore pressure profiles in the previous section showed a fairly good agreement with experimental observations mainly in the early stage of electrokinetic process. During this stage, the stress range was similar to that of the self-weight experiments, so that the use of the self-weight consolidation parameters would have been appropriate here. Overall, however, the simulated consolidation using these parameters was slower than the laboratory experimental results. Therefore, in this section material parameters from electrokinetic consolidation tests were

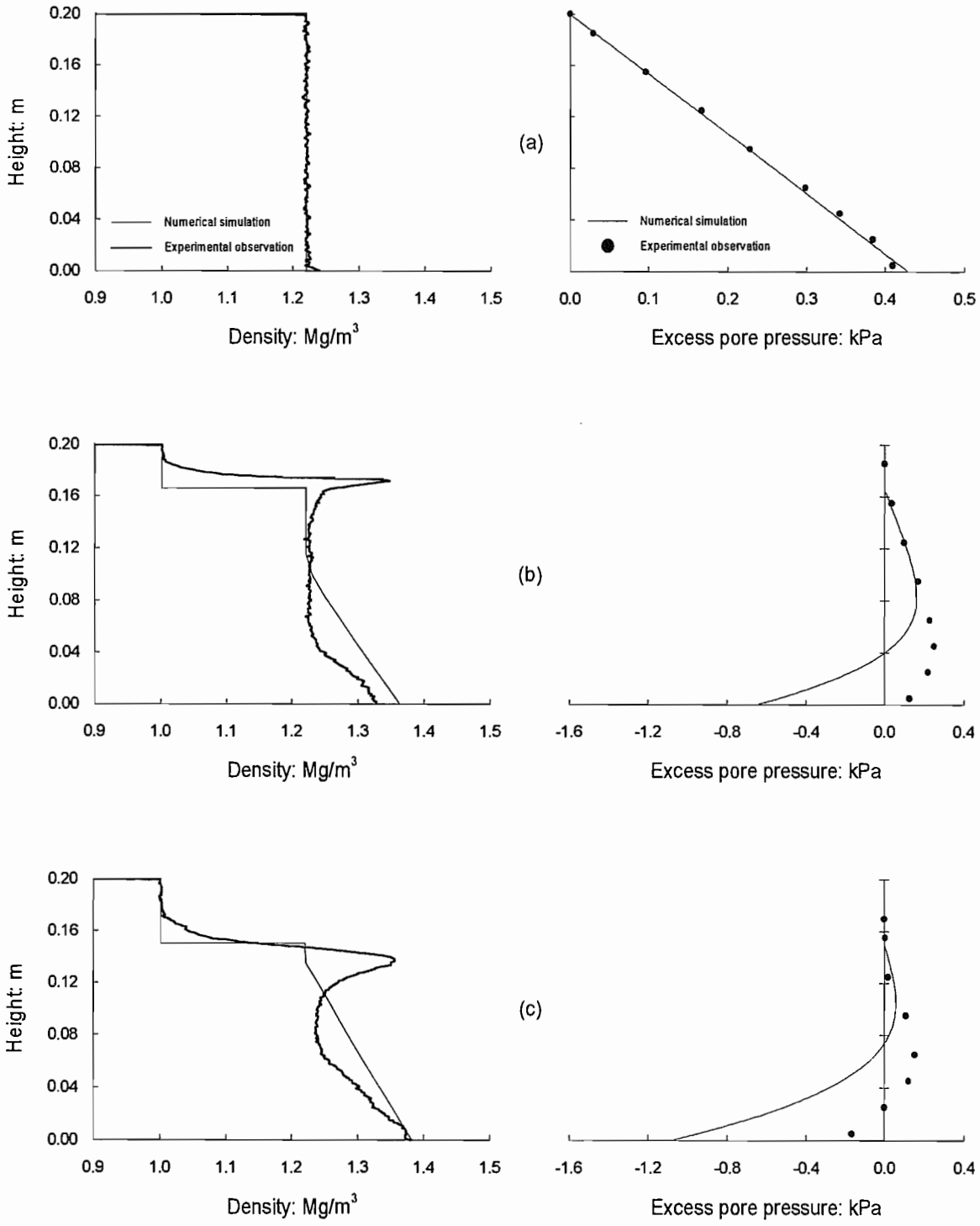

Figure 6.20 Numerical simulation of density and excess pore pressure profiles, experiment KE2: (a) 0 hr; (b) 12 hr; (c) 23 hr

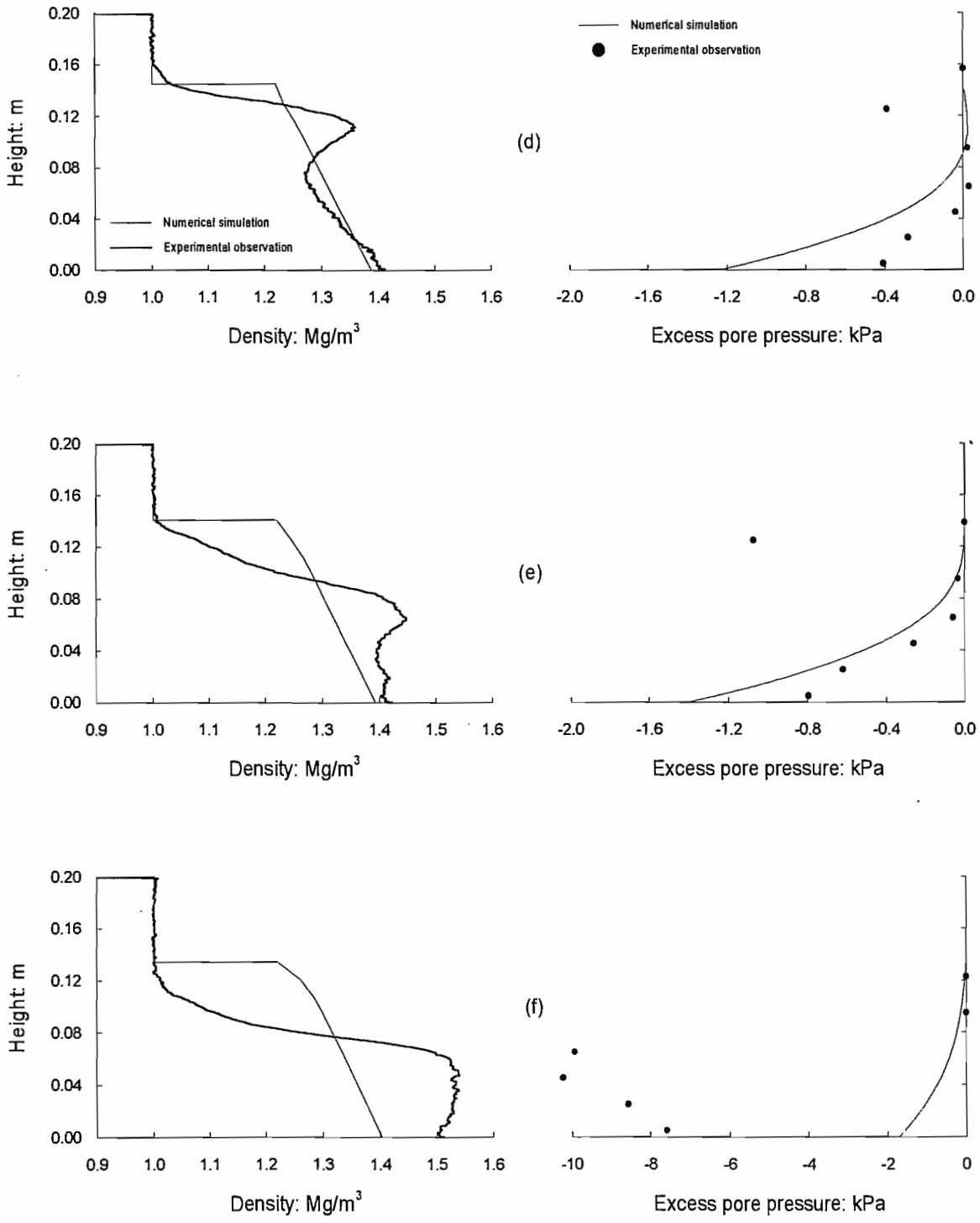

Figure 6.20 Continued: (d) 28 hr; (e) 34 hr; (f) 46 hr

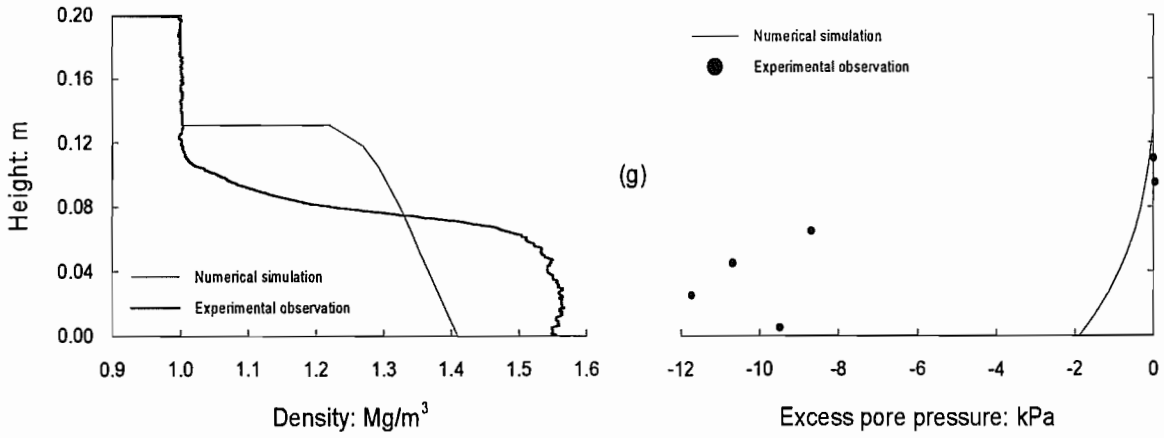

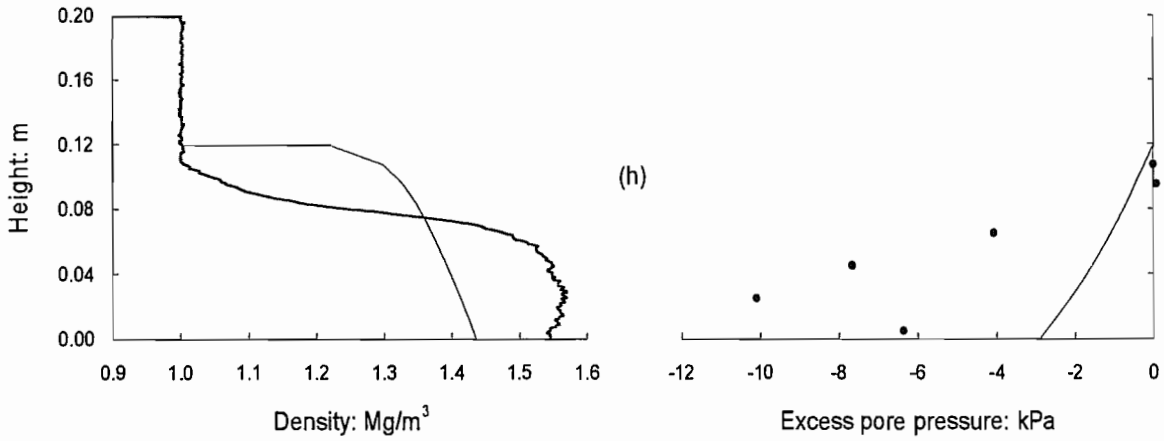

Figure 6.20 Continued: (g) 54 hr; (h) 70 hr

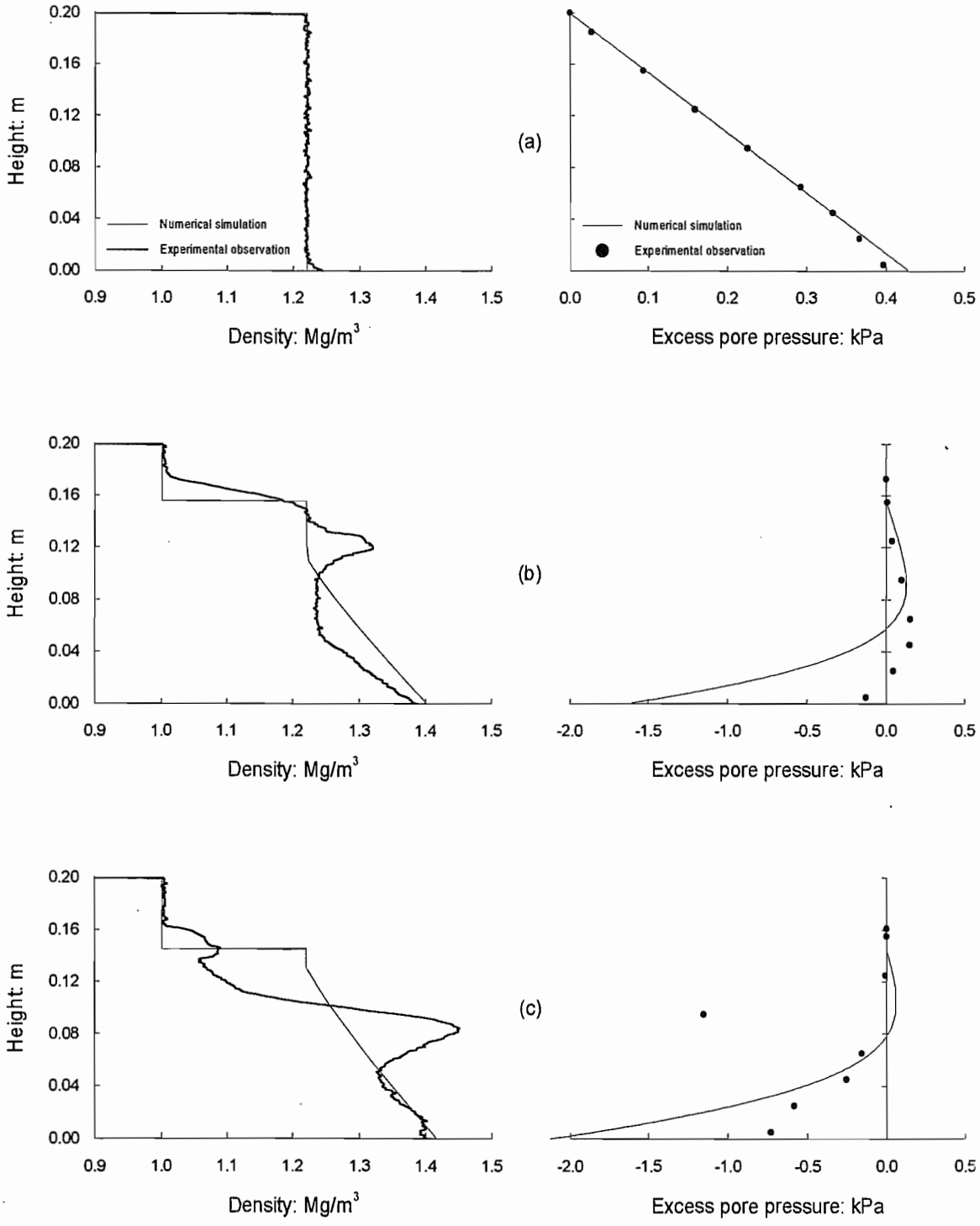

Figure 6.21 Numerical simulation of density and excess pore pressure profiles, experiment KE3: (a) 0 hr; (b) 12 hr; (c) 18 hr

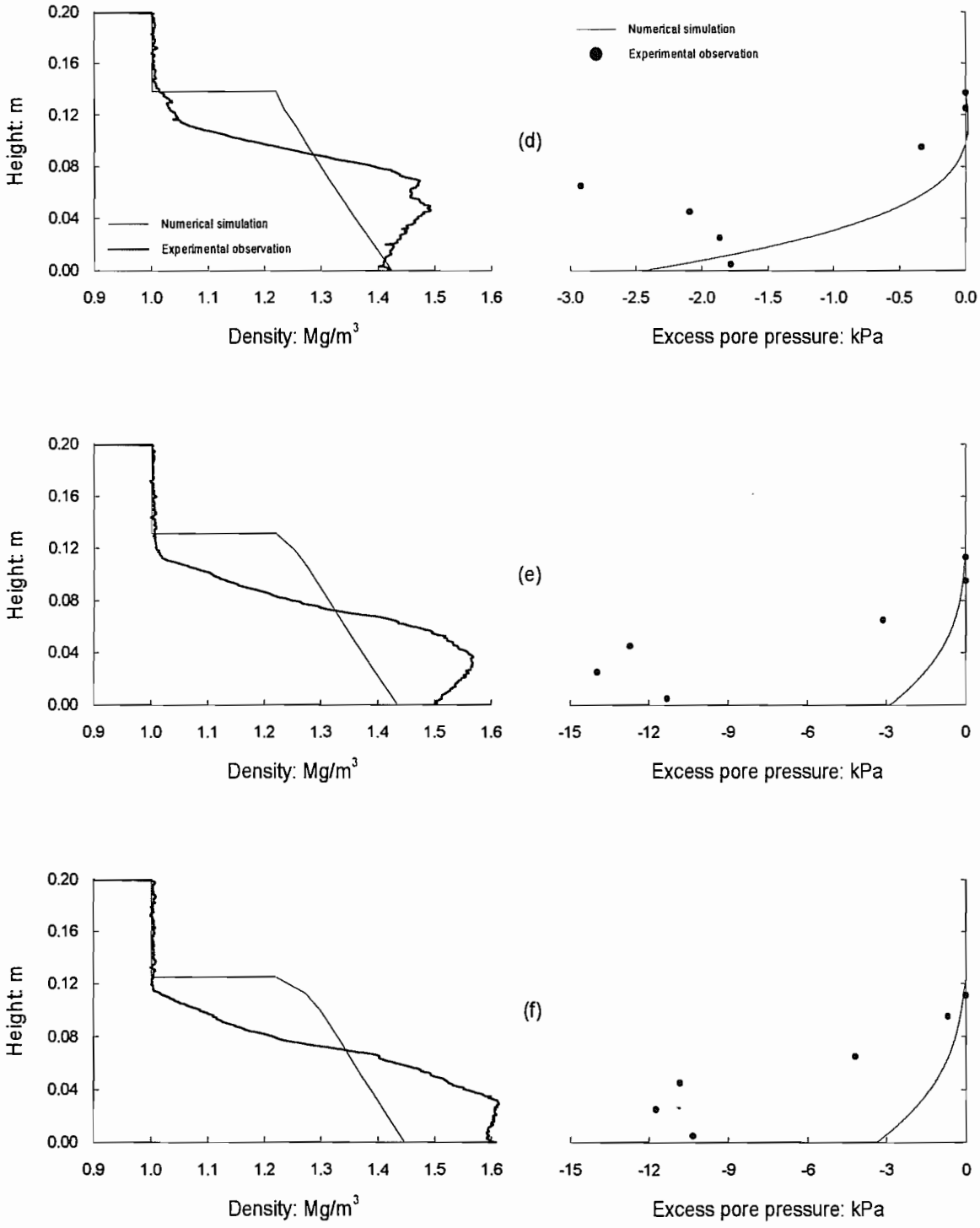

Figure 6.21 Continued: (d) 23 hr; (e) 30 hr; (f) 40 hr

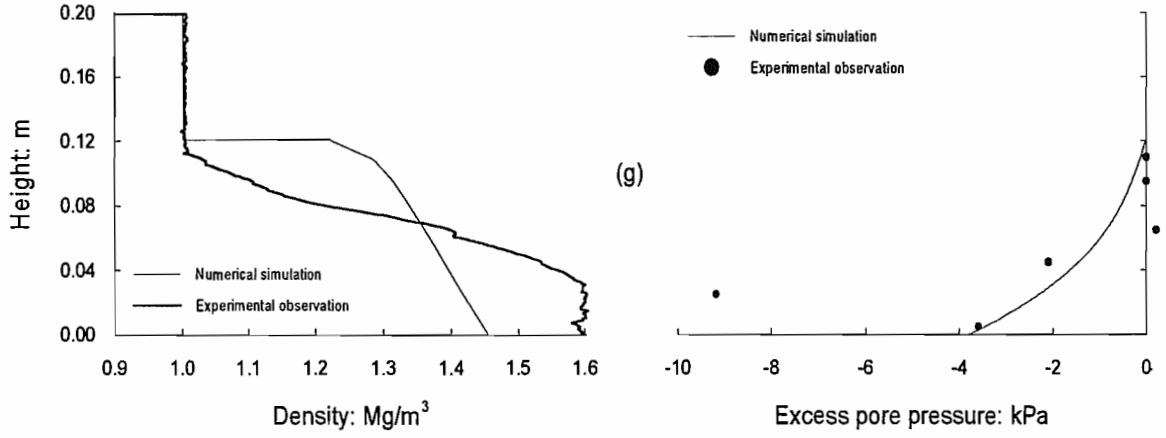

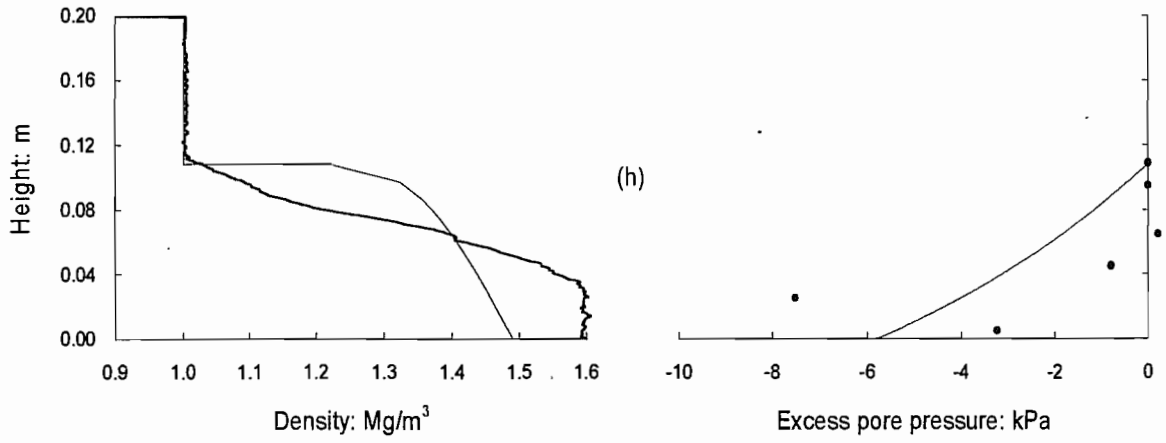

Figure 6.21 Continued: (g) 49 hr; (h) 63 hr

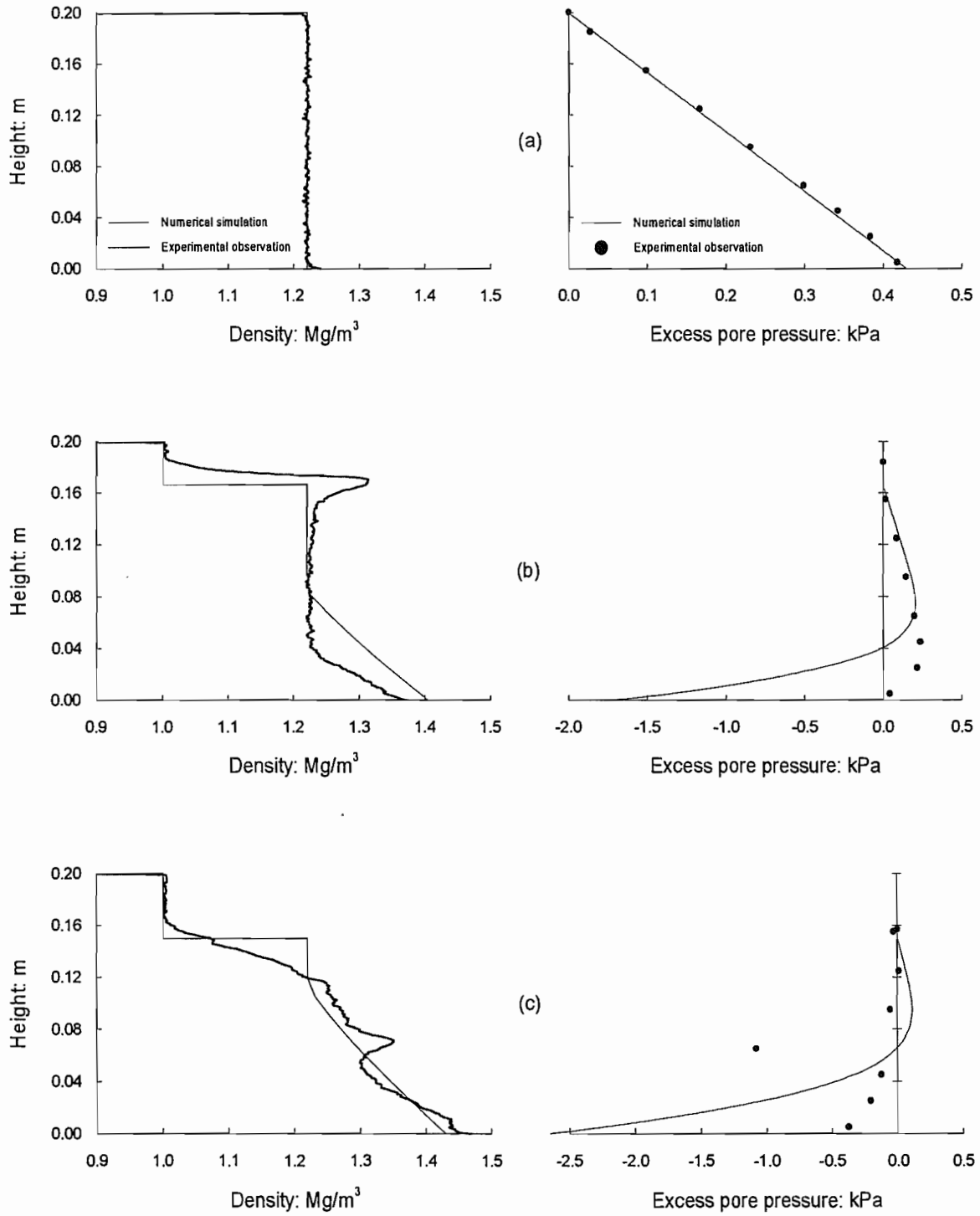

Figure 6.22 Numerical simulation of density and excess pore pressure profiles, experiment KE4: (a) 0 hr; (b) 6 hr; (c) 12 hr

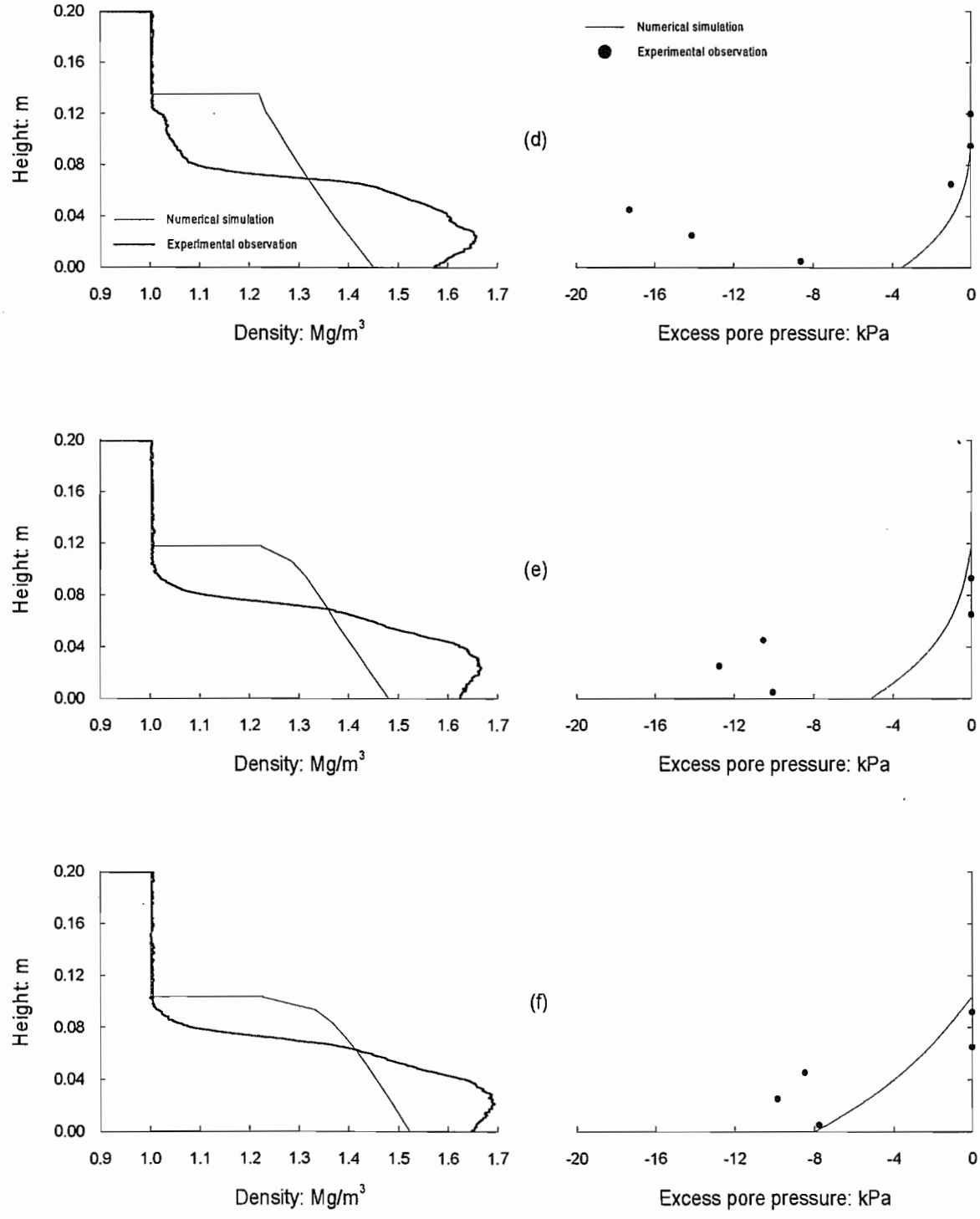

Figure 6.22 Continued: (d) 20 hr; (e) 40 hr; (f) 71 hr

used to simulate soil behaviour under the influence of electrokinesis, as a test of the model.

6.6.2.1 Determination of Hydraulic Permeability

During the electrokinetic process, there may be changes in hydraulic permeability and compressibility. However, it was not possible to measure directly the hydraulic permeability under the influence of electrokinesis.

As the coefficient of hydraulic permeability is inversely related to excess pore pressure (Equations (6.28) and (6.32)), it can be estimated by giving values of negative pore pressures measured during the electrokinetic process. Numerical simulations of excess pore pressure presented in Section 6.6.1 showed that there was a big difference between simulated and measured profiles in the later stage resulting in the difference in density profiles. Therefore, hydraulic permeability under electrokinesis has been estimated by considering the development of negative pore pressures and the corresponding density changes in the later stage of electrokinetic process.

Negative excess pore pressures developed under electric field strength of 10, 20, and 30 V in the later stage of electrokinetic process were approximated to -12, -14, and -18 kPa respectively (Section 4.5.1). The estimation of hydraulic permeability was based on test KE3, and the value of hydraulic permeability for electrokinetic consolidation was determined as 2.25×10^{-7} m/sec. The electroosmotic permeability for numerical simulations was chosen as 1.32×10^{-8} $m^2/V \cdot sec$ from the experimental data reported in Section 5.4.1. The estimated negative pore pressure and the corresponding density in the final stage of electrokinetic process under different electric field strengths are given in Table 6.4, by comparison with measured values.

Table 6.4 Comparison between calculated and measured negative pore pressure

Test series	Numerical simulations		Experimental observations	
	Pore pressure	Density	Pore pressure	Density
KE2	-5.7 (kPa)	1.52 (Mg/m^3)	-11.8 (kPa)	1.54 (Mg/m^3)
KE3	-11.5 (kPa)	1.62 (Mg/m^3)	-12.2 (kPa)	1.61 (Mg/m^3)
KE4	-17.2 (kPa)	1.7 (Mg/m^3)	-18.1 (kPa)	1.7 (Mg/m^3)

6.6.2.2 Determination of the Coefficient of Consolidation

As already stated, numerical simulations using the parameters from self-weight consolidation test required 590 hours of the electrokinetic process in order to complete electrokinetic consolidation. However, in fact, electrokinetic consolidation tests reported in

Section 4.5.1 completed approximately 70 hours of the electrokinetic process under different electric field strengths (see Table 6.3). This was the main reason that numerical simulations of density and excess pore pressure profiles in the later stage did not fit the real profiles well (Section 6.6.1.2) with the input parameters taken from self-weight consolidation test. Therefore, the coefficient of consolidation has been estimated as 1.91×10^{-7} m^2/sec based on the completion of consolidation resulting from 100 hours of the electrokinetic process.

6.6.2.3 Evaluation of the Coefficient of Compressibility Determined by k_h and C_v

The coefficient of compressibility can be calculated simply from Equation (6.2) by giving the values of estimated hydraulic permeability (Section 6.6.2.1) and the coefficient of consolidation (Section 6.6.2.2); the calculated value for compressibility was 0.12 m^2/kN. Figure 6.23 shows the representative compression curve for electrokinetic consolidation obtained from tests KE2 to KE6 on a logarithmic scale (see also Figure 5.2). In order to satisfy the value of the coefficient of compressibility, 0.12 m^2/kN, void ratios at the beginning and the end of consolidation should be in the range between 5.6 and 2.4, and the corresponding effective stresses between 0.07 and 4 kPa respectively. As seen, the range of void ratio during electrokinetic consolidation tests was between 6.2 and 1.7. Therefore, the range of void ratio estimated from the coefficient of compressibility is reasonable, and hence the hydraulic permeability and the coefficient of consolidation. The compression index for electrokinetic consolidation was determined as 1.82 from the effective stress and void ratio relationship as shown in Figure 6.23. Input parameters used in numerical simulations for electrokinetic consolidation are given in Table 6.5.

6.6.2.4 Surface Settlement

Figure 6.24 shows numerical simulations of surface settlement for electrokinetic consolidation tests. Measured settlements were based on the lower level of soil surface during the electrokinetic process (see Figure 4.21(b)). Simulated settlement curves show that the consolidation process is faster than that calculated with the parameters from self-weight consolidation test. Calculated surface height was lower than the real height in the early stage of electrokinetic process. However, as seen, simulations fit the measured settlement well in the later stage of electrokinetic consolidation. It can also be seen that the higher the applied electric field the better the prediction.

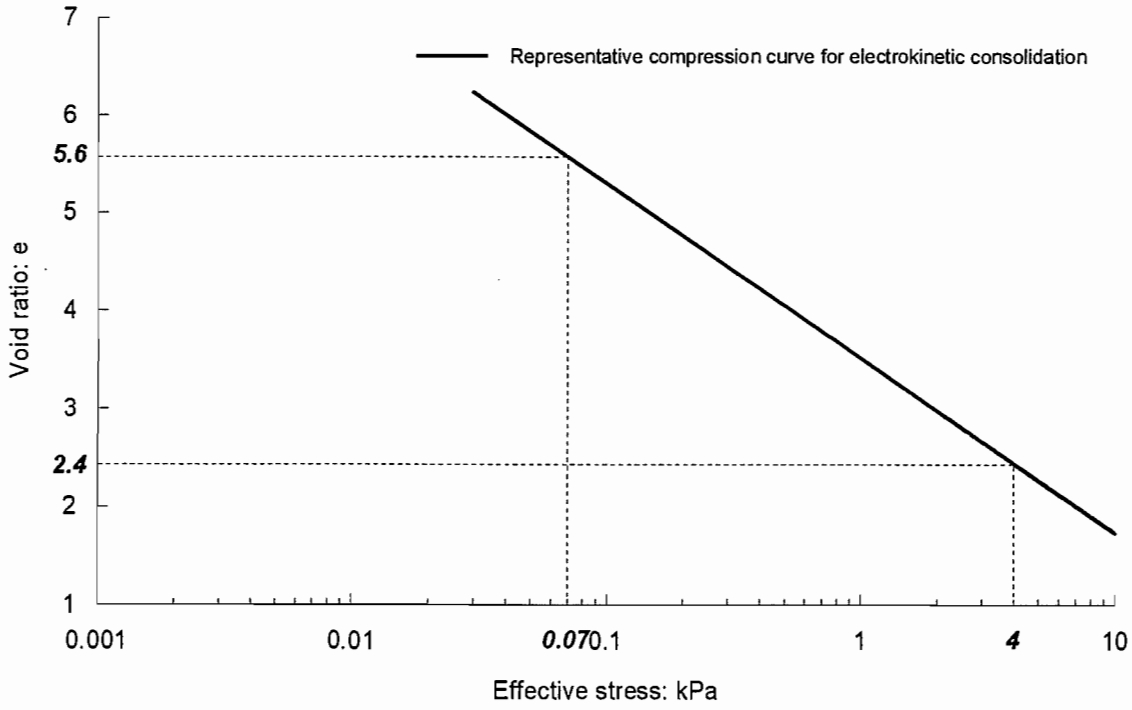

Figure 6.23 Ranges of void ratio and effective stress estimated by the coefficient of compressibility for electrokinetic consolidation tests

Table 6.5 General input parameters for electrokinetic consolidation

Parameter	Value
Initial height (m)	0.2
Initial slurry density (Mg/m^3)	1.22
Overlying water density (Mg/m^3)	1.001
Specific gravity	2.61
Duration (hr)	100
Void ratio at zero effective stress	6.32
Void ratio at the beginning of consolidation	6.1
Effective stress at the beginning of consolidation (kPa)	0.04
Compression index	1.82
Coefficient of compressibility (m^2/kN)	0.12
Hydraulic permeability (m/sec)	2.25×10^{-7}
Coefficient of consolidation (m^2/sec)	1.91×10^{-7}
Electroosmotic permeability ($m^2/V \cdot sec$)	1.32×10^{-8}

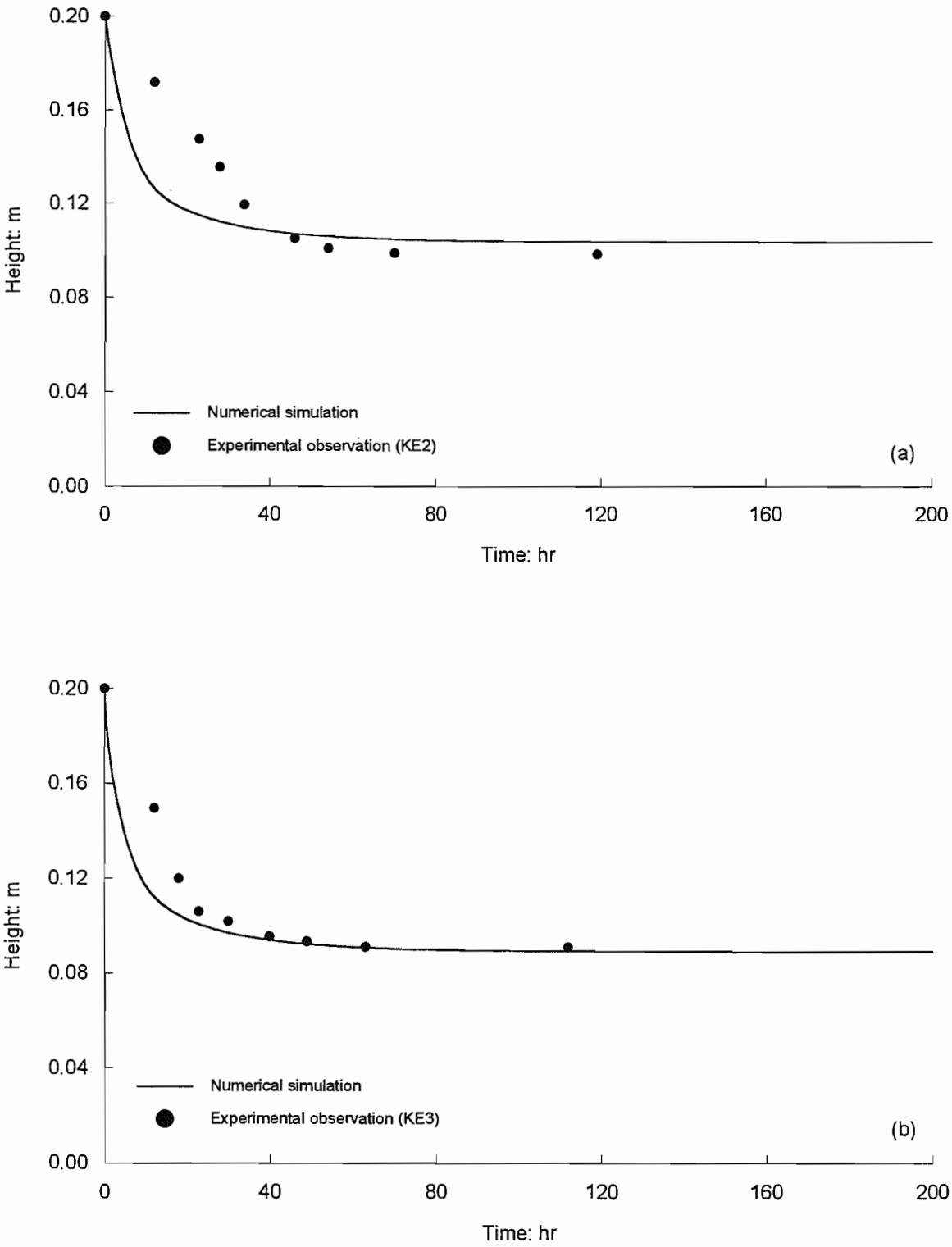

Figure 6.24 Numerical simulation of surface settlement with respect to time result: (a) experiment KE2; (b) experiment KE3

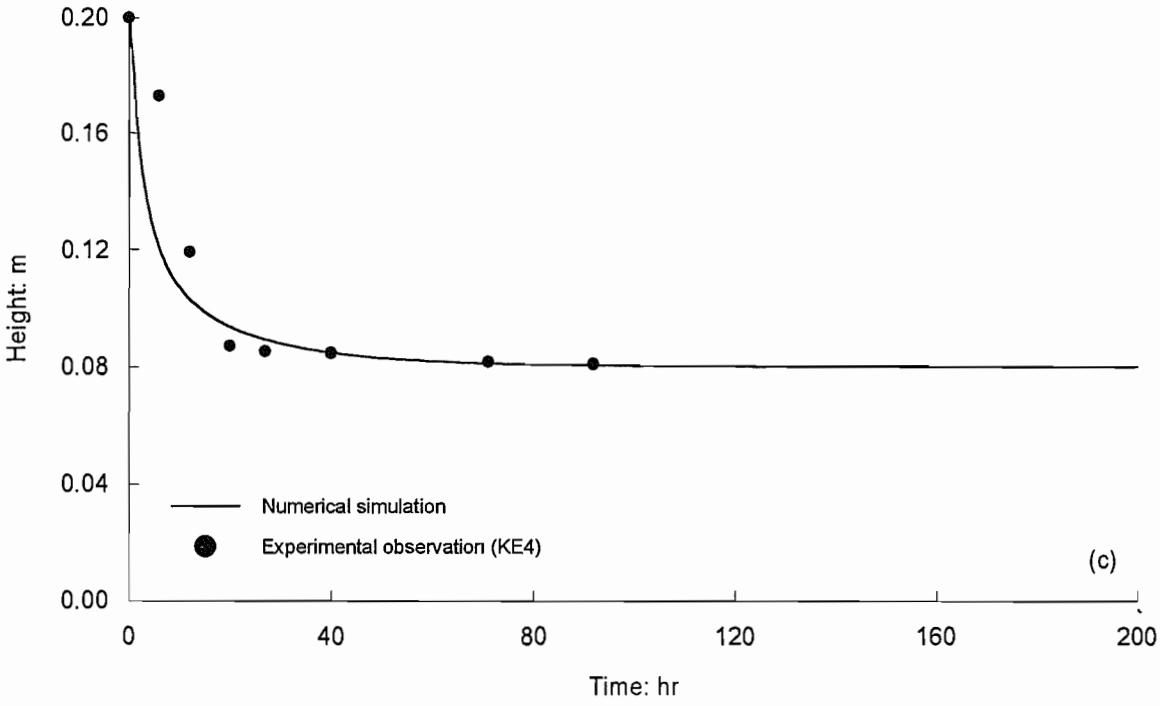

Figure 6.24 Continued: (c) experiment KE4

6.6.2.5 Density and Excess Pore Pressure Profiles

Figures 6.25 to 6.27 show numerical simulations of density and excess pore pressure profiles for electrokinetic consolidation tests. Calculated surface settlement curve showed faster settling in the early stage of electrokinetic process (Figure 6.24). This is clearly seen in density profiles. Using the coefficient of consolidation from electrokinetic consolidation tests, negative pore pressure developed at the base of the sample under the electric field strength of 10 V was approximately -2.7 kPa for test KE2, which is quite different from real measurement as shown in Figure 6.25(b). Consistently, the changes in density were also fast. This difference in simulated and measured profiles has been caused by nonlinearity in voltage gradient across the electrodes with time as reported in Chapter 4. However, the voltage gradient across the electrodes was fixed as initial applied voltage gradient in the analytical model and therefore simulations in the early stage of electrokinetic process did not fit the real profiles well. Similar results can also be seen in tests KE3 and KE4; for the first 18 and 12 hours for tests KE3 and KE4 respectively (see Figures 6.26(b), (c) and 6.27(b), (c)).

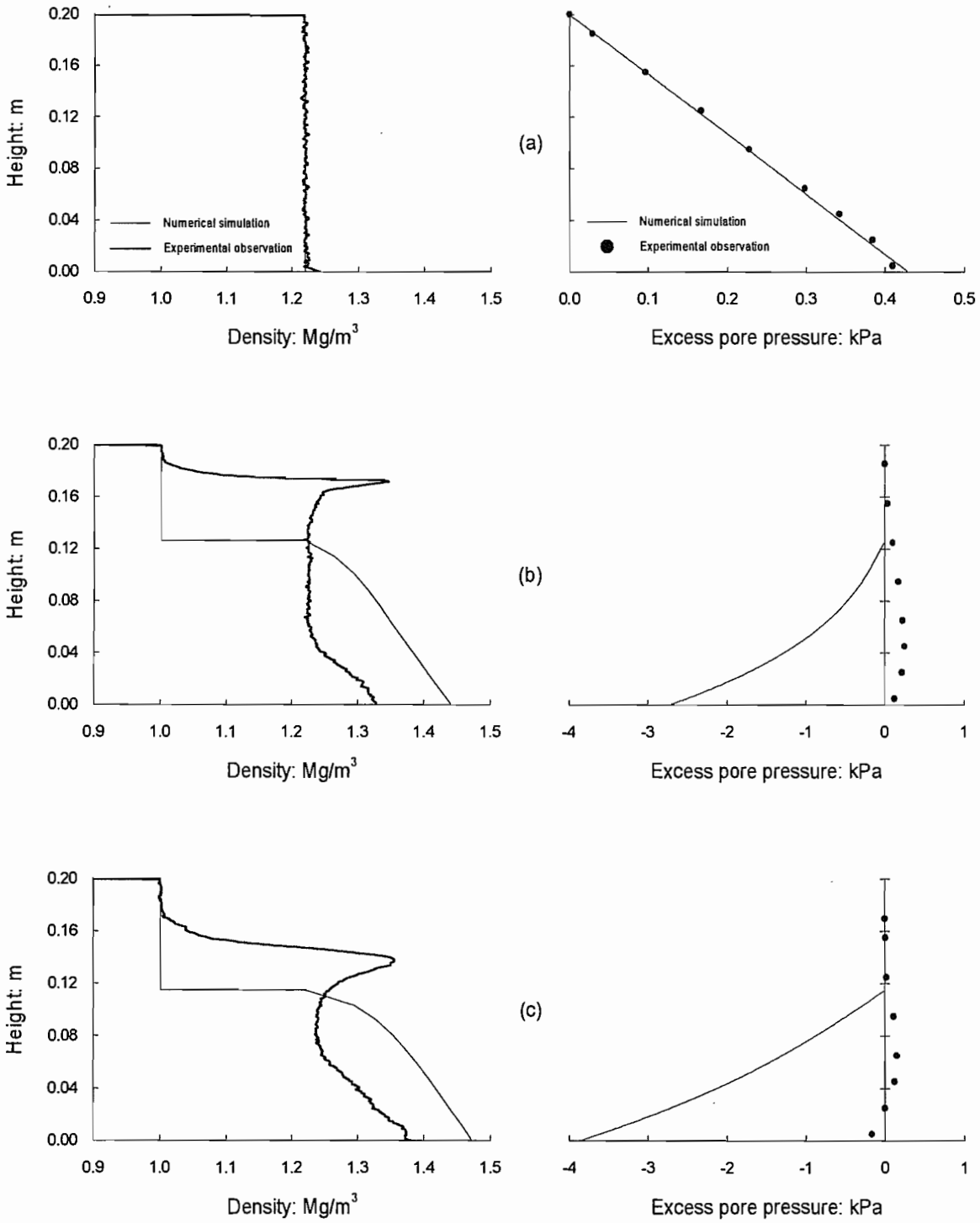

Figure 6.25 Numerical simulation of density and excess pore pressure profiles, experiment KE2: (a) 0 hr; (b) 12 hr; (c) 23 hr

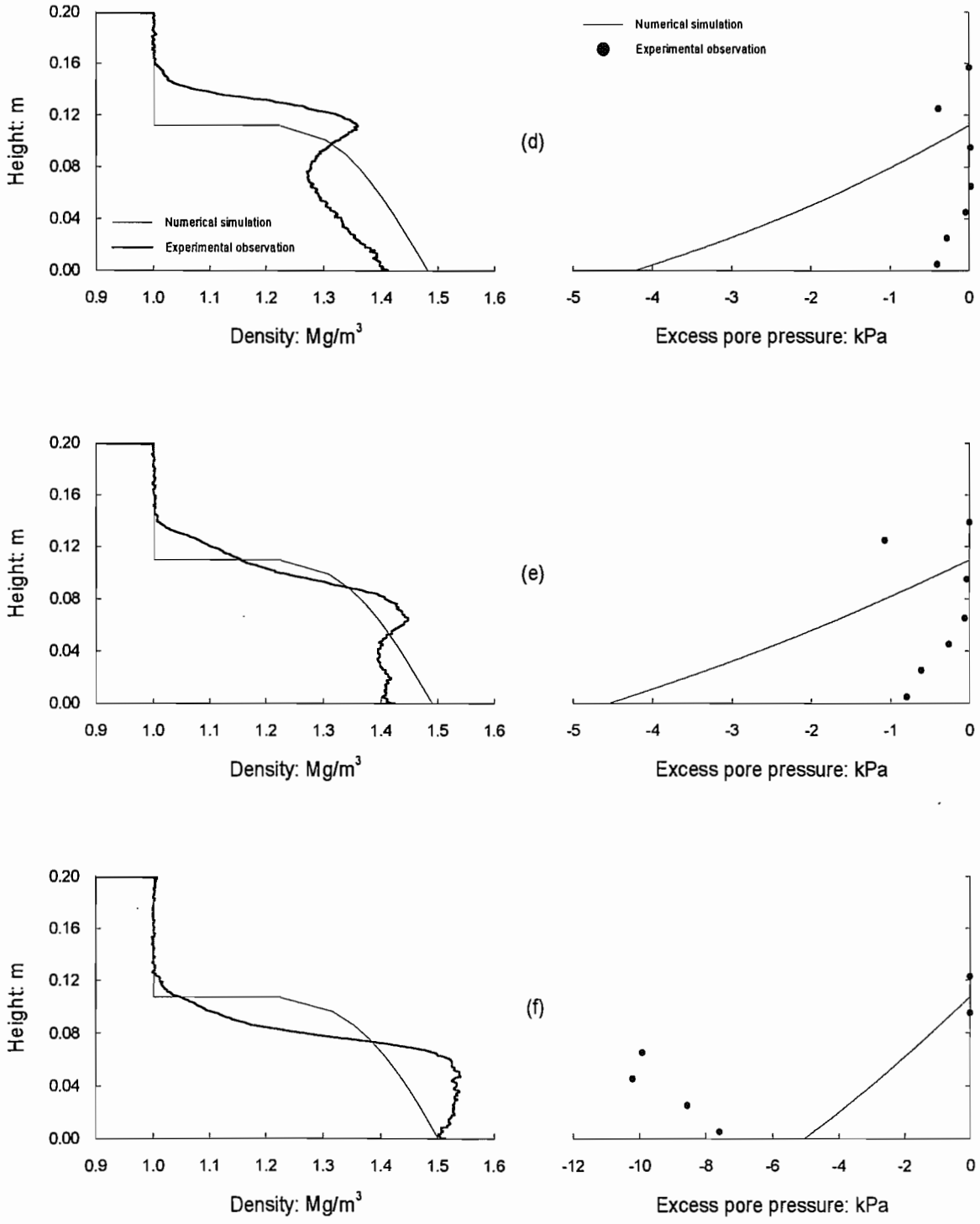

Figure 6.25 Continued: (d) 28 hr; (e) 34 hr; (f) 46 hr

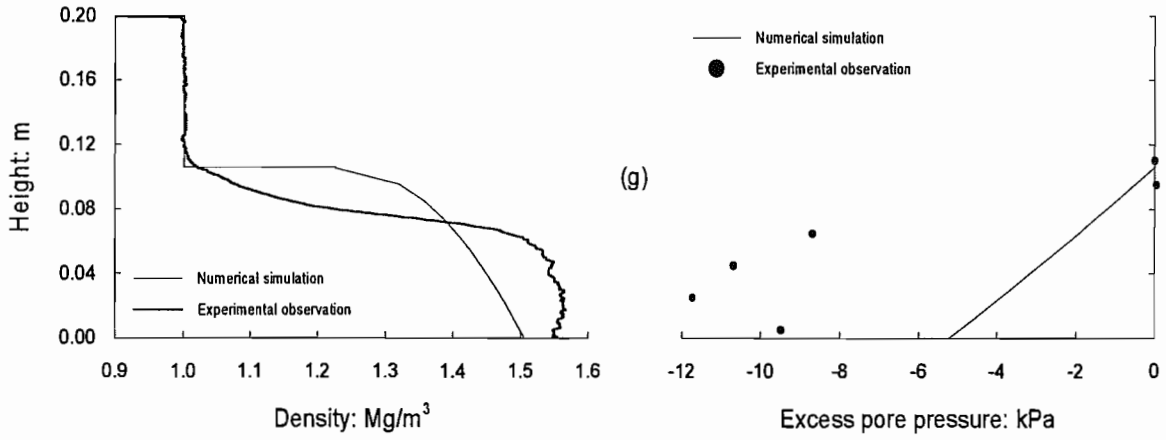

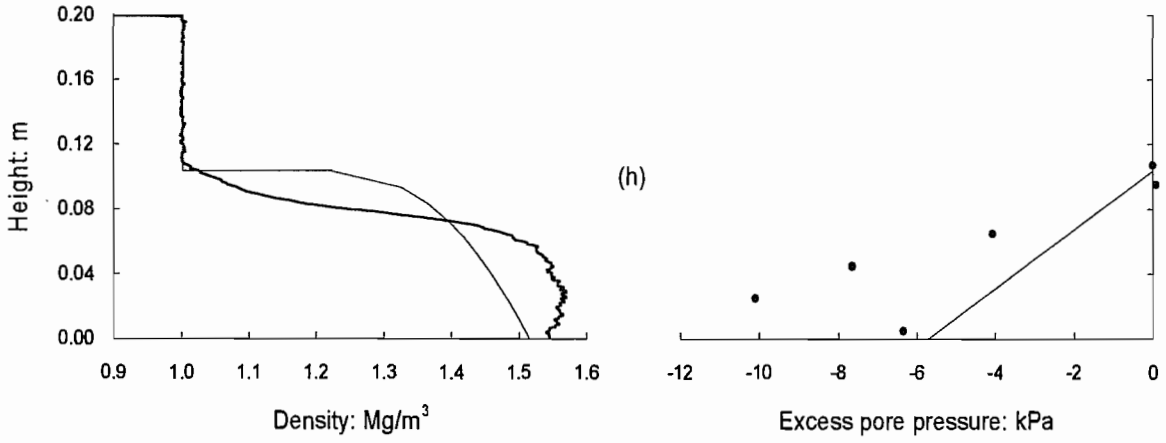

Figure 6.25 Continued: (g) 54 hr; (h) 70 hr

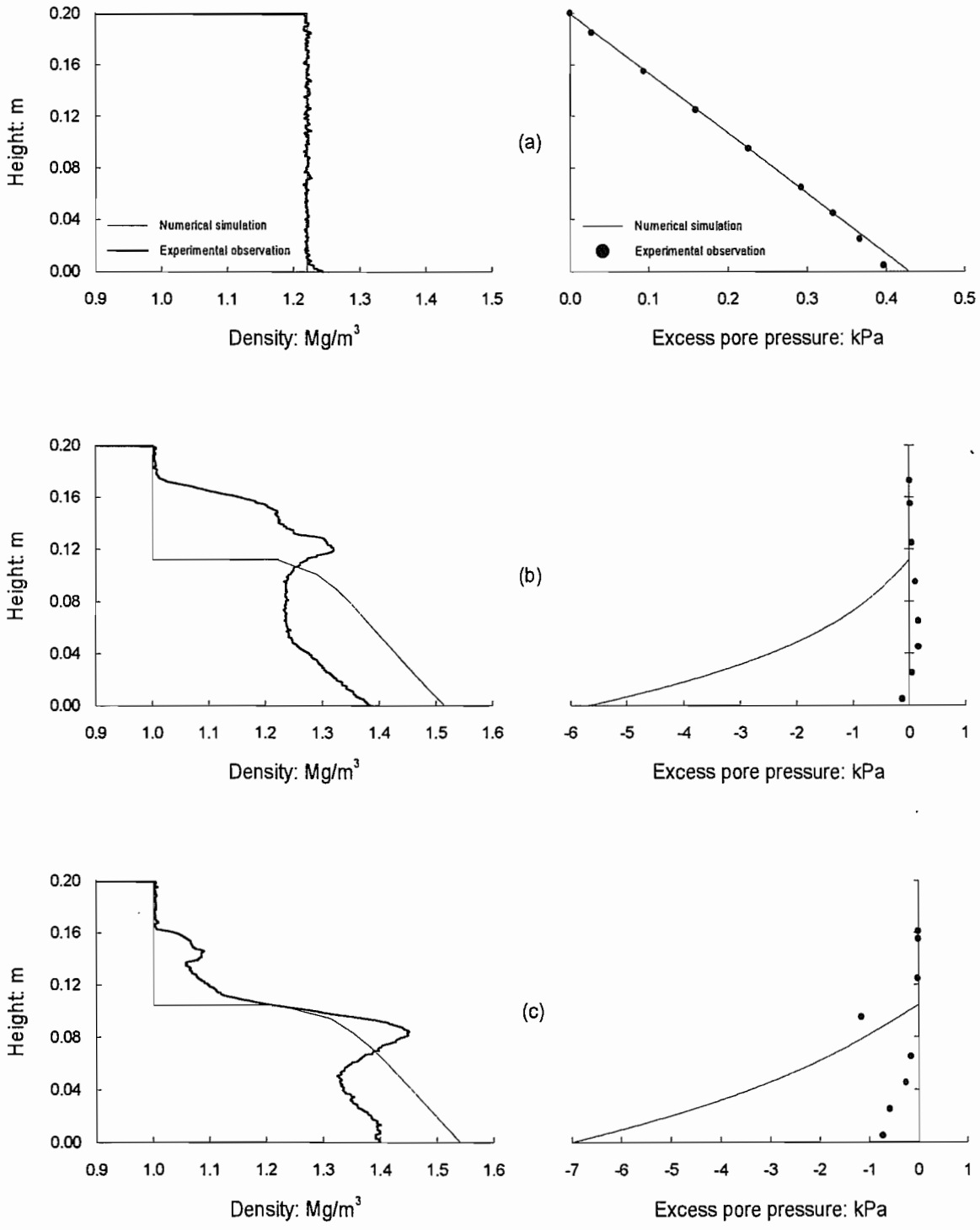

Figure 6.26 Numerical simulation of density and excess pore pressure profiles, experiment KE3: (a) 0 hr; (b) 12 hr; (c) 18 hr

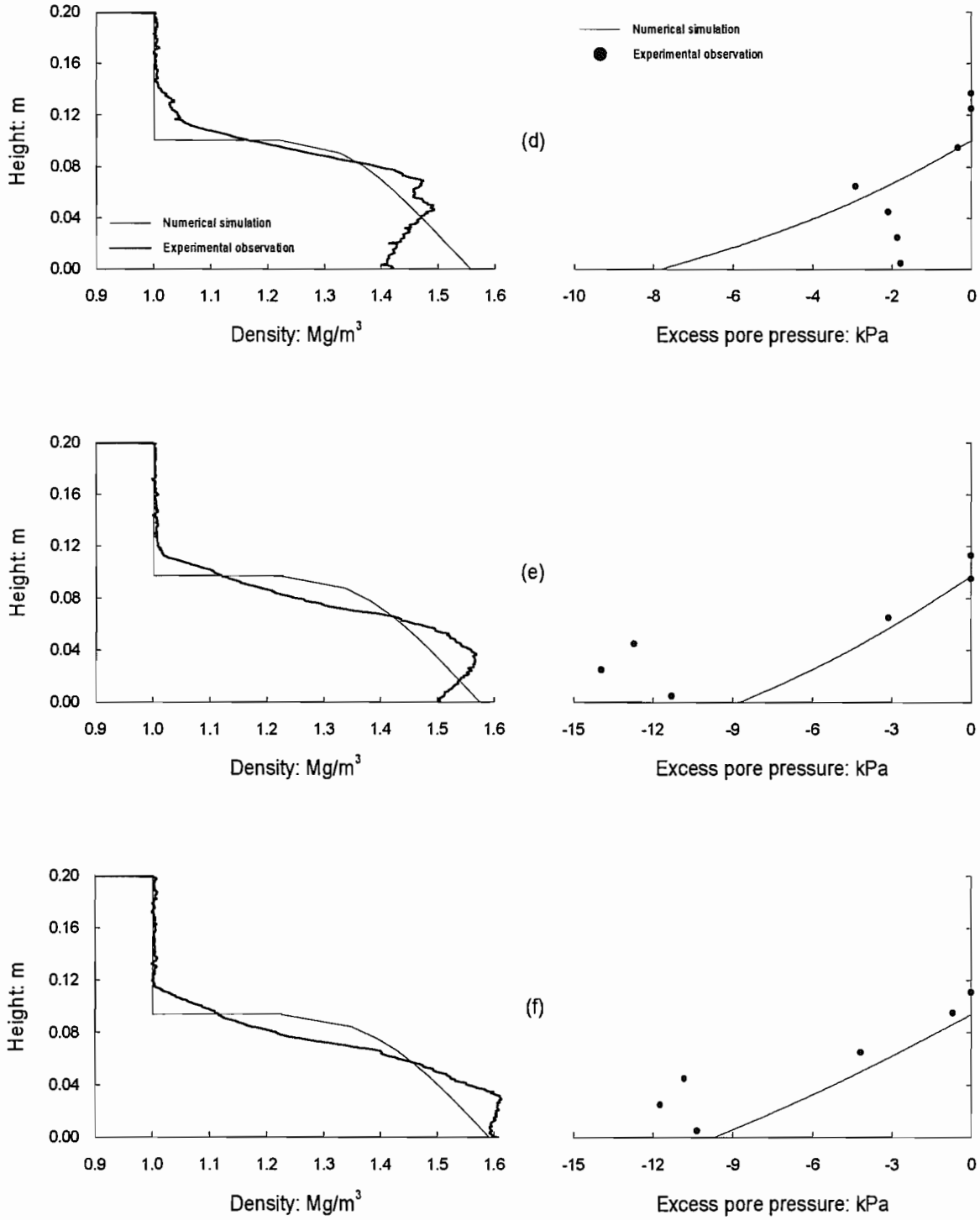

Figure 6.26 Continued: (d) 23 hr; (e) 30 hr; (f) 40 hr

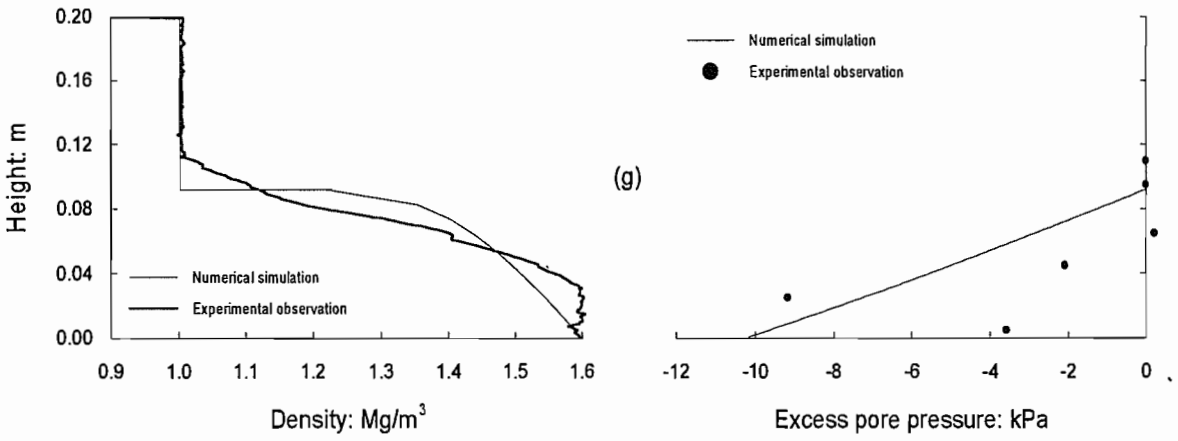

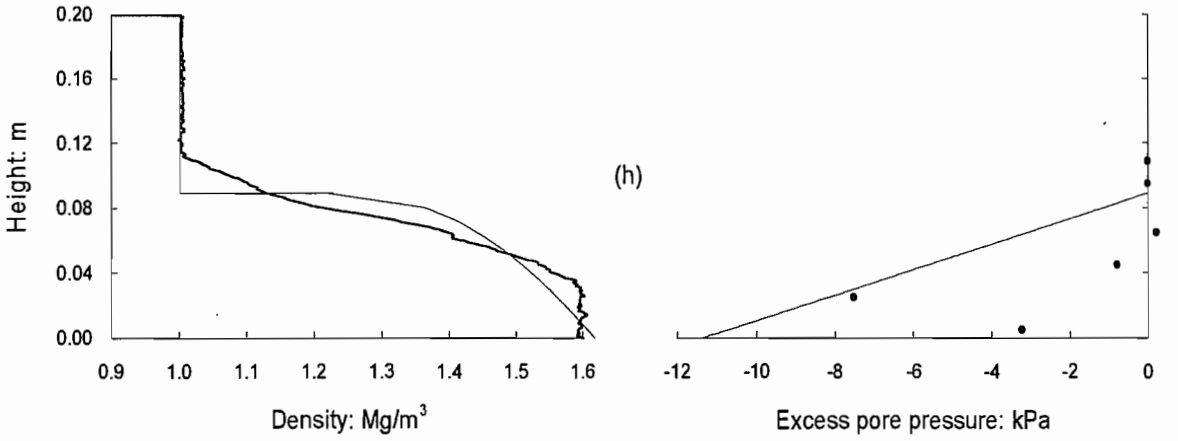

Figure 6.26 Continued: (g) 49 hr; (h) 63 hr

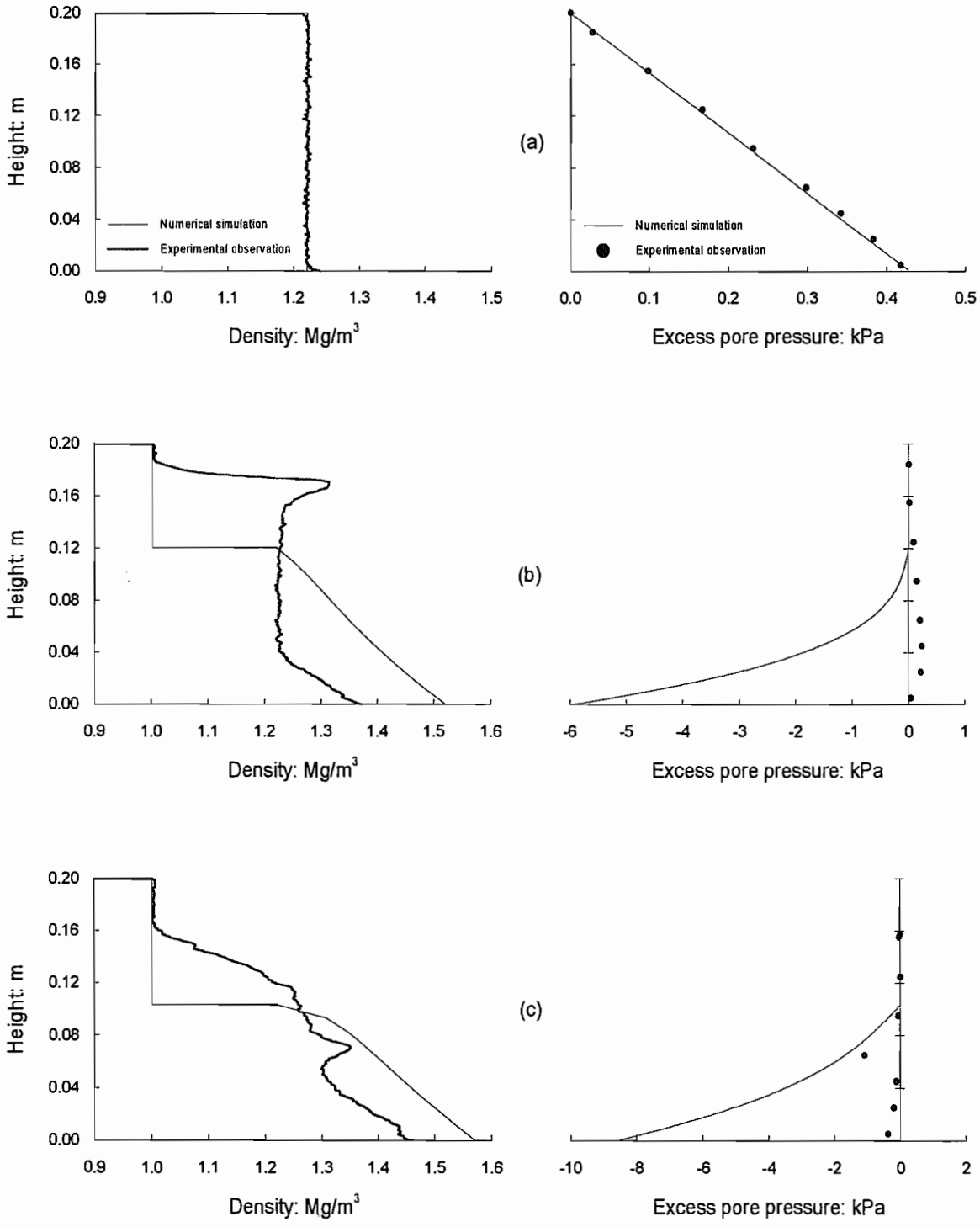

Figure 6.27 Numerical simulation of density and excess pore pressure profiles, experiment KE4: (a) 0 hr; (b) 6 hr; (c) 12 hr

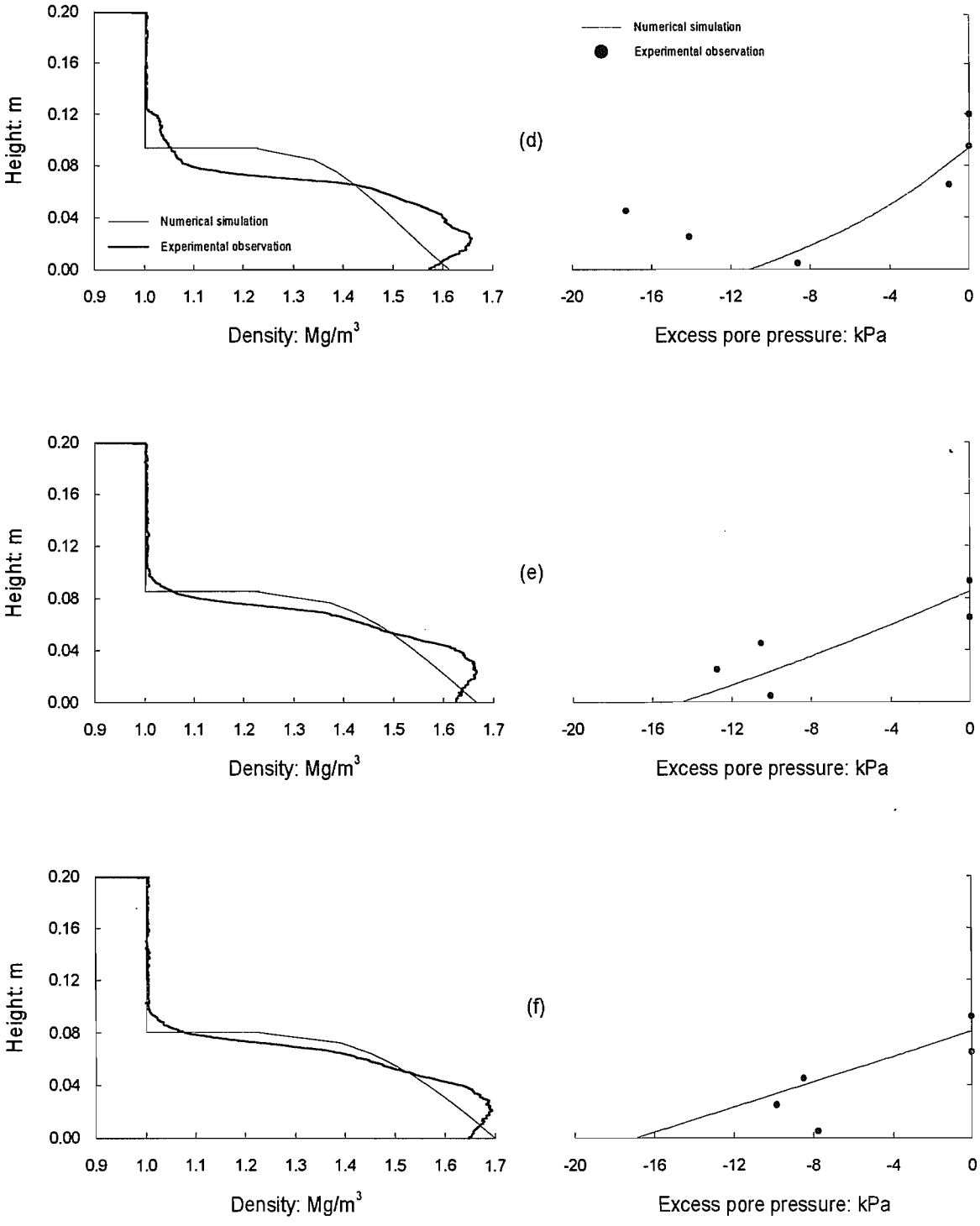

Figure 6.27 Continued: (d) 20 hr; (e) 40 hr; (f) 71 hr

6.7 Summary and Discussion

The diffusion equation governing the electrokinetic consolidation parameter ξ was solved with assumptions of small strain and constant coefficients of consolidation, hydraulic permeability, and electroosmotic permeability. The first stage was a consideration of the self-weight consolidation process corresponding to zero applied voltage, in which case the parameter ξ becomes the excess pore pressure u_e. In this case, a suitable value of the coefficient of consolidation was obtained by finding the best fit between calculated and measured excess pore pressures at some intermediate time. The complete solution then gives excess pore pressure as a function of depth and time. The surface settlement and density changes were then calculated from these excess pore pressures. The overestimation of effective stress due to the small strain assumption has been improved by iteration based on the concept of mass conservation, which results in remarkably good agreement between simulated and measured surface settlement and density profiles.

Under the influence of electrokinesis changes were observed in the soil parameters, such as the coefficient of consolidation, hydraulic permeability, and the compression index. Therefore, similar procedures to those described above were used to determine the appropriate coefficient of consolidation by estimating the hydraulic permeability which gives the best fit to the final negative excess pore pressure and density profiles. Numerical simulations using soil parameters from electrokinetic consolidation tests showed better agreement with real measurements in the later stage of electrokinetic process as those constant coefficients were estimated for the final stage of electrokinetic process.

Despite using soil parameters from electrokinetic tests, numerical simulations were not able to predict the development of denser layer and negative excess pore pressure in the cathode region during the electrokinetic process. This situation has arisen from the assumptions made in the analytical solution about the electroosmotic permeability and the applied voltage gradient. The electroosmotic permeability was assumed to be constant with time, and to have the same value throughout the bed. The applied voltage gradient was assumed to be constant in the small strain solution used as the initial condition for the iteration. This implies that the voltage difference was also constant. During the iteration, there was a constant voltage difference between the top and bottom of the soil bed, and the corresponding gradient increased as the bed thickness reduced. This behaviour is presented in Figure 6.28. Neither the assumption about electroosmotic permeability or the assumption about the voltage gradient were totally realistic; in particular, they changed locally near the cathode due to the changes in zeta potential.

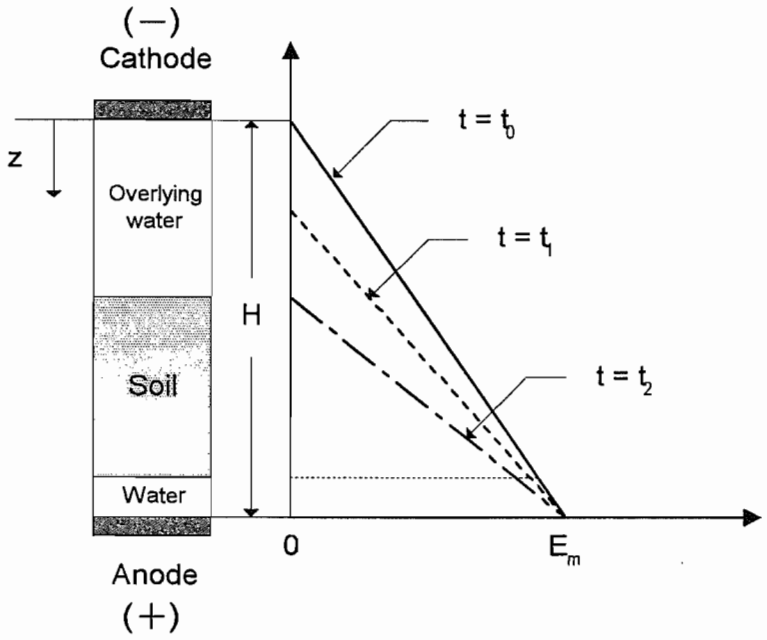

Figure 6.28 Variation of electrical gradient during numerical simulation

If the electroosmotic permeability is taken to be 1.18×10^{-8} m^2/V·sec instead of 1.32×10^{-8} m^2/V·sec, the maximum difference in excess pore pressure is 10 % lower. However, the corresponding density profiles are hardly changed. The explanation for this lies in the linear relationship between void ratio and logarithm of effective stress, so that a 10 % change in effective stress corresponds to a much smaller change in void ratio or density. Actually, the value of hydraulic permeability was chosen so that the predicted excess pore pressure at the base was equal to the measured value. There is then no difference in predictions with the two values of electroosmotic permeability. In fact, the soil parameter that affects the prediction is the ratio k_e/k_h, and this is determined by the excess pore pressure at the base. The other information that is necessary to use the model is the slope of C_c of the linear relationship between void ratio and logarithmic effective stress, along with the consolidation rate associated with the value of C_v from an excess pore pressure profile.

CHAPTER 7 CONCLUDING REMARKS

7. CONCLUDING REMARKS

7.1 Introduction

The research described in this thesis considered the behaviour of soft soil due to the application of an electric field. A laboratory testing programme examined the influence of various electric field strengths on the consolidation process, and a simple predictive model was developed. This final chapter summarises the principal conclusions of the work, and suggests some possible directions for future research.

7.2 Summary and Conclusions

An electrokinetic cell was designed and developed in order to study the fundamental behaviour of soft soil settling and consolidating subjected to an electric field. Unlike electrokinetic research described in the literature, which typically examine average volume changes, the measurements conducted here were able to investigate local compression behaviour of soil sample. The electroosmotic permeability was investigated experimentally and evaluated theoretically. Using the existing analytical model based on small strain theory with the new addition of the concept of mass conservation, predictions of surface settlement and density change due to an electric field were made. The main conclusions from this work can be summarised in the following sections.

7.2.1 Experimental Considerations

The electrically induced surface settlement was greater in magnitude and faster in rate than that under self-weight stresses. The dissipation rate of excess pore pressure has been found to be directly related to the applied electric field strength. It has also been revealed by the measurement of density throughout the soil sample that the electrically induced compression process initially occurred both in the anode and cathode regions. The rapid increase in density occurred as expected in the anode region was induced by the increase in effective stresses via the dissipation of excess pore pressures due to the effect of electroosmosis. This is suggested to be the most significant process during the electrokinetic consolidation. The development of the denser layer at the soil surface was caused by the additional effects of electrokinesis, such as electrochemical reaction (pH change), which eventually resulted in the development of nonlinear voltage gradient within the soil sample. The density and excess pore pressure profiles also identified that the electroosmotic water flow, which affects the variation of pore pressure and swelling, was directly related to the applied electric field strength during and after the electrokinetic process.

This pattern was evident in all the electrokinetic tests.

The movement of acid and base fronts (the migration of ions) due to electrolysis under the influence of electrokinesis has been demonstrated experimentally and identified by the measurement of pH during and after the electrokinetic process. It is suggested that the neutralisation initially occurred at the soil surface (cathode region) due to the initial low pH of the soil sample, and moved towards the anode with the advancing base front. Due to the different ionic mobilities and the electroosmotic water flow, the base front was found to be restricted to the cathode region and hence the zone of neutralisation was also close to the cathode. The development of low electrical conductivity zone was identified by a number of voltage profiles measured throughout the soil samples; the voltage gradient near the cathode increased due to the increase of resistance via the reduction of electrical conductivity in that region. The increase of voltage gradient near the cathode generated greater electroosmotic water flow, resulting in the development of suction.

The initially occurring rapid compression in the cathode region (soil surface) was mainly due to the increase of zeta potential via the increase of pH. The increase of zeta potential would be expected to generate suction near the soil surface via greater electroosmotic flow in that region, although this was not able to be observed due to the limited number of pore pressure ports. The excess pore pressure and pH profiles also support the view that the development of a denser layer in the cathode region was caused by the electrochemical reactions due to the migrating ions. The electrochemical reaction also results in the development of nonlinear voltage gradients within the soil sample.

7.2.2 Theoretical Considerations

The simple diffusion equation with constant coefficients has been taken as the starting point for a model prediction of self-weight and electrokinetic consolidation. The normal small strain assumption, equivalent to the boundary remaining fixed, made in previous solutions of the equation has been replaced by boundary movement coupled with the requirement of conservation of mass. The soil parameters of compressibility and permeability clearly change as consolidation proceeds, but it has proved possible to identify constant values that represent the soil behaviour over the stress ranges examined.

For the self-weight consolidation behaviour, remarkably good agreement has been demonstrated between the measured and simulated density and excess pore pressure profiles. For the electrokinetic consolidation behaviour, the theoretical model does not allow for changes in zeta potential, so that it cannot be expected to simulate the density increase seen at the surface in the early stages. However, it is able to predict the surface settlement well and also the later distributions of pore pressure and density.

The appropriate determination of soil parameters, such as C_c, C_v, k_h, and k_e, are very important in numerical simulations. Therefore, if the model is to be used to predict the electrokinetic consolidation of a soil, a single experiment must be carried out to establish the necessary soil parameters, such as k_e/k_h, C_c, and C_v. These values can then be used to predict the results of different magnitudes of electric field.

7.3 Contribution of this Thesis

This thesis has two main contributions; one is the interpretation of experimental data and one is model development. The experimental results have identified the importance of different processes in electrokinetic consolidation, including changes in zeta potential inferred from pH measurements, and they have also confirmed that the consolidation is governed through the increases in effective stress.

The small strain solution of the simple diffusion equation with constant coefficients has been developed to incorporate some measures of large strain. This has allowed remarkably good prediction of the electrokinetic consolidation observed in the experiments.

7.4 Areas for Future Research

In order to improve the understanding of the electrokinetic process and to examine the analytical model used in this study, following future investigations are required.

The influence of zeta potential and nonlinear voltage gradient have been shown to be significant in the compression of soft soils particularly in the cathode region. Therefore, more frequent measurements of density, pore pressure, local voltage, and pH are required in the region of moving surface.

Zeta potential has different response with different soil type (e.g. kaolinite and montmorillonite), so that a wider variety of soil types should also be used to broaden the scope of the work. Maintaining the pH condition of sample is also beneficial for both variation of zeta potential and voltage gradient.

Different initial soil conditions (e.g. initial height and density) are necessary in order to examine the analytical model and the approach to predict settlement and density. The stress history is relevant to the subsequent electrokinetic response, so that further research is needed for soils consolidated to higher stress levels.

Bibliography

Acar, Y. B., Gale, R. J., Putnam, G., Hamed, J., and Wong, R. L. (1990). Electro-chemical processing of soils: theory of pH gradient development by diffusion, migration, and linear convection. *J. Envir. Sci. Engrg. ASCE*, 25(6), 687-714.

Acar, Y. B., Hamed, G. J., and Putnam, G. (1991). Acid/base distributions in electrokinetic soil processing. *Transportation Res. Rec.* 1288, 23-33.

Acar, Y. B. and Gale, R. J. (1992). Phenol removal from kaolinite by electrokinetics. *J. Geotech. Engng. ASCE*, 118(11), 1837-1851.

Acar, Y. B., Alshawabkeh, A. N., and Gale, R. J. (1992). A review of fundamentals of removing contaminants from soils by electrokinetic soil processing. *Envir. Geotech.*, 321-330.

Acar, Y. B. and Alshawabkeh, A. N. (1993). Principles of electrokinetic remediation. *Envir. Sci. Technol.* 27(13), 2638-2647.

Acar, Y. B., Hamed, J. T., Alshawabkeh, A. N., and Gale, R. J. (1994). Removal of cadminm (II) from saturated kaolinite by the application of electrical current. *Geotechnique* 44(2), 239-254.

Acar, Y. B. and Alshawabkeh, A. N. (1996). Electrokinetic remediation. I: pilot-scale tests with lead-spiked kaolinite. *J. Geotech. Engng. ASCE*, 122(3), 173-185.

Alves, M. C. M. (1992). *Comportamento de sedimentacao e adensamento de uma lama vermelha.* Ph.D. thesis, PUC-Rio. (In Portuguese.)

Atkinson, J. H. (1993). *An introduction to the mechanics of soils and foundations through critical state soil mechanics.* McGraw-Hill Book Company.

Atkinson, J. H. and Evans, J. S. (1985). Discussion. *Geotechnique* 35(3), 378-380.

Atkinson, J. H., Evans, J. S., and Ho, E. W. L. (1984). Non-uniformity of triaxial samples due to consolidation with radial drainage. *Geotechnique* 34(3), 353-355.

Banerjee, S., Horng, J., Ferguson, J., and Nelson, P. (1990). Field scale feasibility of electrokinetic remediation. *Rep. presented to USEPA, Land Pollution Control Div., University of Washington, Seattle.*

Been, K. (1980). *Stress-strain behaviour of a cohesive soil deposited under water.* D.Phil. thesis, University of Oxford, UK.

Been, K. (1981). Non-destructive soil bulk density measurement by X-ray Attenuation. *Geotech. Testing J. ASTM*, 169-176.

Been, K. and Sills, G. C. (1981). Self-weight consolidation of soft soils: an experimental and theoretical study. *Geotechnique* 31(4), 519-535.

Bjerrum, L., Moum, J. and Eide, O. (1967). Application of electroosmosis to a foundation problem in a Norwegian quick clay. *Geotechnique* 17(3), 214-235.

Bowden, R. K. (1988). *Compression behaviour and shear strength characteristics of a natural silty clay sedimented in the laboratory.* D.Phil. thesis, University of Oxford, UK.

Bruell, C. J., Segall, B. A., and Walsh, M. T. (1992). Electroosmotic removal of gasoline hydrocarbons and TCE from clay. *J. Envir. Engng. ASCE*, 118(1), 68-73.

Butterfield, R. and Johnston, I. W. (1980). The influence of electroosmosis on metallic piles in clay. *Geotechnique* 30(1), 17-38.

Casagrande, L. (1949). Electroosmosis in soils. *Geotechnique* 1(3), 159-177.

Casagrande, L. (1952). Electro-osmotic stabilization of soils. *J. Boston Soc. Civ. Engrs.* 39(1), 51-83.

Casagrande, L., Loughney, R. W., and Matich, M. A. J. (1961). Electro-osmotic stabilization of a high slope in loose saturated silt. *Proc. 5th ICSMFE, Paris*, 2, 555-561.

Chappell, B. A. and Burton, P. L. (1975). Electro-osmosis applied to unstable embankment. *J. Geotech. Engng. ASCE*, 101(8), 733-739.

Craig, R. F. (1992). *Soil mechanics.* 5th Ed. Chapman & Hall.

Das, B. M. (1983). *Advanced soil mechanics.* Int. Ed. McGraw-Hill Book Company.

Dean, J. A. (1970). *Lange's handbook of chemistry.* 11th Ed. McGraw-Hill Book Company.

Elder, D. McG. (1985). *Stress strain and strength behaviour of very soft sediment.* D.Phil. thesis, University of Oxford, UK.

Elder, D. McG. and Sills, G. C. (1984). Time and stress dependent compression in soft sediments. *Proc. ASCE Symp. On Prediction and Validation of Consolidation, San Francisco*, 425-444.

Esrig, M. I. (1968). Pore pressures, consolidation, and electrokinetics. *J. Soil Mech. Fdns. Div. ASCE*, 94(4), 899-921.

Eykholt, G. R. (1997). Development of pore pressures by nonuniform electroosmosis in clays. *J. Hazardous Materials* 55, 171-186.

Eykholt, G. R. and Daniel, D. E. (1994). Impact of system chemistry on electroosmosis in contaminated soil. *J. Geotech. Engng. ASCE*, 120(5), 797-815.

Fannin, R. J. (1986). *Geogrid reinforcement of granular layers on soft clay - a study at model and full scale.* D.Phil. thesis, University of Oxford, UK.

Feldkamp, J. R., and Belhomme, G. M. (1990). Large-strain electrokinetic consolidation: theory and experiment in one dimension. *Geotechnique* 40, 557-568.

Fetzer, C. A. (1967). Electroosmotic stabilization of west branch dam. *J. Soil Mech. Fdns. Div. ASCE*, 93(4), 85-106.

Francescon, M. (1983). *Model pile test in clay - stresses and displacements due to installation and axial loading*. Ph.D. thesis, University of Cambridge, UK.

Gibson, R. E., England, G. L., and Hussey, M. J. L. (1967). The theory of one-dimensional consolidation of saturated clays-I. *Geotechnique* 17, 261-273.

Gladwell, J. K. (1965). Practical application of electro-osmosis. *N.Z. Engng*. 20(2), 66-72.

Goldman, L. J., Greenfield, L. I., Damle, A.S., Kingsbury, G. L., Northeim, C. M., Truesdale, R. S., and Roulier, M. H. (1986). Design, construction and evaluation of clay liners for waste management facilities. *EPA/530-SW-86-007-F*.

Gray, D. H. and Mitchell, J. K. (1967). Fundamental aspects of electro-osmosis in soils. *J. Soil Mech. Fdns. Div. ASCE*, 93(6), 209-236.

Gray, D. H. (1970). Electrochemical hardening of clay soils. *Geotechnique* 20(1), 81-93.

Gray, D. H., and Somogyi, F. (1977). Electro-osmotic dewatering with polarity reversals. *J. Geotech. Engng. ASCE*, 103(GT1), 51-54.

Gue, S. S. (1984). *Ground heave around driven piles in clay*. D.Phil. thesis, University of Oxford, UK.

Hamed, J., Acar, Y. B., and Gale, R. J. (1991). PB(II) removal from kaolinite by electrokinetics. *J. Geotech. Engng. ASCE*, 117(2), 241-271.

Hamed, J. T. and Bhadra, A. (1997). Influence of current density and pH on electrokinetics. *J. Hazardous Materials* 55, 279-294.

Johnston, I. W. and Butterfield, R. (1977). A laboratory investigation of soil consolidation by electroosmosis. *Austral. Geomech. J.* 7, 21-32.

Kohl, J., Zentner, R. D., and Lukens, H. R. (1961). *Radioisotope applications engineering*. Van Nostrand.

Kynch, G. J. (1952). A theory of sedimentation. *Transactions of the Faraday Society* 48, 166-176.

Lageman, R., Pool, W., and Seffinga, G. (1989). Electro-reclamation: theory and practice. *Chemistry and Industry* 18(9), 585-590.

Li, H. and Williams, D. J. (1995). Sedimentation and self-weight consolidation behaviour of coal mine tailings. *Proc. Int. Symp.Compression and Consolidation of Clayey Soils, Hiroshima*, Japan 875-890.

Lo, K. Y., Inculet, I. I., and Ho, K. S. (1991). Electroosmotic strengthening of soft sensitive clays. *Can. Geotech. J.* 28, 62-73.

Lockhart, N. C. (1981). Sedimentation and electro-osmotic dewatering of coal-washery slimes. *Fuel* 60(10), 919-923.

Lockhart, N. C. (1983a). Electroosmotic dewatering of clays: I. influence of voltage. *Colloids Surf.* 6(3), 229-238.

Lockhart, N. C. (1983b). Electroosmotic dewatering of clays: II. influence of salt, acid, and flocculants. *Colloids Surf.* 6(3), 239-251.

Lockhart, N. C. (1983c). Electroosmotic dewatering of clays: III. influence of clay type, exchangeable cations, and electrode materials. *Colloids Surf.* 6(3), 253-269.

Lockhart, N. C. and Stickland, R. E. (1984). Dewatering coal washery tailings ponds by electro-osmosis. *Powder Technol.* 40, 215-221.

Lomize, G. M., Netushil, A. V., and Rzhanitzin, B. A. (1957). Electro-osmotic processes in clayey soils and dewatering during excavations. *Proc. 4th ICSMFE, London*, 1, 62-67.

Mise, T. (1961). Electro-osmotic dewatering of soil and distribution of pore water pressure. *Proc. 5th ICSMFE, Paris*, 1, 255-257.

Mitchell, J. K. and Yeung, A. T. (1990). Electro-kinetic flow barriers in compacted clay. *Transportation Res. Rec.* 1288, 1-9.

Mitchell, J. K. (1993). *Fundamentals of soil behaviour*. 2nd Ed. New York: Wiley.

Nyirenda, Z. M. (1989). *The piezocone in lightly over consolidated clay*. D.Phil. thesis, University of Oxford, UK.

Pamukcu, S., and Wittle, J. K. (1992). Electrokinetic removal of selected heavy metals from soil. *Envir. Progress* 11(3), 241-250.

Pamukcu, S. (1997). Electro-chemical technologies for in-situ restoration of contaminated subsurface soils. *The Electronic Journal of Geotechnical Engineering (EJGE)*.

Pane, V. and Schiffman, R. L. (1985). A note on sedimentation and consolidation. *Geotechnique* 35(1), 69-72.

Penn, M. L. M. (1997). *Electrokinetic soil remediation: effects of pH, temperature and chemical reactions*. Ph.D. thesis, University of Cambridge, UK.

Perry, W. (1963). Electro-osmosis dewaters foundation excavation. *Constr. Methods Equip.* 49(9), 116-119.

Probstein, R. F. and Hicks, R. E. (1993). Removal of contaminants from soils by electric fields. *Science* 260, 498-503.

Rowe, R. K., Quigley, R. M., and Booker, J. R. (1995). *Clayey barrier systems for waste disposal facilities*. Chapman & Hall.

Rødsand, T., Acar, Y. B., and Breedveld, G. (1995). Electrokinetic extraction of lead from spiked Norwegian marine clay. *Geoenvironment 2000, Geotechnical Special Publication 46*, 1518-1534.

Segall, B. A., O'Bannon, C. E., and Mathias, J. A. (1980). Electroosmosis chemistry and water quality. *J. Geotech. Engng. ASCE*, 106(10), 1148-1152.

Segall, B. A. and Bruell, C. J. (1992). Electroosmotic contaminant: removal processes. *J. Envir. Engng. ASCE*, 118(1), 84-100.

Shang, J. Q. (1997). Electrokinetic dewatering of clay slurries as engineered soil covers. *Can. Geotech. J.* 34, 78-86.

Shang, J. Q. (1997). Electrokinetic sedimentation: a theoretical and experimental study. *Can. Geotech. J.* 34, 305-314.

Shang, J. Q. (1998). Electroosmosis-enhanced preloading consolidation via vertical drains. *Can. Geotech. J.* 35, 491-499.

Shang, J. Q. and Lo, K. Y. (1997). Electrokinetic dewatering of a phosphate clay. *J. Hazardous Materials* 55, 117-133.

Shapiro, A. P., Renaud, P. C., and Probstein, R. F. (1989). Preliminary studies on the removal of chemical species from saturated porous media by electroosmosis. *PhysicoChemical Hydrodynamics* 11(5/6), 785-802.

Shapiro, A.P. and Probstein, R. F. (1993). Removal of contaminants from saturated clay by electroosmosis. *Envir. Sci. Technol.* 27, 283-291.

Sills, G. C. and Elder, D.McG. (1984). The transition from sediment suspension to settling bed. *Estuarine Cohesive Sediment Dynamics, Berlin*. 192-205.

Sills, G. C. (1995). Time dependent processes in soil consolidation. *Proc. Int. Symp. Compression and Consolidation of Clayey Soils. Hiroshima*, Japan 875-890.

Sills, G. C. (1998). Development of structure in sedimenting soils. *Phil. Trans. R. Soc. Lond.* 356, 2515-2534.

Sposito, G. (1984). *The surface chemistry of soils*. Oxford University Press, Inc., New York.

Sprute, R. H. and Kelsh, R. H. (1982). Electrokinetic densification of solids in a coal mine sediment pond - a feasibility study. *U.S. Dep. Interior, Bur. Mines Rep. Invest.* 8666, 1-31.

Stewart, D. I. and West, L. J. (1996). Electrokinetic soil decontamination - effect of local resistivity variations. *Proc. 2th Int. Congress on Environmental Geotechnics, Osaka*, 10, 1101-1106.

Tan, K. H. (1993). *Principles of soil chemistry*. 2nd Ed. Marcel Dkker, Inc.

Tan, T. S., Yong, K. Y., Leong, E. C., and Lee, S. L. (1990). Sedimentation of clayey slurry. *J. Geotech. Engng. ASCE*, 116(6), 885-898.

Terzaghi, K. (1936). The shearing resistance of saturated soils and the angles between the planes of shear. *Proc. 1st Int. Conf. Soil Mechanics*, 1, 54-56.

Thevanayagam, S., and Wang, J. (1994). Flow behaviour during electrokinetic soil decontamination. First International Congress on Environmental Geotechnics, Alberta, Canada, July 10-15.

Ting, C. M. R. (1990). Controlled gradient consolidation of soft soils with reference to the development of K_o. Ph.D thesis, Polytechnic of East London, UK.

van Olphen, H. (1977). *An introduction to clay colloid chemistry*. 2nd Ed. New York: Wiley.

Vane, L. M. and Zang, G. M. (1995). Electrokinetic soil remediation: impact of aqueous phase properties on soil surface charge and electroosmosis efficiency. *Proc. EPA 21st Annual RREL Research Symposium* 202-206.

Vane, L. M. and Zang, G. M. (1997). Effect of aqueous phase properties on clay particle zeta potential and electro-osmotic permeability: implications for electro-kinetic soil remediation processes. *J. Hazardous Materials* 55, 1-22.

Wade, M. H. (1976). Slop stability by electroosmosis. *Proc. 29th Canadian Geotechnical Conference, Vancouver*, 10, 44-66.

Wan, T. Y. and Mitchell, J. K. (1976). Electroosmtic consolidation of soils. *J. Geotech. Engng. ASCE*, 102(5), 473-491.

West, L. J. and Stewart, D. I. (1995). Effect of zetal potential on soil electrokinesis. *Geoenvironment 2000, Geotechnical Special Publication 46*, 1535-1549.

Wroth, C. P. (1984). The interpretation of in situ soil tests. Géotechnique 34, No. 4, 449-489.

Yeung, A. T. (1990). *Electro-kinetic barrier to contaminant transport through compacted clay*. Ph.D. dissertation, University of California, Berkeley.

Yeung, A. T., Chung, M., Corapcioglu, M. Y., and Stallard, W. M. (1995). One-dimensional experimental studies on electrophoresis of clay. Geotech. Special Publication No. 46, Geoenvironment 2000, 2-2, 1564-1575.

Yeung, A. T., Hsu, C., and Menon, R. M. (1997). Physicochemical soil-contaminant interactions during electrokinetic extraction. *J. Hazardous Materials* 55, 221-237.

Appendix

General Solution to the Consolidation Equation

The differential equation of Terzaghi's consolidation theory governing one-dimensional consolidation and the dissipation of excess pore pressures is expressed as:

$$\frac{\partial u_e}{\partial t} = C_v \frac{\partial^2 u_e}{\partial z^2} \tag{A.1}$$

where C_v is the coefficient of consolidation ($k_h/\gamma_w m_v$).

To solve Equation (A.1), it is assumed that the excess pore pressure, u_e, is the product of two functions of z and t:

$$u_e = F(z)\,G(t) \tag{A.2}$$

where $F(z)$ is a function of z and $G(t)$ is a function of t.

Substitution of Equation (A.2) into Equation (A.1) yields:

$$\frac{\partial u_e}{\partial t} = F(z)\frac{dG(t)}{dt} = F(z)\,G'(t) \tag{A.3}$$

and

$$\frac{\partial^2 u_e}{\partial z^2} = G(t)\frac{d^2F(z)}{dz^2} = F''(z)\,G(t) \tag{A.4}$$

From Equations (A.1), (A.3), and (A.4):

$$F(z)\,G'(t) = C_v F''(z)\,G(t) \tag{A.5}$$

or

$$\frac{F''(z)}{F(z)} = \frac{G'(t)}{C_v G(t)} \tag{A.6}$$

The left-hand side of Equation (A.6) is a function of z alone and is independent of t whilst the right-hand side of the equation is a function of t alone and is independent of z. Therefore, they must be equal to a constant, $-B^2$. So:

$$F''(z) = -B^2 F(z) \tag{A.7}$$

A solution to Equation (A.7) can be given by:

$$F(z) = A_1 \cos Bz + A_2 \sin Bz \tag{A.8}$$

where A_1 and A_2 are constants.

The right-hand side of Equation (A.6) can be written as:

$$G'(t) = -B^2 C_v G(t) \tag{A.9}$$

The solution to Equation (A.9) is given by:

$$G(t) = A_3 \exp(-B^2 C_v t) \tag{A.10}$$

where A_3 is a constant.

Combining Equations (A.2), (A.8), and (A.10):

$$u_e = (A_1 \cos Bz + A_2 \sin Bz) A_3 \exp(-B^2 C_v t) = (A_4 \cos Bz + A_5 \sin Bz) \exp(-B^2 C_v t) \tag{A.11}$$

where A_4 is $A_1 A_3$ and A_5 is $A_2 A_3$.